

On the Melting Behavior of
Cyclic 1,4-Butylene Terephthalate
for Ring-Opening Polymerization and
on Polycondensation by Enzymatic Catalysis

Doctoral Thesis

with the aim of achieving a doctoral degree

Doctor rerum naturalium

at the Faculty of Mathematics, Informatics and Natural Sciences Department of Chemistry
University of Hamburg

Submitted by

Björn Neuer

(born in Hamburg)

Hamburg, April 2020

The practical work for this thesis has been prepared at the Institute for Technical and Macromolecular Chemistry at the University of Hamburg in the research group of Professor Dr. Gerrit A. Luinstra from July 2012 to November 2016.

The disputation took place on June 19, 2020.

Reviewers: Prof. Dr. G. A. Luinstra
Priv. Doz. Dr. C. Wutz

The evaluated dissertation has been revised, the final version has been approved on November 23, 2020.

Table of contents

List of Publications	IV
List of Poster Contributions	IV
List of Abbreviations	IV
1 Summary	1
2 Zusammenfassung	5
3 Introduction and State of Knowledge	11
3.1 ROP of cyclic polyester oligomers.....	13
3.1.1 Mechanistic aspects of metal-catalyzed ROP.....	13
3.1.2 Preparation of aromatic polyesters by ROP.....	15
3.2 Macrocyclic oligomers (MCOs)	18
3.2.1 Accessibility of MCOs of polyesters	20
3.2.1.1 Extraction	21
3.2.1.2 Cyclo-depolymerization (CDP)	22
3.2.1.3 Chemical synthesis	25
3.3 Options for reduction of the cBT polymerization temperature.....	26
3.4 Sustainable polyesters by polycondensation.....	29
4 Scope of work	33
5 Results and discussion	35
5.1 Reduction of the melting temperature of cBT by recrystallization	35
5.1.1 Analytical methods.....	35
5.1.1.1 DSC	35
5.1.1.2 ¹ H NMR spectroscopy	37
5.1.1.3 MALDI-TOF.....	39
5.1.1.4 GPC(THF) of low-melting MCOs	41
5.1.1.5 SEM.....	43
5.1.2 Manipulation of the melting temperature of cBT by precipitation with variation of solvent polarity	44
5.1.3 Isolation of low-melting cBT (LM-cBT) by utilization of low-boiling solvents.....	48
5.1.4 Extraction of cBT.....	51
5.1.4.1 Influence of extraction method.....	51
5.1.4.2 Influence of solvents on the extracted fraction.....	53
5.1.4.3 Effects of scale-up on extraction with cyclohexane.....	55
5.1.4.4 Extractions using fused silica frits with other pore sizes.....	60
5.1.4.5 Change of cBT grain size on the extraction process.....	63

5.1.4.6	Extraction of CBT100 with supercritical carbon dioxide	71
5.1.5	Crystal structure of extracted cBT dimers and trimers	73
5.1.6	Concluding remarks on the isolation of LM-cBT	75
5.2	Effect of MCO mixtures on the thermal behavior	78
5.2.1	Provision with additional aromatic and aliphatic lactones	79
5.2.1.1	Preparing of the aromatic and aliphatic lactones	79
5.2.1.2	Melting and crystallization behavior of the monomers	82
5.2.1.3	Glass transition	83
5.2.2	Effect of chemical structure on thermal behavior in mixtures of aromatic and aliphatic MCOs.....	84
5.2.2.1	General observations of the DSC measurements.....	85
5.2.2.2	Combinations of the aromatic with the aliphatic MCOs.....	86
5.2.2.3	Combinations of the aromatic MCOs among each other.....	105
5.2.3	Interpretation of the results of the monomeric mixtures	118
5.2.3.1	The melting temperature	118
5.2.3.2	Formation of a low-melting fraction.....	119
5.2.3.3	Supercooling and short-term hindrance of crystallization.....	119
5.2.3.4	Long-term crystallization (> 4 d)	120
5.2.3.5	Glass transition and the subsequent melting process.....	121
5.3	Enzyme- and metal-catalyzed polycondensation of a new bio-based polyester	122
5.3.1	Characterization of the diacid Pripol by ¹³ C NMR	122
5.3.2	Polycondensation of Pripol and 1,3-propanediol	123
5.3.2.1	Precondensation	124
5.3.2.2	Transesterification and the final polyesters.....	127
5.3.2.3	Exemplary polyurethane preparation from prepared polyesterol.....	135
6	Experimental Part	137
6.1	Materials	137
6.2	Analytical Measurements	138
6.3	Reduction of melting temperature of cBT by separation	140
6.3.1	Manipulation of the melting temperature of cBT by precipitation with variation of solvent polarity	140
6.3.1.1	Time and temperature dependency of precipitation of cBT oligomers.....	140
6.3.1.2	Variation of solvent polarity	141
6.3.2	Isolation of low-melting cBT (LM-cBT) by utilization of low-boiling solvents.....	143
6.3.2.1	Separation of cBT in presence of transesterification catalyst in CHCl ₃	143
6.3.2.2	Isolating of low-melting cBT (LM-cBT) from single solvent system	144

6.3.2.3 Isolating of low-melting cBT (LM-cBT) by precipitating from a solution in CHCl ₃ with cyclohexane	144
6.3.3 Isolation of LM-cBT by extraction	145
6.3.3.1 Small-scale iterative extractions	145
6.3.3.2 Larger-scale extractions (>100 g cBT) with frits continuously passed by a solvent.....	147
6.3.3.3 Extraction of CBT100 with supercritical carbon dioxide	149
6.3.3.4 Ring-opening of cBT with 1-butanol as reference for analytics	149
6.4 Mixtures of MCO and their influence on the thermal behavior	150
6.4.1 Preparation of aliphatic and aromatic lactones	150
6.4.1.1 Pseudo-high dilution synthesis	150
6.4.1.2 Depolymerization of PBI in dilution	153
6.4.1.3 Depolymerization in bulk	153
6.5 Enzyme- and metal-catalyzed polycondensation of a new bio-based polyester	154
6.5.1 Polycondensation of polyesters.....	154
6.5.1.1 Metal- and auto-catalyzed polycondensation.....	155
6.5.1.2 Enzyme-catalyzed polycondensation.....	155
6.5.2 Exemplary synthesis of a polyurethane elastomer.....	155
7 H- and P-Clauses and Disposal	157
7.1 Safety ^{258–260}	157
7.2 Disposal.....	160
7.3 Usage of CMR substances ^{258,259}	161
8 References	162
9 Acknowledgements and Credits.....	177
Statutory Declaration	179

List of Publications

J. Gebhard, B. Neuer, G. A. Luinstra, A. Liese, Enzyme- and Metal-Catalyzed Synthesis of a New Biobased Polyester, *Org. Process Res. Dev.* **21** (9), 1245–1252 (2017).

M. Lahcini, S. Elhakioui, D. Szopinski, B. Neuer, A. El Kadib, F. Scheliga, M. Raihane, F. J. Baltá Calleja, G. A. Luinstra, Harnessing synergies in tin-clay catalyst for the preparation of poly(ϵ -caprolactone)/halloysite nanocomposites, *Eur. Polym. J.* **81**, 1–11 (2016).

List of Poster Contributions

Rheological behavior of high molecular weight poly(1,4-butylene adipate) synthesized by ring-opening polymerization, Annual European Rheology Conference (AERC), Nantes 2015.

Ultra-High Molecular Weight Biodegradable Polyesters Synthesized by Non-Enzymatic Ring-Opening Polymerization (ROP), Macromolecular Symposium, Freiburg 2016.

List of Abbreviations

ΔC_p	Change in specific heat capacity
ΔH_c	Heat of crystallization
ΔH_m	Heat of fusion
$\Delta H_{m, theo}$	Theoretically expected heat of fusion
ΔH_{cc}	Heat of cold crystallization (beyond glass transition before melting)
AV	Acid value
Ar	Argon

Ar-H	Aromatic hydrogen atoms
BDO	1,4-Butanediol
Bu	Butyl moiety
Cat	Catalyst
cBA	Cyclic 1,4-butylene adipate
cBI	Cyclic 1,4-butylene isophthalate
cBS	Cyclic 1,4-butylene succinate
cBT	Cyclic 1,4-butylene terephthalate
CDP	Cyclodepolymerization
cEI	Cyclic 1,2-ethylene isophthalate
cET	Cyclic 1,2-ethylene terephthalate
CY	Cyclohexane
CHCl ₃	Chloroform
cPI	Cyclic 1,3-propylene isophthalate
cPT	Cyclic 1,3-propylene terephthalate
DABCO	1,4-Diazabicyclo[2.2.2]octane
DCM	Dichloromethan
DMAP	4-(Dimethylamino)pyridine
DMlph	Dimethyl isophthalate
DP	Degree of polymerization
DSC	Differential scanning calorimetry
EDO	1,2-Ethanediol
ED-ROP	Entropically-driven ring-opening polymerization
Exp. no.	Number of experiment
G'	Storage modulus in oscillatory rheology measurements
G''	Loss modulus in oscillatory rheology measurements
GC-MS	Gas chromatography coupled to mass spectrometry
GPC	Gel permeation chromatography
HFIP	1,1,1,3,3,3-Hexafluoroisopropanol
HM-cBT	High-melting cyclic 1,4-butylene terephthalate
lphCl ₂	Isophthaloyl chloride
LM-cBT	Low-melting cyclic 1,4-butylene terephthalate
MALDI-TOF	Matrix-assisted laser desorption/ionization spectrometry with time-of-flight detection
MCO	Macrocyclic oligomer

Me	Methyl moiety
M_n	Number average molecular weight
mol-%	Molar percent
η	Steady state shear viscosity
$ \eta^* $	Complex shear viscosity from oscillatory rheology
M_w	Weight average molecular weight
NMR	Nuclear magnetic resonance
Oct	2-Ethylhexanoate
oDCB	1,2-Dichlorobenzene
PBI	Poly(1,4-butylene isophthalate)
PBT	Poly(1,4-butylene terephthalate)
<i>PDI</i>	Polydispersity index
PDO	1,3-Propanediol
PET	Poly(1,2-ethylene terephthalate)
PPT	Poly(1,3-propylene terephthalate)
Pr	Propyl moiety
Pripol	Pripol™ 1012
R	Universal gas constant ($R \approx 8.31446 \text{ J}\cdot\text{K}^{-1}\cdot\text{mol}^{-1}$)
RI	Refraction index
ROP	Ring-opening polymerization
RTM	Reaction transfer molding
scCO ₂	Supercritical carbon dioxide
T_g	Glass transition temperature
T_m	Melting temperature
TerCl ₂	Terephthaloyl chloride
TFA	Trifluoroacetate
THF	Tetrahydrofuran
TMS	Tetramethylsilane
UV	Ultraviolet light
vol-%	Percent by volume
ω	Angular frequency in oscillatory rheology measurements
w_i	Mass fraction of component <i>i</i>
<i>w/v</i>	Ratio of weight to volume
wt-%	Percent by weight
X	Conversion

1 Summary

This thesis is divided into three parts. The first two parts deal with the ring-opening polymerization (ROP) of lactones, which is a viable route to polyesters. The high melting temperature of aromatic lactones like e.g. cyclic 1,4-butylene terephthalate (cBT) however limits their utilization, especially in reaction injection molding (RIM). The objective of the first two parts of this study was to evaluate possible ways of reducing this crucial parameter for an easier processing of cBT. In the third part, the polycondensation of a sustainable polyester by a metal- and an enzyme-catalyzed route were compared and evaluated.

Low-melting cBT (LM-cBT) could be obtained by extraction of commercially available cBT (CBT100, IQ Tec), which has a melting temperature up to 200 °C. The melting temperatures of the LM-cBT were mostly below 170 °C. The amount of hydroxyl end groups, crucial for ring-opening polymerization, could usually be reduced to below 0.5 mol-% (or below the detection limit of ^1H NMR spectroscopy). Extraction in a heated setup (standard solid extraction setup, setup of KNÖFLER-BÖHM or of TWISSELMANN) was more advantageous than in the simpler setup of SOXHLET with respect to yield and final melting temperature. Cyclohexane proved to be the more effective solvent over chloroform or tetrahydrofuran. Scaled-up extractions with cyclohexane from 20 g to up to 340 g of extraction material led to a similar yield-time curve, melting behavior and amount of impurities in the extracts. The porosity of the extraction frit used was varied (porosity G0, G1, G2) giving extracts with a similar melting behavior at a temperature below 170 °C and an amount of hydrolyzed cycles below 0.3 mol-%. The smallest pores (G2) resulted in the highest yield (44 compared to 38 and 20 wt-%). CBT with different grain sizes or laced with unprocessed cBT or PBT granulate were extracted to increase the yield and to reduce clogging of the frit observed before. Best results regarding yield as well as the melting temperature were achieved by usage of roughly grinded, coarse cBT (56 wt-%, 162 °C). SEM pictures of extraction residues showed the presence of three layers: 1) an amorphous inner area with small crystallites (edge length up to 5 μm) as observed in the starting material, 2) an intermediate layer with an increased number of crystallites ($\leq 15 \mu\text{m}$, often $< 5 \mu\text{m}$), whose thickness appears to be dependent on the yield, and 3) an outer layer consisting of a maze of plates ($\leq 15 \mu\text{m}$) without an amorphous phase of various thickness. A recrystallization process during extraction and a preferred extraction of the amorphous material is proposed to explain formation of this outer layer. A further optimization of the extraction conditions seems possible on basis of this first evaluation of the extraction of LM-cBT.

Further investigations were carried out concerning the literature-known precipitation of the cyclic oligomers from cBT, which are known to cause the higher melting temperatures. Experiments with mixtures of 1,2-dichlorobenzene and cBT with addition of a second low-boiling solvent (chloroform or toluene) were conducted. The temperature during the precipitation was found to be of major influence, not the solvent itself. Similar precipitates were obtained by adding various volume fractions of the second solvent according to analysis by DSC, MALDI and ^1H NMR. The addition of the more polar CHCl_3 at 60 °C led to the elimination of cBT fractions melting above 160 °C, while a higher-melting cBT fraction precipitated days after the addition of toluene at 108 °C.

Further procedures for obtaining LM-cBT were explored without the use of high-boiling solvents for ecological and economic reasons. It was possible to isolate LM-cBT with melting temperatures of below 170 or even 150 °C from solutions or suspensions of the commercial available cBT in chloroform or cyclohexane in yields of up to 79 wt-%. All combinations however showed drawbacks in space-time yield on account of long precipitation times when using chloroform (three days), of low yield (about 1 mol-%) if cyclohexane was applied or of formation of additional high-melting fractions in scale ups of mixtures of chloroform and cyclohexane.

A second approach to reduce the melting temperature of cBT in the preparation of random copolyesters is the exploiting of a melting point depression in the mixtures. Three further aromatic macrocyclic oligomers (MCOs) besides cBT and two aliphatic lactones were prepared and the mixtures analyzed by DSC. These monomers were cyclic 1,4-butylene isophthalate, cBI, cyclic 1,3-propylene terephthalate, cPT, and cyclic 1,3-propylene isophthalate, cPI, as well as cyclic 1,4-butylene adipate, cBA, and cyclic 1,4-butylene succinate, cBS.

All these cyclic monomers were soluble in each other judging from the dependency of melting, crystallization and glass transition temperature, T_m , T_c and T_g , on the sample composition. The changes especially of the melting temperatures were, however, small.

Structurally similar aromatic monomers in combination with one of the two aliphatic monomers generally led to a comparable melting behavior. One particular aromatic monomer showed a comparable melting behavior with the aliphatic monomers, i.e. cBA and cBS, despite their different melting temperatures (cBA 95 °C, cBS 69 °C). This is consistent with the thermodynamic basic considerations on mixing theory. A higher heat of fusion, ΔH_m , was generally found for cBA-containing mixtures, indicating a higher crystallinity if a similar molar heat of fusion is assumed.

Crystallization of cBA or cBS is less pronounced with cPT than with cBT present judged from the fitting of T_c with the monomeric ratio. It results in a more effective reduction of T_m of cPT than of cBT. The diol having an odd or even number of methylene groups obviously affects the crystallization for monomers with such short distance between the polar ester groups significantly. A smaller reduction of the melting temperature was noticed for the mixture cPT/cPI with only the odd-numbered diol present compared to cBT/cBI with its even-numbered diol. This effect has not been observed for mixtures with aliphatic monomers because it was overpowered by the presence of an isophthalate moiety and its disturbance of the alignment of the cycles during crystallization. A dominating hindrance of crystallization combined with lower melting temperatures was the result for mixtures of cBI or cPI with either the two aliphatic monomers cBA or cBS.

A low-melting fraction, whose origin is not identified yet, was noticed in most mixtures. A remarkably low melting temperature is formed in the mixture of cBT and cPT, the monomers with the highest melting temperatures of the pure monomers in this study. A small fraction with eutectic properties appears for blends of cBI or cPI with cBA with their maximum concentration at about equimolar ratios of the monomers.

Additionally, a short-term hindrance of crystallization affects all mixtures of aliphatic and aromatic monomers and most combinations of the aromatics with each other concluding from the supercooling ΔT_{sc} found and the amount of crystalline fraction (by means of ΔH_m). It is intensified by an isophthaloyl moiety. A long-term crystallization of cBI/cBA mixtures was noticed after short-term hindrance to crystallization.

For a pronounced supercooling, the presence of the odd-numbered PDO is advantageous, most preferably in combination with isophthalate (i.e. cPI). However, even the presence of both PDO and isophthalate in a mixture is no guarantee for a high depression.

An influence of the chain length on the hindrance to crystallization was noticed comparing mixtures of cBA or cBS with cBT or cPT but not with cBI or cPI. The presence of isophthalate has a dominating influence in case of the latter, like for the melting behavior, while the effect of the diol is secondary. No noteworthy difference in supercooling has been observed comparing cBS to cBA mixtures. Mixtures of cPT with an aliphatic monomer however possess a higher supercooling than those of cBT, especially for low amounts of cPT (maximum between 20 and 40 mol-%).

The presence of either of the two cycles with small repetition units in mixtures, i.e. cBS or cPT (compared to cBA or cBT and the isophthalate alternatives, respectively), resulted in an increased crystallinity after mixing in DSC measurements. The effect of the odd number of carbon atoms in cPT, which has been observed for the melting behavior, was found to be of

negligible importance for this impairing long-term behavior. This is not consistent with previous reports, but it may stem from the small distance between the polar groups in this

A glass transition was observed for all monomers and for almost all mixtures. Exceptions were combinations of cPT with cBA and mixtures with a high content of cBA. This was ascribed to the ease of crystallization of these monomers and differences in chain conformation affecting crystallization. A free volume higher than estimated by the FOX equation was recognized in mixtures containing a monomer readily crystallizing in pure state. This is similar to the observed conditions for formation of a low-melting fraction.

The amount of amorphous phase formed is smaller in cBA mixtures than in cBS mixtures according to the change in specific heat capacity, ΔC_p . Additionally, the presence of terephthalate reduces the amorphous fraction further compared to isophthalate.

A maximal extent of cold crystallization, ΔH_{cc} , is noticed in cBA mixtures with a fraction of approximately 50 mol-% (except for those with cPT). The presence of cBA obviously facilitates the reorganization of its partner MCO at $T_g < T < T_m$.

A different behavior was noticed for cBS mixtures with isophthalate regarding their glass transition. Their T_g s follow the FOX equation. A high fraction of amorphous phase was recognized in these blends as expected from the hindered crystallization mentioned above.

CBS mixtures with terephthalate-containing monomers reveal a free volume higher than expected from the FOX equation. The amorphous fraction is decreasing with an increasing amount of aromatic MCO. Only cBT/cBA mixtures undergo, however, a noticeable cold crystallization.

The length of the diol in the isophthalate had only little influence on the glass transition and cold crystallization. In contrast, the diol length of the second MCO, if based on terephthalate, significantly affects not only the (cold) crystallization behavior, but also determines the amount of vitreous or crystalline phase as well. A similar behavior was observed for cBT with cPI or cBI and for cPT with cPI or cBI, respectively. An about constant amorphous phase and increasing crystalline phase with increasing cBT content was observed, while an increasing cPT amount resulted in transformation of amorphous into crystalline phase. Only amorphous phase of rather constant extent was observed in mixtures of cBI with cPI as expected from the hindrance in crystallization by the isophthalate moiety.

The third part of this thesis dealt with the comparison of an enzyme-catalyzed and of a metal-catalyzed polycondensation. The effect of the lower temperature for enzyme utilization was of special interest. The monomers *Pripol*TM 1012 (Pripol) and 1,3-propanediol (PDO) have been chosen for this study. Both monomers are obtainable from renewable resources.

This study has been carried out in cooperation with the Technical University of Hamburg.¹ The monomers as well as the polyesters seem thermally stable at temperatures of up to 220 °C during synthesis even without an inert atmosphere. Structurally identical linear polyesters were obtained in metal-, enzyme- and autocatalyzed reactions accordingly to GPC, NMR and rheological measurements despite the different temperature programs.

A molecular weight M_w of 26.7 kg · mol⁻¹ (in GPC) was obtained by enzyme catalysis with *CalB immo* at only 80 °C. A further increase of the M_w would only have been possible in a reasonable time with a temperature higher than applicable for enzyme catalysis or with an optimized reactor set up for an improved removal of the byproduct water. A shift of the stoichiometry is thereby to be avoided, which is especially important during the precondensation step of the slow enzymatic reaction. A higher molecular weight of up to $M_w = 84.6$ kg · mol⁻¹ was accessible by metal-catalyzed polycondensation on account of the higher temperature and the hence more effective removal of the byproduct.

A polyurethane elastomer could easily be synthesized from a polyester made from Pripol and PDO to prove the general usefulness of such a polyester in such applications. The polyester was therefore prepared on a modified route to ensure hydroxy end groups of the polymer chains. The thermal and mechanical properties of the obtained polyurethane are similar to those of comparable polyurethanes from other renewable resources.

2 Zusammenfassung

Diese Dissertation ist in drei Teile gegliedert. Die ersten beiden Teile behandeln die ringöffnende Polymerisation (ROP) von Lactonen, was einen nützlichen Weg zu Polyestern darstellt. Die hohe Schmelztemperatur von aromatischen Lactonen, wie z.B. von cyclischem 1,4-Butylenterephthalat (cBT), begrenzt jedoch deren Anwendung. Das Ziel der ersten beiden Teile dieser Studie bestand in der Evaluierung von Wegen zur Reduktion dieses begrenzenden Faktors um eine einfachere Verarbeitung von cBT zu ermöglichen. Im dritten Teil wurde die Polykondensation eines nachhaltigen Polyesters per Katalyse mit Enzym sowie mit Metallkomplex verglichen und bewertet.

Niedrigschmelzendes cBT (LM-cBT) konnte durch Extraktion von kommerziell verfügbaren cBT erhalten werden. Die Schmelztemperatur konnte dabei von 200 °C des cBT auf

unterhalb von 170 °C für das isolierte LM-cBT gesenkt werden. Die für die ROP entscheidende Menge an Hydroxylendgruppen konnte üblicherweise laut ¹H-NMR-Spektroskopie auf Werte unter 0.5 mol-% oder sogar unterhalb der Nachweisgrenze reduziert werden. Die Extraktion in einer beheizten Apparatur (Standard-Feststoffextraktion, Extraktion von KNÖFLER-BÖHM oder TWISSELMANN) war hinsichtlich Ausbeute und Schmelztemperatur vorteilhafter als ein einfacher Aufbau nach SOXHLET. Cyclohexan erwies sich im Vergleich zu Chloroform oder Tetrahydrofuran als das effektivere Extraktionsmedium. Die Skalierung der Extraktionen mit Cyclohexan von 20 g auf bis zu 340 g Extraktionsgut führten zu vergleichbaren zeitlichen Verläufen der Ausbeute, des Schmelzverhaltens und des Anteils an Verunreinigungen in den Extrakten in Abhängigkeit der Extraktionszeit. Die Variation der Porosität der verwendeten Extraktionsfritte (Porosität G0, G1 und G2) führte zu Extrakten mit einem ähnlichen Schmelzverhalten (unterhalb 170 °C) und ähnlichen Anteilen an hydrolysierten Zyklen (unterhalb 0.3 mol-%). Die höchsten Ausbeuten wurden mit den kleinsten Poren (G2) erhalten (44 gegenüber 38 und 20 wt-%). Die Korngrößen des zu extrahierenden cBTs wurden variiert und gemahlenes cBT wurde sowohl mit unverarbeiteten als auch mit PBT-Granulat versetzt, um durch Variation der Schüttdichte die Ausbeute zu erhöhen und das zuvor beobachtete Verstopfen der Fritte zu reduzieren. Die besten Ergebnisse hinsichtlich Ausbeute und Schmelztemperatur wurden dabei durch Verwendung von grob gemahlenem cBT erzielt (56 wt-%, 162 °C). SEM-Aufnahmen von Extraktionsrückständen zeigten die Bildung von drei Schichten: 1) Ein amorpher innerer Bereich mit kleinen Kristalliten (Kantenlänge bis zu 5 µm), vergleichbar zu dem Ausgangsmaterial. 2) Eine Zwischenschicht mit einer erhöhten Anzahl an Kristalliten (≤15 µm, oft <5 µm), deren Dicke von der Ausbeute abhängig zu sein scheint. 3) Eine äußere Schicht, bestehend aus einem Netzwerk von Plättchen (≤15 µm) von unterschiedlicher Dicke ohne erkennbares amorphes Material. Ein Rekristallisationsprozess während der Extraktion und eine bevorzugte Extraktion des amorphen Materials ist höchstwahrscheinlich die Ursache für die Ausbildung der äußeren Schicht. Eine weitere Optimierung der Extraktionsbedingungen scheint auf der Grundlage dieser ersten Bewertung der Extraktion von LM-cBT möglich zu sein.

Weitere Untersuchungen wurden bezüglich einer aus der Literatur bekannten Ausfällung von denjenigen Oligomeren durchgeführt, die die höheren Schmelztemperaturen verursachen. Hierzu wurden Experimente mit Mischungen von 1,2-Dichlorbenzol und cBT durchgeführt, zu denen ein zweites, niedrigsiedendes Lösungsmittel (Chloroform oder Toluol) dosiert wurde. Es zeigte sich, dass die Temperatur während der Ausfällung und nicht das Lösungsmittel selbst einen bestimmenden Einfluss hat. Ähnliche Fällungsfractionen

entsprechend der Analyse durch DSC, MALDI und $^1\text{H-NMR}$ wurden durch Zugabe verschiedener Volumenfraktionen des jeweils zweiten Lösungsmittels erhalten. Die Zugabe des polarerer CHCl_3 bei $60\text{ }^\circ\text{C}$ führte zur Eliminierung der oberhalb von $160\text{ }^\circ\text{C}$ schmelzenden cBT-Fractionen, während eine höher schmelzende cBT-Fraktion noch Tage nach der eigentlichen Fällung mit Toluol bei $108\text{ }^\circ\text{C}$ bildete.

Alternative Vorgehen wurden evaluiert um die hochsiedenden Lösungsmittel aus ökologischen und wirtschaftlichen Gründen zu vermeiden. LM-cBT mit Schmelztemperaturen unter 170 oder sogar $150\text{ }^\circ\text{C}$ konnte aus Lösungen oder Suspensionen des kommerziell verfügbaren cBT direkt mittels Chloroform oder Cyclohexan in Ausbeuten von bis zu $79\text{ wt-}\%$ isoliert werden. Alle Kombinationen zeigten jedoch Nachteile wie lange Ausfällungszeiten für die Verwendung von Chloroform (drei Tage), eine geringe Ausbeute (etwa $1\text{ mol-}\%$) mit Cyclohexan oder die Bildung zusätzlicher hochschmelzender Fractionen in Scale-Ups von Mischungen aus Chloroform und Cyclohexan.

Ein zweiter Ansatz zur Verringerung der Schmelztemperatur von cBT bei der Herstellung von statistischen Copolyestern ist die Ausnutzung einer Schmelzpunkterniedrigung innerhalb der entsprechenden Mischungen. Zu deren Evaluierung wurden drei weitere aromatische makrozyklische Oligomere (MCOs) sowie zwei aliphatische Lactone hergestellt und die Gemische mittels DSC analysiert. Diese Monomere waren cyclisches 1,4-Butylenisophthalat, cBI, cyclisches 1,3-Propylenterephthalat, cPT, und cyclisches 1,3-Propylenisophthalat, cPI, sowie cyclisches 1,4-Butylenadipat, cBA, und cyclisches 1,4-Butylensuccinat, cBS.

Alle Monomere waren zufolge der Abhängigkeit der Schmelz-, Kristallisations- und Glasübergangstemperatur, T_m , T_c und T_g , von der Probenzusammensetzung miteinander mischbar. Die Änderungen, insbesondere der Schmelztemperaturen, waren jedoch gering.

Strukturell ähnliche aromatische Monomere in Kombination mit einem der beiden aliphatischen Monomere führten im Allgemeinen zu einem vergleichbaren Schmelzverhalten. Ein aromatisches Monomer zeigte jeweils mit beiden aliphatischen Monomeren cBA und cBS ein ähnliches Schmelzverhalten, trotz deren unterschiedlichen Schmelztemperaturen (cBS $69\text{ }^\circ\text{C}$, cBA $95\text{ }^\circ\text{C}$) und im Einklang mit den thermodynamischen Grundlagen der Mischungstheorie. Im Allgemeinen wurde für cBA-haltige Gemische eine höhere Schmelzenthalpie, ΔH_m , gefunden, was auf eine höhere Kristallinität hindeutet, sofern von einer ähnlichen molaren Schmelzenthalpie ausgegangen wird.

Die Kristallisation von cBA oder cBS scheint in Anbetracht des Kurvenverlauf von T_c in Abhängigkeit des Monomerverhältnisses mit cPT schlechter zu sein als mit cBT. Dies führt zu einer effektiveren Reduktion der T_m von cPT durch cBA oder cBS als von cBT. Die Länge

des Diols bzw. die gerad- oder ungeradzahlige Anzahl an Methylengruppen im aromatischen MCO beeinflusst offensichtlich entscheidend die Kristallisation bei Monomere mit solch einem kurzen Abstand zwischen den polaren Estergruppen. In Gegenwart von nur aromatischen MCOs wurde für die Mischung cPT/cPI im Vergleich zu cBT/cBI mit einem jeweils nur geradzahligen oder ungeradzahligen Diol eine geringere Reduktion der Schmelztemperatur festgestellt. Dieser Effekt wurde nur durch die Anwesenheit einer Isophthalat-Einheit mit einer Verzerrung der üblichen Zick-Zack-Struktur der kristallisierten Oligomerzyklen überlagert. Eine gehinderte Kristallisation kombiniert mit niedrigeren Schmelztemperaturen war das Ergebnis bei der Mischung von cBI oder cPI mit einem der beiden aliphatischen Monomere.

In den meisten Mischungen wurde eine niedrigschmelzende Fraktion festgestellt, deren Identität noch nicht feststeht. Bei der Kombination von cBT und cPT, den Monomeren mit den höchsten Schmelztemperaturen der reinen Monomere in dieser Arbeit, wird jedoch eine bemerkenswert niedrige Schmelztemperatur beobachtet. Eine kleine Fraktion mit eutektischen Eigenschaften scheint für Mischungen von cBI oder cPI mit cBA mit ihrer höchsten Menge bei etwa äquimolaren Verhältnissen der Monomere gebildet zu werden.

Zusätzlich ist bei allen betrachteten Gemischen von aliphatischen mit aromatischen Monomeren und bei den meisten Kombinationen der aromatischen untereinander eine kurzfristige gehinderte Kristallisation zu beobachten, wie aus der jeweiligen Unterkühlung (Supercooling) ΔT_{sc} und dem Anteil an kristalliner Fraktion (in Form von ΔH_m) zu schließen ist. Ein Isophthaloylrest verstärkt die Hinderung, vermutlich aufgrund von dessen Abweichung von einer linearen Kettenform. Langfristig war bei cBI/cBA-Gemischen jedoch trotz der kurzfristigen Kristallisationshinderung eine ausgeprägte Kristallisation zu beobachten.

Für eine ausgeprägte Unterkühlung ist das Vorhandensein des ungeradzahligen PDOs vorteilhaft, am besten in Kombination mit Isophthalat in einem Monomer (d. h. cPI). Es hat sich jedoch gezeigt, dass selbst das Vorhandensein von PDO und Isophthalat in einer Mischung keine Garantie für ein hohes ΔT_{sc} darstellt.

Ein Einfluss der Kettenlänge auf die Hinderung bei der Kristallisation wurde bei Gemischen der aliphatischen Monomere cBA oder cBS mit cBT oder cPT festgestellt, jedoch nicht mit cBI oder cPI. Die Anwesenheit von Isophthalat ist auch hier, vergleichbar wie beim Schmelzverhalten, dominant, während die Auswirkung der Kettenlänge sekundär ist. Es wurde kein bemerkenswerter Unterschied in der Unterkühlung beim Vergleich von cBS- zu cBA-Gemischen beobachtet. Mischungen von cPT mit einem der aliphatischen Monomer

besitzen jedoch im Vergleich zu solchen mit cBT ein höheres ΔT_{sc} , insbesondere bei einem geringen Anteil von cPT (maximal zwischen 20 und 40 mol-%).

Das Vorhandensein von cBS oder cPT in den Gemischen, also von einem der zwei linearen, kurzkettigen Zyklen (verglichen mit den jeweiligen Alternativen cBA oder cBT bzw. den Isophthalat-Varianten), führte zu einer höheren Kristallinität zwischen zwei aufeinanderfolgenden DSC-Messungen. Die Auswirkung der ungeraden Anzahl von Kohlenstoffatomen im cPT erwies sich als vernachlässigbar für dieses Langzeitverhalten. Dies steht nicht im Einklang mit früheren Berichten, kann aber auf die geringe Entfernung zwischen den polaren Gruppen in dieser Studie zurückzuführen sein.

Ein Glasübergang wurde für alle Monomere und für fast alle Mischungen beobachtet. Ausnahmen waren Kombinationen von cPT mit cBA und solche mit einem sehr hohen cBA-Gehalt. Die Abweichung bei diesen Gemischen kann durch die hohe Kristallinität und durch die Unterschiede in der Kettenflexibilität erklärt werden, die die Kristallisation beeinflussen. Ein freies Volumen, das höher war als durch die FOX-Gleichung berechnet, wurde in Mischungen mit einem alleine leicht kristallisierenden Monomer beobachtet. Dies ist ähnlich zu den beobachteten Bedingungen für die Bildung einer niedrighschmelzenden Fraktion.

Der Anteil an amorpher Phase ist entsprechend der jeweiligen Änderung der spezifischen Wärmekapazität ΔC_p in cBA-Gemischen geringer als in cBS-Gemischen und bei Anwesenheit von Terephthalat kleiner als bei Isophthalat.

Die Kaltkristallisation, ΔH_{cc} , war in cBA-Gemischen maximal bei gleichen Anteilen der Monomere (außer bei denen mit cPT). CBA erleichtert offensichtlich die Reorganisation des jeweiligen zweiten MCOs bei $T_g < T < T_m$.

Ein abweichendes Verhalten hinsichtlich ihres Glasübergangs wurde bei den cBS-Mischungen mit isophthalathaltigen MCOs im Vergleich zu den cBA-Mischungen beobachtet. Ihre T_g s stimmen gut mit der FOX-Gleichung überein und es wurde ein hoher Anteil an amorpher Phase festgestellt, wie durch die oben erwähnte gehinderte Kristallisation zu erwarten war.

CBS-Gemische mit terephthalathaltigen Monomeren zeigen ein höheres freies Volumen als durch die FOX-Gleichung berechnet. Die Menge an amorpher Fraktion nimmt mit zunehmender Menge an aromatischem MCO ab. Nur bei cBT/cBA-Gemischen kommt es zu einer merklichen Kaltkristallisation.

Die Länge des an Isophthalat gebundenen Diols hat nur geringen Einfluss auf den Glasübergang und die Kaltkristallisation. Im Gegensatz dazu beeinflusst die Diollänge im zweiten MCO, sofern dieses Terephthalat beinhaltet, nicht nur die (kalte) Kristallisation signifikant, sondern bestimmt auch die Menge an Glas- und Kristallphase. Ein ähnliches

Verhalten wurde für cBT mit cPI oder cBI und für cPT mit cPI bzw. cBI beobachtet. Ein nahezu konstanter amorpher Anteil (laut ΔC_p) und eine größere kristalline Fraktion wurden mit steigendem cBT-Anteil beobachtet, während eine Erhöhung des cPT-Anteils zu einer Umwandlung der amorphen in eine kristalline Phase führte. In Mischungen von cBI mit cPI wurde nur amorphe Phase mit einem relativ konstantem Anteil beobachtet, wie aufgrund der gehinderten Kristallisation durch die Isophthalatgruppe zu erwartet war.

Der dritte Teil dieser Arbeit befasste sich mit dem Vergleich einer enzymkatalysierten mit einer metallkatalysierten Polykondensation. Der Effekt der niedrigeren Reaktionstemperatur bei der Enzymverwendung war von besonderem Interesse. Die Monomere *Pripol*TM 1012 (Pripol) und 1,3-Propandiol (PDO) wurden für diese Studie ausgewählt. Beide Monomere sind aus nachwachsenden Rohstoffen herstellbar. Diese Studie wurde in Zusammenarbeit mit der Technischen Universität Hamburg durchgeführt.¹ Sowohl die Monomere als auch die Polyester scheinen bei Temperaturen von bis zu 220 °C während der Synthese selbst ohne inerte Atmosphäre stabil zu sein. Strukturell identische lineare Polyester wurden laut GPC-, NMR- und rheologischen Messungen trotz der unterschiedlichen Temperaturprogramme mittels metall-, enzym- und autokatalysierten Reaktionen erhalten.

Ein Molekulargewicht von $M_w = 26.7 \text{ kg} \cdot \text{mol}^{-1}$ (per GPC) wurde durch Enzymkatalyse mit *CalB immo* bei nur 80 °C erhalten. Eine weitere Erhöhung des M_w wäre in einer angemessenen Zeit nur bei einer höheren Temperatur, die nicht von den verwendeten Enzyme toleriert wird, oder mit einem auf die Entfernung des Nebenproduktes Wasser optimierten Reaktor möglich gewesen. Eine Verschiebung der Stöchiometrie musste bei allen Reaktionen vermieden werden, was besonders während der Vorkondensation der langsameren enzymatischen Reaktion entscheidend war. Ein höheres Molekulargewicht von bis zu $M_w = 84.6 \text{ kg} \cdot \text{mol}^{-1}$ war per metallkatalysierte Polykondensation aufgrund der höheren Temperatur und der besseren Destillation des Nebenproduktes zugänglich.

Es konnte ein Polyurethanelastomer aus einem Pripol/PDO-Polyester hergestellt werden, um die allgemeine Verwendbarkeit eines solchen Polyesters für solche Anwendungen zu demonstrieren. Der Polyester musste dabei auf einem gegenüber der metallkatalysierten Polykondensation leicht modifizierten Weg hergestellt werden, um Hydroxylendgruppen der Polymerketten sicherzustellen. Die thermischen und mechanischen Eigenschaften des erhaltenen Polyurethans ähneln denen vergleichbarer Polyurethane aus anderen nachwachsenden Rohstoffen.

3 Introduction and State of Knowledge

The use of plastics has some benefits compared to using “traditional” materials as paper, wood or metal. Especially the unique combination of properties makes plastic interesting like its low weight, versatility, durability, easy processing, e.g. by injection molding, and effective production regarding costs, resources and energy.² The worldwide production of plastics (without fibers) increased from 225 to 348 million tons between 2004 and 2017.^{3–6} In Germany as well as in greater Europe (EU27, United Kingdom, Norway and Suisse), the largest amounts were used in packaging (35 and 40 %, respectively) followed by building and construction (22 and 20 %), automotive (12 and 10 %) and electrical and electronic applications (7 and 6 %) in 2016.^{5,7}

Over the last decades, the importance of sustainable approaches increased considerably. Polymers from renewable resources are evaluated and find their place in industrial applications, among them various polyesters.⁸ Polyesters have some characteristics making them interesting polymers for recycling. Usually, they are used as thermoplastic materials, making a reuse by mechanical recycling realizable. This goes along with an industrial trend of replacing thermoset plastics by thermoplastic ones.⁹ The cleavable ester linkages in polyesters allow a regain of used fabrics in composites, usually the most expensive part of a composite. Hence, polyesters can be an opportunity to reduce the carbon footprint and to lower the overall costs of products at the same time.

Polyesters can effectively be prepared by two polymerization methods, step growth reactions in means of polycondensation of suitable bifunctional monomers or chain growth reactions in terms of ring-opening polymerization (ROP) of the respective cyclic oligomers.

Polycondensation is the well-established process for production of the majority of polyesters in lab and industry.¹⁰ However, it always suffers from the necessity of removing small byproducts as e.g. water or methanol. These byproducts are formed in the reaction and have to be removed from the reaction mixture to shift the reaction equilibrium to the products. The reaction equilibrium constant for aliphatic polyesters is in the range of 1 to 10.¹¹ Hence, elevated temperature and reduced pressure are usually necessary.

Over the years, a high number of different monomers for polyesters from renewable resources have been evaluated to improve the sustainability of this route. The comparatively simple reaction settings facilitate the use of a vast range of raw materials. The evaluation of polymers therefrom is still going on in most cases with respect to their suitability for industrial application.

ROP on the other hand has features making this method in a number of fields superior to polycondensation, especially for applications like composite preparation. By ROP, a higher degree of polymerization (DP) is possible¹² with comparable or even lower polydispersity^{12–15} in a much shorter reaction time (minutes instead of hours).^{16–18} For example, ROP with titanium catalysts is up to 10 times faster than a comparable polycondensation.^{19,20} A polymerization with a titanium or tin catalyst at 190 °C is possible in 3-5 min.²⁰

Furthermore, the ROP process is generally environmentally more friendly than polycondensation:¹²

- In ROP, in contrast to polycondensation, no build-up of small by-products takes place, which have to be separated from the reaction mass with some effort. This additionally eliminates the restraints of polycondensation reactions caused by mass-transport-limitations.
- Little or no heat is produced as long as cyclic monomers without or with only very little strain are used.¹² This makes isothermal processing possible and therefore expensive and time-consuming heating and cooling cycles gratuitous. This is obviously preferred by industry, especially if the resulting polymer crystallizes fast, as in the case of Poly(1,4-butylene terephthalate), PBT, allowing short cycles.²¹
- ROP can often be carried out in bulk without any mixing after a first initial homogenous distribution of a catalyst, making utilization of a solvent or stirrer for the polymerization obsolete.¹²
- The monomers of ROP are automatically in perfect stoichiometric balance of the respective functional groups, so that this problem of most polycondensation reactions is avoided (especially in small-scale reactions).¹²
- The molecular weight of the product polyester can be readily adjusted by ROP by adding the respective amounts of suitable chain transfer agents.²²

The viscosity of molten cyclic monomers is usually water-like (e.g. about 36 mPa·s at 190 °C in case of cyclic 1,4-butylene terephthalate (cBT) to obtain PBT)^{19,23,24}. This low viscosity and thus its effectiveness in impregnating combined with the properties mentioned above make the preparation of polyester by ROP highly interesting for reactive injection molding towards thermoplastic products.^{22,25,26} Besides, interesting results have been gained for the manufacture of composites with numerous fillers from e.g. clay²⁷ or silica²⁸ over graphene²⁹ to carbon nanotubes³⁰.

Aromatic polyesters are one often-employed group of polymers because of their high service temperature of about 200 °C. PBT is one of these. It has a good heat resistance, a

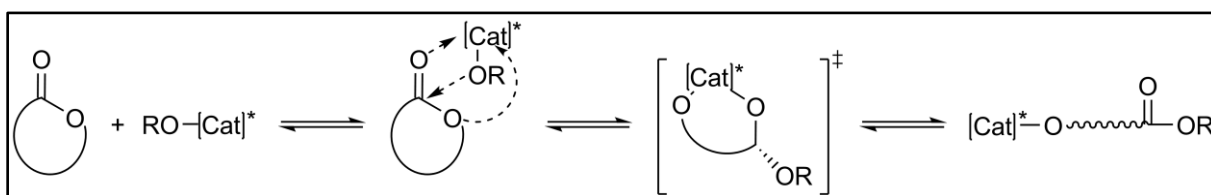
high dimensional stability, stiffness and good insulating properties, even at high temperatures or in presence of water.³¹

PBT is semicrystalline and processible by injection molding, which makes this its main processing method as molding material and resin.^{24,31,32} Most of its applications are in the fields of electrical or electronic appliances and of automotive (including auto electronics).³¹ In 2012, 830 000 t of PBT were consumed worldwide (including blends) and an increase of the demand to 1 650 000 t is expected until 2025.³¹ PBT profits e.g. in automotive from a growing orientation towards safety, efficiency and comfort, opening applications for PBT in parts of reversing cameras, trunk opening or in battery-powered vehicles with their bearings, housings or bezels and the additional sensors, connectors and connector strips, control units or charging plugs.^{31,33}

Additionally, PBT is used in blends with other polyesters like poly(1,2-ethylene terephthalate), PET, or with other polymers such as polycarbonate or acrylonitrile styrene acrylate.³¹ Its compounds are high-performance materials with application of several fillers, reinforcing materials and additive compounds enabling to tailor its properties for different applications.³⁴

3.1 ROP of cyclic polyester oligomers

3.1.1 Mechanistic aspects of metal-catalyzed ROP



Scheme 1: Catalyzed ring-opening polymerization (with R being the moiety of an alkoxide or of the polymer chain).

ROP of lactones usually has to be catalyzed. This is accomplished in very most cases by metal complexes (like titanium(IV) 1-butanolate ($\text{Ti}(\text{O}n\text{Bu})_4$), titanium(IV) 2-isopropylate ($\text{Ti}(\text{O}i\text{Pr})_4$), di-1-butyltin(IV) oxide (Bu_2SnO), tin(II) 2-ethylhexanoate ($\text{Sn}(\text{Oct})_2$), stannoxane etc.)^{13,35–40} or by lipase enzymes¹². In some cases, catalysis by organic bases is possible, too. BRØNSTEDT acids (in a reasonable catalytic concentration) only react with chain ends,

not with inner ester groups.²⁴ The following chapters mainly deal with the most common ROP by metal catalysis.

Metal-catalyzed ROP proceeds by a coordination-insertion mechanism, basically according to the one TEYSSIÉ *et al.* published originally for the ROP of ϵ -caprolactone with various aluminum(III) alcoholates and is schematically summarized in Scheme 1.⁴¹ Many detailed examinations of the ROP mechanism in bulk polymerizations have been carried out by DAHLMANN, KRICHELDORF and more.^{13,42–48} However, most studies deal with aliphatic lactones, especially ϵ -caprolactone and L,L- as well as D,L-dilactids, but a transfer of the findings to aromatic systems is generally made because of the great structural similarity of the participating groups. It was shown at least for some aluminum catalysts that the carbonyl oxygen atom of an ester group is coordinated by an empty orbital of the active catalyst, possessing at least one alkoxide-metal bond, which is basically a LEWIS acid activation of the carbonyl group.⁴⁹ Afterwards, the alkoxide from the ester bonds to the metal atom while the alkoxide from the metal is transferred to the former carboxyl carbon atom of the ester supposing a transient orthoester of the metal. This transfer of the alkoxide part of the internal ester of a cycle to the metal results in the formation of a chain or in its growth, if the initial alkoxide (“OR”) at the metal is already an oligo- or polymer chain.¹³

The exchange of the alkoxide group was found to be fast (for tin compounds).⁵⁰ For some catalysts as Sn(Oct)₂ or antimony(III) oxide, an initiation step must take place in which the active alkoxide-metal bond is obtained.^{42,44,51} If there is more than one alkoxide ligand at a metal, potentially every bond can react in the described way, but not all at the same time.¹³ A surprising difference in activity of catalysts with the same central atom, as e.g. Ti(O*i*Pr)₄ and Ti(O*n*Bu)₄, suggests a remaining of at least one alkoxide on the metal atom or an unresolved and significantly less likely high influence of the alkoxide end group of a chain on its growth at the distanced catalyst during ROP in bulk.⁵²

From a thermodynamic perspective, entropy is the main driving force for ROP. Only with strained rings (mainly with less than 14 ring atoms), enthalpy makes up a noticeable contribution.⁵³ The entropy involved can be distinguished in: the translational entropy, especially present in diluted systems, and the conformational entropy, dominant in the polymeric species, if only few conformations of the lactones are possible, which are not affected by the degree of dilution.¹² ROP of large lactones without ring strain as of most aromatic cyclic esters is in most cases an entropy-driven ROP (ED-ROP).^{19,54,55}

There is always an equilibrium between ring-opening and ring-closing in case of polyesters as there is in every other reversible entropy-driven reaction. Therefore, usually more than

70 % of the material are cycles when polymerization is carried out in high dilution, in some cases even more than 90 %, while only about 2 % are cycles in bulk polymerizations.⁵³ Besides, generally a higher amount of cycles is to be expected at higher conversions. (This equilibrium is further discussed in chapter 3.2, p.18 ff.)

Several kinetic studies of ROP of cBT have been carried out. The reaction equations, the rate constants for polymerization initiation and propagation steps and the corresponding activation energy have been determined for the reaction of cBT in bulk. Their relevance for this thesis is limited, so they are just mentioned briefly here. They comprise studies

- of changes in the DP by Gel permeation chromatography (GPC) in chloroform(CHCl_3)/1,1,1,3,3,3-hexafluoroisopropanol (HFIP) mixtures,⁵⁶ whose results have to be considered carefully because of the quick changes during ROP,⁵⁷
- of changes in light transmittance,³⁸
- by multiwave oscillation rheology at different temperatures from 220 to 250 °C,⁵⁷
- by dielectric analysis utilizing changes of the ionic conductivity by transformation of liquid monomer to solid polymer (although the relationship between the molecular structure and the macroscopic dielectric behavior is not disclosed completely)^{58,59} and
- by using an ultrasonic technique evaluating the time or temperature evolution of ultrasonic velocity and attenuation.⁶⁰

3.1.2 Preparation of aromatic polyesters by ROP

Some prominent examples for ROP of aliphatic monomers have been mentioned in the previous chapter in context of the mechanistic aspects of ROP. They mainly deal with ϵ -caprolactone and dilactides. Recently, some attention was additionally drawn to ROP of cyclic butylene succinate as well.^{61,62} High M_n of 100 000 $\text{g} \cdot \text{mol}^{-1}$ and more were reported for ROPs of various aliphatic lactones and various catalysts.^{12,63,64} Such high molecular weights are rarely reported for synthesis by polycondensation and only if some additional effort concerning vacuum and catalysts etc. is made, especially if the low PDI of 1.5 to 2.6 in ROP reactions has to be obtained as well.^{61,65–67} However, the preparation of aliphatic polyesters has mainly been of interest for determination of mechanical details because of their low melting and glass transition temperatures (T_m and T_g), and the resulting limited number of applications is limited (some polycaprolactone, polylactides etc. excepted).²⁴

ROP of aromatic lactones is more challenging than of aliphatic monomers. The lactones as well as the polymers generally exhibit higher melting temperatures and a lower solubility. The rapid crystallization of many partly aromatic polyesters makes processing further challenging and limits the diffusion of unreacted monomeric material significantly.¹² There are a number of publications on the polymerization of partly or completely aromatic lactones, not limited to ROP of cBT. For example, the ROP of cyclic 1,2-ethylene isophthalate (cEI) was conducted by YODA *et al.* as early as 1968.⁶⁸ They polymerized cEI even without complete melting of the monomer at a temperature above 265 °C (melting point 327 °C). At 270 to 290 °C, MONVISADE *et al.* obtained a *DP* of 20-55 with 3 mol% Bu₂SnO in 8 to 12 hours.⁶⁹ CET, which is closely related to cBT, has been polymerized at 285 °C in 10 min with a *DP* of 80 by Burch *et al.* in 2000.⁷⁰ Less common polymers as poly(ethylene 2,6-naphthalenedicarboxylate) (PEN) and poly(butylene 2,6-naphthalenedicarboxylate) (PBN) have been prepared by ROP catalyzed by Bu₂SnO or Ti(O*i*Pr)₄, as well.³⁶ However, the following paragraphs summarize publications related to ROP of cBT as this monomer is of central importance in this thesis.

The structure of PBT by ROP of cBT is generally the same as of PBT by polycondensation.⁵⁶ PBT prepared by ROP however exhibits a higher crystallinity than PBT by polycondensation resulting in more brittle products.^{19,56,71–75} PBT by polycondensation is reported in literature to have a heat of fusion of about 35 – 50 J·g⁻¹,²⁴ while that of polymerized cBT is circa 55 – 70 J·g⁻¹ as measured by ISHAK, KARGER-KOSCIS *et al.*⁵⁵ and during the experimental part of this work. Besides, ring-opened PBT was found to possess a very high nucleation density.⁷⁶ As in most ROPs of lactones, the completeness of ROP of aromatic cyclic esters is dependent:²⁴

- on the purity of the lactones
- on their complete mixture with the initiator before the increase of viscosity during polymerization prohibits any further mixing and
- on a polymerization rate high enough to forestall freezing of the reaction by crystallization of monomers or polymers at $T < T_m$.

Polymerization and crystallization happen simultaneously in ROP as long as the temperature is below the melting temperature of PBT (below about 225 °C).⁷⁷ Polymerizing below that temperature has not only successfully been accomplished but is even generally advantageous. Thermal cycling of the machinery, e.g., can be avoided by exploiting the simultaneous polymerization and crystallization of the polymer, which allows production cost saving.⁷⁸

A difference in crystallization was found for PBT prepared by ROP below and above 200 °C irrespective of catalysts (with cBT with a melting temperature between 115 and 200 °C in

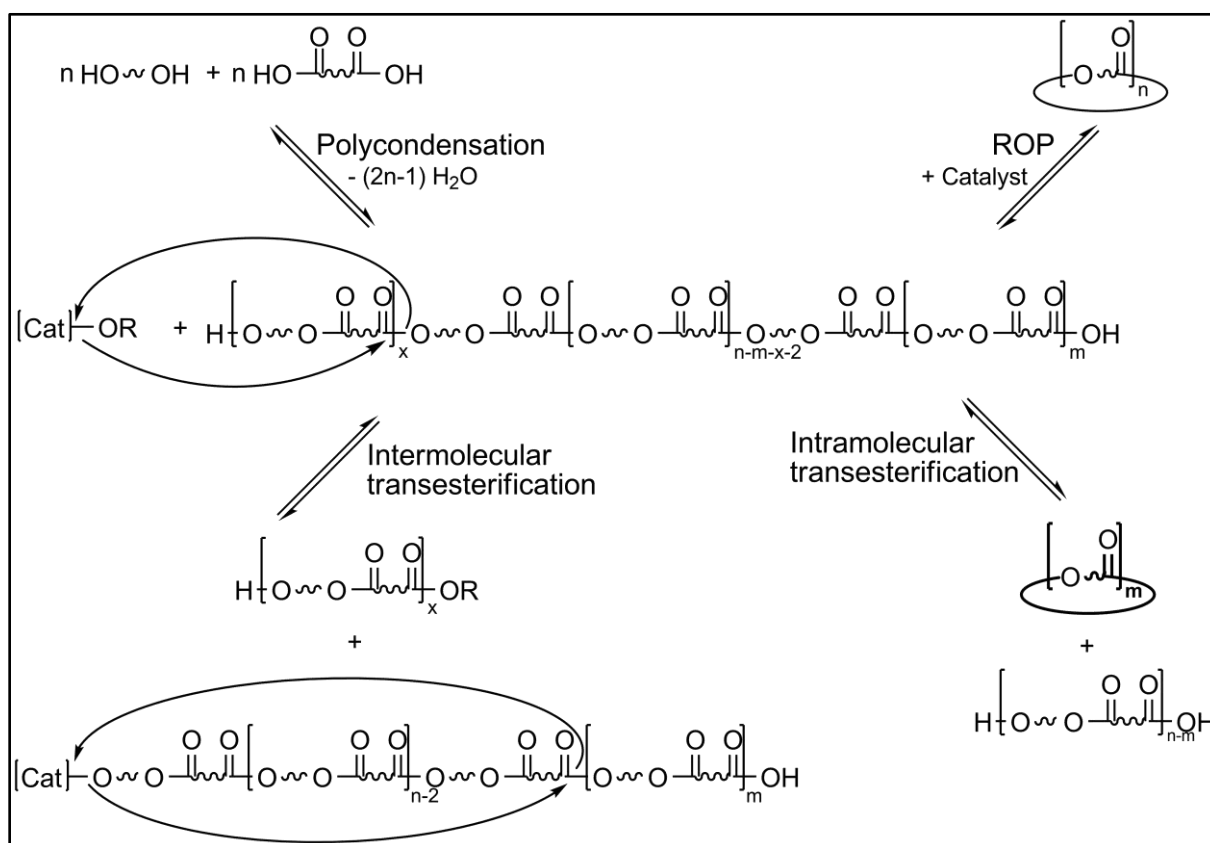
literature).^{19,21,24,55,79–83} An increase in crystallinity was observed with an increase of polymerization temperature with butyltin(IV) chloride dihydroxide ($\text{BuSnCl}(\text{OH})_2$) as catalysts, but the contrary was seen with stannoxane and titanium(IV) 2-ethylhexanoate ($\text{Ti}(\text{Oct})_4$) by MACKNIGHT, WINTER *et al.* in 2005.³⁸ Crystallization was faster with stannoxane than with $\text{Ti}(\text{Oct})_4$. An “unusual type” of spherulites was noticed in polymerization at low temperature with catalysis by $\text{BuSnCl}(\text{OH})_2$ and $\text{Ti}(\text{Oct})_4$ compared to the “usual type” at higher crystallization temperature. The lower the temperature, the number average molecular weight (M_n) or the conversion, the faster was crystallization and the larger the defects in crystallinity.³⁸ These findings are in good agreement with those of KARGER-KOCSIS *et al.*²¹ and WU *et al.*⁷⁶ The latter observed highly disordered spherulitic crystallites in ROPs below 200 °C, whose fraction became more prominent, while the fraction of three-dimensional spherulitic morphology decreased. No general dependence of the achieved M_n or the polydispersity index (*PDI*) on the softening temperature of the polymer was observable in the exploration of ROP by the three different catalysts at temperatures between 185 and 205 °C by MACKNIGHT, WINTER *et al.*³⁸ Polymers were obtained with the different catalysts with a similar M_n (between 30 and 60 $\text{kg} \cdot \text{mol}^{-1}$) and a *PDI* of about 2.6 as well as a comparable glass transition and melting temperature. The choice of catalyst did however have a significant effect on monomer conversion, induction time and the required polymerization time.

At the beginning of the commercial exploration of cBT at *General Electric*, researchers overcame some difficulties with polymerization of cBT at temperatures below 200 °C by initially treating it with silica as BRUNELLE reported in a review in 2008.²⁰ By this procedure, the slow and incomplete polymerization at a temperature between 190 and 200 °C caused by the presence of carboxylic acid groups and anhydrides has been significantly improved. Successful ROPs of cBT at a temperature of about 190 °C were published by BRUNELLE *et al.* in 1998, too.¹⁹

KARGER-KOCSIS *et al.* found in their investigations that generally the same conversions are possible for ROP at 150 °C and 190 °C, only in a longer time (according to viscosity).⁵⁵ They conducted polymerization of cBT at temperatures down to 145 °C. Between 145 and 160 °C, they faced incomplete melting of the monomer and further an overlapping of melting and polymerization peak in measurements by differential scanning calorimetry (DSC).²¹ Their results comprise the successful polymerization at comparatively low temperatures and the possibility of annealing of the product. However, it should be considered that rather varying values (between 115 and 200 °C) are given for the melting temperatures of cBT.^{19,21,24,55,79–83}

WANG, GU *et al.* polymerized cBT with a reduced melting temperature at 190 °C. This cBT was prepared accordingly to a patent by PHELPS at *Cyclics Corporation* from 2004 (see chapter 3.3, p. 26 ff.). PBT with enhanced toughness and elongation at break was obtained in these explorations.⁵⁴ Evidence for not completely molten cBT was found, if standard monomer was polymerized, which acted as “heterogeneous” nucleating agent (in monomeric state), while the cBT composition with a lower melting temperature melted completely. They concluded that the unmolten cBT residues were stress concentration points and thus led to a higher brittleness. A reduction in polymerization rate of the “normally”-melting cBT was suggested additionally, caused by the crystallizing of converted cBT.

3.2 Macrocyclic oligomers (MCOs)



Scheme 2: Inter- and intramolecular transesterifications in polycondensation and ROP (R represents any alkyl moiety).

In polyesters, there is always an equilibrium between linear and cyclic chains, whether or not a catalyst is present and irrespective of whether the polymer was prepared by step-

growth or by chain-growth reaction. Especially in case of aromatic polyesters with their stiff aromatic building blocks, the formation of macrocyclic oligomers (MCOs) is common. The fraction of MCOs in bulk is usually only about 0.5 – 5 wt-% of the polymer depending on the type of polyester and its preparation process.^{21,24,84} In contrary, almost only MCOs are present in highly diluted systems (of below 3 % (w/v)).¹²

Routes towards cyclic esters by catalysis are more common and of interest for this study, mostly due to their higher reaction rate (Scheme 2). A catalyst can react with an existing polymer chain following the pattern described for ROP via the same transition state (compare to chapter 3.1.1, p. 13f). As soon as a polymer chain is bonded at the catalyst, mainly with a metal center, reaction can take place in an intermolecular transesterification with another chain or an intramolecular transesterification. In the first, a part of the polymer is exchanged with the alkoxide of the catalyst (not presented in detail in Scheme 2, see also chapter 3.1.1). The latter, intramolecular transesterification (backbiting), leads to a cycle with m repetition units and a chain remaining bonded to the metal with a length decreased by m repetition units.

The formation of MCOs has been verified for many lactones by KRICHELDORF *et al.*¹³ They observed smaller M_n by viscometry and vapor pressure osmometry, as it had been expected according to their end group analysis with ¹H NMR spectroscopy.

Most cyclic esters are formed as families of cycles of different sizes, each cycle possessing individual physical properties, which is especially true for aromatic esters.^{51,85–88} The formation of very small and very large cycles is statistically unlikely.^{89,90} It was noted that often at least about 95 % of the cycles have 100 ring atoms at maximum but more than 300 are possible, too.⁵³ It has been noticed at the end of the last century that at the begin of a reaction cycles are mostly created for statistical reasons, while smaller cycles are entropically preferred and build up during the further reaction progress (as long as no ring-strain is present).⁹¹ Additionally, the surplus of smaller rings at the end is caused by the statistically much more likely attack of the catalyst at an interior than at a terminal ester group, especially when the polymer chains become longer.²⁴

Catalysts, especially on basis of metals, show different activity for intramolecular transesterification. KRICHELDORF *et al.* observed the following increase in activity for cycle formation between catalysts: aluminium(III) 2-propanolate ($\text{Al}(\text{O}i\text{Pr})_3$) (almost no transesterification), zirconium(IV) *n*-propanolate ($\text{Zr}(\text{O}n\text{Pr})_4$), $\text{Ti}(\text{O}n\text{Bu})_4$, tributyltin(IV) methanolate (Bu_3SnOMe), dibutyltin(IV) dimethanolate ($\text{Bu}_2\text{Sn}(\text{OMe})_2$).¹³

The presence of cycles is not accounted for in the CAROTHERS equation, which describes the general relation between DP and reaction progress in dependence of the stoichiometric

ratio for step growth reactions. A first theoretical approach for the description of the ring-chain-equilibrium in AA/BB polyester systems including the ring-chain equilibrium have been made and experimentally proven for poly(1,10-decamethylene adipate) by JACOBSON and STOCKMAYER^{89,90} in 1950. They developed expressions for number and weight average of the DP of chains and cycles, for the weight fraction of rings, and they calculated different ring size distributions for thermodynamically and kinetically prepared MCO compositions. They pointed out that while the size of thermodynamically obtained MCOs decline with $DP^{5/2}$, the size depends on $DP^{3/2}$ for those from kinetical control.⁹² Besides, they have shown the average molecular weight of the cycles to be smaller than those of the chains and that below a critical concentration of monomer (in high dilution) only cycles are formed.

The last observation had already been applied to the synthesis of macrocycles in form of the *RUGGLI-ZIEGLER dilution principle* as early as 1912 and 1934, respectively.^{93–95} The principle's quintessence is the finding that lower concentration of reagents leads to a higher amount of cyclic molecules and a lower DP . This concept represents the principal basis for all MCO preparation methods as described below (chapter 3.2.1 Accessibility of MCOs of polyesters).

A deeper insight into the conditions under which and the ways of how cycles are formed was gained by the calculations of STEPTO *et al.* (also for irreversible step growth reactions)^{96,97} and the correlations of GORDON and TEMPLE.^{98,99} The latter two calculated kinetic schemes of step growth reactions with the assumption of a continuous competition between cyclization and chain-growth during the whole polymerization. Their findings agree well with those of the *RUGGLI-ZIEGLER dilution principle*, i.e. the increase in the MCOs' fraction with dilution. They supplemented the principle by the prediction of an increase of the MCO fraction with conversion. A summary including new strategies for synthesis of cyclic oligomers and polymers has been composed by KRICHELDORF in 2010.⁹²

3.2.1 Accessibility of MCOs of polyesters

A key issue of utilization ROP for polyester preparation is the accessibility of suitable cyclic monomers, which are usually MCOs of the corresponding polymer. The following chapter only deals with the preparation of polyester lactones due to the topic of this work, although interesting results have as well been published for e.g. ROP of amides^{100–104}, olefins (in metathesis)^{105–113} or ether ketones^{114–119}.

A few polyester-based MCOs are commercially available. These are mostly aliphatic. A comprehensive list of commercial aliphatic lactones and of those readily prepared from commercial products has recently been listed by HODGE.¹² Examples besides the commonly known ϵ -caprolactone or D-, L- or D,L-lactide are ω -pentadecalactone^{12,120} or α -, β -, and γ -cyclodextrins¹². The only aromatic MCO commercially available was cBT, which can be polymerized to PBT and which was sold by *IQ Tec*, the successor of a *GE* spin-off enterprise, until 2016.¹²¹

There have been a number of publications on the preparation of very different MCOs in the last hundred years. Some of these are applicable to preparation of aromatic MCOs as well. The following chapters are focused on these. First isolation of aromatic MCOs was realized by their extraction from the corresponding polyester (chapter 3.2.1.1). The yield of this method is generally low due to the very low amounts of cycles (< 5 %). A more efficient preparation is possible by cyclo-depolymerization (CDP) in bulk or in dilution (chapter 3.2.1.2), p. 22 ff.) or by chemical synthesis (chapter 3.2.1.3, p. 25 f.). In CDP, an existing polymer chain is transformed partly or completely into MCOs by intramolecular backbiting. In chemical synthesis, the MCOs are separately built up from usually chemically reactive precursors like, in the case of polyesters, mostly acid chlorides or esters.

3.2.1.1 Extraction

The first reported isolation of an aromatic MCO was that of the cyclic 1,2-ethylene terephthalate (cET) trimer from a PET film at DuPont in 1945.¹²² The extraction was repeated for the cET di-, tri-, and tetramer (in low yields of 1.3 – 1.7 wt-%) and supplemented by its polymerization by GOODMAN *et al.* 1960.⁵¹

Extraction of cycles from polyesters of terephthalic acid and 1,2-ethanediol (EDO), 1,3-propanediol (PDO) and 1,4-butanediol (BDO) with dichloromethane or a mixture of dichloromethane and ethanol (40 and 60 wt-%, respectively,) was realized as well.⁸⁸ The respective MCO compositions were reported to consist in the case of PET mainly of trimers and in those of poly(1,3-propylene terephthalate) (PPT) and PBT surprisingly of dimers.

The number of MCOs extracted from partly aromatic polyesters was further extended by WICK and ZEITLER in 1983.⁸⁷ They used polyesters of not only terephthalic but phthalic and isophthalic acid as well, combined with different alkyl diols. All reports have in common the small quantities of cyclic compounds isolated from the polymers, which diminishes the attractiveness of this route for a preparative purpose.

3.2.1.2 Cyclo-depolymerization (CDP)

CDP uses the thermodynamically controlled equilibrium between polymer chain and MCOs to depolymerize an existing polymer to MCOs. Its principles have already been mentioned above (introduction of chapter 3.2). Strategies for CDP differ depending on whether it is carried out in bulk or in dilution. CDP is however usually catalyzed in both cases, mostly by alkoxide metal complexes as named above for catalysis of ROP or transesterification. Especially titanium(IV) alkoxides or dibutyl tin alkoxides have found to be very efficient catalysts, so far.²⁴

The fraction of MCOs in dilution is significantly higher than in bulk. Actually, at concentrations below 3 % (w/v) the equilibrium is clearly on the side of MCOs while in bulk usually less than 2 wt-% are MCOs.¹² In dilution, the intramolecular CDP leading to cycles is firstly statistically much more favored than the intermolecular transesterification and is secondly driven by the gain in entropy. This is in agreement with both the *RUGGLI-ZIEGLER dilution principle*⁹³⁻⁹⁵ and the findings of STEPTO *et al.*^{96,97} and of GORDON and TEMPLE^{98,99} cited above.

3.2.1.2.1 CDP in bulk with isolation of MCOs by distillation

The preparation of MCOs in bulk is only effectively possible if they are distilled off during the process because the equilibrium lies heavily on the side of the polymer chain (usually 95-99 wt-% are linear).¹² Therefore, only volatile MCOs can be prepared by this route. Hence, mostly aliphatic MCOs are accessible via CDP in bulk. Aromatic or partly aromatic MCOs are usually not distillable at a temperature below the degradation temperature even at ultra-high vacuum (judging from the respective melting temperatures).^{36,69,123-129}

CAROTHERS, mostly accompanied by SPANAGEL, prepared over 40 aliphatic MCOs in the 1930s with yields of raw distillate between 30 and 85 %.^{35,130-133} In contrast, there are few examples of aromatic MCOs isolated by depolymerization in bulk reactions. The first publication was on the cyclic dimer of poly(1,2-ethylene isophthalate) by BERR at DuPont in 1955. It was isolated as crystalline sublimate during polycondensation in 10 to 15 % yield in respect to the theoretically possible polymer, but not utilized or characterized any further.¹³⁴

Phthalate macrocycles with EDO, 1,5-pentanediol, 1,6-hexanediol or triethylene glycol as alcohol component have been isolated by CDP in bulk combined with distillation by EHRHART in 1968.¹³⁵ The MCOs were distilled off together with the excess of respective diol in very different yields at high vacuum and temperature. 3.6 wt-% Ti(*On*Bu)₄ or tin(IV) oxalate were utilized as catalyst.

CBT oligomers, mainly the cyclic dimer, were identified for the first time at a source for mass spectrometry (MS) with electron impact ionisation.^{88,136} At 200 °C, first oligomers were observed, at 330 °C, a sudden thermal decomposition took place freeing mainly cyclic dimer and at 380 °C, mainly larger cyclic oligomers were present. Similarly, the pure cET dimer was collected at the surroundings of processing equipment for PET by NAGAHATA in 2000.¹³⁷

This route has mostly been disregarded because of the generally limited numbers and quantities of aromatic MCOs accessible combined with the high demands on the equipment, despite the high product purity obtainable by CDP in bulk with distillation.

3.2.1.2.2 CDP in dilution

CDP in dilution is usually carried out by refluxing or heating the respective polymer in a suitable, high-boiling solvent in a concentration of 2 % (w/v) or less. As catalyst, tin complexes are common as they convert the polymer fast and are not too water sensitive. However, they are not readily quenchable and have to be removed after CDP for avoiding unintentional ROP. The other commonly used catalysts are based on titanium and are quenchable by hydrolysis which, on the other hand, makes strictly anhydrous conditions during CDP necessary. Other metal complexes, on basis of e.g. antimony have been explored as well.⁷⁰

The conversion of polymer to MCOs is generally substantially higher than that in CDP in bulk with a yield of up to 85 %. On the other hand, CDP in dilution is paired with high amounts of solvent, with the necessity of separating the MCOs from the usually high-boiling solvent as well as from polymeric and oligomeric linear species.¹² Additionally, a relatively long reaction time has been reported with values between 30 min (for a few reactions utilizing tin or titanium catalyst) to 8 d, most being between 1 and 4 d.^{24,138–141}

It has been shown that the solubility of the polymer in the solvent used for CDP is crucial as the rate of depolymerization is depressed in case of not complete solubility.^{24,70} The dilution ratio of the solvent itself alters the ratio of the different oligomers being formed during CDP, which has been reported for PET.¹¹⁶ The temperature during CDP has no influence on the depolymerization rate or the ratio of the cyclic oligomers formed above a threshold, as investigated by BRUNELLE *et al.* for cBT.²⁴

Different solvents have been successfully applied for CDP of different partly aromatic polyesters. Mostly aromatic and halogenated solvents are used, particularly 1,2-dichlorobenzene (oDCB) has been employed widely. Further solvents in publications are 1,2-xylol or 1-methylnaphthalene, e.g.

BRUNELLE *et al.* from *Cyclics Corporation* patented the CDP 1995 and 1997.^{20,138,139,142} The depolymerization of PBT, PET and poly(1,2-ethylene 2,6-naphthalene dicarboxylate) was herein emphasized in diluted solutions of less than 0.3 M (in respect to the structural units) with yields of 33 – 90 %. They were carried out in the aromatic solvents 1,2-xylene, chlorobenzene, naphthalene, toluene, tetramethylbenzene, methylnaphthalene, oDCB and their mixtures, with 1 – 5 mol-% tin or titanium complexes as catalysts (Bu_2SnO or $(\text{Ti}(\text{O}i\text{Pr})_4$, e.g.) and with heating to a temperature of 140 to 280 °C. Preferentially, the depolymerization was carried out in a plug-flow tube reactor.¹³⁹ Interestingly, they found the molar concentration of cycles in solution to be the same (about $0.05 \text{ mol} \cdot \text{L}^{-1}$) for every experiment, except for very low concentration, where the presence of end-groups limited the number of cycles formed.²⁰

In 1997 SEMLYEN *et al.* prepared cBT by CDP in oDCB in yields of up to 70 %. They admittedly diluted the PBT by a relatively high ratio of 1.4 % (w/v) and used relatively long reaction times of 72 h.¹¹⁶

Furthermore SEMLYEN *et al.* published CDPs of PET in 1-methylnaphthalene in different dilution ratios of 3 or 10 wt-% with different catalysts in 24 h reaction time.¹⁴³ The highest yield of 30 wt-% cET was obtained in higher dilution – in accordance with the theories cited before^{89,90,93–99} – and with zinc(II) acetate as catalyst. The presence of a second cyclic oligomer species with ether defects was noticed in these experiments.

HODGE *et al.* published the preparation of various cyclic alkylidene isophthalates via CDP in polymer solutions of 1 – 2 % (w/v) in oDCB or chlorobenzene with Bu_2SnO as catalyst in 2000.¹⁴⁴ After 12 h, an almost maximal yield was observed, but not a thermodynamically equilibrated system, which was only seen after up to 10 d of reflux (monitored by gel permeation chromatography (GPC) in chloroform). The formation of cyclic diol/diacid adducts occurred for cycles smaller than 16 ring atoms with a yield close to 90 % and for larger cycles with a yield of about 72 %. The working group around HODGE prepared cyclic 1,2-ethylene naphthalene-2,6-dicarboxylate by a comparable method in yields of up to 93 % from solutions of its corresponding polymer in oDCB.¹⁴⁵

CDP in dilution can be discriminated in CDP in solution and CDP in suspension, but the differentiation is vague. The general principles of RUGGLI, ZIEGLER, STEPTO, GORDON, TEMPLE *et al.*^{93–99}, summarized above, apply in both cases, although there tend to be differences in the properties of the resulting MCO compositions. BURCH *et al.* at *DuPont* investigated the effect of the solubility on CDP and discovered a dependency on the cycle distribution and hence on the melting temperature of the resulting MCO composition.⁷⁰ They depolymerized different partly aromatic polyesters in diphenylether solution as well as in

suspension with saturated hydrocarbons as hexadecane. CDP in solution led to a kinetic distribution of ring sizes because of the high dilution of the cycles and hence to broadly distributed ring sizes (in accordance with the theory of JACOBSON and STOCKMAYER^{89,90}). They showed a lower melting temperature of the MCOs. CDP in suspension was thermodynamical controlled and resulted in a narrow distribution with a higher melting temperature.

After findings of enrichment of cET oligomers in supercritical fluids, especially in supercritical carbon dioxide (scCO₂),^{146,147} the CDP of PBT and extraction of the resulting cBT by supercritical fluids was established by WEIJERS *et al.* in 2006.¹⁴⁸ Fast cycle formation and solvation was observed at comparatively high temperatures and pressures of 230 °C and 250 bar, while the mass transfer of the loaded supercritical phase was rate determining. Supercritical pentane showed an even higher solubility power for cBT in that study.

3.2.1.3 Chemical synthesis

Most strategies for chemical synthesis of MCOs are kinetically controlled reactions. First chemical synthesis of MCOs was carried out by ZAHN *et al.* and REPIN and PAPANIKOLAOU (with assistance by ZAHN).^{85,149–151} CET and cBT oligomers were prepared by reaction of the respective dicarboxylic acid chlorides with the respective diol or by the reaction of respective linear oligomers of diacid chloride and diol in very high dilution of less than 0.005 M, often less than 0.001 M, of repeating units in benzene or oDCB. The reaction took up to 8 d of reflux with *N,N*-dimethylaniline or magnesium powder as catalyst.

Avoiding diacid chlorides, BURCH *et al.* at *DuPont* established the synthesis of various MCOs from the dihydroxy alkyl esters of the aromatic acids in 2000.⁷⁰ The respective dihydroxy alkyl ester was heated in a solution of up to 0.1 M in hexadecane together with a titanium(IV) or aluminum(III) alkoxide catalyst while solvent and the correspondent glycol by-product were distilled off. Besides, some MCOs (terephthalic or isophthalic acid with neopentyl glycol) were prepared by reacting the respective dimethyl ester with the diol. The adaptability of this method to continuous process was emphasized.

A different approach of transesterification to avoid diacid chlorides was made by NAGAHATA *et al.* by reacting a diacid glycol with a dimethyl ester.¹⁵² The dimer of cyclic 1,2-ethylene isophthalate was prepared from ethylene glycol diacetate and dimethyl isophthalate in cyclohexane with sodium ethanolate. Formed methyl acetate was distilled off azeotropically. The reaction did only work with strictly dried solvents and reagents.

Researchers at *General Electric* developed an effective pseudo-high dilution synthesis, in which the corresponding reactive species are present in only very low concentrations while

the product MCOs enrich in the solution. Multi-kilogram scales and final MCO concentrations as high as 0.5 M have been realized via this route.^{12,153}

First attempts were patented with the simultaneous addition of Bisphenol A (in slight excess of 3 – 5 mol-%) and terephthaloyl or isophthaloyl chloride solutions to a solution of octadecyltrimethylammonium chloride. It led to final MCO concentrations of about 0.3 M.¹⁵⁴

An alkaline mediated pseudo-high dilution synthesis of aromatic carbonate MCOs from bisphenol A bis(chloroformate) in a two-phase system of aqueous sodium hydroxide and dichloromethane was published by BRUNELLE *et al.* at *General Electric* in 1991.¹⁵⁵ Reaction took place at 0 or about 40 °C, depending on the target cycle, with catalytic amounts of trimethylamine or 4-(dimethylamino)pyridine (DMAP) present.

Pseudo-high dilution synthesis was adapted to give cyclic oligomers of polyester and patented in the following years.^{156,157} Carboxyl diacid chlorides and diols or bis(hydroxyalkyl) ester were continuously dosed to a solution containing stoichiometric amounts of base like triethylamine and catalytic amounts of an unhindered amine like 1,4-diazabicyclo[2.2.2]octane (DABCO) (2 – 5 %) or quinuclidine. Amines, especially unhindered ones, do not only act as proton acceptor, but also as a nucleophilic catalyst. MCOs of ten different polyesters were synthesized with a yield of 49 – 85 %, respectively, within hours at maximum, including cBT, cET and cBI.^{12,19} With the same method more challenging MCOs were synthesized, too, like those of poly(1,4-ethylene 1,6-naphthalene dicarboxylate) and poly(1,4-butylene 1,6-naphthalene dicarboxylate).^{36,126} A polymer-supported variant has been developed by HODGE *et al.*, which is mentioned here for the sake of completeness.¹⁵⁸ It involves a protection-deprotection strategy and has the advantage that formed cycles can simply be filtered off, while linear species stay bonded to the polymer matrix. However, its applicability is restricted to MCOs of polymers of the AB-type and the yield was reported to be below 50 % (for oligoamides).

3.3 Options for reduction of the cBT polymerization temperature

The lowest possible polymerization temperature is determined by the melting temperature of the MCOs used to obtain a minimum mobility of the monomers, if the efforts of a solid state polymerization are to be avoided. ROP of cBT below the melting temperature of PBT has been extensively investigated and even already utilized for preparation of composites

and RTM (reaction transfer molding) despite its disadvantages, as pointed out in the previous paragraphs (chapter 3.1.2, p. 15 ff.).^{26,56,83,159–161}

The various oligomers of cBT possess different melting temperatures, for instance. The dimer, tetramer and pentamer of cBT was found to melt at a higher temperature than a composition of cBT (dimer 194-199 °C^{87,162,163}, tetramer 247 – 251 °C^{150,162,163}, pentamer 207 °C¹⁶³, compared to 200 °C for completely molten cBT in the cited reference). However, the cBT trimer melted at 168 °C. The measured values at least of the dimer, trimer and tetramer were verified by BRUNELLE *et al.* in 1998.¹⁹

A manipulation of the melting point of a MCO composition was realized by changing the fractions of the individual oligomers within this composition. This was noticed first by BURCH *et al.* for compositions of cET, which is structurally closely related to cBT and which was already cited above.⁷⁰ A broad distribution of ring sizes, obtained by a kinetic preparation route in solution, leads to a lower melting temperature of the composition than a narrow one resulting from a thermodynamic equilibrium from synthesis in suspension. The dependency of the melting temperature of a MCO composition on the fractions of the enclosed oligomers is probably the reason for the different melting ranges of cBT compositions stated in literature.^{19,21,24,55,77,79–83}

A first way to reduce the melting temperature of cBT purposefully by 15 to 70 °C was established by removing the majority of the cBT tetramer, according to a patent by PHELPS.¹⁶⁴ As noted above, the tetramer is the highest melting oligomer usually present in cBT mixtures. The removal was realized, among other methods, by fractional crystallization from solutions in aromatic and mostly halogenated hydrocarbons like oDCB. A solution of up to 5 wt-% cBT was first generated by heating. The precipitation of the cyclic tetramer was subsequently initiated by cooling or by adding a non-solvent like pentane or another short-chained hydrocarbon, which preferentially causes the tetramer to crystallize. The polymerization of cBT with a reduced melting temperature led to PBT with a reduced brittleness and improved mechanical properties as toughness or elongation at break, as outlined above (chapter 3.1.2, p. 15 ff.).⁵⁴

In case of copolymers prepared by ROP, the melting temperature of the mixture of monomers can be reduced in an easier way by just using a mixture of the employed monomeric building blocks. This could take place in form of comonomers (*co*-MCOs) or by mixing the respective monomers with utilization of their colligative properties. The first makes some effort necessary for preparation of the respective comonomers with a fixed ratio of the

respective building blocks. Each prepared comonomer is restricted to one copolymer with one ratio of monomeric units.^{19,70} The latter is easily applicable to existing monomers.

Preparation of *co*-MCOs was carried out in form of *co*-cyclization by BRUNELLE *et al.* in 1998.¹⁹ They prepared cyclic 1,2-ethylene terephthalate-*co*-butylene terephthalate, c(BT-*co*-ET), by condensing BDO, EDO and terephthalic acid in pseudo-high dilution (compare to chapter 3.2.1.3, p. 25 ff.). A lower melting temperature of c(BT-*co*-ET) comonomers (with a ratio of 1:9 of BT to ET units) was observed in ED-ROPs than compared to the pure monomers cBT or cET and even to a mixture of cET and cBT in the same ratio of 1:9. The obtained polymer had no significantly reduced melting temperature (in respect to PET). These results are in good agreement with those of Burch *et al.* in 2000.⁷⁰ The latter failed to additionally establish a transesterification of cBT and cET, (according to mass spectrometry analysis), although they claimed to have strictly maintained transesterification conditions, particularly excluding water from the reaction.

Mixing cyclic monomers permits simple variations in the monomers, in the ratios of these and hence in the prepared polymers, although a smaller reduction of the melting temperature has probably to be accepted. To optimize the polymerization temperature of the mixtures, it is inevitable to evaluate the influences of the ratio of the different monomers in the mixtures on the melting behavior. However, in the few studies of mixtures of different cyclic monomers, the focus was mostly on the reduction of the crystallinity of the resulting polymer (in PBT, e.g.¹⁶⁵) or on varying its properties but less on the effect on the melting temperature.

Mixtures of cyclic hexamethylene terephthalate and ϵ -caprolactone have been polymerized in various fractions by MUÑOZ-GUERRA *et al.* in 2008¹⁶⁶ as well as by MARTÍNEZ DE ILARDUYA and MUÑOZ-GUERRA *et al.* in 2010¹⁴¹. They had a closer look at the thermal and mechanical properties of the resulting polymers but did not mention any further characterization of the monomer mixtures. However, they recognized a lower reactivity and a lower product M_w with smaller ring size of their MCOs while the other polymer properties and its structure seemed unchanged.

In another article, cBT was mixed with cyclic cyclohexyl-1,4-dimethene terephthalate and polymerized by MUÑOZ-GUERRA *et al.*, too.¹⁶⁷ Again, no information about the melting temperature of the mixtures itself was given. In ROP, a conversion of 92 – 97 % was accomplished and a $M_w = 30 - 50$ kDa.

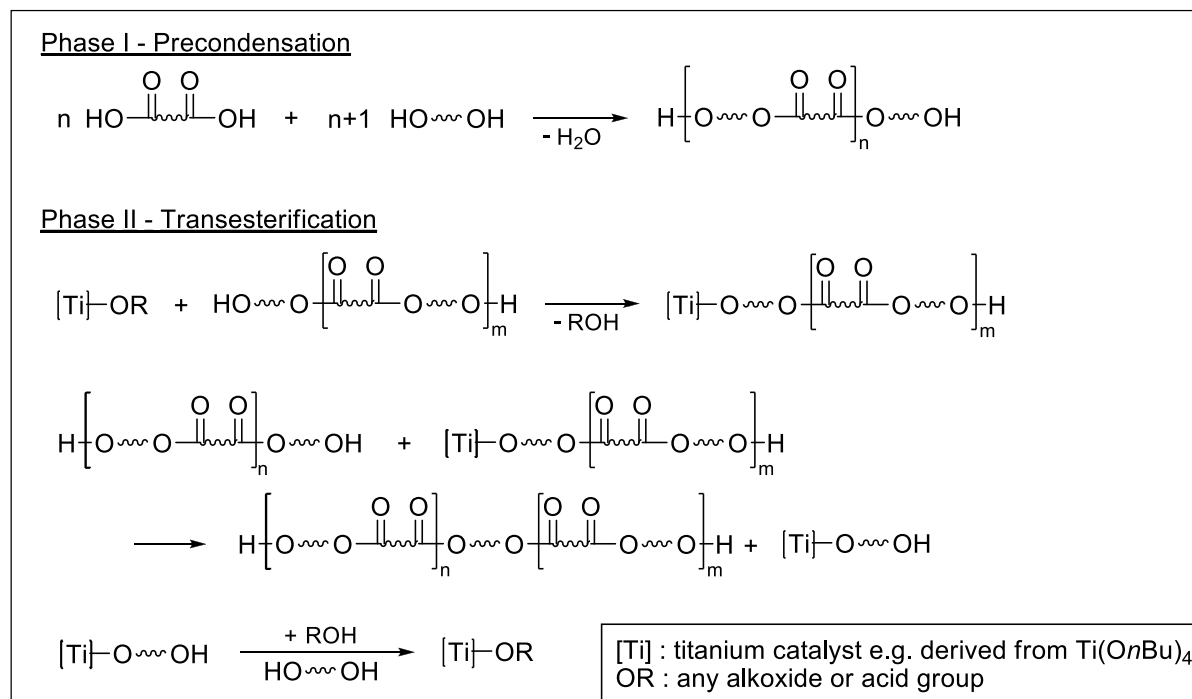
Copolymerization of cET and cEI in chloroform solution was published by MONVISADE *et al.* in 2008. No analysis of the undissolved monomer mixture was carried out.⁶⁹

The investigation of the copolymerization of cBT and pentadecalactone in bulk by DUCHATEAU *et al.* in 2016 revealed a eutectic copolymer.¹⁶⁸ PBT segments were found to be

present in the poly(pentadecalactone) lattice but not vice versa. In the same article, a limitation of the achievable molecular mass of polymerized cBT of $70 \text{ kg}\cdot\text{mol}^{-1}$ was described, even with carefully conditioned cBT. A characterization of the monomeric mixture was not reported, especially with respect to its melting temperature.

3.4 Sustainable polyesters by polycondensation

Although polycondensation has some disadvantages over ROP, it is a versatile tool in the preparation of polyesters from various monomers with a simpler process than for ROP. The formation of ester bonds from diol and diacid is thermodynamically not an observable equilibrium. Hence, the formed by-product, mostly water or methanol, is removed to progress the reaction. Often diols with small chain length are employed, e.g. EDO, PDO or BDO, which are easily distilled off together with the formed byproduct. Therefore, the (usually more volatile) diol is used in excess and a precondensation step at comparatively milder conditions is performed.^{169,170} Oligomers are formed in this precondensation step as in every step-growth polymerization.¹⁶⁹ This phase may predominantly be autocatalyzed by the acid functionalities, but the concentration of acid decreases with progressing conversion to ester and the role of an additional catalyst becomes more important. The molecular weight is increased in this second phase mostly by transesterification and removal of formed diol (Scheme 3).^{13,41,171} Metal-based catalysts like e.g. titanium(IV) alkoxides, antimony(III) oxides and manganese(II), calcium(II), magnesium(II) or zinc(II) acetates are commonly applied for the transesterification catalysis at temperatures between 180 to 280 °C.¹⁷²



Scheme 3: The predominant reactions in the polycondensation of a diol and a diacid with precondensation and transesterification phase, the latter being catalyzed by a titanium(IV) alkoxide.

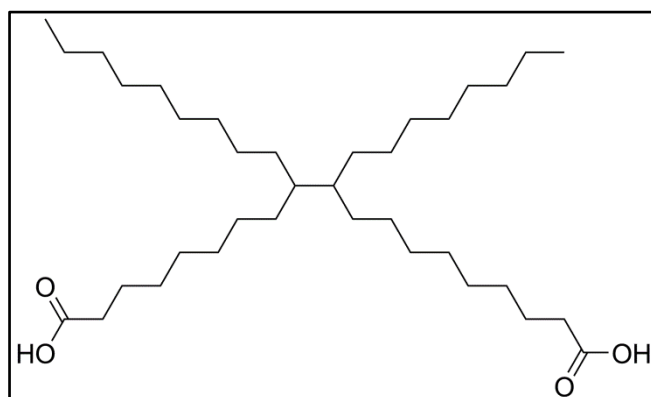
There is an ongoing interest in the modification of this route to more sustainable or “green” conditions with additional regard of the economic aspects (overall costs) and the necessary auxiliaries.^{173,174} A reduction of the polymerization temperature is possible, when using highly active catalysts like enzymes^{175–178}, which have the additional advantages of being highly selective and usually non-toxic.^{179–181} Enzymes are already a versatile tool in organic synthesis, e.g. for production of high-fructose corn syrup (HFCS)¹⁸², of *L-tert-leucine*¹⁸³ or of surfactants.^{184,185}

Inactivation of the enzymatic activity at elevated temperature is a major restriction, which limits enzyme usage in industrial processes. However, the immobilization of suitable enzymes, e.g. on an acrylic resin, has been proven to give a substantial improvement of its thermal stability. Enzymes in this form remain active for a longer time and can be reused several times at temperatures between 60 and 80 °C.^{186,187} This temperature furthermore allows polymerization of aliphatic polyesters in bulk. An additional advantage of the immobilization is the possible separation and removal of the resin after the reaction. Thus, there is no catalyst left in the polymer to induce undesired degradation reactions, or which might even be potentially harmful as it might be the case for metal catalysis.

The avoidance of the reaction conditions of metal catalysis by utilization of the highly active enzymes as catalysts combined with their high selectivity moreover allows the further expansion of the suitable monomers. More complex monomers from renewable sources as well as those with additional functionalities can be included in the range of possible starting materials. Enzymatic catalysis allows the presence of reactive groups like e.g. siloxanes, epoxy entities or double bonds with prevention of side reactions like e.g. alcohol dehydration¹⁸⁸, double bond isomerization or ORDELT saturation of a double bond.¹⁸⁹ The presence of such functionalities in catalysis by metal are highly likely to cause major side reactions.

Some effort has consequently been made in the last decades in researching enzyme-catalyst polycondensation. Various enzymes have been tested with peroxidases, cellulases, cutinases and lipases being the most prominent representatives.^{181,190–193} It became clear that *lipase B* from *Candida antarctica* has the broadest substrate spectrum and generally the highest activity for polycondensation.^{194,195}

The disadvantage of the comparatively mild reaction conditions in catalysis by enzyme is often a limitation of the achievable molecular weight because of a limitation in the removal of the formed by-product by distillation. One interesting application for a low molecular mass polyester is in polyurethane synthesis as soft block component, e.g. for short polyester chains from fatty or dimerized fatty acids with their long carbon chains. An example for such dimerized fatty acids is *Pripol™ 1012* (Pripol), which is produced by dimerization of C18 vegetable oil fatty acids. It is claimed by the producer to be partly unsaturated (0-1 double bonds per molecule) (proposed structure in Scheme 4).¹⁹⁶ Such polyesters are of particular interest regarding the carbon footprint, especially if not only the diacid component but also the diol component stems from renewable resources. PDO is such a diol of interest as it can readily be prepared from glycerin by fermentation.^{197–199} The evaluation of such polyurethanes including their precursors have been subject of large interest in the last years in order to find sustainable supplements for the so important polyurethanes.^{200–206}



Scheme 4: Structural proposal of *Pripol™ 1012* (Pripol).¹⁹⁶

However, there is still a lack of information for polyester synthesis in the combination of enzymatic catalysis and monomers from renewable resources. Despite the obvious differences, there is very little information comparing the performance and the formed products by catalysis with a highly active enzyme or with a metal complex at its higher temperatures.

4 Scope of work

This work consists of two sections, the first dealing with the ROP of cBT, the second with the comparative polycondensation of a sustainable polyester by enzyme and by metal catalysis.

ROP of cBT can be utilized to obtain high-molecular weight PBT in shorter reaction times than possible by polycondensation. Methods providing cBT with a reduced melting temperature are desirable for this. They lead to a reduced processing temperature (as in RTM, e.g.) and possibly even to improved mechanical properties due to a reduced brittleness of the final polymer.⁵⁴ Two different approaches have been pursued to evaluate the feasibility of this goal. Both utilize the fact that cBT consists of a composition of cycles of different sizes, as the vast majority of MCOs do. The highest melting temperature of a cBT composition is the result of a colligative effect of these different oligomers. It can thus be significantly lower for a composition than one would expect from the melting temperatures of the isolated oligomers. The various melting temperatures of cBT published so far are probably due to this fact.^{19,21,24,55,79–83}

The first route towards cBT with a lower melting temperature is the manipulation of the composition of the oligomers within a cBT batch, which has only rarely been addressed in literature before. In these reports, the high-melting cBT tetramer was fractionally separated from the composition. Details on the temperature or solvent dependencies were not given, which would be useful for further optimization. A deepening of the insights was pursued in this study. The insights gained hereby led to the purposive extraction of low-melting cBT (LM-cBT) from a cBT composition as possible alternative, which was extensively evaluated. The yield of this LM-cBT was monitored in dependence on solvent or solvent combination, time and temperature.

The second approach deals with the mixing of monomers. Several publications considered the mixing of cyclic monomers for ROP to alter the properties of the resulting polymer, but only very limited data is available on the effect of the mixing on the melting temperature of monomeric mixtures, despite promising results for comonomers and eutectic copolymers. The three aromatic MCOs cyclic 1,4-butylene isophthalate (cBI), cyclic 1,3-propylene terephthalate (cPT) and cyclic 1,4-butylene isophthalate (cPI), which are structurally closely related to cBT, and two aliphatic lactones, cyclic 1,4-butylene adipate (cBA) and cyclic 1,4-butylene succinate (cBS), have been prepared and mixed in various ratios. The thermal properties of mixtures among the aromatic MCOs and of each of the aromatic MCOs with

one of the two aliphatic MCOs have been analyzed by DSC. The resulting effects were analyzed regarding the influence of the enclosed structural units in the cyclic monomers.

The second section of this thesis deals with the evaluation of polycondensation by combining the utilization of monomers from renewable resources with the mild process parameters of a catalysis by an active enzyme. Therefore, linear aliphatic polyesters were prepared from Pripol and PDO. The reaction has been catalyzed by the lipase *CalB immo* by *c-LEcta*, which is immobilized on an acrylic resin. One objective was to explore the maximal molecular weight achievable by catalysis with this immobilized enzyme at its maximal operation temperature of 80 °C. The constitution of the formed polyester products, i.e. the occurrence of side reactions, was compared to those obtained by metal-catalyzed reactions with $\text{Ti}(\text{OnBu})_4$ at 220 °C, which is one of the processes routinely employed for production of various polyesters like poly(butylene terephthalate) or poly(trimethylene terephthalate) as mentioned above. The resulting polyester has been exemplarily used in preparation of polyurethane elastomer as proof of concept for a possible application of this polymer.

5 Results and discussion

5.1 Reduction of the melting temperature of cBT by recrystallization

A possible route for lowering the melting temperature of cBT was found by PHELPS in precipitating a higher-melting oligomer from the cBT composition by fractional separation from the composition.¹⁶⁴ A significant reduction of the melting temperature of about 15 to 70 °C was reported. The effects of temperature or solvent polarity on the precipitation were not given. These dependencies were further investigated in this study. Therefore, time and temperature dependent precipitation of cBT were explored from oDCB, from mixtures of oDCB with CHCl_3 or toluene, from CHCl_3 and from CHCl_3 mixed with cyclohexane (CY).

Additionally, the isolation of cBT with a reduced melting temperature was extensively evaluated by extraction of fractions from cBT compositions like e.g. the commercial product CBT100 (IQ Tec). The low-boiling solvents as CHCl_3 , CY and THF were therefore utilized. Isolated fractions of cBT were analyzed by means of DSC, ^1H NMR, MALDI-TOF (matrix-assisted laser desorption/ionization spectrometry with time-of-flight detection), SEM and GPC.

5.1.1 Analytical methods

The general descriptions of the various analytical methods applied during this study are given in this chapter. Possible general observations in the different methods are listed if they concern the entirety of the measured samples. The results for CBT100 are discussed. CBT100 is a commercial composition of oligomers prepared by depolymerization in solution on a larger scale. It was hence chosen as starting material for manipulations in this study. Its results serve as a benchmark.

5.1.1.1 DSC

The DSC measurements consisted of two cycles of heating and cooling of the sample under a nitrogen atmosphere. The initial melting during the first cycle is considered, if not stated otherwise, because the initial properties of the cBT composition are regarded most

interesting for further processing of isolated fractions, e.g. for ROP or RTM processes. The glass transition temperature (T_g) was calculated according to ASTM D3418/IEC1006 (i.e. the midpoint temperature on the tangent between on- and endset of T_g).²⁰⁷ Hence the resulting ΔC_p is proportional to the amorphous fraction in the sample.

The repeatability of DSC measurements was mostly found to be good, sometimes even excellent for 1st and 2nd cycle of a DSC measurement and for subsequent measurements of the same DSC sample. The crystallization process was found to be less homogeneous than the melting of different DSC samples of the same cBT batch. The deviation of the crystallization temperature was at about ± 10 °C (mainly caused by divergence of some individual samples); the deviation for melting was at about ± 4 °C. It was probably caused by inherent fluctuations of the crystallization processes itself. The enthalpy of melting was generally smaller in the 2nd cycle than in the 1st probably caused by incomplete crystallization in the short time of a DSC measurement.

A typical melting behavior of a polymorphic substance was observed²⁰⁸ with several melting endotherms. Overlapping of the second melting endotherm with cold crystallization was observed in many cases for heating and cooling rates during the second heating segment of $10 \text{ K}\cdot\text{min}^{-1}$ (Figure 1). The peak form of a eutectic mixture was observed in some isolated cBT fractions with a reduced melting temperature. The melting temperature during the second heating cycle in DSC measurement was below 180 °C in these cases and above 185 °C otherwise, usually around 195 °C.

Considering all cBT samples obtained during this study, the chance for a batch of LM-cBT seems to be higher if a higher amorphous fraction in the respective cBT batch was detected by means of a high ΔC_p especially during the second heating cycle. This relation was not observed in all samples. No sample was measured with a high T_m and a high ΔC_p , but a few with a low T_m and a low ΔC_p .

The melting of CBT100 shows several endotherms in the range of 120 to 200 °C with major maxima mostly around 140, 155 and 185 °C (Figure 1). The melting behavior is dominated by overlap of melting endotherms of different oligomers with melting point depression. An impressive cold crystallization exotherm is observed during the second heating before melting. Glass transitions were detected during cooling and second heating, sometimes even during first heating at about 24 °C (20 °C during cooling segment). The existence of a glass transition in the monomer mixtures may be unexpected but comprehensible considering the size of the cycles and the oligomeric nature of the aromatic MCOs.

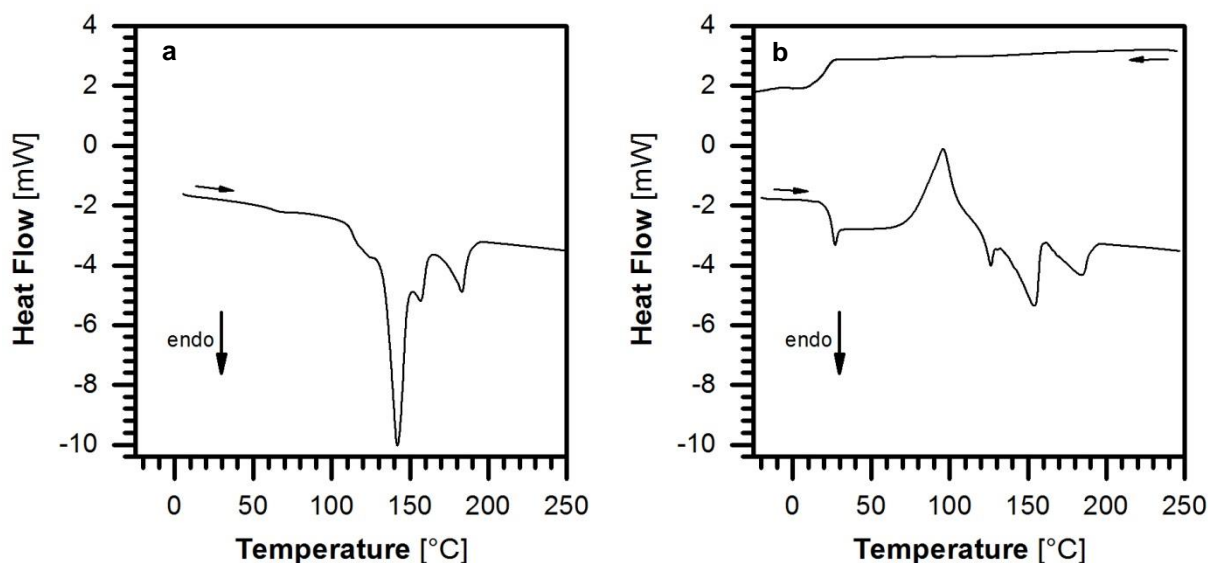


Figure 1: DSC traces of CBT100 during a) first heating (initial melting) and b) cooling and second heating.

5.1.1.2 ^1H NMR spectroscopy

^1H NMR spectra were recorded for gaining insight into the amount of hydrolyzed rings, of degradation during processing and into the ratio of oligomeric to polymeric character of the cBT batch.

The signal of the methylene group next to the hydroxyl group resulting from the opening of cBT ($-\text{CH}_2\text{-OH}$) was found at 3.7 ppm. Less than 5 mol-% hydrolyzed cycles were usually found for all of the samples as calculated from its integral and the integral of the resonance of the internal methylene group ($-\text{CH}_2\text{-CH}_2\text{-O-}$) at around 2.0 ppm (Equation 1). The ratio was calculated assuming the most probable case of hydroxy termination at only one end of the chain. It should be noted that even small amounts of hydroxy terminated chains significantly alter the products by ROP, e.g. and have hence to be considered.

$$\text{Ratio hydroxyl end groups} = \frac{\int_{3.6 \text{ ppm}}^{3.8 \text{ ppm}} (-\text{CH}_2\text{-OH})}{\int_{3.6 \text{ ppm}}^{3.8 \text{ ppm}} (-\text{CH}_2\text{-OH}) + \frac{\int_{1.9 \text{ ppm}}^{2.1 \text{ ppm}} (-\text{CH}_2\text{-CH}_2\text{-O-})}{2}} \cdot 100 \quad (1)$$

The signal of the corresponding methylene group next to the ester group ($-\text{CH}_2\text{-O-}$) overlapped with the resonance of HFIP (1,1,1,3,3,3-Hexafluoroisopropanol), which had to be added in small amounts in order to obtain a solution of CBT100 (as well as of high-melting fractions of cBT isolated in this study). It could hence not be used for any calculations.

Degradation may result from elimination and transesterification processes next to the mentioned hydrolysis of cycles. This is manifested by a shifting of the peaks of the aliphatic backbone causing additional peaks in the range of 2.5 to 1.5 ppm.

The ratio of small and large oligomers has been calculated to characterize the various cBT fractions further. The peak of the aromatic protons at 7.87 ppm is characteristic of small cyclic oligomers and is absent in the polymer with a peak at 8.1 ppm.^{52,148} The oligomeric ratio was calculated by the ratio of the integral at 7.87 to that at 8.07 ppm and itself (Equation 2). It hence specifies the molecular fraction of small oligomer repetition units.

$$\text{Oligomeric Ratio} = \frac{\int_{7.8 \text{ ppm}}^{8.0 \text{ ppm}} (\text{Ar}^{\text{Oligomer-H}})}{\int_{7.8 \text{ ppm}}^{8.0 \text{ ppm}} (\text{Ar}^{\text{Oligomer-H}}) + \int_{8.0 \text{ ppm}}^{8.4 \text{ ppm}} (\text{Ar}^{\text{Polymer-H}})} \cdot 100 \quad (2)$$

The signal at 7.87 had previously been reported to originate from the dimer without any proof for this assignment.¹⁴⁸ Correlation of the ratio from NMR to the signal of the dimer and trimer in GPC (THF as eluent) was observed in this work but could not be related to one oligomer or to a combination of some (see next section on p. 39 and Figure 5). Hence, the ratio is referred to as oligomeric ratio in this study. The ratio has not been determined before and so comparable values are not available. CBT with 100 mol-% oligomers has never been characterized. It should be noted that no direct correlation between the oligomeric ratio and the melting temperature has been recognized so far. However, LM-cBT usually possesses a higher oligomeric ratio than CBT100. The lack of direct correlation is most probably due to the determination of the thermal behavior by colligative properties of the cBT oligomers.

Commercial CBT100 showed in five measurements an average oligomeric ratio of 33.7 ± 0.0 mol-% and a fraction of chains of 1.9 ± 0.6 mol-% (exemplary spectrum in Figure 2, values in Table 1).⁵² An elevated ratio of small cycles was observed for all isolated fractions with a reduced T_m in this work. The amount of hydrolyzed cycles was reduced by most procedures.

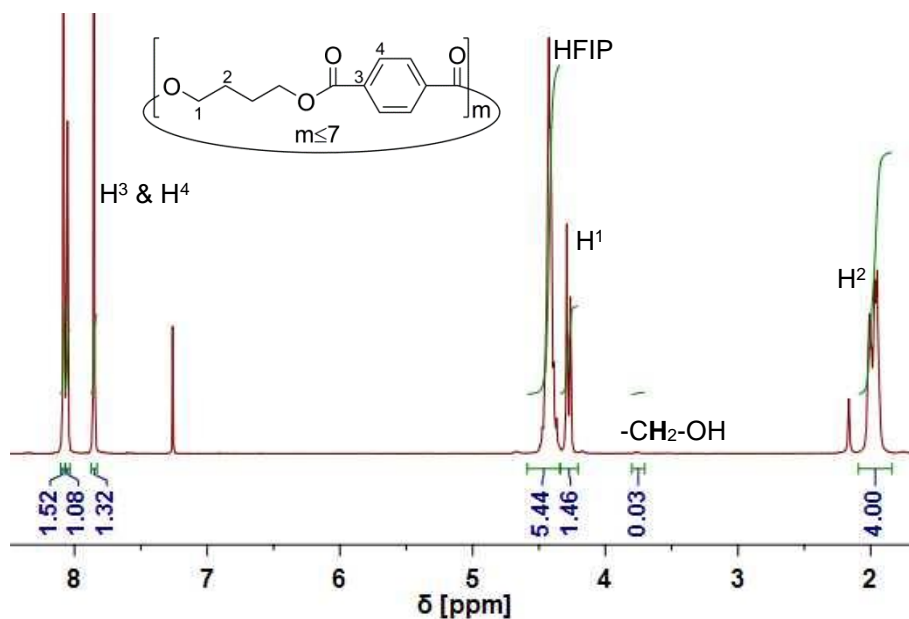


Figure 2: ^1H NMR spectrum of CBT100 in CDCl_3 spiked with drops of HFIP.

Table 1: ^1H NMR results of the five measurements of CBT100 in CDCl_3 spiked with HFIP and the oligomeric ratio and the ratio of hydroxyl end groups calculated thereof.

	$\text{Ar}^{\text{Polymer}}\text{-H}$ 8.4-8.1 ppm	$\text{Ar}^{\text{Polymer}}\text{-H}$ 8.1-8.0 ppm	$\text{Ar}^{\text{Oligomer}}\text{-H}$ 8.0-7.8 ppm	$\text{-CH}_2\text{-OH}$ 3.8-3.6 ppm	$\text{-CH}_2\text{-CH}_2\text{-}$ 2.1-1.9 ppm	Oligomeric Ratio [mol-%]	Ratio hydroxy end groups [mol-%]
cBT #1	151.36	105.26	130.18	1.98	400.00	33.66	0.99
cBT #2	149.72	106.11	130.17	2.65	400.00	33.72	1.33
cBT #3	149.59	107.17	130.65	4.78	400.00	33.72	2.39
cBT #4	148.22	105.41	128.56	4.92	400.00	33.64	2.46
cBT #5	152.28	107.53	132.13	4.42	400.00	33.71	2.21
Average	---	---	---	---	---	33.69	1.88

5.1.1.3 MALDI-TOF

MALDI-TOF was utilized for determination of cyclic and linear species present in the respective sample, the latter stemming from ring-opening during the preparation procedure or during the ionization and volatilization processes in MALDI. A molecular weight distribution was not derived from the spectra as ionization, evaporation and flight behavior of the different oligomers of the various species may differ and are not known. The evaluated

repeating units of the rings and chains are mentioned here to give an impression and to allow a first comparison of isolated fractions. The data generally match the conclusion from GPC analysis (if samples could be analyzed by GPC, chapter 5.1.1.4).

Sodium(I) and silver(I) trifluoroacetate (NaTFA and AgTFA) were used as ionization aids with a dithranol matrix. More intense signals were obtained with AgTFA, but with more side or degradation products observable, too. It is unclear whether AgTFA enhances degradation or simply causes a more efficient ionization of the linear species than NaTFA. AgTFA was usually used in order to obtain comprehensive information about the samples. Addition of HFIP was necessary in some samples to obtain solutions. No effects on peaks and peak intensity were found (with utilizing Dithranol and AgTFA).

A good detection of the ratio of cyclic to opened species seems to be obtained by MALDI. Similar relations between the signals of cyclic and linear species were found by MALDI-TOF and ^1H NMR for cycles purposely opened with 1-butanol.

No correlation was however found between MALDI-TOF peak intensities and melting temperatures in DSC measurements as was to be expected because thermal behavior is a result of the colligative effects within the composition of oligomers in cBT. However, smaller cycles were generally found for extracted LM-cBT with their lower melting temperature.

The presence of cycles with an odd number of repeating units seems higher. These species were mostly detected by MALDI-TOF. No or only comparatively small signals were even observed for species with six repeating units. A disfavor of all species with an even number of repeating units by MALDI-TOF spectrometry is not likely and is hence excluded as reason for the observation.

Samples of CBT100 possess peaks of cyclic oligomers with a number of repeating units of mainly 3 – 7 and indicated signals for rings with 8 – 14 units (Figure 3). Traces of linear chains (hydroxy terminated by an excess of 1,4-butanediol) were found for 7 to at least 14 repeating units.

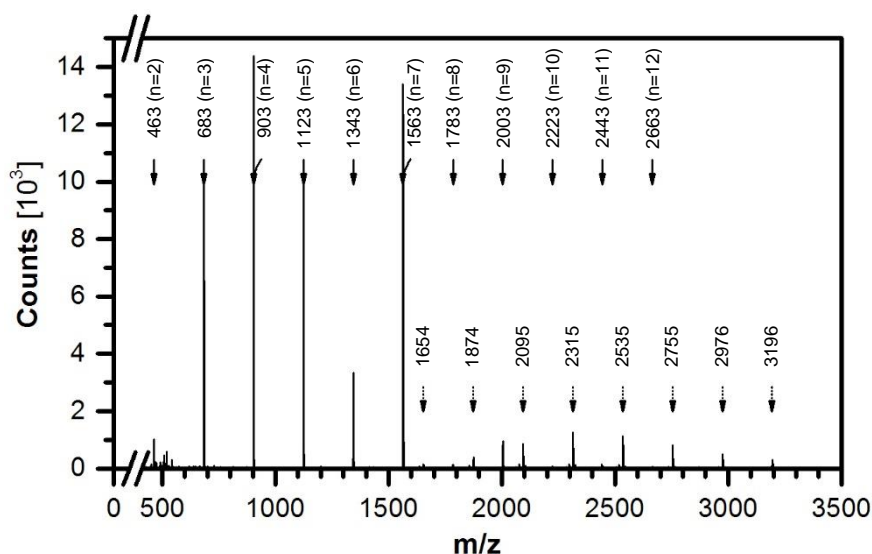


Figure 3: MALDI-TOF spectrum of CBT100 with Dithranol and NaTFA. Series of $[n\text{-MCO} + \text{Na}]^+$ (solid arrows at the top) and series of hydroxy terminated linear chains (dotted arrows at the bottom).

Electrospray ionization (ESI) spectrometry as another mild ionization method was evaluated as well. Mainly degradation products were detected and research was not pursued.

5.1.1.4 GPC(THF) of low-melting MCOs

Only some extracted fractions could be analyzed by GPC with THF as eluent. LM-cBT fractions were often found to be soluble in CHCl_3 and mostly in THF or dichloromethane. Separation of the molecular weight was achieved in these cases by a GPC column for separating low molecular weight compounds. The detection was achieved by means of the number-sensitive absorption of UV light and of the mass-sensitive change of the refraction index (RI). Both detection methods resulted in similar relations between the different peaks (Figure 4).

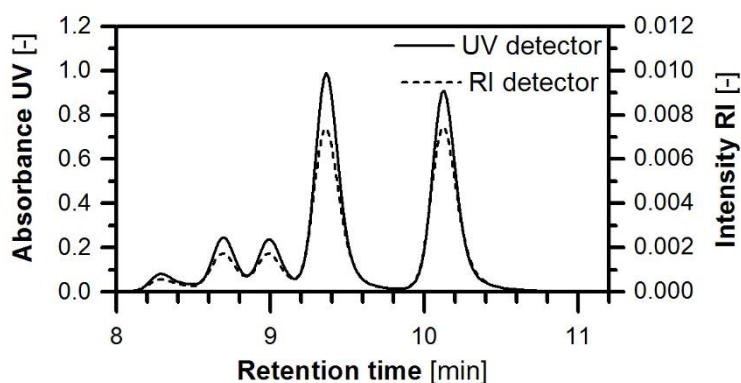


Figure 4: Exemplary GPC trace of UV and RI detector of cBT extracted by THF (sample 1).

The order of the oligomers by their integral fraction was consistent for most evaluated LM-cBT samples: trimer \gg dimer \gg pentamer \geq tetramer \geq hexamer (Figure 5). The only exception was an extraction of CBT100 by THF, where the order of dimer and tetramer was switched and the difference of their integrals smaller. The oligomeric ratio calculated from ^1H NMR does not generally match the fraction determined by GPC of one of the oligomers. Various oligomers must contribute to the respective peak representing the oligomers in ^1H NMR. The order determined from integrals in GPC does in general agree with the peak intensities in MALDI-TOF spectra, although some deviations were noticed especially for oligomers, which were present only in small amounts. This may be attributed to variations in flight probabilities during measurements. No obvious relationship was found for the integrals with the melting endotherms in DSC measurements as discussed for MALDI spectra. This highlights once more that the melting (and crystallization) behavior are determined by colligative interactions rather than single oligomers.

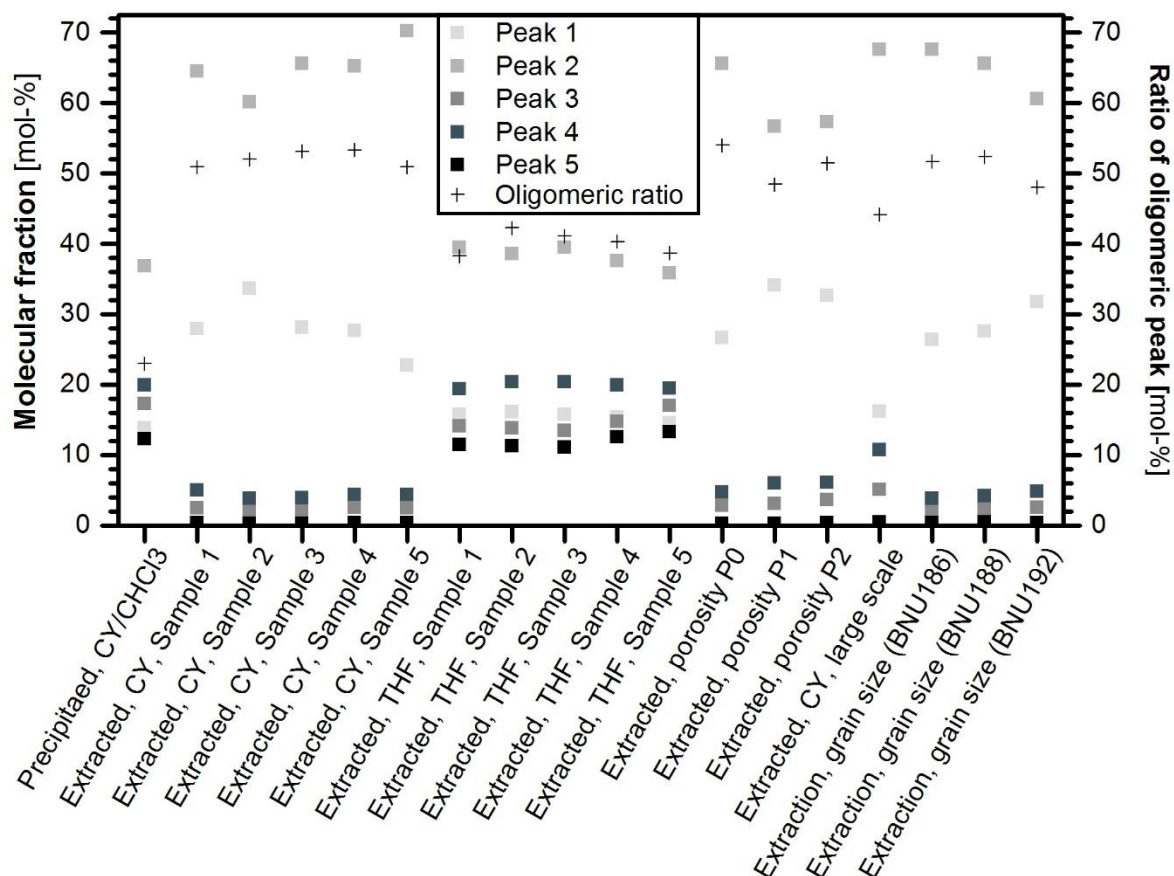


Figure 5: Molecular fractions of the peaks from oligomeric GPC with THF as eluent (UV detection) in different samples collected through this study (square markings and left axis) and the comparison with the oligomeric ratio by ^1H NMR (cross markings and right axis).

5.1.1.5 SEM

SEM pictures of CBT100 were taken to compare the appearance of the granulate before and after extraction. For CBT100, the pictures show plates of about 3 – 5 μm side length in an amorphous matrix on the surface and in cross-section (Figure 6). Additionally, scattered crystallites were observed with an edge length of 3 – 15 μm .

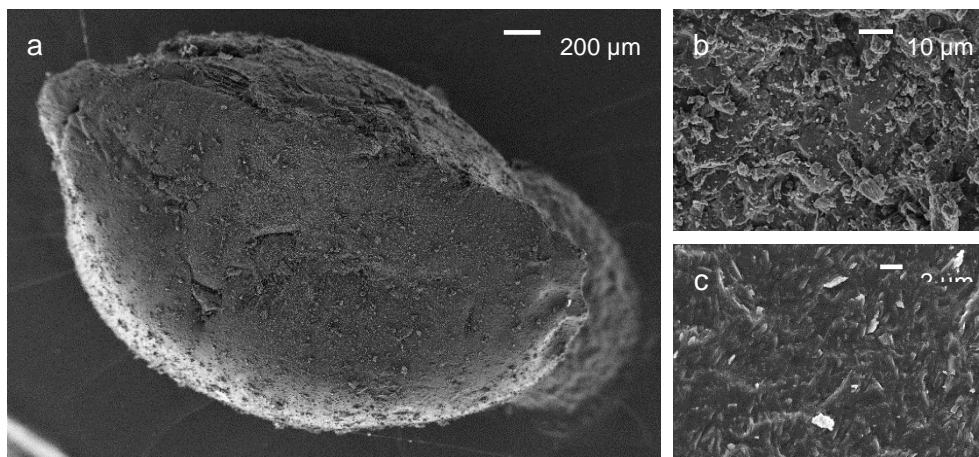


Figure 6: Images of CBT100 by SEM a) in top view, b) expansion from top view and c) expansion from internal phase in cross section (a & c by InLens detector, b by SE2 detector).

5.1.2 Manipulation of the melting temperature of cBT by precipitation with variation of solvent polarity

The experiments outlined in this section had the objective to gain a deeper insight into the isolation of LM-cBT by selective precipitation as was described in principle by PHELPS.¹⁶⁴ Among other things, he patented the reduction of the melting temperature of a cBT composition by precipitating the tetramer by addition of a non-solvent to in particular low-concentrated solutions of about 5 wt-% cBT. Information on the influence of different solvents or the solvent volume on the precipitation behavior was not mentioned or disclosed. To close these gaps of knowledge, the precipitation was carried out by the stepwise addition of a second solvent with a higher or lower polarity index than the solvent oDCB (CHCl_3 or toluene, respectively). Both solvents had proven in preliminary tests to be capable of solving at least some amount of LM-cBT from CBT100.

A transesterification catalyst was present as in the patent described, in this case tin(II) 2-ethylhexanoate, SnOct_2 , to obtain comparable results to the patent and quick equilibrating of the distribution of oligomer sizes. Samples were taken 25 min after addition of the respective volume of solvent to allow equilibration and were immediately filtrated afterwards. The temperature of the mixture of CBT100 in oDCB was reduced after 2.5 h of reflux at 180 °C to the boiling temperature of the second solvent (108 °C for toluene, 61 °C for CHCl_3) before addition of the second solvent was started.

Precipitation of high-melting cBT was faster and more complete in experiments with the more polar CHCl_3 than with toluene. The difference in temperature during precipitation between both experiments seems to be the major reason for this difference because differences in the precipitate's behavior are notable even before addition of solvent. The yield of precipitated cBT within the withdrawn samples as well as the melting behavior and the composition are similar independent of the used solvent or of the second solvent being present. Its fraction seems to be mainly dependent on the temperature during precipitation. Only little more precipitate was isolated from the samples at 61 °C (with addition of CHCl_3) compared to separation at 108 °C (with toluene) (10.9 ± 0.6 wt-% compared to 8.7 ± 0.4 wt-%, Figure 7a and b, square markings). The yield of cBT within the withdrawn samples was determined as the mass of cBT isolated by filtration related to the mass of cBT theoretically present in the sample volume (including solid and solved fractions). The difference in the fraction of precipitated cBT was not reflected in the thermal behavior. Only one melting endotherm was found at above 200 °C in the first heating segment in DSC measurement (Figure 7a and b, round markings) for all samples independent of the used precipitation solvent or the solvent composition. The same is true for the heat of fusion, normalized by the mass (ΔH_m), which is indicated in the diagrams by the markings size to allow comparison. The color of the markings was chosen to illustrate the change in melting temperature from red for CBT100 over orange to light green for a reduced highest melting temperature and to dark red if it is increased. A corresponding thermal behavior was found during the cooling and the second heating segment as described for the first heating segment of DSC (not shown).

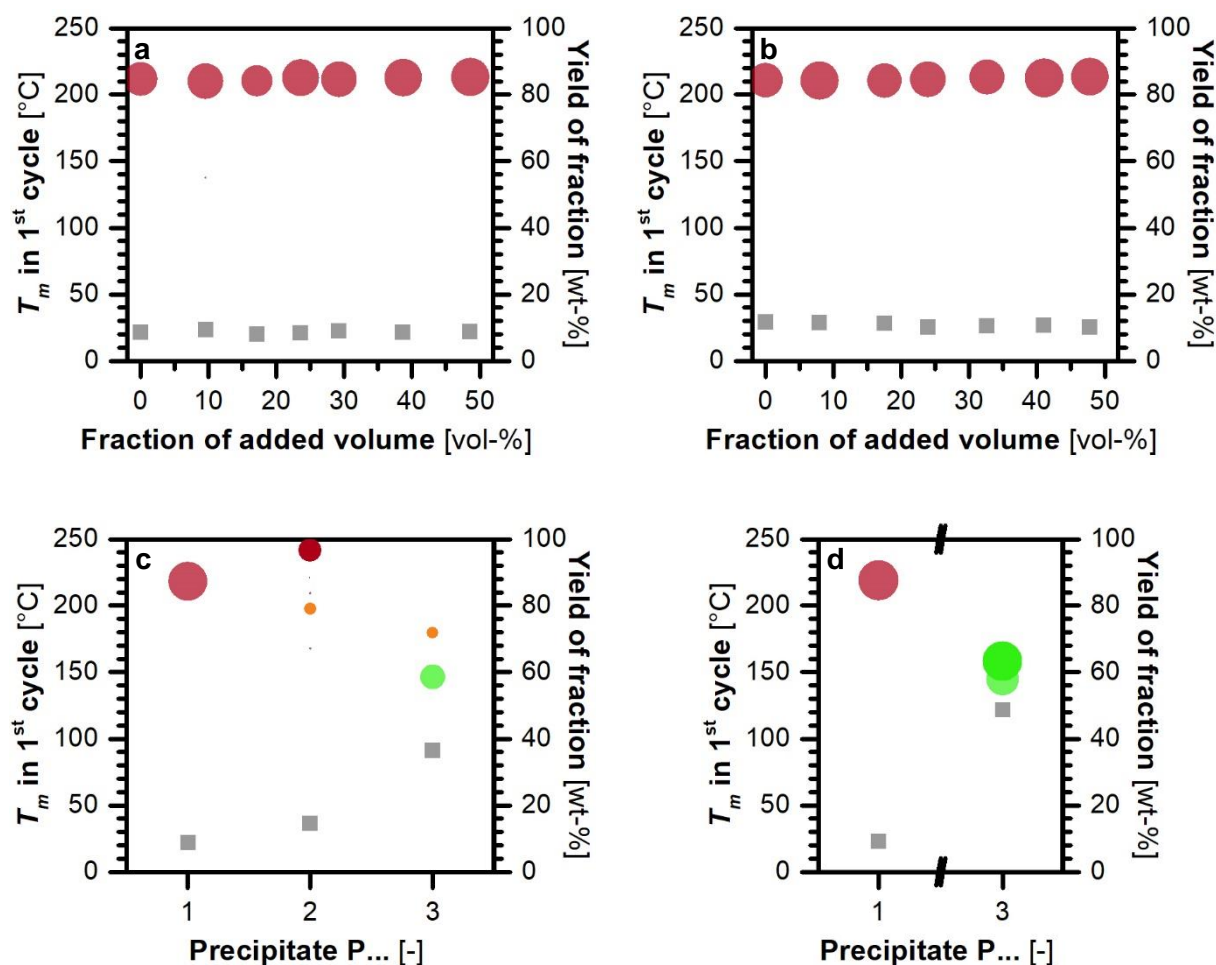


Figure 7: Melting temperatures during initial melting in DSC measurement (points with size indicating ΔH_m) and yield (squares) of cBT obtained by addition of a) & c) toluene b) & d) CHCl_3 . Precipitates a) & b) from samples after stepwise addition of the second solvent, c) & d) from final mixture of oDCB with an equal volume of the second solvent.

The final product after evaporation of the last filtrate gave a cBT batch with a melting temperature of 158 °C for CHCl_3 /oDCB and 180 °C for toluene/oDCB mixtures in a yield of 48.7 and 36.4 wt-%, respectively (precipitate P3, Figure 7c and d). The suspension was filtrated in hot in both experiments directly after taking of the last sample, giving a high-melting precipitate (precipitate P1). A melting temperature of about 220 °C was found for these fractions. In case of toluene addition (at 108 °C), additional precipitate of 14.5 wt-% formed after this first filtration within three days and was filtered off (precipitate P2), resulting in a cBT fraction with complete melting at 242 °C.

The composition of all withdrawn samples according to MALDI was similar, independent on the used solvent (Figure 8). The comparison of the MALDI spectra allows a first estimation of possible differences between the samples despite the uncertainty that they represent the true

ratios of the oligomers. The samples, which precipitated in the presence of CHCl_3 and thus at lower temperatures, possess in average slightly higher counts for larger MCOs than those obtained in presence of toluene. The MALDI spectra of all samples have most intense peaks for cycles with 3 or 2 repetition units accompanied with still intense signals for 4 and 5. Additional small to very small signals for 6 to 10 repetition units are in most cases observed with the signal for 7 being the most intensive one. The finally isolated, low-melting fraction interestingly showed a similar MALDI spectrum to those of the samples taken during solvent addition with their higher melting temperatures. The higher-melting precipitates P1 and P2 usually exhibited most intense signals for larger cycles (≥ 4 repetition units with the signal for 4 often being dominant) in MALDI. The latter was expected from the description of the patent of PHELPS.

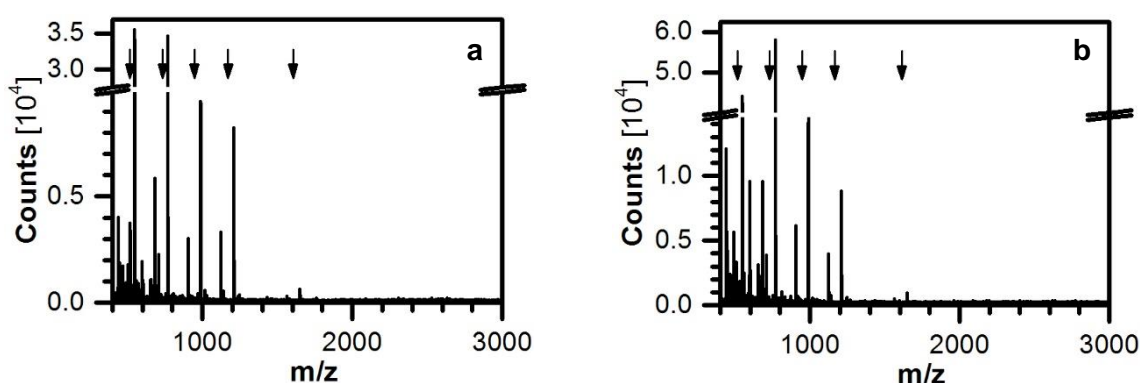


Figure 8: MALDI of samples precipitated from oDCB after addition of a) 24 vol-% toluene or b) 24 vol-% CHCl_3 . The arrows indicate the signals of the Na or Ag agglomerates of the cycles with 2 to 5 and 7 repetition units.

The percentage of opened cycles in the precipitates was at a constant level for the samples withdrawn from the mixtures at 61 and 108 °C and in the first precipitate separated while in hot condition (P1) according to ^1H NMR (Figure 9a). The value was higher than in CBT100 despite drying CBT100 prior to the manipulation (about 6 or 7 mol-% vs. 2 mol-%). This similar behavior of the samples and P1 is in accordance with the similar melting temperatures observed in DSC. A constant amount of degraded cBT was observed in NMR in all these samples. The higher melting fraction P2, which precipitated from the toluene containing mixture after days, contains a ratio of hydroxyl-terminated chains similar to CBT100. This suggests a more or less unselective precipitation of a part of the solved oligomers. Lower amounts of oligomers were determined than in CBT100 for all samples precipitated to give the final LM-cBT product (Figure 9b). Interestingly in this aspect is that the precipitate P1 of both experiments differs significantly from the samples taken during the

stepwise addition of the solvent. The longer time necessary for complete separation of P1 from the mixture may be the reason for this change in ring size distribution. This shift to apparently larger cycles is unexpected as a reason for it is not obvious. A transesterification giving larger rings is not likely at the applied temperatures despite the presence of catalyst, according to the experiences with CBT100. The longer processing time might also explain the slightly higher part of hydroxyl termini in P1 compared to the samples taken before. The smaller amount of oligomers of P1 (of both precipitations) and P2 corresponds well with the high melting endotherms observed in DSC in this case. For the LM-cBT isolated as P3, a very low part of hydroxyl terminated chains (<1 mol-%) and an increased oligomeric ratio compared to CBT100 (>40 mol-%) were determined.

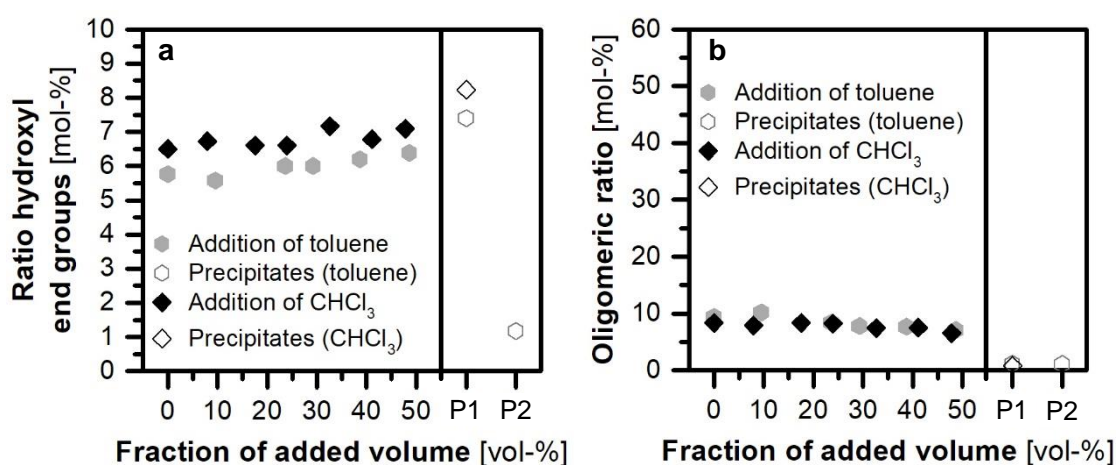


Figure 9: Results from ¹H NMR spectra in respect to the ratio a) of hydroxyl end groups and b) of oligomers with oligomeric character of cBT precipitated samples by addition of toluene CHCl₃ to a solution of cBT in oDCB as well as precipitates P1 and P2 (with constant fraction of solvents).

5.1.3 Isolation of low-melting cBT (LM-cBT) by utilization of low-boiling solvents

Further experiments were carried out with suspensions of CBT100 in CHCl₃ and in cyclohexane (CY), which is low-boiling as well. This seems favorable, after the derived effect of the temperature during precipitation on the properties of the thereby isolated cBT. The use of a low-boiling solvent is preferable over the high-boiling solvents used by PHELPS¹⁶⁴ with respect to economic and environmental effects. Some effort is necessary to strip isolated LM-cBT from higher-boiling solvents. Usually, preparation, manipulation and separation of aromatic MCOs is made in chlorinated aromatics as 1,2-dichlorobenzene (179 °C),

sometimes long-chained hydrocarbons as hexadecane (287 °C) or rarely in substituted aromatics as 1,2-xylene (144 °C). All tested separations by precipitation from the screened low-boiling solvents showed, however, issues regarding yield and/or melting behavior despite generally promising results.

From suspensions in CHCl_3 , fractions of LM-cBT were obtained in yields of up to 73 wt-% with melting temperatures below 170 °C and a suppressed crystallization in the cooling segment of DSC measurements. The amount of hydrolyzed MCOs was only about 0.1 mol-% but of the oligomers with 22 mol-% (according to $^1\text{H NMR}$) even smaller than in CBT100 (34 mol-%). No signs of degradation were observed. Unfortunately, it takes a long time, usually days, for the oligomers causing the higher melting MCOs to precipitate and hence until the low-melting fraction could be isolated by distillation from the filtrate.

To accelerate the precipitation, the less polar CY was screened as alternate solvent. Its solvation power proved to be not high enough to keep a significant amount of LM-cBT: The yield was only 1 wt-% (after removal of the cBT insoluble in reflux). However, the small isolated fraction of LM-cBT inhibited a moderate melting temperature of 172 °C, but a high amount of oligomers of 61 mol-% and no noteworthy fraction of opened rings. Nevertheless, these results prompted to use the combination of CHCl_3 and CY to obtain an adequate low-boiling solvent.

CY was added as precipitation solvent to a solution of CBT100 in CHCl_3 and the mixture was refluxed for equilibration. The formed precipitate was filtered off (Figure 10, precipitate P2). The high-melting insoluble fraction of cBT was removed prior to addition of precipitation solvent (giving precipitate P1) to obtain insight into the precipitating effect of CY. Similarly high yields of LM-cBT (precipitate P3) precipitated in hot condition as without CY, but in only 30 min instead of days. A further decrease of time without an extensive minus in yield seems possible but was not investigated. By addition of an equal volume of CY to the suspension, cBT with a melting temperature below 150 °C and a hindered crystallization by means of DSC measurements was recovered in 79 wt-% yield (Precipitate 1 - 3). A low oligomeric ratio of less than 26 mol-% was noticed for the LM-cBT in $^1\text{H NMR}$ and very low amounts of opened cycles of 0.1 mol-% like in utilization of CHCl_3 alone. Degradation of the MCOs during processing was negligible, which is consistent with observations in MALDI spectra. The unequivocal identification of the ring sizes in the LM-cBT was not possible by MALDI-TOF. The respective fractions showed signals of various ring sizes, mostly with 2 to 7 repeating units, and very small signals for larger cycles as well. The spectra of the higher-melting precipitates consisted, however, mainly of signals for cycles with 5 or less repeating units and comparatively more signals of various degradation products or impurities.

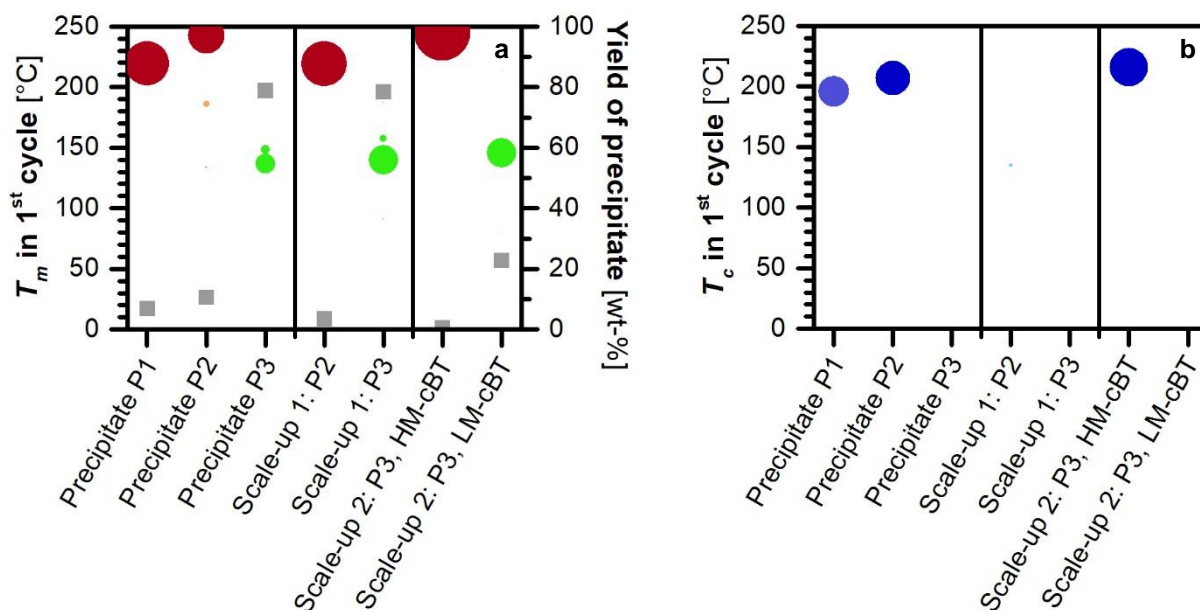


Figure 10: a) Melting and b) crystallization temperatures according to DSC of precipitations of cBT from mixtures of CHCl_3 with CY (size of markings indicate ΔH_m) and yield of respective fraction (squares). Precipitate 1 is the CHCl_3 insoluble fraction, Precipitate 2 was filtrated after addition of CY and Precipitate 3 is the cBT in the filtrate thereof, LM-cBT of scale-ups is the equivalent to Precipitate 3 with HM-cBT isolated thereof.

An additional melting endotherm of comparatively small ΔH_m was observed in doubled size experiments (Figure 10a, Scale-up 1). Melting temperatures above 240 °C were found for this fraction, which had formed in the filtrate shortly after filtration. The melting temperatures were usually lowered in mixtures with other oligomers by colligative effects. The formation of this high-melting cBT (HM-cBT) is probably caused by the prolonged processing times for hot filtration. HM-cBT fraction precipitated from a filtrate containing only LM-cBT selectively (according to quick removal of solvent and DSC measurements of one part of this filtrate) (Figure 10a, Scale-up 2). A formation of larger cycles with time can be ruled out in these cases as no transesterification catalyst was present and these reactions are regarded as comparatively slow, especially at the applied temperatures. This issue hampers an unrestricted usage of this method for reproducible isolation of LM-cBT, but demonstrates the general applicability of low-boiling solvents for isolations of LM-cBT instead of the commonly used high-boiling ones.

5.1.4 Extraction of cBT

An extraction of cBT fractions with a reduced melting temperature than CBT100 is another possible route to circumvent the disadvantages of PHELPS' method to a certain extent by these actions:

- The utilization of a low-boiling instead of a high-boiling solvent makes drying processes less energy intensive and thus ecologically and economically friendlier (compare to chapter 5.1.3, p. 48 ff.).
- Less heating and cooling steps are necessary than in the method suggested by PHELPS.
- The precipitation of oligomers is uncertain with respect to the necessary time and to completeness. This can be evaded by using the temporal reliable process of extraction.
- The procedure of PHELPS is limited to low concentrations (5 to 10 wt-%) caused by limited solvation, which limits the amount of LM-cBT by precipitation and filtration.

Extraction does not suffer from these restrictions. A constant exchange of the solvent is simply possible. The focus of this study was the demonstration of the applicability of the extraction process for isolation of LM-cBT. Therefore, various extraction methods, solvents and different states of comminuting of the cBT pellets have been explored and scale-up experiments have been carried out. The low-melting fraction of cBT showed a higher solubility in all explored solvents. Hence, the cBT in the extraction solvent and its properties, not the remaining cBT after extraction, was of main interest.

5.1.4.1 Influence of extraction method

Two different extraction methods were explored: extraction according to SOXHLET and according to KNÖFLER-BÖHM (Figure 11). In the first, evaporated solvent is led to a condenser to return through the extraction material back to the reservoir. In the latter, the evaporated solvent is additionally used to heat the apparatus including frit and extraction material. CY was chosen as extracting agent after the, in principle, promising results mentioned above (chapter 5.1.3, p. 48 ff.). The flask with solvent was repeatedly exchanged for a new one with "fresh" solvent and the respective content was separately analyzed to obtain insight into the time dependent extracts. The initial melting endotherms during the first heating segment of DSC measurements of the extracted fractions are given by the colored marks (peak temperatures). The color from red to green indicates the temperature in relation to the melting temperature of CBT100 as described above. The size of these markings correlates to

the respective ΔH_m , again. The results for the residue in the extraction thimble after extraction are given under “R” on the x-axis. The accumulated yield of cBT extracted from the CBT100 at the respective time is marked with grey, semitransparent squares.

Partially, fractions with lower melting temperatures are formed by the method of SOXHLET, but less reliably than by extraction according to KNÖFLER-BÖHM. By the latter method, cBT fractions with rather constant melting temperatures and in higher yields were obtained.

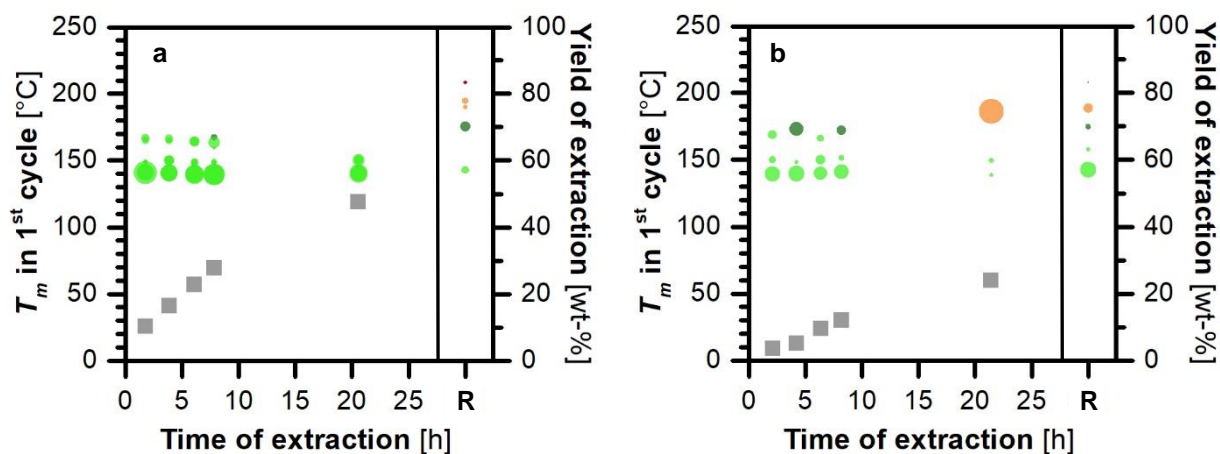


Figure 11: Results of the iterative extraction of CBT100 with CY as solvent according to a) to KNÖFLER-BÖHM and b) to SOXHLET. (Round markings stand for T_m with indication of the relative ΔH_m by their size and grey squares for the total yield of extracted cBT at the respective time).

Similar cBT fractions were obtained by both methods in respect to the oligomeric ratio and the amount of hydrolyzed or degraded cycles according to ^1H NMR spectroscopy (Figure 12). The oligomeric ratio calculated from the aromatic signals are some of the highest observed in this study (52 ± 1 and 53 ± 4 mol-%, resp.). A low amount of opened cycles was further calculated for both extractions (0.5 ± 0.2 and 0.3 ± 0.1 mol-%) that apparently proceeded without further degradation. Further exploration of the extraction of cBT was carried out with the setting of KNÖFLER-BÖHM as result of these findings.

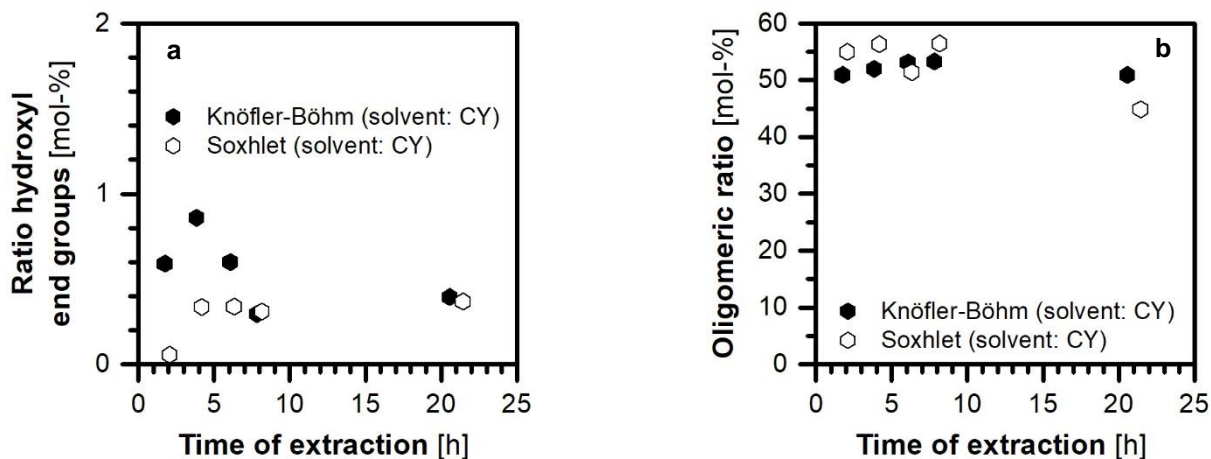


Figure 12: Evaluation of ^1H NMR samples of the extractions of CBT100 by the two extraction methods: a) fraction of hydroxyl end groups (determined by the ratio of $-\text{CH}_2\text{-OH}$) and b) ratio of oligomeric character (according to aromatic signals).

5.1.4.2 Influence of solvents on the extracted fraction

The influence of the solvent polarity and water miscibility on the extraction according to KNÖFLER-BÖHM procedure was explored by comparing the results of extraction with CY to those with CHCl_3 or THF. All three solvents have a low boiling temperature of 81, 61 and 65 °C, respectively. CY may have a higher boiling temperature but showed some advantages regarding the extraction of LM-cBT over CHCl_3 and THF despite a smaller yield of extracted cBT (grey semitransparent squares in Figure 11a and Figure 13).

The extraction with all three solvents yielded cBT with a melting temperature below 170 °C (Figure 11a and Figure 13). The extracts by CHCl_3 however contained a fraction of high-melting cBT in all samples that eluted before 4 hours (see chapter 5.1.3, p. 48 ff.).

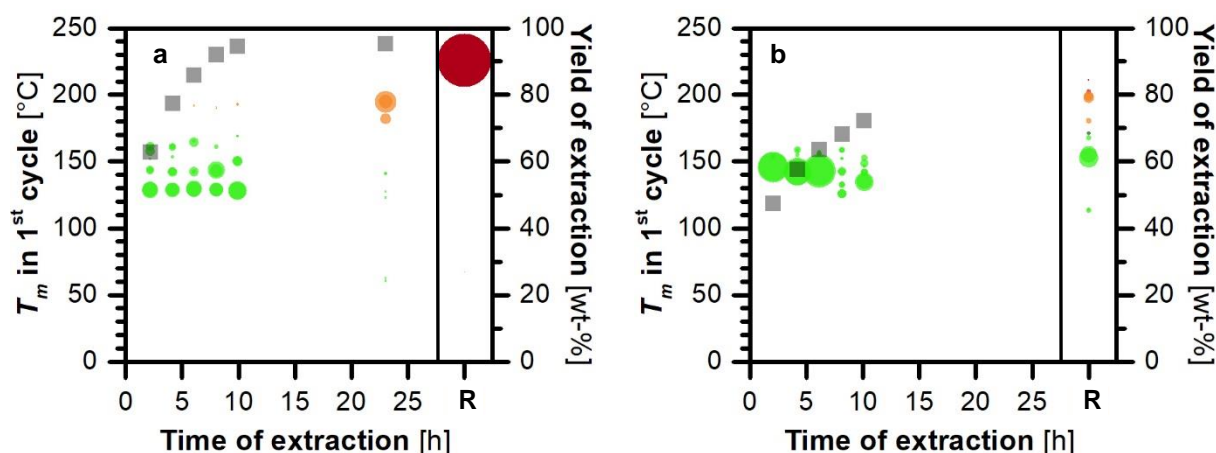


Figure 13: Results of the iterative extraction of CBT100 according to KNÖFLER-BÖHM with a) CHCl_3 and b) THF, to compare to Figure 11a. (Colored markings stand for T_m with indication of the relative ΔH_m by their size and grey, semitransparent squares for the total yield of extracted cBT).

The solubility in CHCl_3 seems to be too high to allow a separation of the cBT by extraction. It effectively dissolves all cBT except the highest-melting oligomers from the CBT100 composition. The frit after CHCl_3 extraction contains only cBT with very high melting temperatures ($T_m > 225$ °C), while a variety of melting endotherms between 142 – 208 or 114 – 212 was found for the residues of CY and THF, respectively. This agrees well with the smaller yield of LM-cBT obtained with the latter two solvents. The existence of endotherms at lower temperatures than in CBT100 is probably caused by the colligative interaction of the different oligomers once more.

The melting temperatures of the extracted fractions with THF are slightly smaller than those of the CHCl_3 extractions within the first two hours of extraction and of those with CY (respective upper limit of melting peaks and endset temperatures for THF, CHCl_3 and CY of below 160 & 175, 162 & 168, 166 & 178). It is not clear if a more polar solvent generally extracts lower-melting cBT fractions (at least at the beginning) or if it is only an artefact in the DSC measurements. Later fractions of the CHCl_3 extraction have a higher melting temperature of 188 – 192 °C (endset 194 – 202 °C). The melting behavior of extracts from the other solvents is constant over the time of extraction.

The higher hydrophilicity of THF leads to a higher effort for water-removal. The measures taken for CHCl_3 and CY are not sufficient for THF. The remained water in THF readily reacted with the cBT cycles. The ratio of opened cycles determined by ^1H NMR spectroscopy (in accordance with general observations in MALDI-TOF) was below 1 mol-% for CY and CHCl_3 but significantly higher for THF (2 – 6 mol-%) (Figure 14a).

The highest concentration of oligomers as estimated from the aromatic signals in ^1H NMR spectroscopy was observed in extractions by CY (52 ± 1 mol-%), increased in extractions by THF (40 ± 2 mol-%) and unchanged with CHCl_3 (34 ± 3 mol-%) in comparison to CBT100 (34 ± 2 mol-%) (Figure 14b).

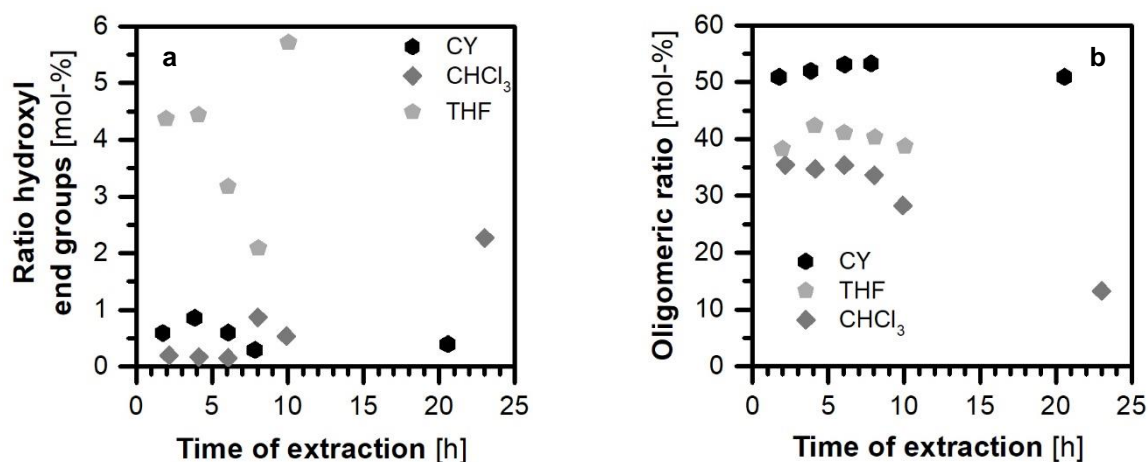


Figure 14: Evaluation of ^1H NMR spectroscopy of CBT100 extractions with different solvents: a) fraction of hydroxyl end groups (determined by the ratio of $-\text{CH}_2\text{-OH}$) and b) ratio of oligomeric character (according to aromatic signals) (Data for CY repeated from Figure 12 for better comparison).

MCOs with an odd number of repeating units were particularly prominent in MALDI-TOF analysis for all extracts. A smaller number of repeating units was observed for extraction by CY than by CHCl_3 or THF. Mainly MCOs with 5 or less repeating units were detected for CY with the peaks of 3 and 5 being generally dominant, those with 7 or less were detected for CHCl_3 and THF with 3 to 5 or 5 and 7 being dominant, respectively. No dependency of the ring size on the extraction time was observed in any case.

All further experiments were carried out with CY. The easy accessibility of cBT fraction of constantly low melting temperatures compared with only small ratios of hydrolyzed cycles and a highly oligomeric character of the products made the extraction with CY superior to those with CHCl_3 or THF.

5.1.4.3 Effects of scale-up on extraction with cyclohexane

Scale-up experiments were carried out for CBT100 extraction with CY. The form of the apparatus had to be adapted to hold a higher mass. The extraction thimble used in the classical setup of KNÖFLER-BÖHM, with cycles of filling with solvent by condensing hot solvent and periodically releasing, was substituted by a frit with the pore size G2. By this, solvent continuously passed through the substrate. This is the standard setup for extraction of solids

in warm state and comparable to that of the TWISSELMANN procedure. The length of the frit was chosen to accommodate the respective amount of CBT100 (130 or 340 g). The diameter was constantly 7 cm.

A similar result was obtained for all scales (including the small scale of 15 g in the classical KNÖFLER-BÖHM apparatus). Similar curves for the yield of extracted cBT with time were obtained (Figure 15) with maximal yields of 48, 44 and 65 wt-%, respectively (reached after various time). The large-scale experiment was prolonged compared to the others to investigate a possible increase of the yield. The lower values of the largest scale in the yield-time curve is probably caused by a longer time of heating before start of extraction due to the higher mass and by clogging of the frit due to “sticking” cBT pellets by partly solvent penetration and solvation. The latter effect was observed for all scales but was more pronounced for a higher fill level of the frit, i.e. for the largest scale.

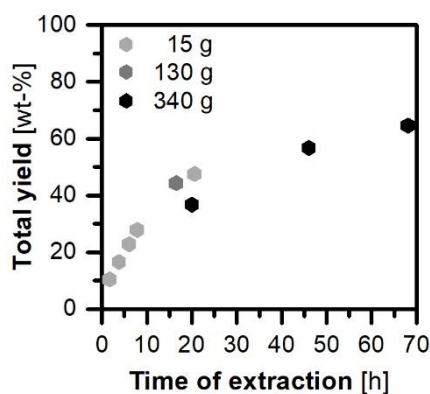


Figure 15: Yield of the extraction of CBT100 with CY (frit porosity G2) in the scales of 15 g (data repeated for comparison from Figure 11a), 130 g and 340 g. Results for 15 g scale obtained by a setup accordingly KNÖFLER-BÖHM, for the others by a setup comparable to TWISSELMANN.

The extracted fractions revealed a similarly low melting temperature in DSC measurements being constant or even decreasing with the time of extraction (Figure 16). Long extraction times as used for the large scale resulted in the presence of additional melting endotherms at a higher temperature in the extracted fractions. Side reactions at long reaction times are probably responsible, assisted by the restriction of solvent flow from the clogging of the frit mentioned above. This behavior is similar to the appearing of high melting fraction during precipitation from CHCl_3 or THF reported above (chapter chapter 5.1.3, p. 48 ff.). The access of higher amounts of LM-cBT by upscaling is successfully proven for moderate extraction times in this set-up. The extraction could be further optimized; complication with respect to the composition is not expected.

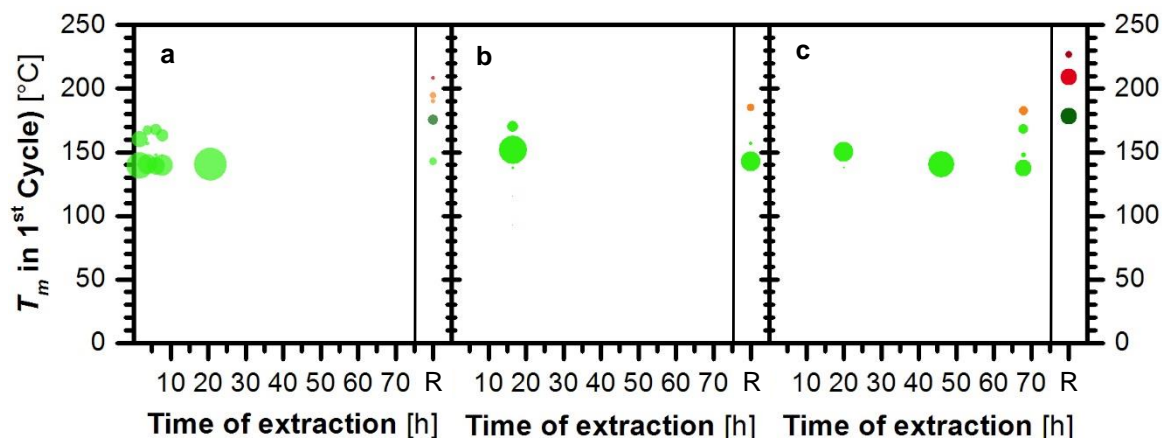


Figure 16: Melting peaks of the fractions extracted from CBT100 with CY (frit porosity G2) in the scales of a) 15 g (data repeated for comparison from Figure 11a), b) 130 g and c) 340 g. The size of the markings indicate the relative ΔH_m , the results for the residue in the frit after extraction are given under R on the x-axis.

The highest counts in MALDI-TOF of the extracts were observed for cycles with up to 5 repeating units accompanied by small signals for 6 and 7. No significant signals for opened species were observable. Contrary, a small decrease of the amount of opened cycles was recognized by ^1H NMR spectroscopy, although it has to be noted that values from ^1H NMR that small will have a substantial uncertainty (Figure 17a). No indications of other degradation during the differently scaled extractions were to be seen. A comparatively high oligomeric ratio was calculated from ^1H NMR data for extractions in all scales, higher for small and medium scale (ca. 51 mol-%), smaller for the large scale (about 44 mol-%) (Figure 17b), which fits the higher-melting endotherms observed in DSC in this case.

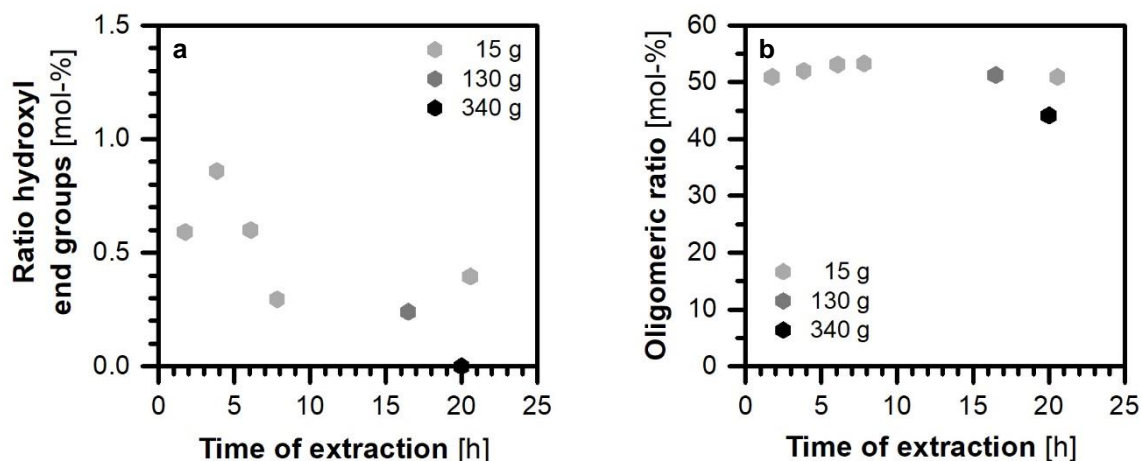


Figure 17: Evaluation of ^1H NMR spectroscopy of the scale-ups with CY regarding a) the fraction of hydroxyl end groups (determined by the ratio of $-\text{CH}_2\text{-OH}$) and b) the oligomeric ratio (according to aromatic signals) (Data for 15 g scale reproduced from Figure 12 for better comparison).

High-melting endotherms were found for the frit residue of the largest scale after extraction (Figure 16, indication “R” on abscissa). The difference to the former experiments was to be expected because of the higher yield of extracted cBT obtained after the longer time.

SEM images give similar impressions for the residues from the medium- and large-scaled experiments (Figure 18), which differ in some aspects from those of CBT100 (chapter 5.1.1.5, p. 43 f.). (The residue from the small-scale extraction has not been analyzed by SEM.) A preferred extraction of the amorphous fraction and possibly a recrystallization process appears to take place. Related rearrangement processes have previously been reported for PET kept in a swollen state (in supercritical fluid) above the T_g for some time.^{209–216}

The outer layer of the pellets from the residues consists of a maze of large plates of up to $15\ \mu\text{m}$, which is generally larger than those observed in CBT100. The residues have no amorphous matrix. It suffered in most samples from mechanic abrasion during isolation. A higher thickness of the outer layer is noticed in samples of the large-scale experiment compared to the medium-sized one.

The inner phase is similar to that of CBT100, which indicates a less intense material loss of this area. Crystalline plates of generally smaller dimensions than in the outer layer (mostly $\leq 5\ \mu\text{m}$) within an amorphous matrix were observed. No difference between the medium and large-scale extraction was noticed in this respect.

An additional intermediate layer was observed in all extracted cBT samples, which is not present in the starting material CBT100. It usually consists of small stacks of small plates

(<15 μm , often <5 μm) and fragments in amorphous matrix. Its crystalline fraction appears increased compared to the inner phase or to CBT100. This suggests a preferred dissolving of amorphous material during extraction and/or a recrystallization process taking place simultaneously to the extraction. The intermediate layer has a sharply defined delimitation to the outer layer and transforms smoothly into the inner layer. Its layer thickness is in a similar range for medium and large scale as expected from the yield. Its distribution however was wider within the samples of the medium than of the large scale with its higher yield of extract (110-430 μm and 173-348 μm).

A small area beneath the outer layer seems to be partially depleted in crystallites within the extraction in largest scale, which had the highest yield at the end. This has been observed in more distinct form in other high yielding experiments discussed below, too (chapter 5.1.4.5, p. 63 ff.).

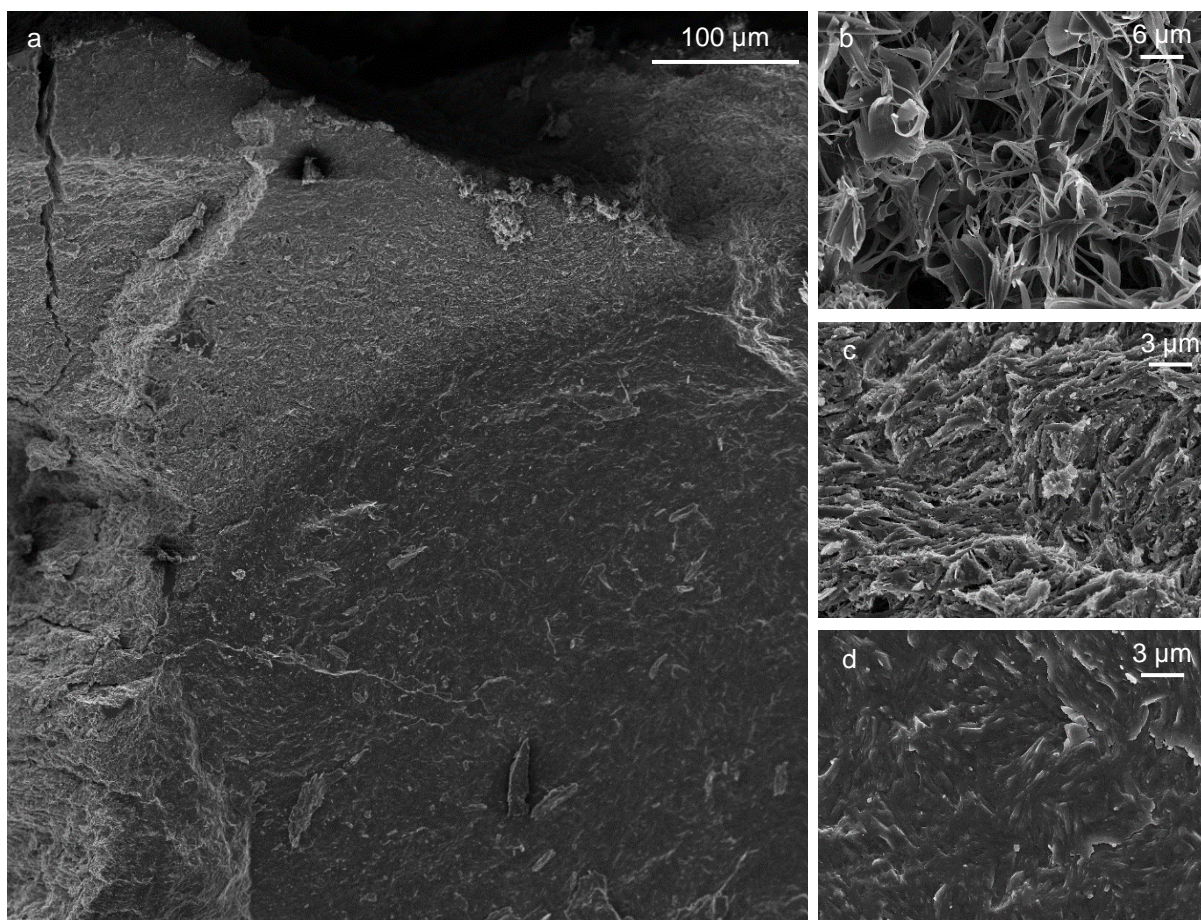


Figure 18: SEM Images from medium-scale extraction (130 g, pore size of frit G2) a) of the three layers (only small remains of outer layer visible in this picture) (by InLens detector), b) of the outer layer (top view by InLens detector), c) of the intermediate layer (by InLens detector) and d) of the inner phase (by InLens detector).

5.1.4.4 Extractions using fused silica frits with other pore sizes

The pore size of the used silica frits was varied to evaluate the influence of the flow rate of the extraction solvent through the extraction space and hence the retention time of the solvent in the frit. Therefore, ca. 130 g CBT100 were extracted with CY utilizing frits with a porosity of G0, G1 and G2 (in compliance with ISO 4793 these are nominal pore sizes of 160 – 250, 100 – 160 or 40 – 100 μm , respectively).

No dependency of the melting temperature on the utilized pore size was found for the extracted fractions. The yield showed a dependency (Figure 19a). LM-cBT was isolated with each pore size possessing multiple melting endotherms with the highest melting peak below 170 $^{\circ}\text{C}$. Its yield in a comparable time increased with decreasing pore size and hence with increasing retention time of the solvent in the frit. A yield of 44.4 wt-% or 37.3 wt-% was achieved with size G2 and G1 in 16 h and of 17.4 wt-% with G0 after 10 h (the yield was already below those with the other frits at this time). This order is unexpected as the passing of the solvent through the cBT in the frit was much faster for larger pore sizes. An intensified clogging of the frit was also observable for the frit with smaller pore sizes, which obviously did not have a major effect on the yield at the scales used in this experiment.

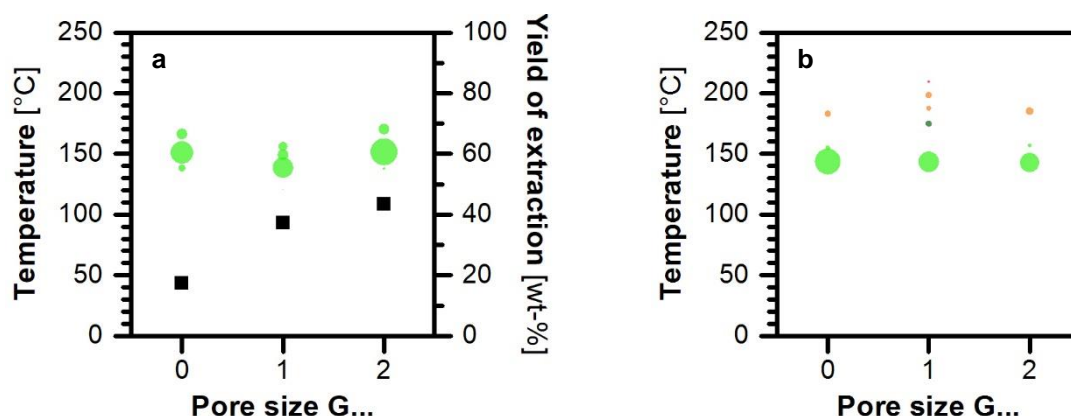


Figure 19: DSC analysis of the melting (with depiction of the respective yield as black squares) of the extraction of CBT100 with CY with utilization of different pore sizes of the frits. a) Results of the extracted fractions and b) of the residues in the frits (the size of the markings indicate the relative ΔH_m). Results after 16 h of extraction for G2 and G1 and 10 h for G0.

The ^1H NMR spectra indicated only remarkably small amounts of opened cycles in all of these experiments (Figure 20). Small signals for opened cycles were detected by MALDI-TOF spectrometry only for extraction with the smallest pore size. A noteworthy high fraction of oligomeric cBT of above 48 mol-% was found for the three variations. The lowest value

was calculated for the frit with the medium-sized pores (54, 48 and 51 mol-%, G0, G1 and G2 respectively).

MCOs with mainly 5 or less repetition units were detected by MALDI-TOF for extractions with the frits with only traces of larger cycles of 6 or 7 repetition units.

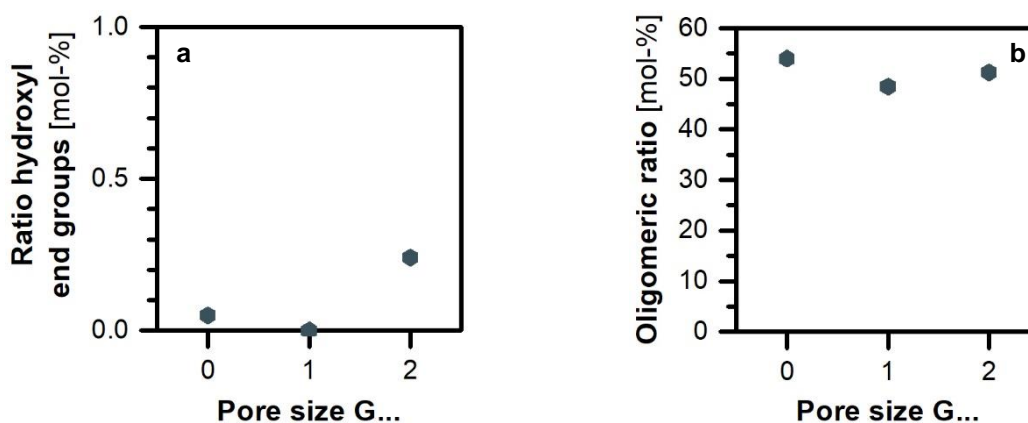


Figure 20: Results of ¹H NMR spectrum evaluation of the extraction of CBT100 with a frit porosity of G0, G1 or G2 with respect to a) the fraction of hydroxyl end groups (determined by the ratio of -CH₂-OH) and b) the oligomeric ratio (according to aromatic signals).

The residues in the respective frit after extraction possessed melting endotherms that were interestingly in part below those of unprocessed CBT100 (Figure 19b). The colligative interaction of the different cBT oligomers in the composition is probably the reason. The intense melting peaks below 160 °C seem to indicate that more material may be extracted to improve the yield.

Images by SEM of samples from the residues resemble those described in the previous chapter with their differences to CBT100 (Figure 21, Figure 22 and Figure 18 for pore sizes G0, G1 and G2). The outer layer consists of a maze of large plates of up to 15 μm (in general larger than in CBT100) without an amorphous matrix. The plates themselves are partly “frayed” from the ends and in case of porosity G2 even completely dissolved in some areas. An internal phase, that is similar to that of unmodified CBT100, indicates an incomplete solvent penetration in this series of extractions too. The number of plates in the inner area seems to be reduced by the extraction in all cases. This observation might be biased as the number of images is limited.

The observed additional intermediate layer in the extracted cBT samples seems to become thicker with decreasing pore size, but this differs in some aspects between the samples of one extraction. It was found to be 35 – 94 μm thick at extraction with frit of the porosity G0 (pores of 150 – 250 μm), with G1 (pores of 100 – 160 μm) 94 – 235 μm and with G2 (pores

of 40 – 100 μm) 110 – 430 μm . This increasing amount of intermediate phase correlates well with the isolated amount of LM-cBT by the extractions.

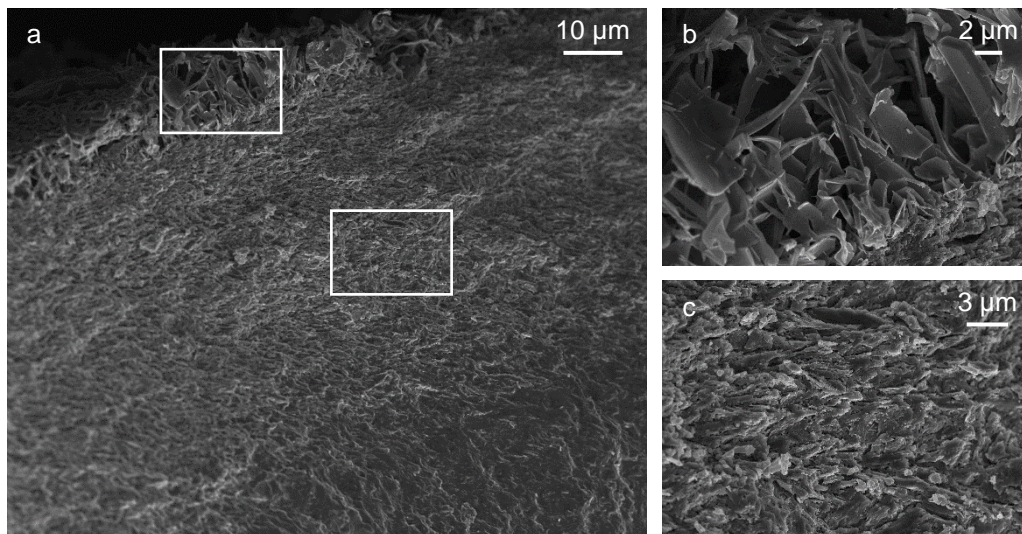


Figure 21: SEM Images (all by InLens detector) after extraction using a frit with pore size G0 a) of the three layers, b) of the outer layer and c) of the intermediate layer.

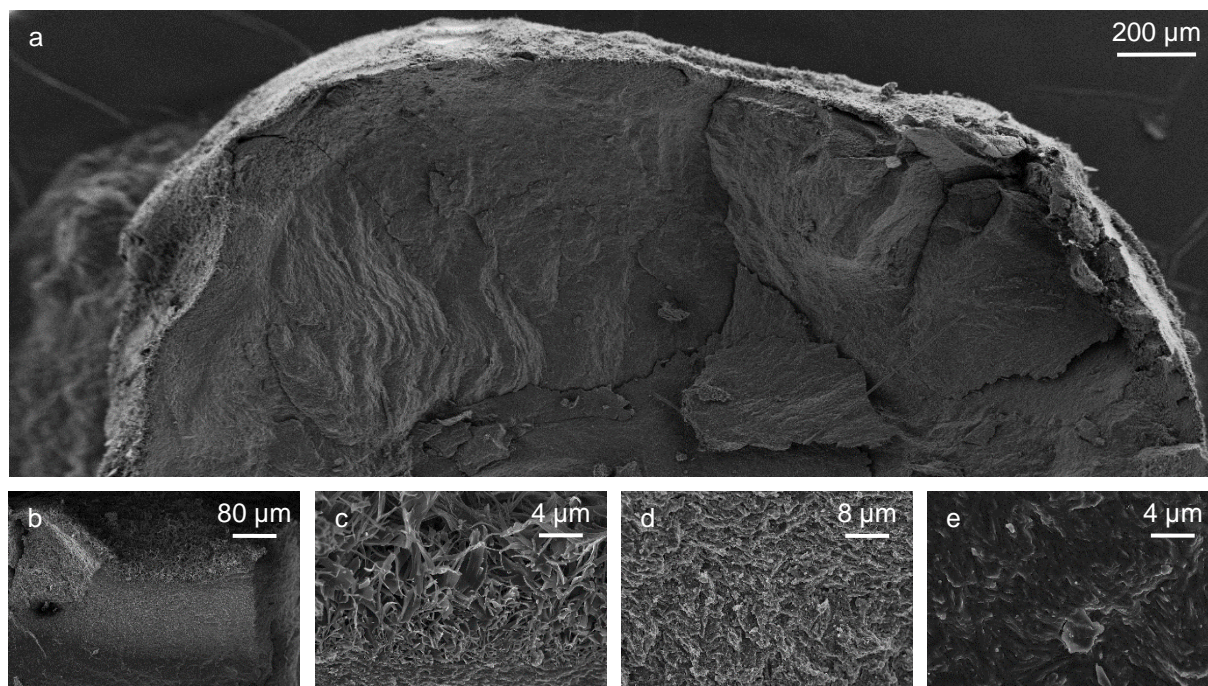


Figure 22: a) SEM Images after extraction using a frit with pore size G1, b) of the three layers (by SE2 or InLens detector, respectively), c) of the border between outer and intermediate layer (by InLens detector), d) of the intermediate layer (by InLens detector) and e) of the inner phase (by InLens detector).

5.1.4.5 Change of cBT grain size on the extraction process

The challenge of clogging of the frit due to sticking of the cBT pellets (see chapter 5.1.4.3 and 5.1.4.4, p. 55 ff.) was addressed by variation of the grain size of the cBT. The effect on the yield was evaluated, which seemed to be limited by the penetration depth of the solvent into the pellets. Extractions of cBT with different degrees of grinding were explored as well as that of grinded cBT mixed with cBT or PBT pellets as spacers in-between.

Grinding was generally found to be challenging because of the brittle nature of cBT. Only fine cBT powder was obtained by various attempts of grinding, e.g. with a rotor speed mill or with a cutting mill, either equipped with sieve rings or grinding inserts of various sizes. A controlling of the grain size was not possible by these methods. Homogenous powder was obtained with a reduction by at least a factor of 9 and an average edge length of about 1/20 compared to the length originally observed in images of CBT100 (estimated from optical microscopy; Figure 23e). All manipulations resulted in a comparable minimal length of particles with an edge length of about 10 to 25 μm (about 1/120 to 1/50 compared to CBT100) due to the mentioned brittle nature of cBT. Hence, alternatives providing possibly less controlled but therefore larger grain sizes were explored.

Manual grinding in a mortar and crumbling of CBT between two steel plates resulted in similar average edge lengths (reduction of length by a factor of about 18) as electrical milling, but with a broader distribution (Figure 23b and d). A more complete and effective decrease of the maximal edge length was accomplished by crumbling between steel plates than by grinding in a mortar (reduction factor about 5 vs. 3). The microscopy images of the less thoroughly grinded cBT met expectations as very finely grinded as well as non-affected cBT pellets can be observed. This is reflected by a comparatively high standard deviation of the average particle size.

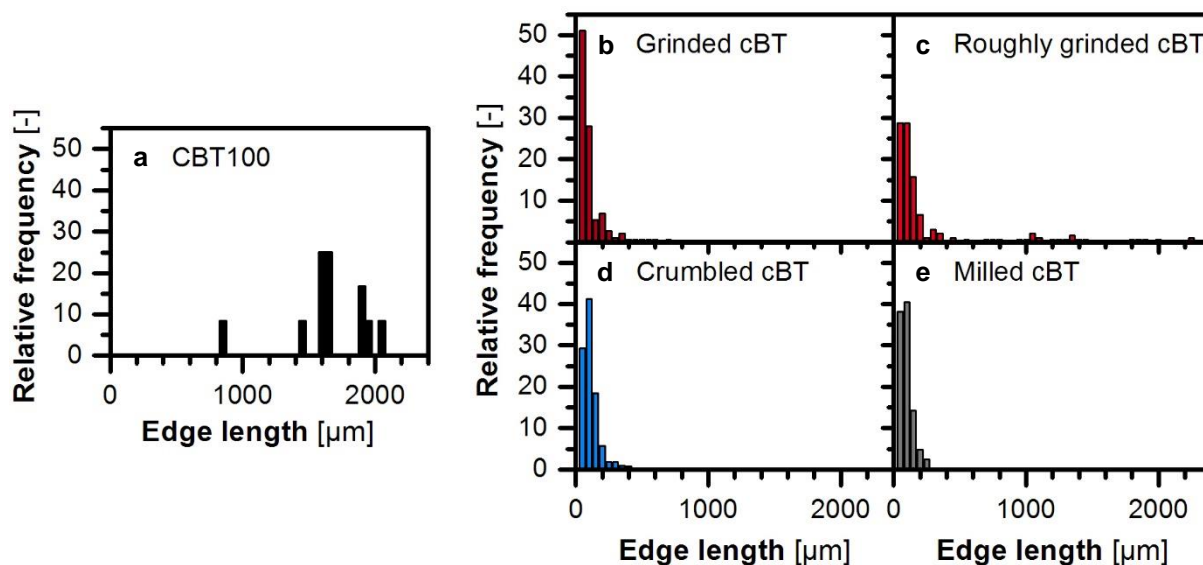


Figure 23: Relative distribution of edge lengths in processed CBT100 according to optical microscopy: a) CBT100 as delivered, b) thoroughly and c) roughly manually grinded in a mortar, d) crumbled between steel plates and e) treated in a rotor speed mill.

The extractions were carried out on a scale of 130 g CBT100. It was placed in a frit with a bottom of fused silica of porosity G0 with CY as solvent. G0 was chosen despite the better yield of G2 because of its lower amount of opened cycles in the extract and the less extensive clogging of the frit allowing a more appropriate comparison of the results (chapter 5.1.4.4, p. 60 ff.). The used cBT types were: cBT finely or roughly grinded in a mortar, cBT granulate just crumbled between steel plates, a mix of roughly grinded cBT and non-processed cBT granulate in a ratio of 1:1 or of cBT granulate mixed with PBT granulate in a ratio of 2:1 (Table 2). The enhancement of solvent flow by passing an argon (Ar) stream through the cBT in the frit by means of a cannula was explored in an additional experiment but did not have an effect on the yield, as expected.

Table 2: Conditions of the extractions of cBT in various grain sizes (in a frit with a porosity G0 and a length of 12 cm).

Exp. no.	Mass of used cBT [g]	Processing of cBT	Additional modification	Time of extraction [h]	Yield of extract [%]
1	130	grinded in mortar		40	1.5
2*	330	grinded in mortar		40	0.3
3	65	grinded in mortar		24	21.4
	65	CBT100			
4	114	grinded in mortar	PBT pellets (63 g)	24	7.7
5	131	roughly grinded		24	55.6
6	130	crumbled		20	39.0
				44	43.5
7	130	milled	Ar flow	9	0.8

*Usage of a longer frit of 26 cm with porosity G2.

5.1.4.5.1 The extracts

LM-cBT was obtained by extraction of all evaluated grain sizes with melting temperatures of about 160 to 166 °C although it was accompanied by an additional high-melting fraction in smaller-scale extraction when using grinded cBT (exp. no. 1 in Table 2). The yield was dependent on the grain size and its distribution as expected (Figure 24a). This also applies for the content of opened cycles and the oligomeric ratio (Figure 25). Two samples of every fraction were measured by DSC (except for the low-yielding extractions with just grinded cBT in different scales, exp. no. 1 and 2 in Table 2) with a close resemblance. The results of only one sample are depicted. A high amount of small cycles was generally obtained in the extracted fractions compared to CBT100 and to the residues after extraction (according to the ratio of the aromatic signals in ¹H NMR and MALDI-TOF). Only in case of the product from extraction of crumbled CBT100 (exp. no. 6), a lower oligomeric ratio that in CBT100 is observed. No correlation was observed between the oligomers in the extracted fractions detected by MALDI and the yield of the fractions nor their melting temperatures. All MALDI spectra of the extracts were dominated by the peaks of the tri- to pentamer. Signals of the tetramer were absent in some extractions (exp. no. 4 and 6). The hexamer was additionally observed in the extraction of coarsely grinded cBT (exp. no. 5), the one with the highest yield.

Extractions with a higher yield exhibit minor signals of impurities in MALDI spectrometry and ^1H NMR spectroscopy. The impurities in CBT100 may have preferably been extracted at the beginning. The low yield extraction of finely grinded CBT100 (without any added “fillers” like cBT or PBT pellets, i.e. exp. no. 1 and 2) resulted in an extract with decomposition products. Additional peaks were noticed in ^1H NMR as well as a yellowish color and an acid odor similar to that of thermally degraded PBT.

The amount of opened cycles calculated from NMR spectra are higher than in CBT100 (>8 vs. 2 mol-%). The utilization of equipment with a frit with pore size G2, which was previously found to lead to a superior yield (at the expense of further impurities) (chapter 5.1.4.4), and of a larger scale (exp. no. 2) actually “improved” the melting behavior of the extract significantly but did not result in an improvement of yield (Figure 24a, exp. no. 1 and 2).

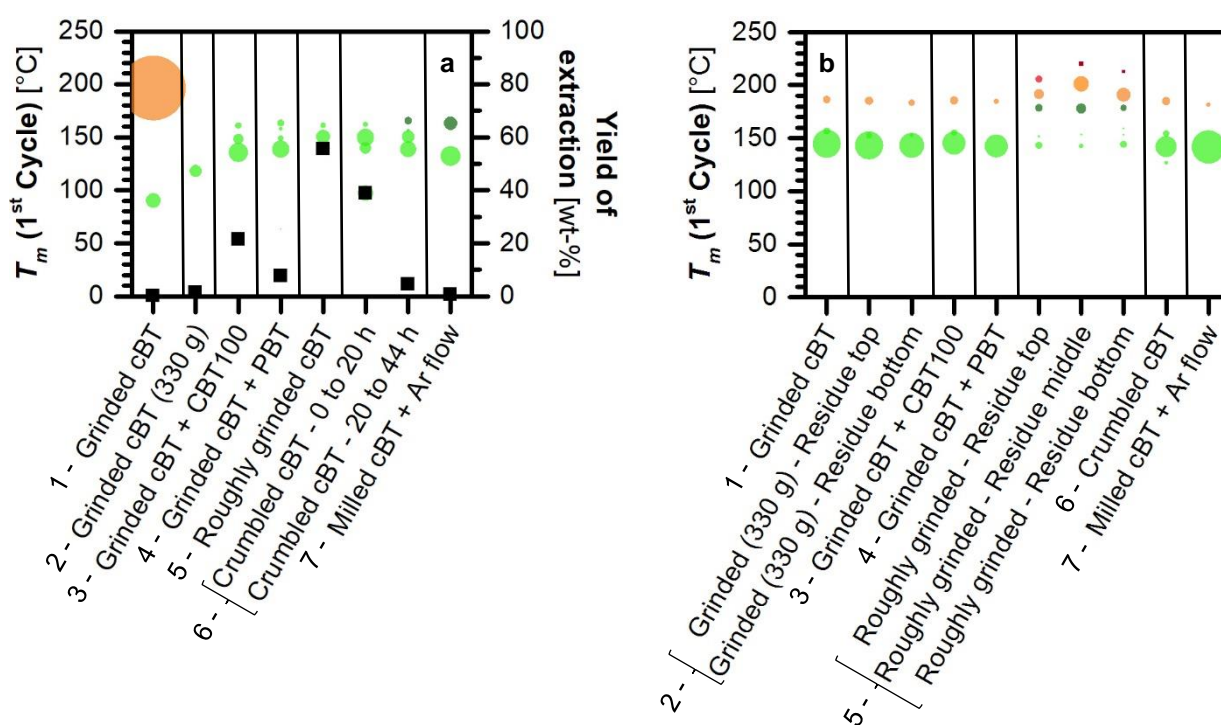


Figure 24: DSC-based analysis of the extraction of differently processed CBT100 (numbers indicate exp. no. from Table 2). a) Melting endotherms (colored markings) and the obtained yields (black squares) of the respective fractions and b) melting endotherms of the residues. The size of the endotherm markings correspond to their respective ΔH_m .

The addition of cBT or PBT pellets to grinded cBT (exp. no. 3 and 4) for loosening the packing of the material resulted indeed in an increase of space-time-yield relative to the extraction of grinded cBT (Figure 24a, exp. no. 3 and 4). It was higher for the utilization of cBT than for PBT pellets. The same amount of cBT was used in both extractions, but the

total volume was higher when additional PBT was present. This additional mass had to be passed and heated by the solvent, which probably caused the different performance. Very similar thermograms were observed for both experiments. ^1H NMR spectra proved the presence of impurities especially in case of added cBT granulate. The ratio of hydroxy termini is significantly lower in both cases than in the extractions of only grinded cBT or in non-treated CBT100 itself (0.4 or <0.1 mol-% for addition of CBT100 or PBT compared to 8.7 mol-% for grinded cBT and 1.9 mol-% for CBT100) (Figure 25a).

Extraction of cBT in coarse grain (only roughly grinded or crumbled CBT100) resulted in a further increase of the yield of LM-cBT. The amount of linear chains is reduced below the detection limit of ^1H NMR spectroscopy (Figure 25a, column 5 to 7). Results of the extraction of crumbled cBT were evaluated after 20 and after 44 h to estimate the effect of prolonged extraction. The melting endotherms were similar but tended to higher values at longer extractions. The space-time-yield decreased drastically during the prolongation (39.0 wt-% after 20 h, 4.5 wt-% after additional 24 h) as observed before in this study (Figure 24a).

The extraction enhanced by an Ar stream for loosening of the extraction material resulted in the mentioned low yield (Figure 24a) and in a small but noticeable amount of linear chains in the extract (Figure 25a, column 8). The latter is probably caused by the degradation observed for extractions of finely powdered cBT.

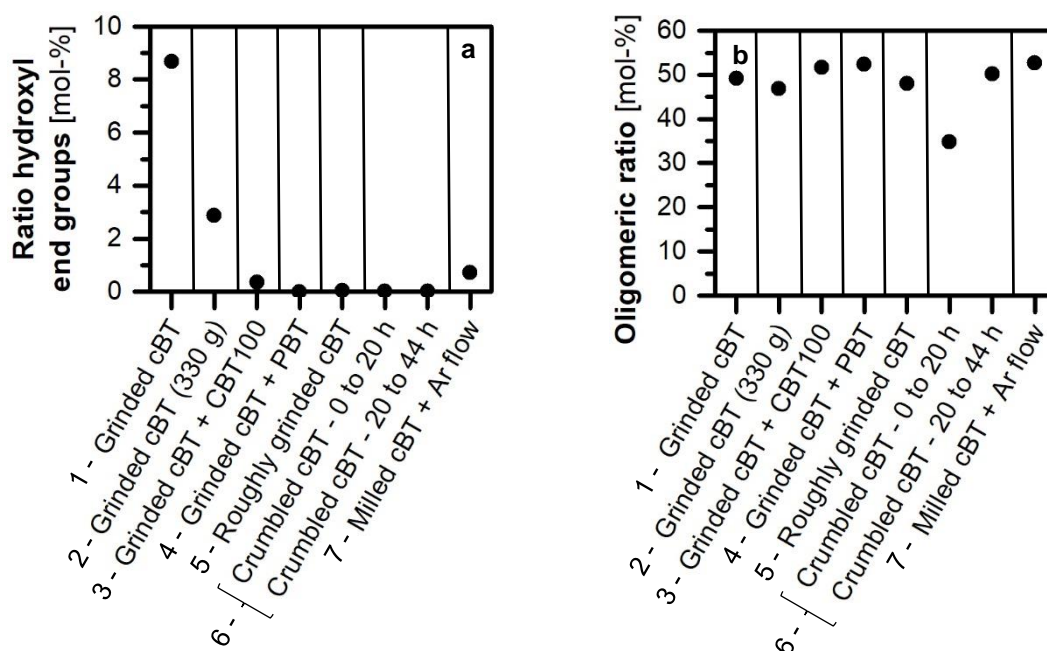


Figure 25: Results of ^1H NMR spectroscopy evaluation for the extractions of differently processed CBT100 (numbers indicate exp. no. from Table 2) in respect of a) the fraction of hydroxyl end groups (determined by the ratio of $-\text{CH}_2\text{-OH}$) and b) the oligomeric ratio (according to aromatic signals).

5.1.4.5.2 The residues after extractions

The melting temperature of the cBT residues after extraction was generally higher if a noticeable yield of extracted fraction was obtained (Figure 26). (The correlation of highest melting temperature and yield are depicted in this figure for extractions with at least 50 g of extraction material (from chapter 5.1.4.3, 5.1.4.4 and this chapter) to avoid scale-related effects in smaller batches.) The residue's melting temperature in dependence of the yield are probably caused by the complex formation of the melting endotherms by interaction of the cBT oligomers amongst each other.

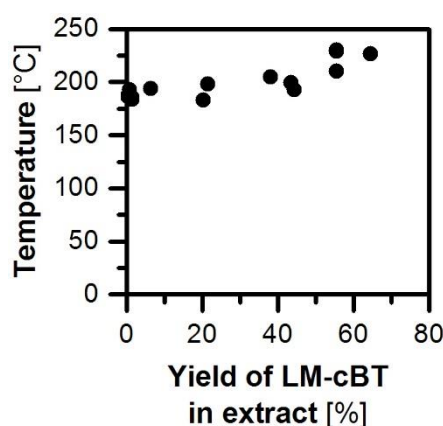


Figure 26: The melting temperature of the residues after extraction in dependence of the yield of cBT extracted therefrom for extractions of 50 g or more CBT100.

MALDI-TOF spectra of samples from the residues showed signals from larger cycles than observed in the extracts. They consisted mainly of signals for cyclic tri- to heptamers with very small peaks for oligomers with 11 or less repetition units. Small but identifiable signals of linear impurities were observed with 8 or less repetition units, which were already observed in CBT100 (chapter 5.1.1.3, p. 39 ff. and Figure 3). The extraction with the highest yield (coarsely grinded cBT, exp. no. 5) resulted in MALDI spectra with a reduced signal of cyclic trimer compared to the other spectra. This can be a hint for a preferred extraction of the trimer.

The SEM images appeared similar to those described in chapter 5.1.4.3 (p. 55 ff.) and 5.1.4.4 (p. 60 ff.). The three different layers are visible within the cBT residues after extraction (Figure 27). Extractions with high yields (>45 wt-% in exp. no. 5 and 6) exhibit a fourth layer with an amorphous appearing and depleted in crystallites right beneath the highly crystalline outer layer as already observed for the large-scale extraction (chapter 5.1.4.3, p. 55 ff.) (Figure 28).

The maze of the outer layer appeared denser in case of high yields than for those with lower yields observed and described. Its crystalline plates had edge sizes in the range of 3 – 17 μm and were partly frayed in all cases regardless of the yield. No relation between the yield and the thickness of the outer layer was found.

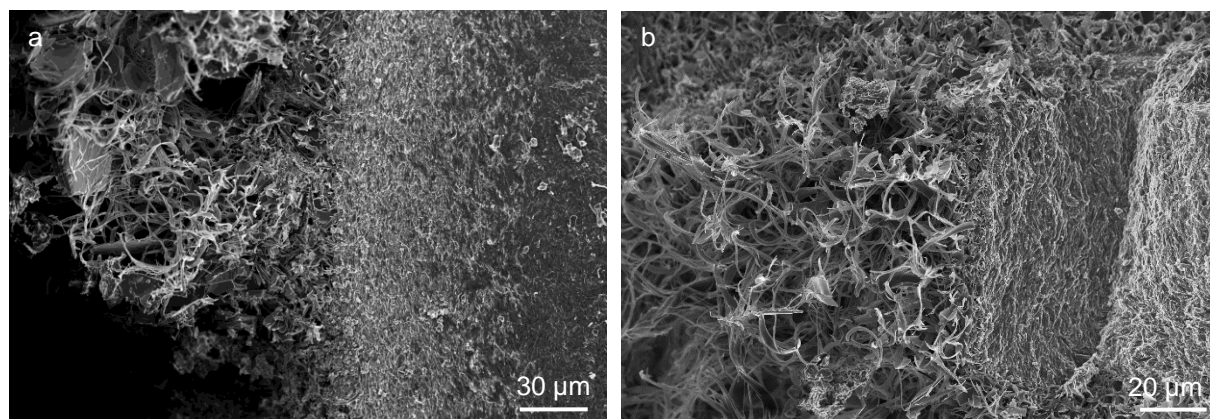


Figure 27: SEM images of the residue after extraction a) of finely grinded cBT (exp. no. 1) and b) of finely grinded cBT in presence of PBT (exp. no. 4).

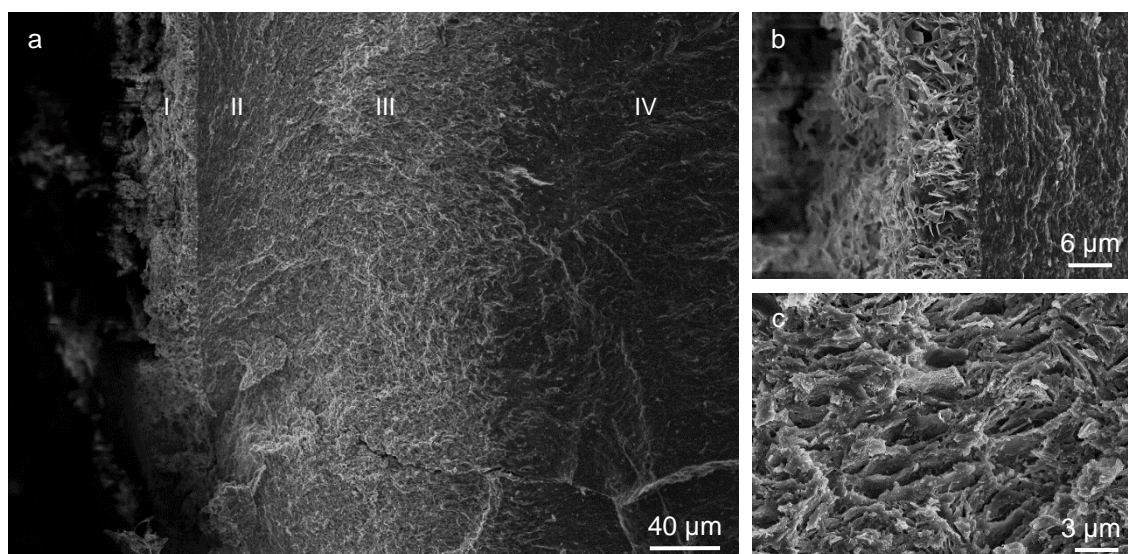


Figure 28: SEM images (all by InLens detector) after extraction of crumbled cBT (exp. no. 6) a) of the 4 layers in overview (indicated by Roman numbers), b) of the outer and the additional layer beneath and c) of the intermediate layer (III).

The inner phase is similar to CBT100 in all cases with its small crystalline plates in an amorphous matrix as observed and described above. It is followed by the intermediate layer described before. Its thickness increases with increasing yield of dissolved cBT (Figure 29). This is the same dependency of the thickness as observed before (chapter 5.1.4.4, p. 60 ff.). The thickness however varies between samples of one probe and they appear to decrease

with depth in the frit (tested for the residue in the frit after the extraction of crumbled cBT). It hence suggests a decrease of the extent of extraction with depth in the extraction vessel. The corresponding DSC thermograms were measured of residue samples from different heights in the frits in case of the extraction of finely grinded cBT (exp. no. 1, two samples) and of crumbled cBT (exp. no. 6, three samples) (Figure 24b). However, the melting temperature is the product of a complex interaction of the different oligomers and could obviously not be measured of just one layer. A decrease of the degree of extraction has been expected in the setup used. The (comparably small) solubility of cBT in the solvent is reached while the solvent passes through the frit.

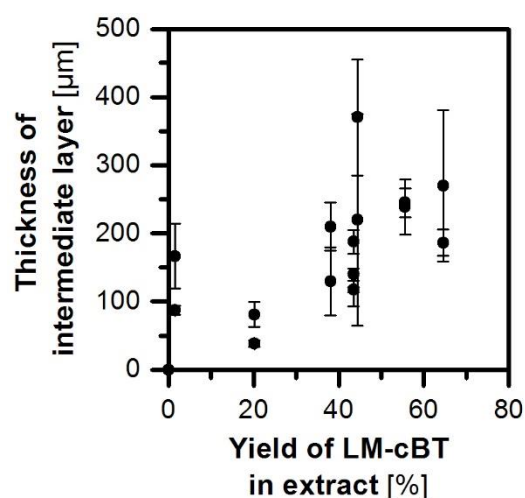


Figure 29: Thickness of the intermediate layer in SEM images of the residues after extraction in dependence of the yield of cBT extracted therefrom for extractions of 50 g CBT100 or more.

The formation of an outer layer consisting of crystalline plates without amorphous matrix can be observed in optical microscopy as well. A crystalline glitter after extraction can be distinguished from the appearance from before (example images in Figure 30 and Figure 31). No discrimination can be made between the different extractions regarding the appearance under an optical microscope.

The lateral length of the cBT particles decreased only at a high yield (>50 wt-%) of extracted LM-cBT and increased elsewhere according to analysis by optical microscopy. The possible explanation is a recrystallization (as mentioned in chapter 5.1.4.3, p. 55 ff.), which takes place during extraction. It forms the maze of larger crystalline plates, which increases the size of the particles. Only a significantly high loss of mass due to extraction can counteract this effect and result in a loss of diameter. Such a decrease in particle size was only observed for the extraction of roughly grinded cBT (exp. no. 5, which had the highest

yield of >55 wt-% (factor to initially found average length of 0.6 – 0.8)). A gain with an average factor between 1.2 and 3.3 was found in all other extractions. The increase during extraction of crumbled cBT (exp. no. 6), where a comparably high yield of about 46 wt-% was obtained, was moderate compared to the other grain sizes (factor of 1.2 – 1.8).

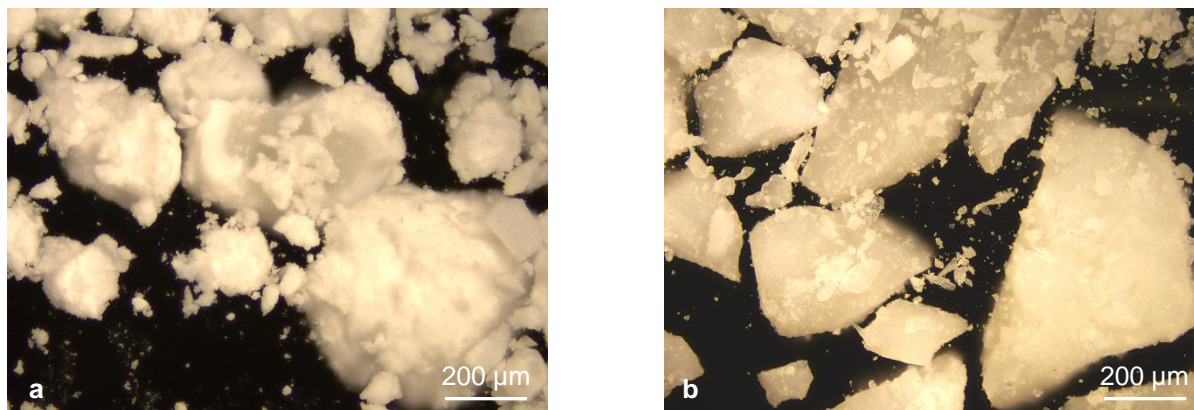


Figure 30: Optical microscopy images of a) the residue after extraction (exp. no. 5) and b) coarsely grinded cBT from before.

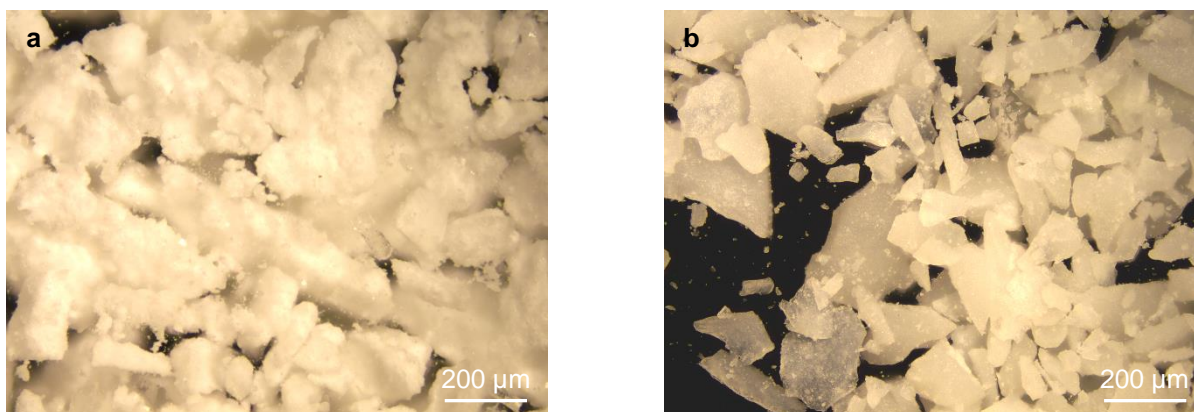


Figure 31: Optical microscopy images of a) the residue after extraction (exp. no. 6) and b) crumbled cBT from before.

5.1.4.6 Extraction of CBT100 with supercritical carbon dioxide

CBT100 was extracted by supercritical carbon dioxide (scCO₂) in cooperation with the Technical University of Hamburg inspired by the depolymerization and extraction experiments at high temperatures and pressures (230 °C, 250 bar) reported before.¹⁴⁸ A small yield of less than 1 wt-% was determined after 45 min, which is in a similar order of magnitude to the solvent extractions with a medium to high yield (chapter 5.1.4.1 to 5.1.4.5). The melting temperature of the first extract (5 min) was below 170 °C but increased

significantly in the later fractions (≥ 15 min) (Figure 32). It is even above those found in the residue after extraction. It should be noted that the small yield of the fractions only permitted a DSC analysis of small quantities. Hence, the found values may not be representative and could not be double-checked.

The ratio of hydroxyl end groups of the extracts (calculated from ^1H NMRs) is in a comparable magnitude to that in CBT100 and is substantially enlarged in the residues after extraction, even though it was carried out for only 45 min (Figure 33a). Hence, a hydrolysis seems to take place during extraction even at the mild temperature of 45 °C.

The extracted cBT has a high oligomeric ratio according to ^1H NMR as observed before for scCO_2 extracts from PBT¹⁴⁸ and similarly for PET^{146,147}, which is higher than any other reported result in this work (Figure 33b). This is supported by MALDI-TOF, where mainly MCOs with 2 or 3 repeating units were detected (in repulsion mode of detector). In later fractions, small signals for cycles with up to 5 repeating units appear, which might be connected to the increase of the global melting temperature of the extracted fractions. Considering only the four extracts, small signals of impurities are present, especially in the first fraction. Both, the presence of smaller cycles and of impurities mainly in the first fraction, go along well with the concept of selective extraction of impurities at the beginning and of the cBT trimer (depletion observed at high yield) suggested above for liquid extraction (chapter 5.1.4.5.1, p. 65 ff.). Hydrolysis might be enhanced through water uptake of up to 1 mol-% during separation of the scCO_2 after extraction.²¹⁷ The MALDI spectrum of the residue after extraction mainly consists of signals for cycles of septamers beside those of di- and trimers and with small signals of impurities. Whether the latter are products of degradation processes or just simply not extracted at this point, still has to be evaluated.

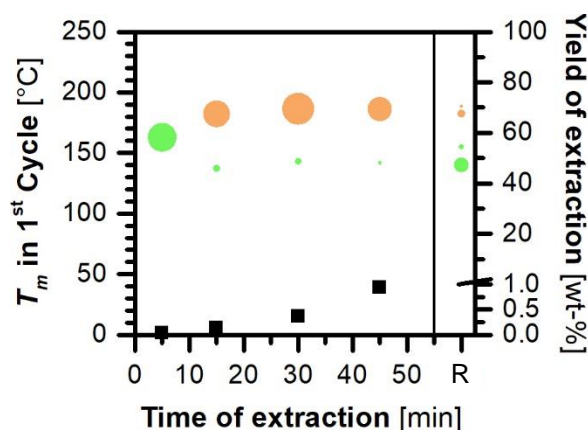


Figure 32: Melting endotherms according to DSC (colored markings, their size correspond to their respective ΔH_m) and the total yield of extract in dependence of time (black squares) of extraction with scCO_2 .

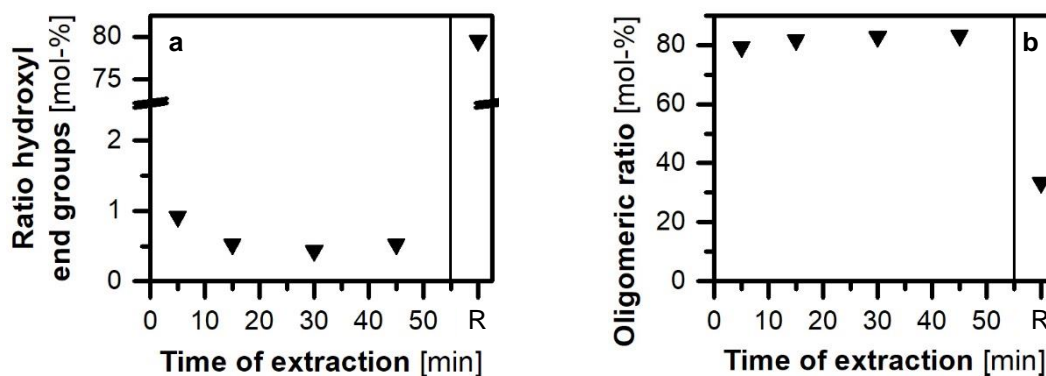


Figure 33: a) The fraction of hydroxyl end groups (determined by the ratio of $-\text{CH}_2\text{-OH}$) and b) the oligomeric ratio (according to aromatic signals) from analysis of ^1H NMR spectroscopy of samples from CBT100 extraction with scCO_2 .

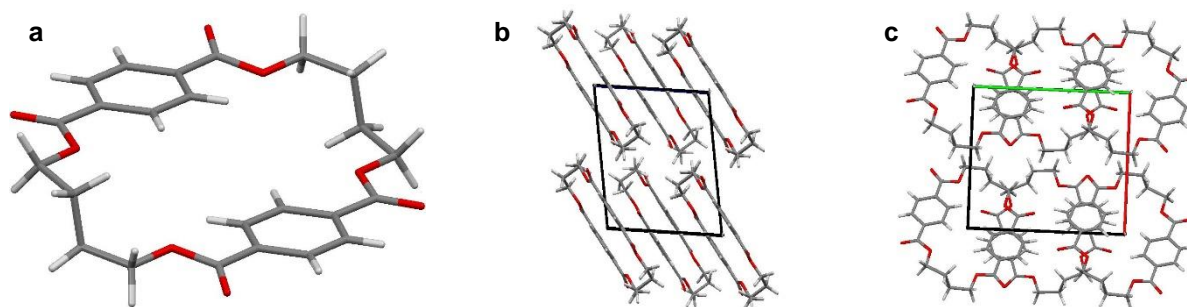
5.1.5 Crystal structure of extracted cBT dimers and trimers

It was possible to selectively crystallize the dimer and trimer of cBT from a solution of extracted cBT. The dimer gives crystals with a monoclinic system (Table 3 and Figure 34) as reported before for the cBT dimer²¹⁸ and similarly for the cET dimer (with a smaller, less distorted cell)^{219,220}. The high stiffness of the comparatively small cyclic dimers combined with the attractive forces between the π -systems probably permit only the formation of these crystals. The aliphatic segments are in *gauche* confirmation as reported for short linear (all aliphatic) polyesters.^{221–230} The aromatic systems are stacked on those of the neighboring molecules, not with the one from the same monomer.

The trimer easily incorporates solvent (chloroform, cyclohexane or THF) in its triclinic system (Table 3 and Figure 35), probably because of its larger ring size and the more flexible character compared to the dimer. The methylene segments are positioned *anti*, which has also been found in longer aliphatic polyesters.^{229,230} Again, two aromatic rings of adjacent oligomers are stacked.

Table 3: Crystallographic data of dimeric and trimeric cBT crystals.

	CBT dimer	Dimer in literature²¹⁸	CBT trimer (+ THF)	CBT trimer (+ CHCl₃)
Crystal system	monoclinic	monoclinic	triclinic	triclinic
Space group	P 2 ₁ /c	P 2 ₁ /c	P-1	P-1
Length a [Å]	10.735	11.006	6.250	6.322
Length b [Å]	11.770	11.926	16.092	16.116
Length c [Å]	8.596	8.489	18.260	18.168
Angle α [°]	90.000	90.000	92.206	92.603
Angle β [°]	98.971	95.742	93.278	91.982
Angle γ [°]	90.000	90.000	93.779	94.116
Volume Cell [Å³]	1073	1109	1828	1843
Molecules per cell	Z=4	Z=2	Z=2	Z=8
Density [mg·m⁻³]	1.36 (calc. 1.36)	1.31 (calc. 1.32)	1.33 (calc. 1.33)	1.39 (calc.1.39)
R factor	11.35 %	N/A	5.71 %	3.24 %

**Figure 34:** a) Crystal structure of cBT dimer, b) packing along b axis and c) along c axis.

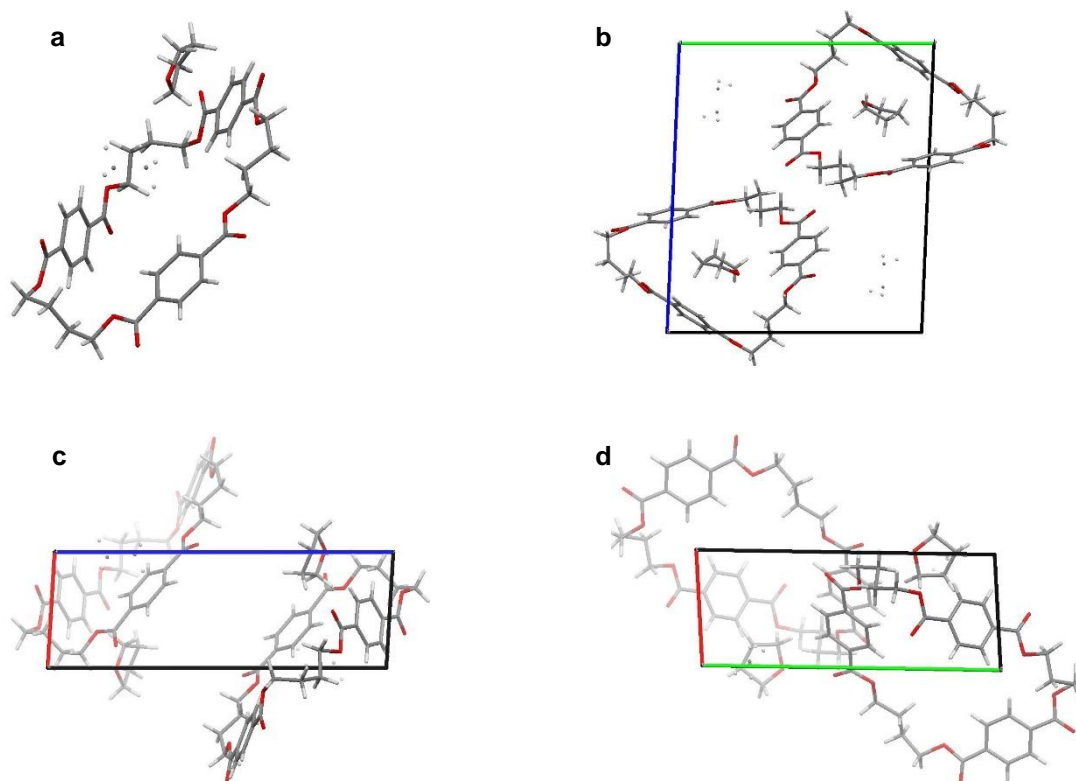


Figure 35: a) Crystal structure of cBT trimer (with incorporated THF), b) packing along a axis, c) along b axis and d) along c axis (with stacking of π -systems).

5.1.6 Concluding remarks on the isolation of LM-cBT

Investigations have been carried out to provide supplement information on the literature-known precipitating of cBT oligomers, which cause a higher melting temperature of a commercially available cBT.¹⁶⁴ Precipitates were obtained by stepwise addition of a low-boiling non-solvent to a solution of cBT in oDCB and analyzed. The temperature during the precipitation was found to be of major influence, not the precipitation solvent itself. Similar precipitates were obtained with addition of various volume fractions of the second solvent regarding analysis by DSC, MALDI and ¹H NMR. The addition of the more polar CHCl₃ at 60 °C led to the elimination of cBT fractions melting above 160 °C, which was not fully accomplished by addition of toluene at 108 °C. A higher melting cBT fraction precipitated days after the initial experiment from the toluene-containing solution.

The utilization of low-boiling solvents was explored after the elucidation of the importance of the temperature during precipitation on the resulting cBT fraction in solution and the possible suitability of CHCl₃ and toluene as solvents for LM-cBT. This avoids high-boiling solvents in the process, which are an issue for ecological and economic reasons. LM-cBT could be

precipitated from chloroform with a melting temperature below 170 °C in a yield of 73 mol-% and with only a small amount of hydroxyl termini (<0.1 mol-%) and a moderate amount of oligomers (22 mol-%), but the precipitation took days. An acceleration was possible by usage of CY giving a product with a comparable melting temperature, no opened rings and a high oligomeric character (61 mol-%) detected by ¹H NMR spectroscopy, but only in a small yield of 1 wt-%. The combination of CHCl₃ and CY resulted in LM-cBT with a melting temperature of even below 150 °C in high yields of up to 79 wt-% and with a ratio of opened cycles of ca. 0.1 mol-% and a moderate oligomeric ratio (26 mol-%). Unfortunately, a cBT fraction with an elevated melting temperature formed in scale-ups during processing.

LM-cBT could be successfully isolated as well by the extraction of CBT100. The extraction in a heated setup according to KNÖFLER-BÖHM procedure showed superior properties to a non-heated setup according to SOXHLET in aspects of yield (48 compared to 24 wt-%) and of the highest melting peak in DSC of the extract (168 and 187 °C). Low ratios of hydroxyl end groups (0.5 ±0.2 and 0.3 ±0.1 mol-%) and high oligomeric ratios (52.0 ±1.0 and 52.8 ±4.4 mol-%) were found in the obtained LM-cBT products of both methods. An evaluation of solvents proved CY to be superior compared to CHCl₃ or THF. Higher yields were obtained with CHCl₃ or THF, but the product obtained by CHCl₃ suffered from additional endotherms at higher temperatures in DSC and the products from extraction with THF made additional efforts for drying necessary to circumvent hydrolyzing of the MCOs.

Scale-ups of the extraction with CY were carried out in a setup for solids (comparable to the TWISSELMANN procedure) from 15 to 130 and 340 g. The results are similar for all scales. The yield-time curve of the largest scale was a little bit flatter than the others. This is probably caused by the longer time needed for heating of the system because of the higher mass of the complete system and by clogging (37 compared to >44 wt-%). The melting behavior of the obtained LM-cBT was similar. Additional melting endotherms were observed after prolonged extraction in the large-scale experiment. The ratio of hydroxyl termini was below 1 mol-% for all scales, the oligomeric ratio probably decreased slightly with increasing scale (52 ±1, 51 and 44 ±8 mol-%).

The pore size of the extraction frit was varied to compare frits with a porosity of G0, G1 and G2 (160 – 250, 100 – 160 or 40 – 100 μm, respectively). A higher yield was obtained with smaller pore sizes, meaning a higher retention time of the solvent, despite an observed clogging especially of these small pores. Multiple melting endotherms were found for all extracts with the highest melting temperature being below 170 °C in all cases. The amount of hydrolyzed rings was small (<0.3 mol-%), higher for small pores with longer retention times. The oligomeric ratio was comparably high for all three pore sizes (51 ±2 mol-%).

Different grain sizes of CBT100 were prepared and extracted with CY in order to investigate the effect of a more intense solid/solvent contact and shorter diffusion ways on the extraction yield and on clogging of the G0 frit. Extracts with the highest melting temperature being between 150 and 166 °C were obtained with all explored grain sizes. The highest yield was isolated by utilization of a coarse grain (56 wt-% in 24 h) combined with a ratio of hydroxyl termini below the detection limit of standard ^1H NMR spectroscopy. The addition of CBT100 or PBT pellets to loosen the extraction material enhanced the yield compared to the utilization of finely grinded CBT100, too (21 and 8 wt-%, respectively, compared to 0.3 wt-%). A comparable amount of hydroxyl end groups was obtained with both setups (0.3 mol-% compare 1.9 ± 0.6 mol-% for CBT100). The amount of impurities was higher when CBT100 was added than for the extraction of only finely grinded CBT100 or in combination with PBT. A break-up of the extraction material by Ar flow in order to increase the yield and prevent clogging had no noteworthy effect.

An increase of the melting temperature of the extraction residue was generally noticed with yield. Additionally, the depletion of cBT trimer in some residue was observed in MALDI-TOF, which is possibly an indication for its preferred extraction. A high concentration of impurities was recognized in the extract shortly after the start of extraction, which might indicate a preferred solving of those as well. Similar observations were made by the extraction of CBT100 pellets with supercritical carbon dioxide (scCO_2). Small, low-melting cBT was extracted in a yield comparable to the liquid extraction with CY.

The occurrence of three type of layers is observable in samples of different extraction residues by SEM: 1) an inner phase, which appears to be similar to CBT100 with few small crystallites (edge length of up to 5 μm) in an amorphous matrix, 2) an intermediate layer of an increased number of crystallites (≤ 15 μm , often ≤ 5 μm), whose thickness seems to be larger for a higher yield, 3) an outer layer consisting of a maze of plates (≤ 15 μm) and a thickness that appears to be dependent on the extraction method but is often distorted because of damaging of the delicate structure during recovery. A smooth transition from the inner phase to the intermediate layer is observed, but a sharp contour line between the intermediate and the outer layer. The outer layer has been observed in optical microscopy (glittering instead of matte appearance), as well. An additional fourth layer with an amorphous appearance is visible between the outer two layers in some high-yield extractions.

A recrystallization seems to take place during extraction forming the outer layer with its larger crystal plates. The reduction of the amorphous fraction in the outer layer suggests a selective solving of amorphous cBT. The particle size increases during extraction (factor 1.2 -

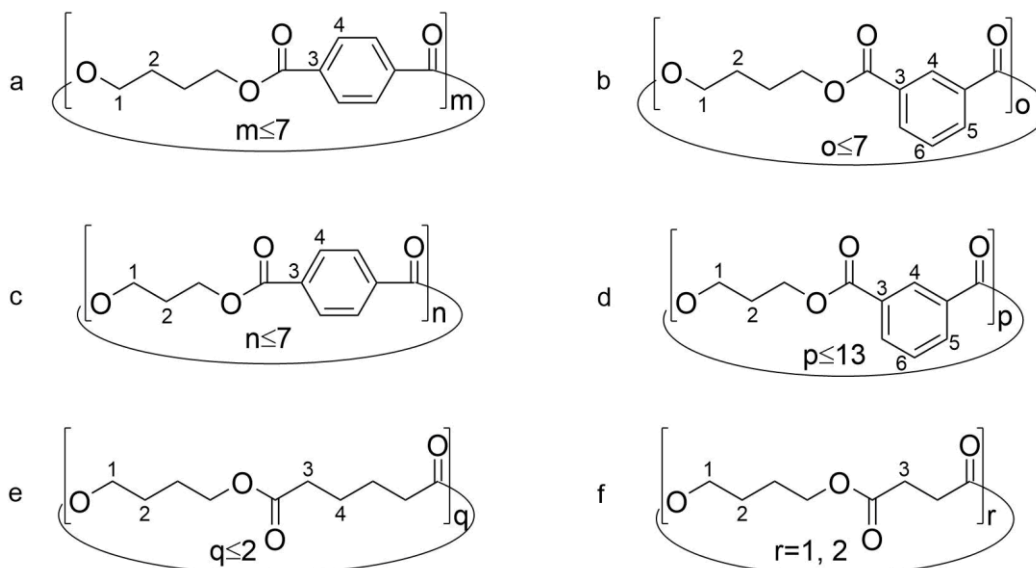
3.3; determined by optical microscopy). The gain in diameter is counteracted by the material loss due to the extraction and a decrease is found for a higher yield (>55 wt-%). The extraction seems to be less intense with increasing depth from the surface of the granules of the extraction material according to determination of the intermediate layer in SEM pictures (despite the similar melting behavior in DSC). There is obviously a potential for a further increase in yield. Extraction has nevertheless proven to be a powerful method for the isolation of cBT with a, in some cases, drastically reduced melting temperature. The resulting LM-cBT was superior compared to preparation by precipitating of oligomers, at least with low-boiling solvents at a low temperature regarding the time necessary and/or the purity.

The using of scCO_2 as extraction agent is a promising procedure, as well, if the co-extraction of impurities respectively the degradation of the cBT can be prevented (e.g. by selective extraction of the degraded products at the beginning or by more extensive exclusion of water). The utilization of other supercritical fluids like e.g. pentane or the combination of scCO_2 with another solvent may further support such an effect next to a further increase in the swelling of the granulate by varying the solvent's polarity and hence an increase of the yield.²¹⁶ The latter effect has already been observed in combined depolymerization-extraction experiments at elevated temperatures of 230 °C and pressures of 250 bar (without regard of the melting temperature of the extracted cBT).¹⁴⁸

5.2 Effect of MCO mixtures on the thermal behavior

Generally, a reduction of the melting temperature of MCOs and hence of the processing temperature can be achieved more simply in case of copolyesters if a melting point reduction by colligative effects of the respective monomeric mixtures can be exploited as discussed in the introduction (chapter 3.3 Options for reduction of the cBT polymerization temperature p. 26 ff.). This route is much more straightforward than isolating low-melting fractions of the respective monomers. The information on the effect of such mixing on the thermal behavior is limited, as is the commercial availability of suitable lactones up to now. Hence, the aromatic lactones cyclic 1,4-butylene isophthalate (cBI), cyclic 1,3-propylene terephthalate (cPT) and cyclic 1,3-propylene isophthalate (cPI) have been prepared and were mixed with cBT (CBT100) and each other. The aliphatic lactones cyclic 1,4-butylene adipate (cBA) and succinate (cBS) were also prepared and combined with the four aromatic MCOs. In the following subchapters, the results of the preparations are described (chapter 5.2.1) and the

results of the DSC studies on the mixtures are summarized and compared to observations reported in literature regarding aliphatic and aromatic polyesters (chapter 5.2.2).



Scheme 5: Monomers used in this study (number of repeating units are stated according to MALDI-TOF experiments): a) cBT, b) cBI, c) cPT, d) cPI, e) cBA and f) cBS.

5.2.1 Provision with additional aromatic and aliphatic lactones

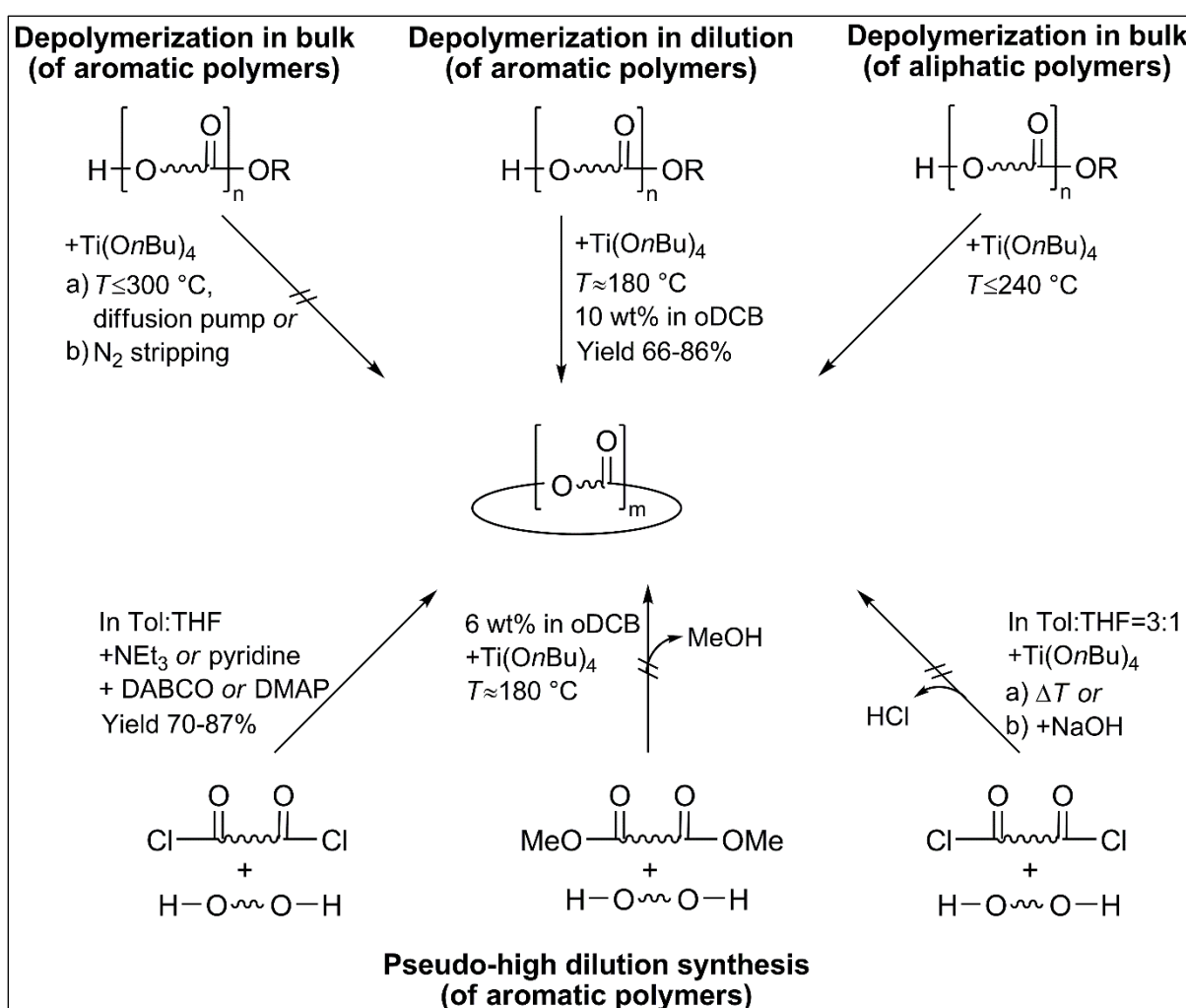
Cyclic 1,4-butyrene terephthalate (cBT) is the only aromatic cyclic monomer commercially available. Two aliphatic lactones and three other aromatic MCOs with a structurally similar repetition unit compared to cBT (Scheme 5) were additionally chosen. The similarity was supposed to facilitate mixing and to gain insight into the effect of structure on the thermal properties of the mixtures at the same time (chapter 5.2.2). A short linear diol with three or four carbon atoms was therefore combined with a linear aliphatic diacid with four or six carbon atoms or with a linear or an angled aromatic diacid.

5.2.1.1 Preparing of the aromatic and aliphatic lactones

Pseudo-high dilution synthesis and depolymerization in bulk as well as in dilution were evaluated as routes to partly aromatic MCOs (Scheme 6). A successful preparation was achieved by pseudo-high dilution synthesis. The depolymerization in dilution was

successfully carried out, as well, but dismissed because of a lengthy reaction and complicated purification.

The aliphatic monomers cyclic butylene 1,4-adipate (cBA) and cyclic 1,4-butylene succinate (cBS) (Scheme 5a and b) were readily prepared by cyclo-depolymerization in bulk of the corresponding polymers in a 5 L steel reactor. The polymers had been prepared by polycondensation from the respective diol and diacid with utilization of $\text{Ti}(\text{OnBu})_4$ as transesterification catalyst directly before their cyclo-depolymerization. The method is basically the same as published by CAROTHERS *et al.* in the 1930s for various monomers^{35,130–133}. It has recently been described by BEREZINA *et al.* for cBS⁶² and extensively for cBA²³¹.



Scheme 6: Explored routes to aromatic and aliphatic MCOs.

The partly aromatic lactones cyclic 1,4-butylene isophthalate (cBI), cyclic 1,3-propylene terephthalate (cPT), cyclic 1,3-propylene isophthalate (cPI) (Scheme 5c to f) were synthesized in pseudo-high dilution. This method was essentially explored by BRUNELLE *et*

al. in the 1990s. High yields (70 – 87 %) and pure products (according to ^1H NMR and MALDI spectra) were obtained when solutions of the reactants, diol and dicarboxylic acid chloride in case of oligoesters, are dosed to a solution of a base like triethylamine or pyridine and a catalytic amount of a sterically less hindered amine as DABCO or DMAP, following the literature.^{19,154–157} Providing dicarboxylic acid chloride in the reaction flask led to a high yield (94 %) with a good purity, as well. Cyclic compounds were mainly formed in these cases because of the low concentration of reaction partners during the whole reaction time. In contrast to reports in literature¹⁹, DMAP did not show a significantly reduced catalytic activity relative to DABCO. Similar yields with rather different degrees of purity were obtained with both catalysts on the different preparation routes explored here for the different aromatic MCOs (e.g. dosing of just the diol or of both reactants simultaneously).

Further routes for the synthesis in pseudo-high dilution were evaluated but dismissed for reasons of yield and product purity. These comprise reactions with heating to accelerate the reaction and/or to remove side products. The transesterification of dimethyl isophthalate with BDO in presence of $\text{Ti}(\text{O}n\text{Bu})_4$ in *o*DCB gave the desired cycles only in almost negligible yield with mainly opened cycles present. The reaction of terephthaloyl dichloride with BDO under removal of HCl gave a high amount of linear esters (according to the amount of BDO end groups (above 20 %)) and almost exclusively polymers (compared to CBT100 in chapter 5.1.1.2 ^1H NMR spectroscopy, p. 37 ff.), questioning the formation of cyclic structures. The same is true for the utilization of sodium hydroxide instead of amines at an elevated temperature.

Depolymerization in dilution was screened in preparing cBI in *o*DCB. The low yield of the batchwise preparation combined with a slow transformation of the previously prepared PBI to cBI (>72 h at 10 wt-% of cBI in *o*DCB) and the cumbersome drying because of the high-boiling, hazardous solvent made this method less favorable. Hence, it was not further pursued. CBI was chosen as model compound instead of cBT in this case because of the easier handling of the corresponding polymer regarding its lower melting temperature and better solubility in organic solvents.

No successful preparation of cyclic aromatic oligomers was established by depolymerization in bulk. The resulting partly aromatic MCOs of this study are not volatile enough to be distilled off. Depolymerization of aromatic polyesters in bulk was explored for PBT and PBI. The first was chosen because of its central meaning for this project, the latter because of its close relation to PBT combined with the promising yields in comparable experiments with poly(1,2-ethylene isophthalate) in literature.¹³⁴ Additionally, the much lower melting temperature of PBI polymer and corresponding MCO promised a less demanding

evaporation of the monomer. Neither the utilization of a temperature above 300 °C nor of a diffusion pump nor of the stripping gas nitrogen (in case of cBI) led to an isolation of mentionable amounts of MCOs according to GC-MS. The thermal degradation was usually high after the extensive heating necessary according to appearance, odor and ¹H NMR spectra.

5.2.1.2 Melting and crystallization behavior of the monomers

The thermal behavior of the monomers relevant for this work has been determined by DSC measurements. Iterative measurements have been carried out to evaluate the changes of the observed behavior over time. The observed key figures for melting, crystallization and glass transition (Table 4) were analyzed regarding the influence of chemical structure of the monomers and compared to literature.

Table 4: Data from DSC measurement of the studied cyclic monomers (data from 3rd DSC run of each sample if not stated otherwise).

	1 st heating segment			1 st cooling segment			2 nd heating segment		
	Lowest T_m [°C]	Highest T_m [°C]	Total H_m [J·g ⁻¹]	High T_c [°C]	T_g [°C]	ΔC_p [J·g ⁻¹ ·K ⁻¹]	Lowest T_m [°C]	Highest T_m [°C]	Total H_m [J·g ⁻¹]
cBT	126.7	182.7	39.7	---	22.3	0.224	129.5	183.7	42.7
cBI	102.3	131.3	2.1	---	18.5	0.435	---	---	---
cPT	188.7	221.6	87.8	172.4	37.6	0.147	184.1	221.4	76.1
cPI	65.8 ¹⁾	120.4 ¹⁾	57.7 ¹⁾	---	30.0	0.415	---	---	---
cBA	---	95.5	145.5	53.2	-41.8 ²⁾	0.055 ²⁾	---	95.2	137.9
cBS	---	69.4	5.7	---	-71.9 ²⁾	0.480 ²⁾	---	45.7	78.0

1) Data from 1st DSC run, not observed in further runs.

2) Data from DSC run for T_g determination with decreasing of the temperature to -90 °C.

It should be noted that the molar heat of fusion for 100 % crystallinity is not known for all of the studied monomers and hence a comparison of their crystallinity is not possible so far. A comparison of the total H_m during the heatings of the DSC measurements is nevertheless informative as differences were rather high and similar molar heat of fusions for perfect crystals can be assumed for similar repeating units as suggested by HYBART *et al.* before.^{232,233}

Multiple melting endotherms were observed for all compounds except cBA, which consists almost exclusively of the cyclic dimer. The different endotherms are the product of colligative

effects of different oligomers in the MCOs. The presence of isophthalic acid in the monomer results in a smaller T_m (i.e. the highest observed melting endotherm) and ΔH_m than of the respective MCO with terephthalic acid instead. The reason is probably a distortion of the supposed zigzag structure caused by the “kink” of isophthalate and leading to a suppression of crystallization reported before for other aromatic polyesters.^{232,234,235} The effect was enhanced by presence of PDO, the diol with the odd number of methylene groups. A melting endotherm was observed for cBI during the first heating cycle of all DSC measurements, for cPI only during the very first heating, but not for any reheating of the same sample even after crystallization at room temperature for more than 21 d. Crystallization could not be observed for neither of the MCOs during cooling in DSC.

An odd number of carbon atoms in the repeating unit of the monomers does not seem to disturb the chain alignment during crystallization per se significantly. This is in contrast to the observations for polyesters, where a general lowering of the melting temperature by odd-numbered diols was recognized.^{232,233} The expected lower melting temperature of MCOs with PDO instead of BDO was only observed in combination with the obstructive isophthalate. The higher T_m and ΔH_m of cPT compared to cBT already known from literature²³⁵ can be explained by the presence of the rigid terephthalate, which “forces” the chains in an oriented structure. The length of the diols and hence the distance between the polar groups and of the π -electron system of the aromatic determines the strength and hence the T_m of the crystals.

The order of T_m and ΔH_m for the aliphatic monomers cBA and cBS follows the rules previously set up:^{233,236} A longer chain makes the monomer more like polyethylene and causes a comparatively higher T_m . The shorter diacid chain prevents an easy alignment and hence crystallization during cooling in the DSC measurements made. ΔH_m during the subsequent heating phase has hence decreased compared to the initial melting ($<80 \text{ J}\cdot\text{g}^{-1}$ instead of $104 \text{ J}\cdot\text{g}^{-1}$ initially). A higher crystallinity was interestingly observed in general for cBS during second heating of the DSC measurements than during the first heating of subsequent measurements days later.

5.2.1.3 Glass transition

The T_g is determined by the chain flexibility. Consistently, it was found to be higher for shorter diols and for the more rigid, aromatic MCOs than for the more flexible, aliphatic monomers. This is in good agreement with previous observations regarding polyesters mentioned before.^{232,233} A difference between terephthalate- and isophthalate-containing oligomers was observed. The increase of free volume granted by the bulky isophthalate

possibly gains importance in monomers with only short diols. The density of polar groups in these and hence the attractive forces between the molecules highly limit the free volume.

Surprisingly, a longer diacid in the two studied aliphatic monomers has the opposite effect on the glass transition compared to the diols and heightens the T_g . This is probably caused by the longer distance between the ester groups that facilitates a short-range orientation and possibly reduces the free volume.

The amount of amorphous phase was higher for monomers with an isophthaloyl than a terephthaloyl moiety, judged from the ΔC_p . It is caused by the alignment of the linear terephthalate-containing monomers.^{232,237,238} The higher amorphous fraction in MCOs with BDO compared to those with PDO can be explained similarly. This dependency of the vitreous amount on the diol length is again not transferable on the length of an aliphatic diacid, where a significantly smaller ΔC_p was found for the longer adipate than for succinate. Obviously, the longer chain remarkably enhances the alignment of the monomers in crystals.

5.2.2 Effect of chemical structure on thermal behavior in mixtures of aromatic and aliphatic MCOs

Mixtures of the five prepared lactones and CBT100 were analyzed in various ratios by at least three iterative DSC measurements consisting of two cycles of heating and cooling and with a delay in time between the measurements of 4 to 25 days for an insight into the extent of solid-state crystallization. Mixing of the samples was completed after the first melting. The focus of the evaluation was on the dependency of melting, crystallization and glass transition on the composition of the respective sample. The influence of the structural units of different diols and diacids in the different monomers on the thermal properties was qualitatively evaluated. The findings were compared to reported observations regarding aliphatic and aromatic polyesters.

The thermodynamic equations for binary mixtures generally apply, among them those for phase transition and colligative effects. Of those, the depression of the melting temperature is probably of the highest interest for this thesis. The respective melting temperature T_m can be calculated for a molecular fraction x_i of a solute by the SCHRÖDER-VAN LAAR equation²³⁹ from the temperature and enthalpy of fusion of the pure solute, $T_{m,i}$ and $\Delta H_{m,i}$, and the universal gas constant R ($R \approx 8.31446 \text{ J}\cdot\text{K}^{-1}\cdot\text{mol}^{-1}$) (assuming that $\Delta H_{m,i}$ is independent of the temperature):

$$\frac{1}{T_m(x_i)} = \frac{1}{T_{m,i}} - \frac{R \cdot \ln(x_i)}{\Delta H_{m,i}} \quad (3)$$

A deviation from the aforementioned correlation can generally be ascribed to non-ideal conditions like an additional exothermal interaction (e.g. electrostatic interactions) or endothermal interaction between the components. However, theoretical calculations are complicated for the mixtures considered here because of the unknown molecular composition of each of the MCOs used. Different oligomers with their different molecular masses are present according to MALDI and GPC analysis, which makes the respective amount of substance and hence the general equations not readily accessible.

CBT, cBI, cPT, cPI and cBS have hence to be considered as mixtures themselves and the mixtures containing them, like those discussed in the following part, have to be regarded as “mixtures of mixtures”. The resulting effects on the thermal properties within these “mixtures of mixtures” have been small and their mathematical description is accordingly complex and effortful, while at the same time prone to errors. Those calculations have therefore not been part of this thesis.

However, similar phase diagrams were found for the different mixtures. An additional low-melting fraction formed in presence of readily crystallizing monomers as cBT, cPT or cBA. Besides, a lower glass transition temperature than expected from the properties of the pure monomers was observed. The presence of a longer diol in the monomer resulted in the reduction of the fraction of amorphous phase. The necessary supercooling for crystallization was enlarged by the presence of isophthalate especially in company with 1,3-propanediol simultaneously leading to a high amount of amorphous fraction in these mixtures.

5.2.2.1 General observations of the DSC measurements

Each DSC sample was measured at least three times to check for change in liquefaction (i.e. softening of glassy regions and melting) and crystallization behavior caused by further mixing with additional DSC runs. The samples were allowed to further crystallize between the measurements by the delay between the different runs. After the first melting, no further shift in melting, crystallization or glass transition points was noticed over the measurements indicating a mixing as complete. The only exception is the mixture of cBI and cPT where a shift with runs was noticeable (Figure 61 and its discussion).

Only values of the third measurement (fourth in case of cPI with cBA or cBS) were used for evaluation if not stated otherwise. Small deviations from seen trends were generally ascribed

to the variance of DSC, which occurred in the measured temperature as well as in the determined heat of fusion, ΔH_m .

In heating segments, multiple melting endotherms were observed for most mixtures. The endset of the highest melting temperature is generally quoted as it is considered as the point of complete melting. Exceptions are the phase diagrams, where the actual maxima of melting endotherms are depicted to allow conclusions on colligative effects. The first melting cycle of each measurement is referred to as initial melting behavior of the composition, which is of essential interest for processing of the monomer mixtures and hence for this study.

In cooling segments, the first occurrence of crystallization, i.e. the high limit of the crystallization peaks was determined as significant value. Weak signals often made peak fitting and determining of peak onsets and maxima prone to errors and hence the limits of the peaks the most reliable values.

Glass transition temperatures, T_g 's, and the correlated change in specific heat capacity, ΔC_p , were determined from data of the second heating according to ASTM D3418/IEC1006 in order to obtain a ΔC_p directly proportional to the amount of amorphous fraction.

5.2.2.2 Combinations of the aromatic with the aliphatic MCOs

Blends of the four aromatic MCOs cBT, cBI, cPT and cPI with cBA or with cBS were studied in DSC. All examined aromatic MCOs seemed to be soluble in the two aliphatic MCOs used and *vice versa*. The mixtures of an aromatic MCO with cBA or cBS showed a similar dependency of the melting temperature (i.e. the melting peak with the highest temperature) and crystallization temperature (in means of start of crystallization) on the fraction of the respective aromatic MCO. Melting and crystallization behavior showed a dependency on the ratio of the monomers. The difference in the melting temperature of the pure aliphatic MCOs cBA and cBS (95 °C to 69 °C) was, however, not found for the melting of the mixtures. These observations are in accordance with the general thermodynamic considerations for the chemical potential in mixing with the kind of "impurity" not being of major importance but its concentration.

The phase diagrams in dependence of the mixture composition appear to belong to soluble substances, more or less pronounced (Figure 36, Figure 37, Figure 43 and Figure 44). The presented phase diagrams consist of the lowest and the highest melting temperature during the initial heating of the third DSC measurement of the samples. They indicate start and end of melting. The data of a fourth DSC measurement (25 d after the 3rd run) had to be used for both combinations of cPI because data of the third run showed a similar behavior but with an agitated baseline.

Generally, mixtures with cBA had a higher ΔH_m during the first heating of a DSC run than those with cBS. An exception are the combinations with cPT, where a similar ΔH_m was measured for comparative mixtures with cBA or cBS. This is not a surprise as cBA generally crystallizes faster and more complete than cBS (according to the melting enthalpies of the pure substances). The crystallinity has not been calculated from this, as the molar enthalpy for 100 % crystallinity has not been determined for the used compounds yet except for cBT.

5.2.2.2.1 Mixtures of the terephthaloyl-containing MCOs cBT and cPT with cBA and cBS

The phase diagrams for blends of the high melting cBT or cPT (melting peak at 183 °C and 222 °C, respectively) with cBA or cBS show the typical behavior of mixable substances (Figure 36 and Figure 37, respectively). A significant increase of the highest melting temperature was observed as soon as cBT or cPT was present in a mixture with cBA or cBS. After this first increase, only a small slope of the curve is noticed. The start of melting, i.e. the lowest melting temperature, seems mainly be determined by the aliphatic component. A rise in temperature is not detected until a high amount of the aromatic monomer is present (>80 mol-% for cBA, >40 mol-% for cBS).

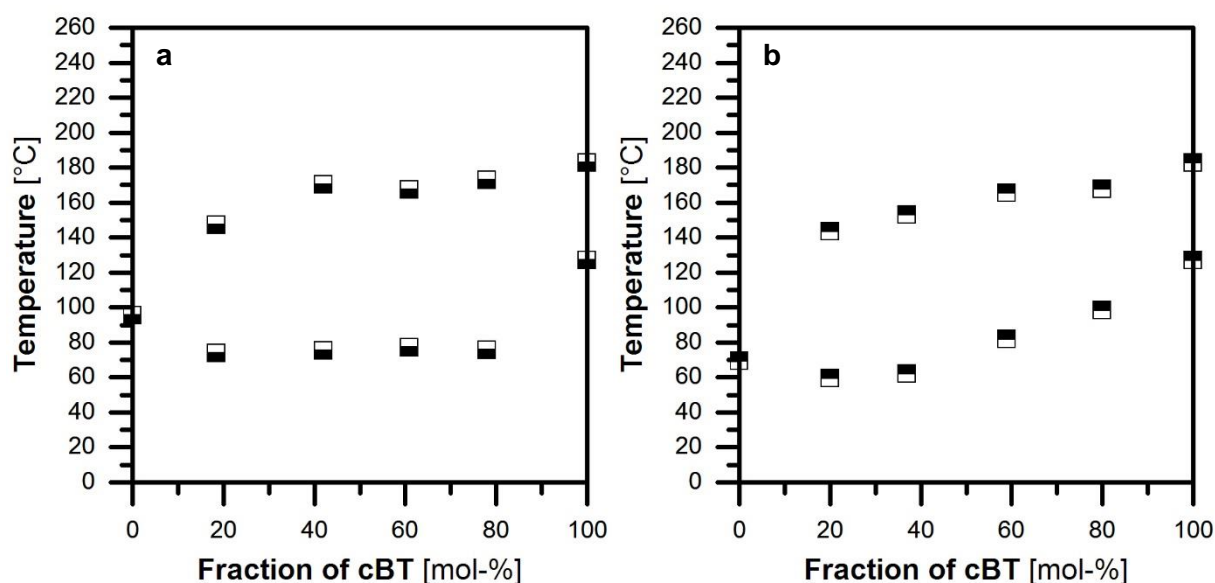


Figure 36: Phase diagram (highest and lowest melting temperature during initial melting in the 3rd DSC run) of mixtures of a) cBT and cBA and b) cBT and cBS.

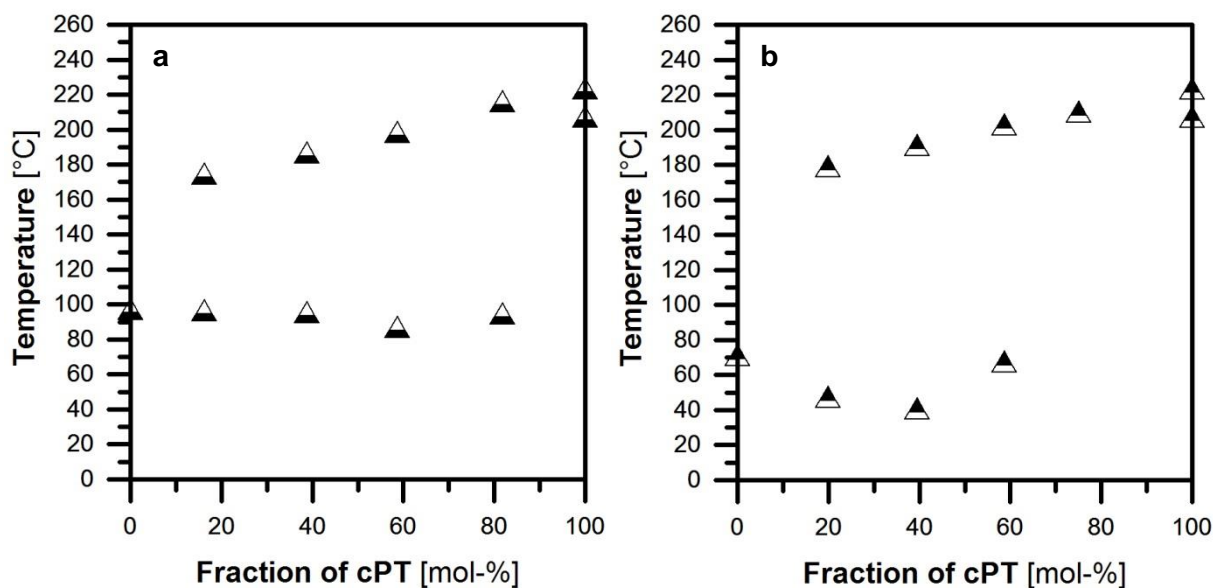


Figure 37: Phase diagram (highest and lowest melting temperature during initial melting in the 3rd DSC run) of mixtures of cPT and a) cBA or b) cBS.

ΔH_m in the mixtures of cBT or cPT with cBA roughly matches the theoretically expected ones, $\Delta H_{m,theo}$, in the first heating of a DSC run (absolute ΔH_m in Figure 38a, normalized values in Figure 39a). $\Delta H_{m,theo}$ of the mixtures were calculated from the experimental values of the pure components, $\Delta H_{m,i}$, proportioned by the respective mass fraction w_i of the components in the sample.

$$\Delta H_{m,theo} = \Delta H_{m,1} \cdot w_1 + \Delta H_{m,2} \cdot w_2 \quad (4)$$

The evaluations of ΔH_m have to be considered carefully as its values from standard DSC measurements are prone to errors. This is why the respective average values from the second and third run were considered. The interpretation of the behavior in means of general trends seems possible although not every fluctuation must be taken as granted without further verification. Only ΔH_m over one complete heating segment is depicted in the diagrams for reasons of clarity. The resulting curves for the normalized ΔH_m are at 100 % for pure components by definition, of course. The method of normalizing ΔH_m (in $\text{J}\cdot\text{g}^{-1}$) by the theoretical value has been chosen to overcome the issue of the unknown ring size of the MCOs and hence the respective amount of substance not being accessible. If those were readily calculable, the concept of excess parameters from thermodynamic correlations and the comparison of the experimental phase diagrams and ΔH_m would be the appropriate method for describing the respective discrepancy.

Crystallization of the mixtures of cBT or cPT with cBA is hindered according to the data from the second heating segment of the measurements. ΔH_m is lower than expected for all mixtures (Figure 39b). This is unexpected because these monomers show more or less extensive crystallization as pure substances, which is in agreement with the reported behavior of analogous polyesters.^{232,233,236} The linear structures of the aromatic MCO and the comparatively longer diol usually cause a fast crystallization. A decreasing ΔH_m with increasing aromatic content is observed, especially for cPT mixes. The faster and more complete crystallization of cBA (deduced from the value of ΔH_m) may cause a kinetic discrimination and hence the observed effect, probably conditioned by its small and flexible cycles (compare ring sizes by mass spectrometry in Scheme 5).

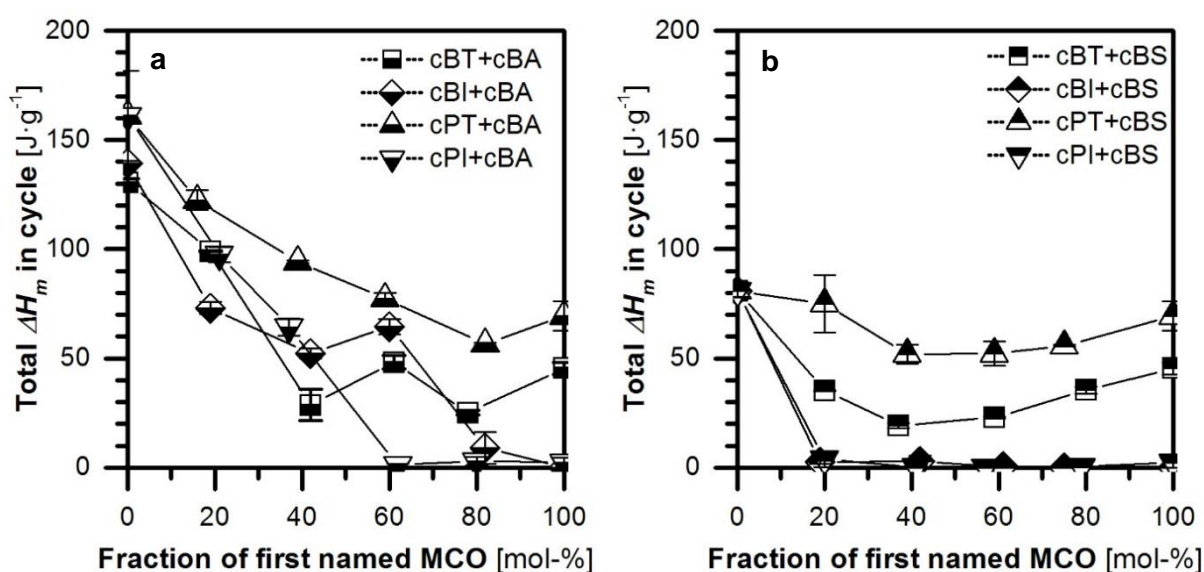


Figure 38: Average ΔH_m of the 2nd cycle of the 2nd and 3rd (or 4th for cPI) DSC run of the mixtures of cBT, cBI, cPT or cPI with a) cBA or b) cBS.

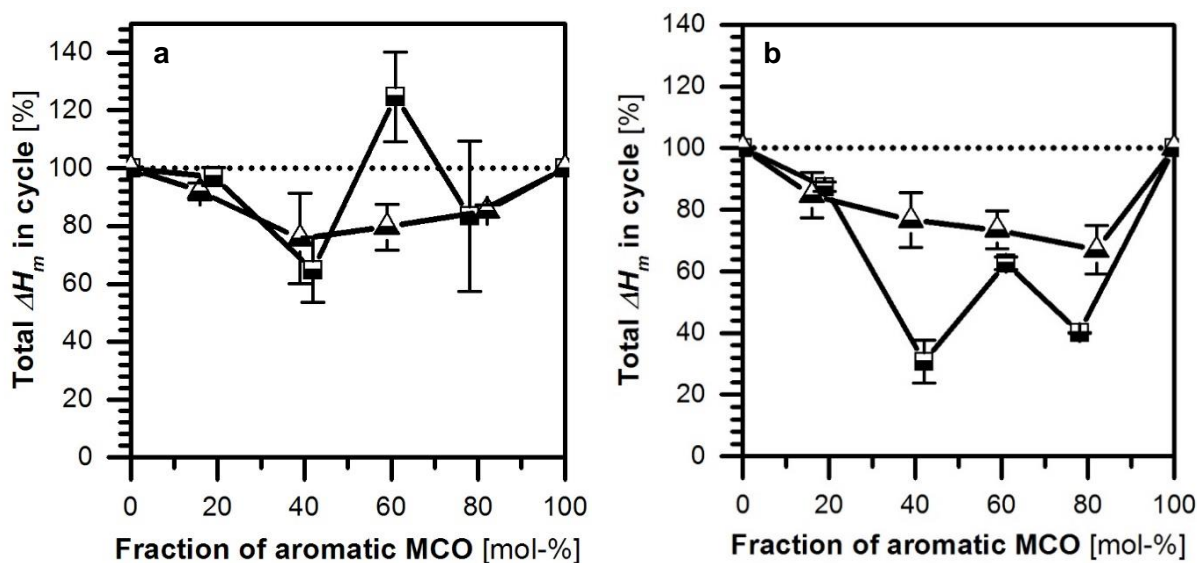


Figure 39: Normalized total ΔH_m (average of values from 2nd and 3rd run in DSC) of mixtures of cBT with cBA (■) and cPT with cBA (▲) during a) the 1st and b) the 2nd heating segment.

The corresponding blends of cBT or cPT with cBS instead of cBA also possess a hindrance of crystallization in the time of a DSC measurement. ΔH_m is below the theoretical expectations during the second heating for all these mixtures (Figure 40b). A synergetic effect takes over at longer crystallization times leading to an increased crystallization of the monomer combination compared to the identical cycles alone. A maximum is observed during the first heating segment, moderate for cBT at about 60 mol-% and high for cPT at ca. 20 mol-% (Figure 40a). The difference may stem from the higher concentration of the polar carboxyl groups, which majorly contribute to the crystal stability. A smaller distance between the polar groups was found to cause a higher specific heat in comparable aliphatic polyesters, which is reflected in the ΔH_m .²³⁶ The existence of a maximum at moderate concentrations of aromatic MCO however is an open question.

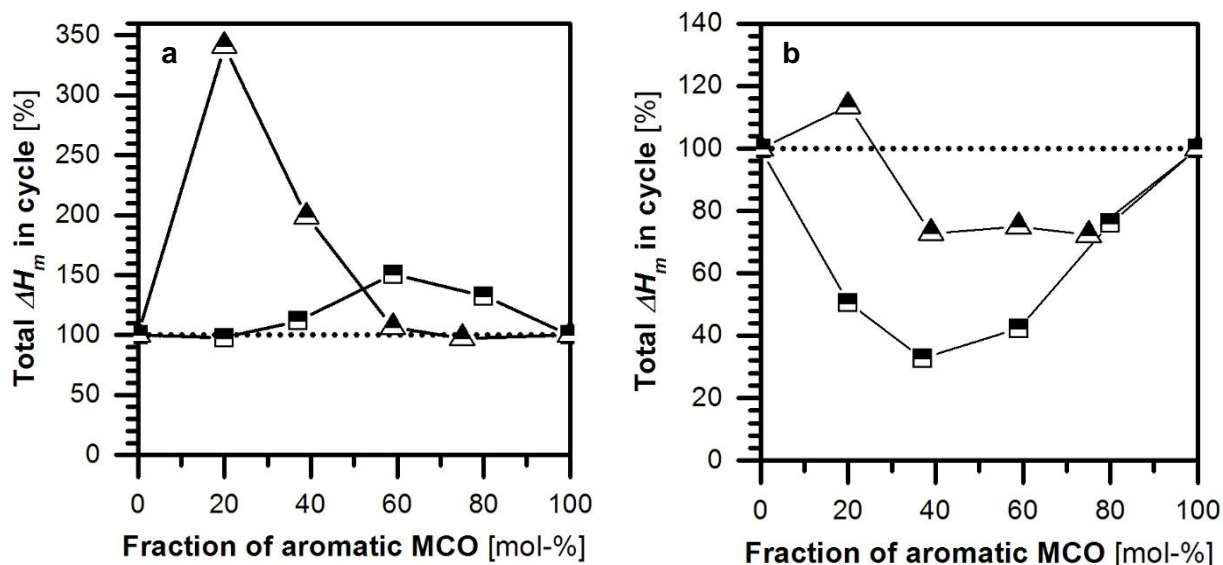


Figure 40: Normalized total ΔH_m of mixtures of cBT (■) or cPT (▲) with cBS during a) the 1st or b) the 2nd heating segment in 3rd DSC runs of the samples (curves of the 2nd run are in agreement but at different levels and hence not displayed).

The crystallization temperature of cBT or cPT with cBA or cBS showed a similar dependency on the composition as observed during the melting despite the different aliphatic monomer and their various diol length. The temperature increases monotonously with the fraction of aromatic MCO (Figure 41). It is shifted to a lower temperature as one would expect for DSC measurements. The obtained curves are superimposable for the two mixtures of one aromatic MCO with the two aliphatic monomers. Previous studies of polyesters showed a dependency of the crystallization on the chain length of the polyester in means of the distance between the polar groups.^{232,236} The enthalpy of crystallization is similar for the comparative mixtures of cBA and cBS with both aromatic MCOs. Cold crystallization was additionally observed in all samples during the second heating except for the fast crystallizing pure cBA, attesting a rearrangement of the crystallites. There is obviously still a potential for crystallization after the cooling segment of a DSC measurement judging from the comparison of ΔH_m of the first and second DSC cycle (compare in Figure 38). Further investigation is needed to deepen the insights into the crystal phases.

A difference in the crystallization behavior between the mixtures of cBT or cPT is seen at low concentrations of the aromatic monomers. Only a small slope of the crystallization temperature in dependence on the cBT fraction has been observed for moderate contents of cBT combined with a sharp drop as soon as its amount is reduced to zero (Figure 41a, no crystallization peak was observed for pure cBS). This curve progression resembles that of

the melting temperature (compare to Figure 36). In mixtures of cPT, the slope is constant over the whole range of the cPT fraction (Figure 41b). Previous studies suggest a hindered formation of crystals by the odd number of methylene groups causing a non-equilibrium orientation and alignment of chains.^{232,233,237,240} CPT itself however exhibits an intense crystallization exotherm ruling out this explanation in this case. It seems more likely that the behavior is caused by the combination of readily crystallizing monomers with an odd and an even number of methylene groups between polar ester groups, the latter having a major influence on strength of crystal bonds. The combination slows nucleation and crystal growth by hindering the alignment of the chains and even producing repulsion in some cases.

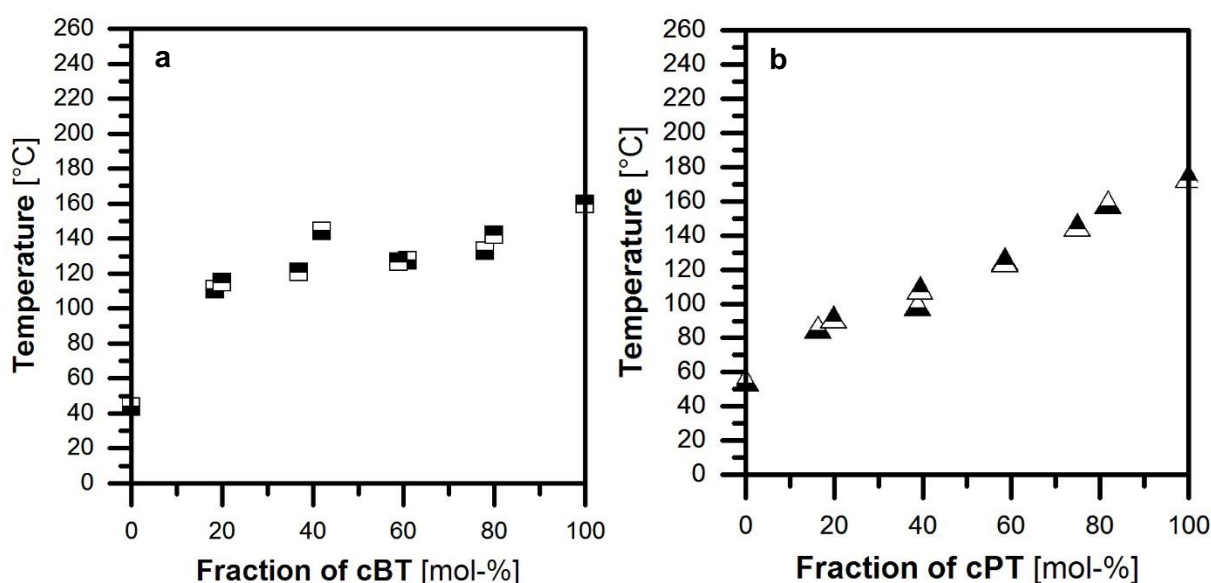


Figure 41: Start of crystallization during 1st cooling in the 3rd DSC run of mixtures of a) cBT with cBA (■) or cBS (□) and b) cPT with cBA (▲) or cBS (△).

The supercooling, ΔT_{sc} , is the difference between the melting and crystallization temperature. It should be considered, that these values have been determined by DSC with a finite heating or cooling rate in this study, which causes a systematic error to the real values determined by infinite slow heating or cooling. The values determined here give however a good indication of the mixtures' properties. ΔT_{sc} of the four mixtures discussed so far is mainly determined by the respective aromatic MCO. It is higher in cPT mixtures than in those of cBT (Figure 42). This is consistent with the more reduced degree of crystallization and the higher melting temperature of cPT mixes compared to those of cBT. The found differentiation between cBT and cPT is in good agreement with the observations of HYBART, PARK, CELLI *et al.* for aliphatic and aromatic polyesters.^{232,233,237} Among other things, a higher supercooling was observed by these groups for polyesters containing a diol with a smaller

and especially an odd number of methylene groups than for even-numbered or longer diols. The dependence of ΔT_{sc} in sample composition with their curve maxima at moderate fractions of aromatic MCOs seems to correlate with the form of the respective ΔH_m curve during initial melting (first heating segment) (compare to Figure 40a). This interestingly indicates a direct correlation between the temperature of crystallization onset and the amount of the formed crystals.

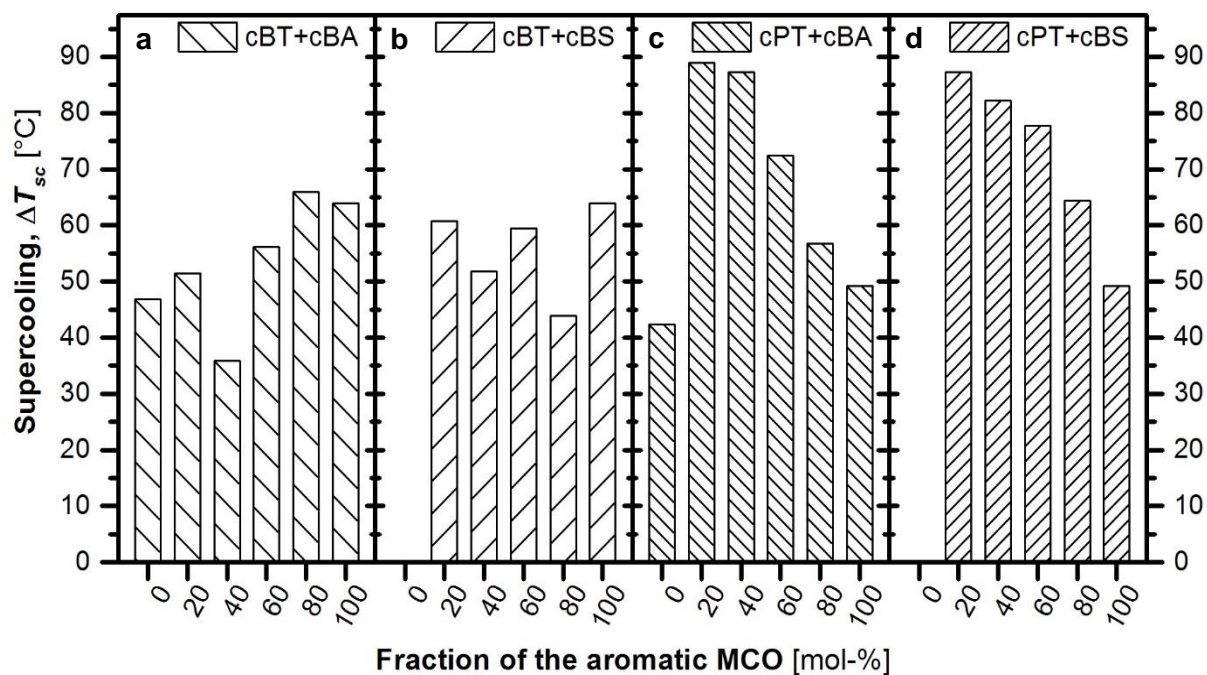


Figure 42: Supercooling of the mixtures of a) cBT/cBA, b) cBT/cBS, c) cPT/cBA and d) cPT/cBS (average of the data from 1st heating in 2nd and 3rd DSC run where applicable).

5.2.2.2.2 Mixtures of the Isophthaloyl-containing MCOs cBI and cPI with cBA and cBS

In mixtures of cBI or cPI with cBA or cBS, only a small reduction of the melting and crystallization temperature of the respective aromatic MCO is observed. CBI has a melting temperature similar to those of the aliphatic MCOs (Figure 43). Pure cPI did not show any melting peak after the very first heating (initial melting at 120 °C) (Figure 44). A similar behavior was observed for both aromatic MCOs. Weak signals and baseline fluctuations complicated the evaluation of the thermograms.

The melting behavior of these four mixtures is dominated by the respective aliphatic component for fractions of cBI or cPI below 60 mol-% (Figure 43 and Figure 44, respectively). Above, the higher melting temperature is almost identical for the respective mixtures with the two aliphatic monomers cBA and cBS (accordingly to theoretical

predictions for the chemical potential of mixtures). It increases slightly with the aromatic fraction. Below this limit, the melting temperature of the two cBA mixtures and of cPI with cBS is similar to that of the respective aliphatic monomer alone. A “plateau” or even a negative slope is observed with increasing content of aromatic MCO. The slopes of the two described curves of the highest melting peak seem to intersect closely to the point of equimolar mixtures, possibly even forming a minimum (upper curves in Figure 43a and Figure 44). The curve belonging to combinations of cBI and cBS exhibit a positive slope with increasing cBI content instead and bend around 50 mol-%.

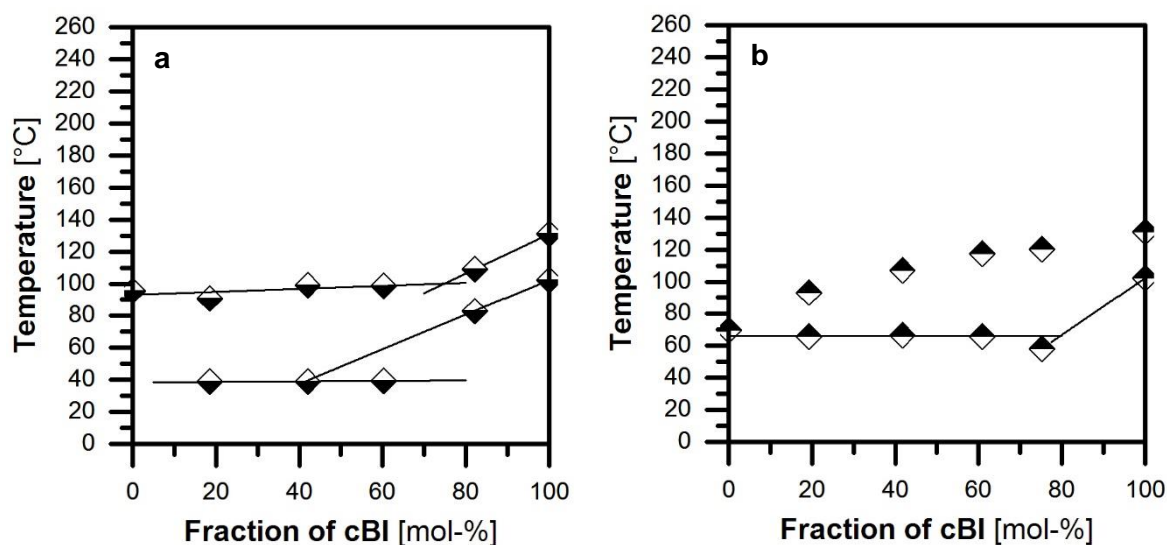


Figure 43: Phase diagram (highest and lowest melting temperature during 1st melting in the 3rd DSC run) of mixtures of a) cBI and cBA and b) cBI and cBS with the display of fittings to lead the eye.

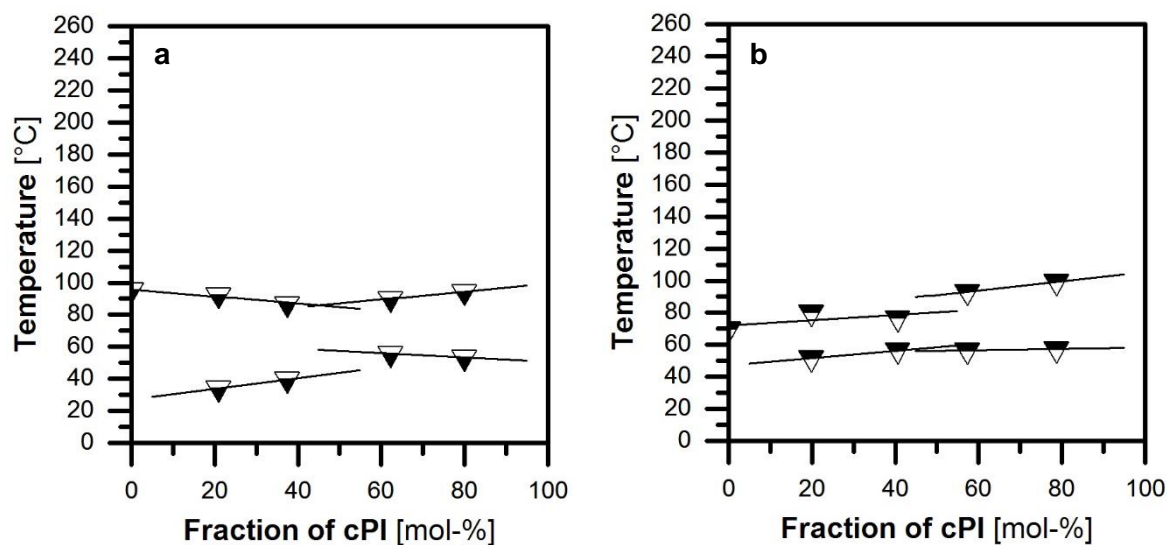


Figure 44: Phase diagram (highest and lowest melting temperature during 1st melting in the 4th DSC run) of mixtures of a) cPI and cBA and b) cPI and cBS with the display of fittings to lead the eye.

It seems evident from the melting temperatures that a crystalline eutectic phase is present in cBA mixtures with cBI or cPI, the low-melting aromatic MCOs. The eutectic mixture has cBA contents of up to 60 mol-% at least. A higher content of aromatic monomer disturbs the formation of this phase leading to the vanishing of the eutectic and of the crystallization peaks as well. A melting endotherm appears at about 40 °C (in a small volume judged by the very small ΔH_m) if both monomers (cBA/cBI or cBA/cPI) are present. This melting temperature is significantly below that of cBA itself (ca. 95 °C). At the same time, the clearly dominant peak exhibits a “tailing” at lower temperatures in case of cBA mixtures with cPI or cBI with contents ≤ 40 mol-% of the aromatic monomer indicating an eutectic mixture (see Figure 45). For higher fractions of cPI or cBI, this “tailing” is difficult to identify because there is an overlap with another, non-influenced melting peak. The mixture with cBS does not show such a behavior. The upper melting temperature of cBI and cBS (in Figure 43b) is generally even higher than that of cBI and cBA (in Figure 43a) despite the lower melting temperature of cBS.

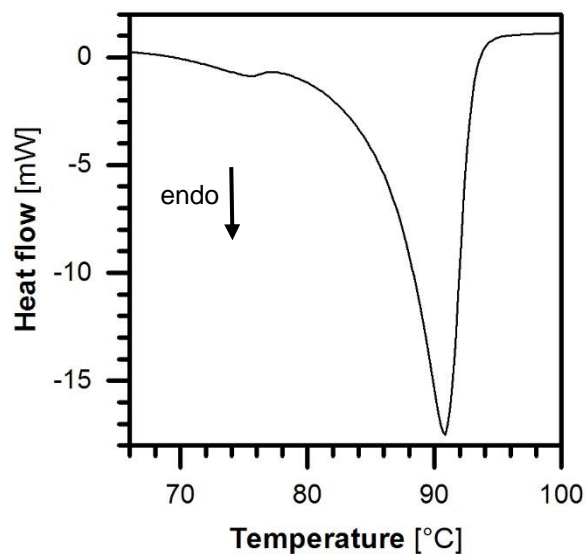


Figure 45: Melting behavior with tailing for the sample cBI:cBA=19:81 during the 1st melting of the 3rd run in DSC.

An increasing crystallization is observed in mixes of cBI and cBA with increasing content of cBI after applying the long period of time between two measurements resulting in an increase in ΔH_m (Figure 46a, absolute values in Figure 38a). Such behavior is not observed for any other of the cBA mixtures but is similar to those of cBS with cBI or cPI (see Figure 49a) and comparable possibly with cPT (Figure 40a). The respective ΔH_m of mixes of cPI and cBA are on the other hand similar to those expected by calculation (Equation 4) during the first heating in the measurements (Figure 46a).

Crystallization of the two mixtures of cBA with cBI or cPI occurs less extensively in the short term (during a DSC measurement) compared to that of pure substances. ΔH_m during the second heating is hence smaller than theoretically expected for both mixtures (except for cBI:cBA=60:40, whose behavior needs further investigation) (Figure 46b, absolute values in Figure 38b). Crystallization exotherms in the cooling segment between the two heatings were observed only for less than 40 mol-% aromatic MCO (Figure 47). These peaks were very sharp with a high heat of crystallization ($>65 \text{ J}\cdot\text{g}^{-1}$). The crystallization temperature of the respective 20:80 mixtures with cBA was reduced remarkably even below that of the pure aliphatic compounds despite of the higher melting temperature of the aromatic compounds of over 120 °C. This decrease is in contrast to the melting observed at significantly higher temperatures. It emphasizes the hindrance of crystallization of cBI and cPI, which seems to be caused by the presence of an isophthalate majority even in presence of readily crystallizing cBA. The aromatic is known to cause slow and only little crystallization.^{232,233,241,242}

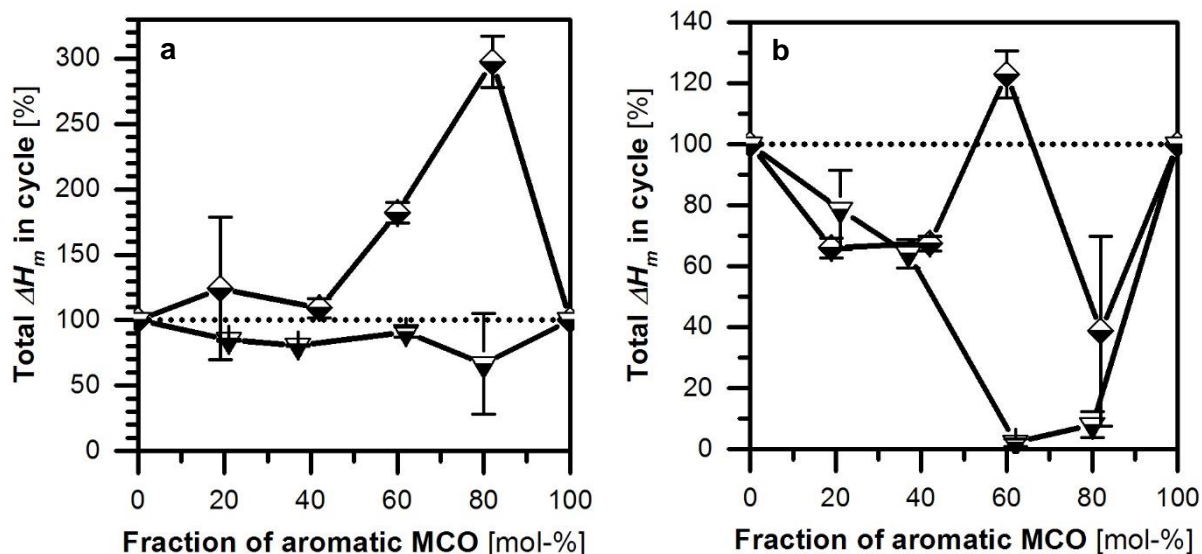


Figure 46: Normalized total ΔH_m of mixtures of cBI (\blacklozenge) or cPI (\blacktriangledown) with cBA during a) the 1st and b) the 2nd heating segment (average values of 2nd and 3rd run in DSC for cBI and of 2nd and 4th for cPI).

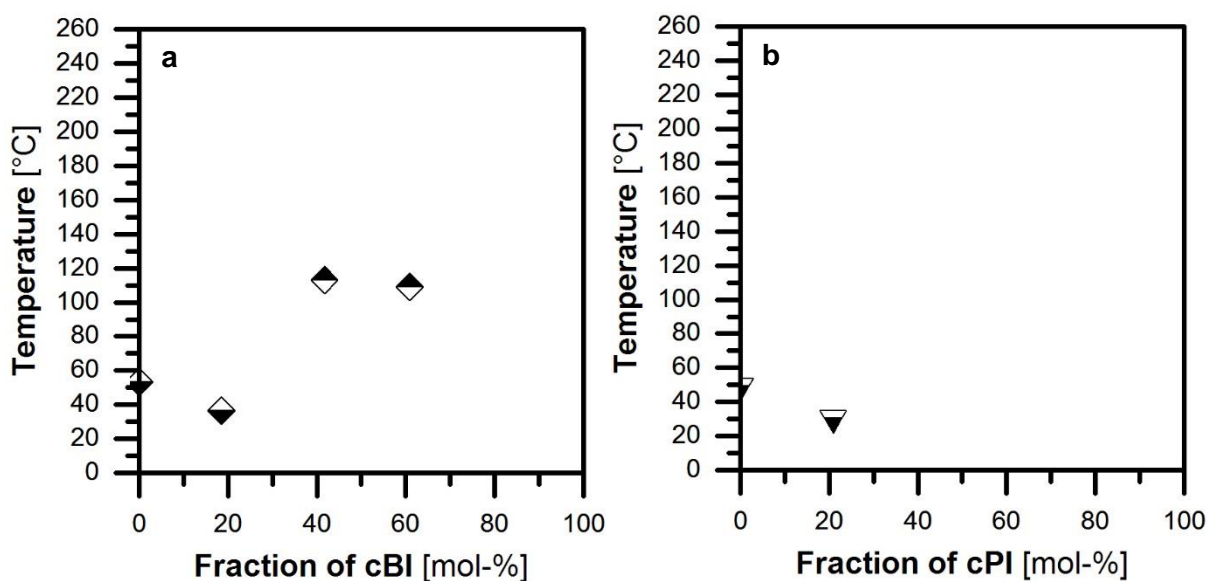


Figure 47: Start of crystallization during 1st cooling of mixtures of a) cBI with cBA (\blacklozenge) or cBS (\blacklozenge) (data of the 3rd DSC run) and b) cPI with cBA (\blacktriangledown) (data of the 4th DSC run, no observed crystallization for cPI and cBS (\blacktriangledown)).

The mixture of cBI and cBA shows a different behavior during the second heating than in the first in all of the three measurements. This is probably related to the mentioned short-term hindrance in nucleation. The behavior is in contrast to that of other investigated combinations of an aromatic and an aliphatic monomer. While an increase of the endset

melting temperature with the fraction of cBI is noticeable during the first heating, during the second melting a decrease of this temperature is recognizable. The more cBI is present, the more difficult is nucleation. The endset melting temperature during the first and second heating of the third DSC measurement are presented (Figure 48, black markings, the value of the 40:60 mixture had to be discarded). Additionally, the values from the second run are presented subjacent in dark grey. The mentioned hindrance in crystallization by the presence of cBI is not overcome in the time of a DSC measurement, but is not noticeable anymore after 4 d, when a regular melting behavior is observed again. The slow crystallizing cBI appears to hinder the crystallization of cBA.

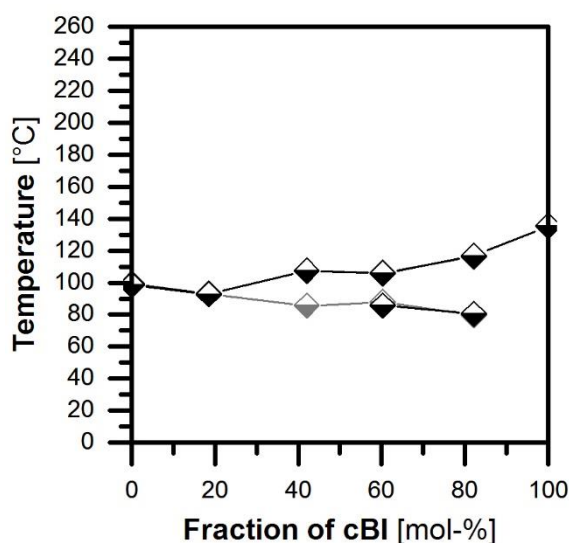


Figure 48: Different curves of melting endset temperatures of cBI:cBA mixtures during 1st (upper curve) and 2nd heating (lower curve) of the 2nd (dark grey) and 3rd run (black, except cBI:cBA= 40:60).

Interestingly, an interaction of cBI or cPI with cBS somehow leads to an enhanced crystallization between two consecutive DSC measurements, but to a hindered one between two runs in one measurement (in contrast to the expectations based on the properties of the pure monomers) (Figure 49, absolute values in Figure 38). All mixtures of cBI or cPI with cBS possessed melting peaks with a significant ΔH_m during the first heating, although neither cBI, cPI nor cBS alone exhibit melting endotherms with a noteworthy ΔH_m (Figure 49a). The high values of the ΔH_m in the figures stem from the normalization with the very small melting endotherms of the pure monomers according to Equation 4. Even comparatively small ΔH_m thus appear as high percentage. It however still gives an impression of the increase of crystallization. The shown data in Figure 49 is obtained only from the third run in DSC for cBI blends and the fourth for cPI as the data from the previous runs were less reliable because of

baseline fluctuations. Nevertheless, the observed behavior was essentially the same in all measurements.

The observed hindrance in crystallization for blends of cBI or cPI with cBS for at least within the period of a cooling segment in DSC measurement is more pronounced than in corresponding cBA mixtures (compare (Figure 49b to Figure 47). No or only almost negligible peaks were detected during the second heating ($< 3 \text{ J}\cdot\text{g}^{-1}$), which are significantly below those expected from calculations. The different behavior of the mixtures of cBI and cPI with cBS respectively with cBA can be explained by the observations of HYBART *et al.*, as well.^{232,233} A polyester with short chains between the carboxyl groups like PET was found to crystallize more slowly than polyesters with long chains as PBT or poly(1,6-hexamethylene terephthalate), but reach a higher final crystallinity. The same seems to be true for mixtures of cBS compared to cBA, if no other readily crystallizing, i.e. a terephthalate-containing monomer, is present.

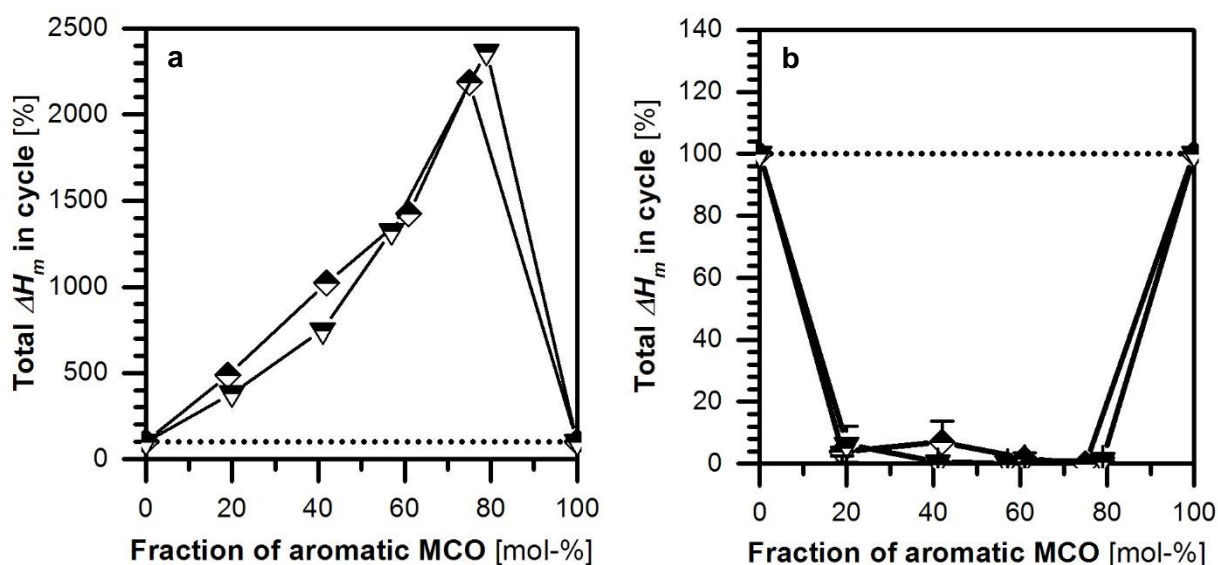


Figure 49: The normalized total ΔH_m of cBS mixtures with cBI (\blacklozenge) and cPI (\blacktriangledown) during a) the 1st or b) the 2nd heating of the 3rd (for cBI) or 4th (for cPI) DSC run.

5.2.2.2.3 Glass transition of mixtures of the aromatic with the aliphatic MCOs

Glass transitions were observed for all mixtures of an aromatic with an aliphatic monomer except for the mixture of the highly crystalline and readily crystallizing monomers cPT and cBA. cPT showed in repetitive DSC measurements no glass transition at all, the ones of cBA were generally only indicated.

Extended cooling to $-90 \text{ }^\circ\text{C}$ was necessary to obtain T_g 's, which was carried out in additional measurements keeping the rest of the method unchanged. Only one glass

transition was observed in all cases in which a glass transition was recognized at all. It has to be mentioned that an erratic baseline complicated the identification of possible additional glass transitions. Therefore, a temperature-modulated DSC experiment (TOPEM® by Mettler Toledo) was carried out in cases of doubt. No additional glass transition was observed in any of those cases.

The general influence of the mixture composition on the glass transition temperature (Figure 53 to Figure 55) underlines the miscibility of the aromatic and the aliphatic monomers as concluded by the interdependency of T_m and T_c . The size of the markings in the figures indicates the ΔC_p during the respective transition. The dashed lines in the diagrams are the fits according to FOX (Equation 5):

$$\frac{1}{T_g} = \frac{w_1}{T_{g,1}} + \frac{w_2}{T_{g,2}} \quad (5)$$

where $T_{g,i}$ is the glass transition temperature of the pure components and w_i is their mass fraction. There are fits that are more accurate than the FOX equation for describing the relationship between the glass transitions and the composition, of course. The FOX equation is generally applicable to comonomers with similar molecular structures, with similar solubility parameters and with only weak intermolecular interaction. It is an adequate testing tool for additional effects present in the mixtures in dependence on the mixture composition and was hence applied in this study. The sealing of the DSC pans to prevent sublimation and evaporation may have altered the found ΔC_p as the pressure may not have been constant. However, changes in pressure and ΔC_p can be considered relatively small. They do not effect observed fundamental trends and are thus neglected here.

Mixtures with cBS showed a dependency of the glass transition on the ratio of the used monomers similar or even according to the FOX equation (Figure 50 and Figure 51). A T_g below that of the FOX equation was observed for combinations of cBS with more than 20 mol-% of a terephthaloyl-containing monomer, i.e. cBT or cPT (Figure 50), resulting in an S-shaped curve with a flattened slope between 20 and 40 mol-%. Additional effects as plasticizing must gain importance with increasing aromatic fraction, but the exact cause for the deviation has not been revealed yet. The glass transition was more intense for cBT and cPT contents below 40 mol-%. A decrease of ΔC_p with the terephthalate content was noticed. It was not reflected by a general increase of total ΔH_m during the subsequent heating (compare to Figure 40).

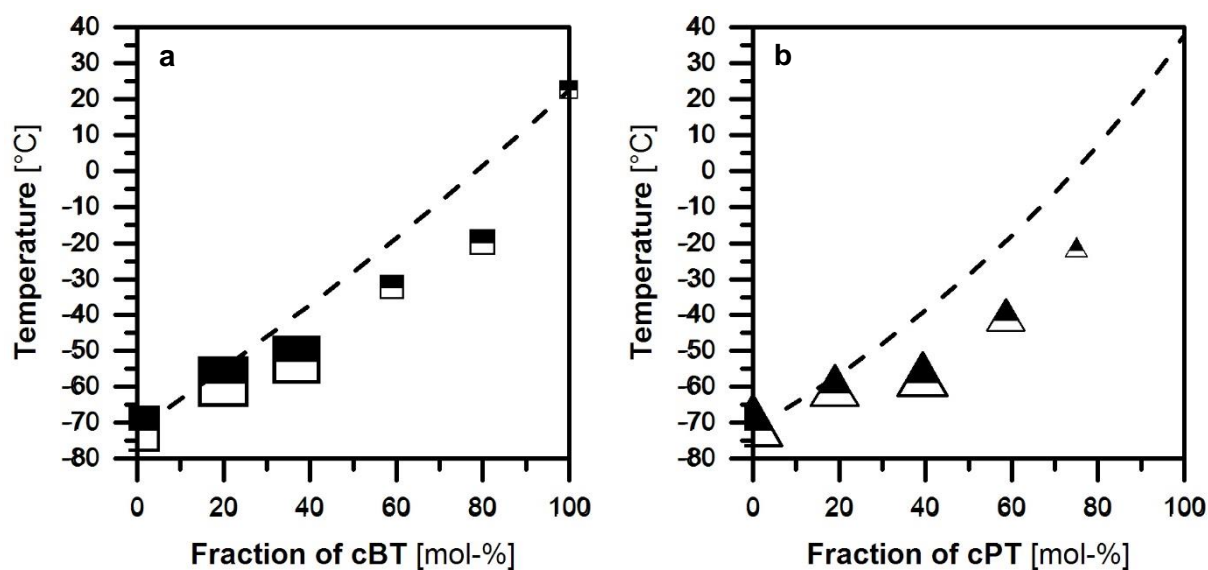


Figure 50: T_g 's of the 2nd heating of the 3rd DSC run of cBS mixtures with a) cBT or b) cPT. The size of the respective marking indicates the ΔC_p .

For blends of cBS and a monomer containing isophthalic acid, the FOX equation seems applicable (Figure 51). Small deviations are possibly caused by the variance of DSC measurements.²⁴³ The glass transitions seem to become less intense for fractions of aromatic MCOs above 60 mol-%. The intense transitions indicate a high fraction of amorphous phase in the sample, which is not present at the beginning of the DSC measurement as no glass transition is initially observed in DSC runs. This is consistent to the different behavior of ΔH_m between the first and second cycle in DSC measurement (Figure 49b) and underlines the deduced hindrance of crystallization for these samples.

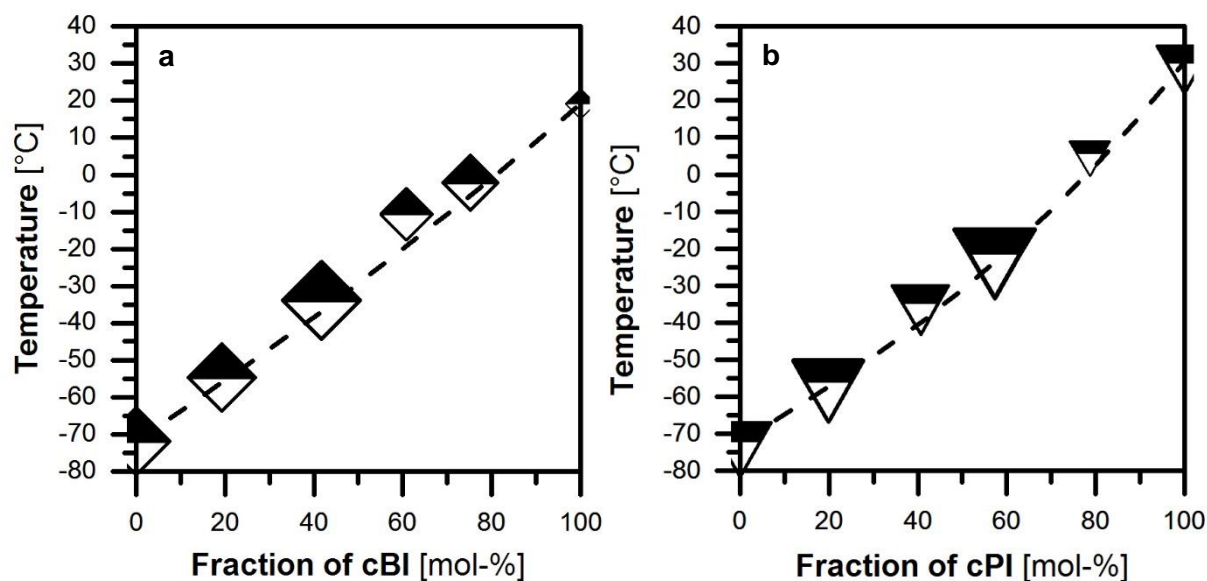


Figure 51: T_g 's in the 2nd heating of cBS mixtures with a) cPT (data from 3rd DSC run) or b) cPI (data from 4th DSC run). The size of the respective marking indicates the ΔC_p .

Only minor cold crystallization in terms of heat of cold crystallization, ΔH_{cc} , occurs in all studied cBS mixtures at a temperature above the glass transition (Figure 52a). This supports the conclusion of a long-lasting hindrance of crystallization deduced from the respective ΔH_m in the two cycles (Figure 49).

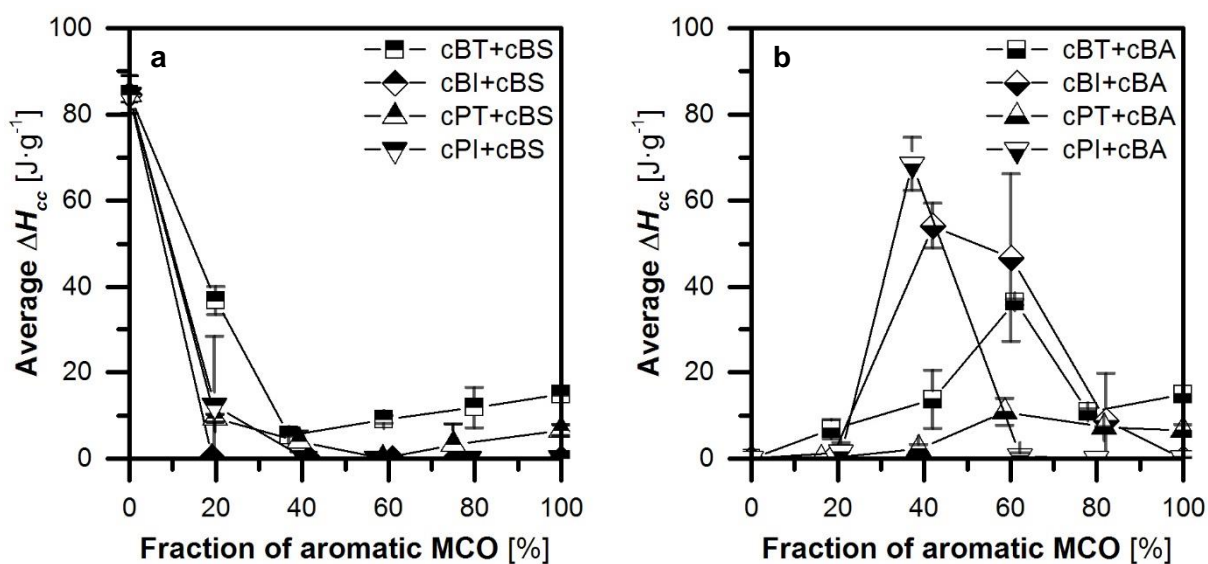
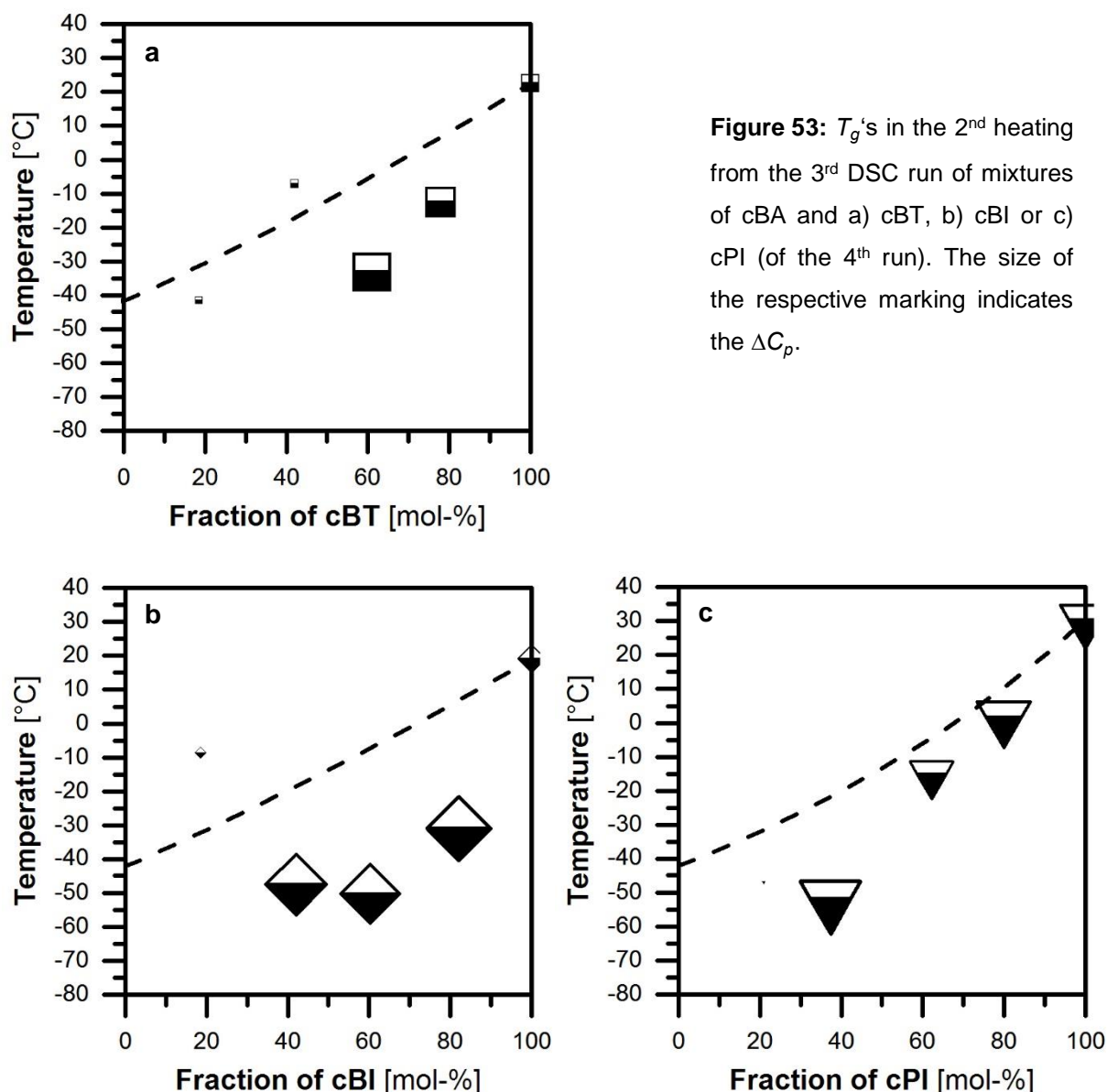


Figure 52: Heat of cold crystallization ΔH_{cc} of 3rd or 4th DSC run of the mixtures of cBT, cBI, cPT and cPI with a) cBS or b) cBA.

Comparing the terephthalate-containing cBS mixes, cBT mixtures exhibit easier nucleation. ΔH_{cc} is below $10 \text{ J}\cdot\text{g}^{-1}$ for all these mixtures, higher for cBT than for cPT. Again, this is consistent with the observations regarding crystallization hindrance conducted from the normalized ΔH_m (Figure 40). It has not been understood so far why pure cBS showed remarkable melting endotherms only after cold crystallization in the second cycle of the DSC measurements, but not in the first cycle of the subsequent measurement.

An additional interaction of the monomers lowers the T_g of cBA mixtures below predictions of the FOX equation, when a significant amount of aromatic monomer is present. The respective T_g deviates from the predictions by at least $10 \text{ }^\circ\text{C}$ (Figure 53). A “plateau” is formed in the cPI/cBA curve between 40 and 60 mol-% cPI. The curves of the T_g vs. the aromatic fraction for higher contents of aromatic MCOs (>40 mol-% for cBT and >20 mol-% for cBI or cPI) do not seem to match the curves formed by samples with smaller content. A high ΔC_p is found in the range of these higher amounts of aromatic MCOs despite only small glass transitions in the pure monomers (except cPI). Very small transitions by means of ΔC_p are detected below this concentration, if any. The intense glass transitions of the cBA blends with a high aromatic fraction have no reciprocal pendant in the curves of the total ΔH_m , which reflects the crystalline parts (Figure 39b and Figure 46b). Only the combination with cPI shows a significantly lowered ΔH_m .

The different influences of cBA and cBS have not been fully understood. Possibly, cBA combines chain flexibility and mobility in its cycles. It results in a fast and comparatively simple arrangement in crystals and hence in a smaller amorphous phase than in cBS. This effect is especially been seen in combinations with MCOs containing the not readily-crystallizing isophthalate.



The similar behavior of cBT and cPT and of cBI and cPI concerning the glass transition is in contrast to findings of HYBART *et al.* for polyesters.^{232,233} They found the T_g more depending on the length of the diol as source of chain flexibility than on differences in structural hindrance caused by different diacids. Therefore, an additional effect caused by the mixing must be taken into account. To assume a significant influence of the aliphatic monomer cBA or cBS seems appropriate as even mixtures with low amounts of cBA or cBS have properties different from the aromatic compound. Furthermore, it is rather interesting that the structurally similar cBA and cBS provoke such a different behavior in combinations with cBI or cPI.

Only a fraction of the mixtures with cBA appears to crystallize during cooling, if any, while the rest vitrifies. A comparatively high free volume in the amorphous phase and

crystallization after first liquefaction (i.e. at $T > T_g$) is the result, especially at a composition near to equimolar. A high ΔH_{cc} was noticed in the cBA combinations during the second heating except for the cPT blends (Figure 52b). Its curve progressions for the mixtures with cBT, cBI or cPI reflect in general lines the deviations of the T_g from the FOX equation. Mixtures of cBA and cPT resemble the cBS mixtures in their cold crystallization behavior. This is consistent with their described tendency to crystallize and the absence of a glass transition.

5.2.2.3 Combinations of the aromatic MCOs among each other

The binary mixtures of the aromatic MCOs with each other showed a similar thermal behavior in general (as expected from general thermodynamic considerations), although no two are alike in all aspects. A close resemblance of the dependency of the melting and crystallization behavior on the composition was observed between the three DSC runs of each sample. Exceptions were the combinations of cBI with cPT and of cBI with cPI. A shift of the measured melting and crystallization transitions to lower temperatures was observed with the number of DSC measurements for the mixtures of cBI and cPT, more pronounced the higher the amount of cBI (Figure 61b). The combination of cBI and cPI possesses, if any, only features with a small enthalpy (in the third run $< 1 \text{ J}\cdot\text{g}^{-1}$ except for pure cBI). Combined with a generally noisy baseline, this did not permit a more detailed examination of the melting and crystallization behavior.

A solubility of the aromatic MCOs in each other can be concluded from the observed dependencies of the properties in DSC. The phase diagrams appear as expected for soluble substances. The thermal behavior is influenced only to a small extent by the fractions of the respective MCOs. The changes with the mixture composition are small in most cases, especially considering the respective differences between the monomers' melting temperatures (highest melting peak of cBT at 183 °C, of cBI at 131 °C, of cPT at 222 °C, of cPI for initial melting in the very first heating at 120 °C). Exceptions are the combinations of cBT with cBI and with cPI, the two monomers with an isophthaloyl moiety. Similar phase diagrams were obtained for both mixtures despite the different diol length of the second monomer (Figure 54). Furthermore, a high similarity of these cBT combinations to those with the aliphatic monomers, cBA and cBS, is obvious (Figure 36). Compared with these, there is a shift to higher temperatures, as one would expect from the melting temperatures of the pure monomers (cBA 95 °C, cBS 65 °C). A difference is the unusual presence of only one crystalline fraction in the sample with cBT:cPI=20:80 (Figure 54b) although several melting endotherms are observed in other compositions.

5.2.2.3.1 Mixtures of cBT with the isophthaloyl-containing MCOs cBI or cPI

The mixtures of cBT with cBI possessed a low-melting fraction similar to that of the mixtures of cBT with the aliphatic MCOs (Figure 54a). Crystallization of these combinations was found to be difficult for high cBI contents. No crystallization endotherm was detected below 40 mol-% cBT (Figure 55a). The relative ΔH_m was found to decrease between 40 and 80 mol-% cBI, connected to its raise from below to above the values calculated by equation 5 (Figure 56a; ΔH_m during first heating, comparable to second heating, which is hence not depicted).

A consistent melting behavior was observed for mixtures of cBT with cPI including the low-melting fraction (Figure 54b). The melting temperature in cPI blends is lower than the other ones measured for cPI in this study. A corresponding crystallization endotherm was not observed during cooling, indicating its slow crystallization (Figure 55b). The relative ΔH_m is below the theoretical expectations over the whole range of the composition during the first heating segment (Figure 56b).

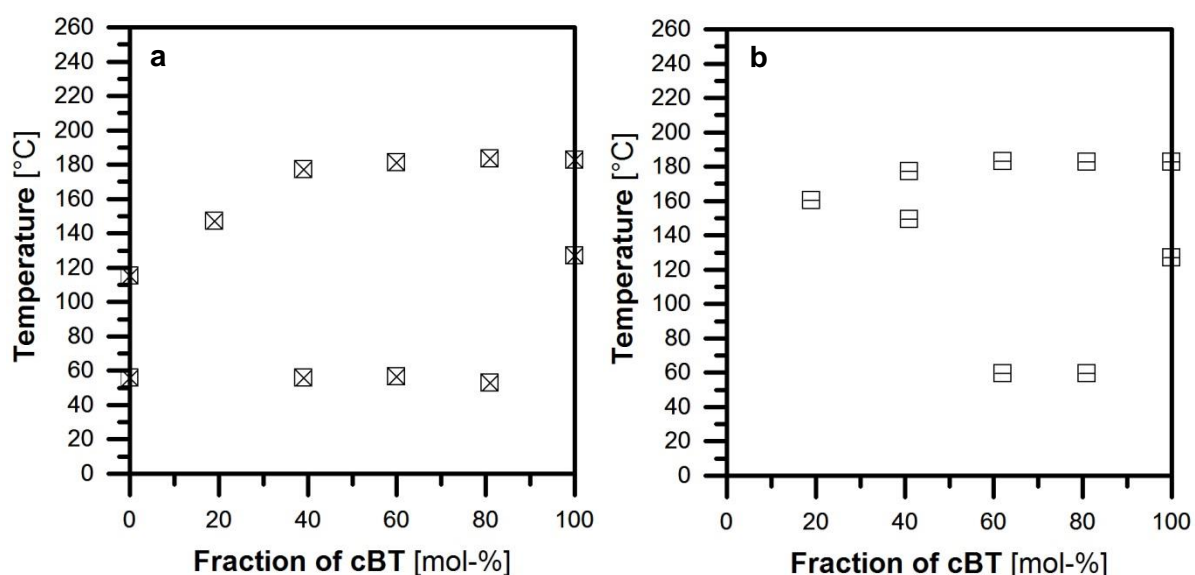


Figure 54: Phase diagram (highest and lowest melting temperature during initial melting in the 3rd DSC run) of mixtures of a) cBT and cBI (excluding lowest melting temperature of cBT:cBI=19:81 because of overlapping with endothermic recrystallization) and b) cBT and cPI.

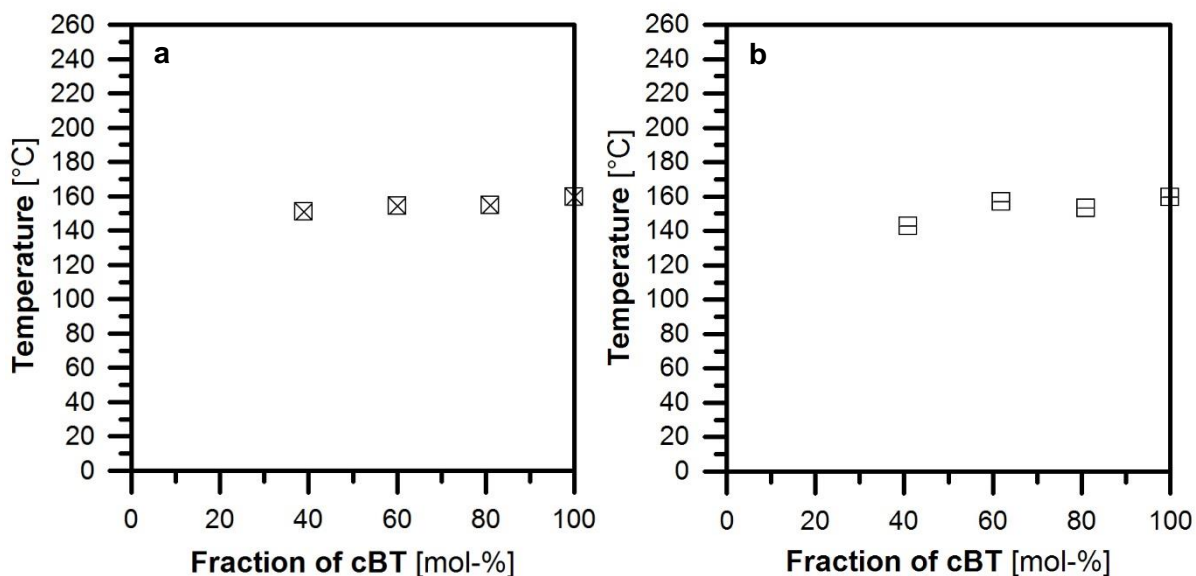


Figure 55: Temperature at start of crystallization of mixtures of a) cBT and cBI and b) cBT and cPI (in 3rd DSC run).

Comparing the thermal properties of the mixtures of cBT with cBI or with cPI, the low-melting fraction interestingly appears to be dependent on the presence of cBT with its larger heat of fusion. A hampered crystallization was observed for high contents of the isophthaloyl-containing monomer with no crystallization endotherm below 40 mol-% cBT (Figure 20). The ΔH_m during first and second heating supports the conclusion of a hindered crystallization for increasing isophthalate fraction. The dependency of the melting process and of the crystallization temperature on the fraction of cBT is less pronounced in mixtures with cPI than with cBI. The plateau values of the higher melting temperature for higher cBT contents has interestingly not been reported for randomly copolymerized poly(1,4-butylene isophthalate-co-terephthalate) with comparative fractions of isophthalate and terephthalate.²⁴⁴ The reason for this could be related to the statistical distribution of two repetition units in the polymer after transesterification during polymerization instead of block-like forms in the MCOs.

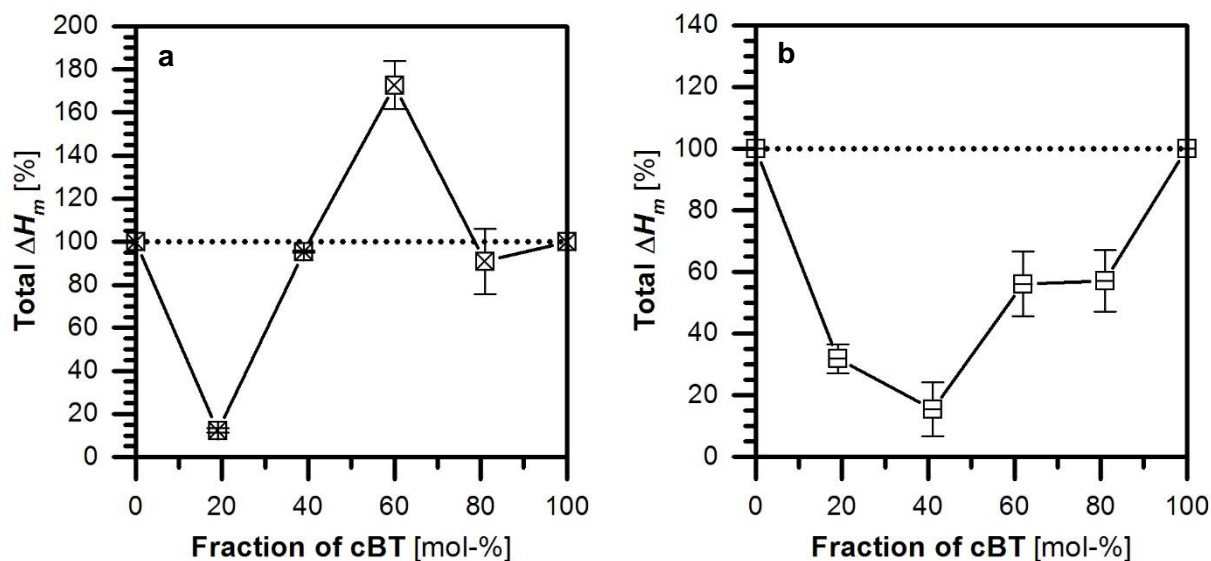


Figure 56: The total ΔH_m relative to calculations by equation 4 a) of cBT and cBI and b) of cBT and cPI during the 1st heating (average of run 2 and 3).

5.2.2.3.2 Mixtures of cPT with cPI

Mixtures of cPT with cPI showed a similar dependency of the highest melting temperature on the sample composition to those of cBT with cBI and with cPI (Figure 57 and Figure 54a and b). This is also true for the crystallization behavior (not depicted). However, a lower melting fraction was not observed for cPT/cPI mixes.

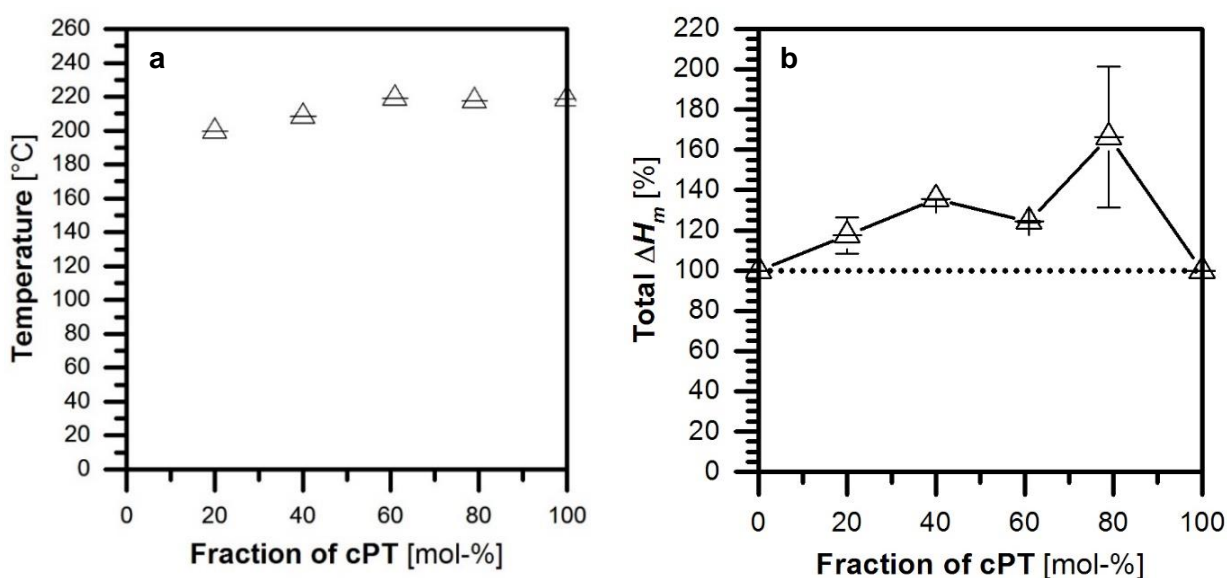


Figure 57: a) Upper melting temperature (during the 1st heating in the 3rd DSC run) of mixtures of cPT with cPI and b) the respective total ΔH_m (average of 2nd and 3rd run) in respect to the values calculated.

5.2.2.3.3 Mixtures of the BDO-containing MCOs cBT or cBI with cPT

The phase diagrams of mixtures of cBT and cPT were found to have a dependency on the composition with the formation of a low-melting fraction (Figure 58a). The highest melting fraction showed only a small variation with changes in the composition. The amount of this lower-melting phase seems to reach a maximum at equimolar fractions. The total ΔH_m is slightly but reproducibly higher than the expected value (Figure 59a). This is also true but less obvious in the second heating segment.

A similar behavior has been observed for mixtures of cBI with cPT. A composition-dependent phase diagram has been observed with a low-melting fraction, maximal at about equimolar amounts, and only little shifting of the highest melting peak with the altering of the composition (Figure 58b). Again, the total ΔH_m is especially in the first heating segment of each DSC run slightly but reproducibly above the expected values (Figure 59b).

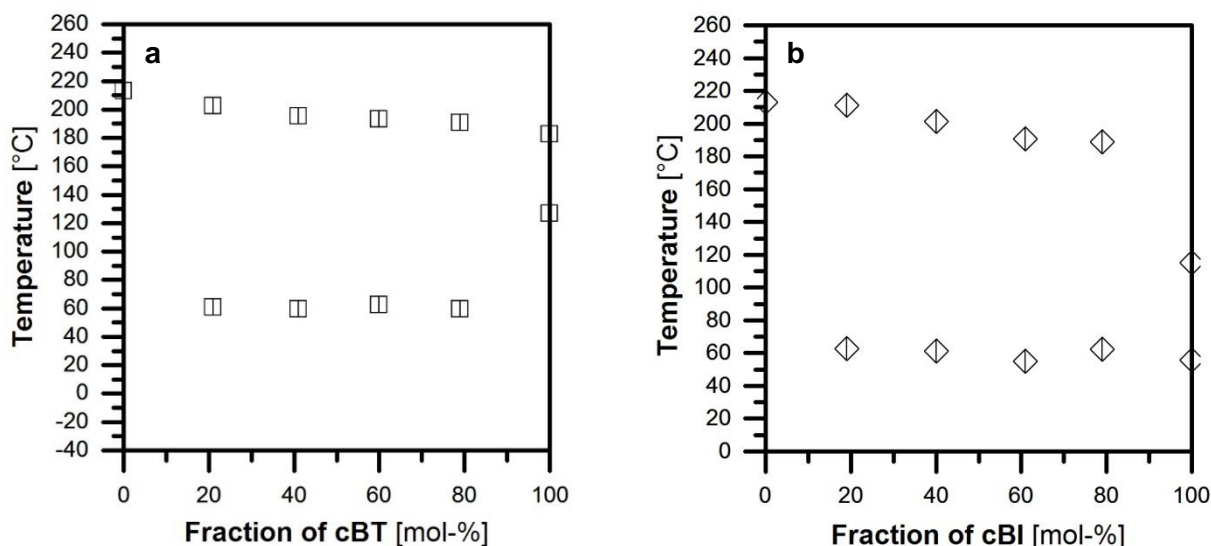


Figure 58: Phase diagram (highest and lowest melting temperature during initial melting in the third DSC run) of mixtures of a) cBT and cPT and b) cBI and cPT.

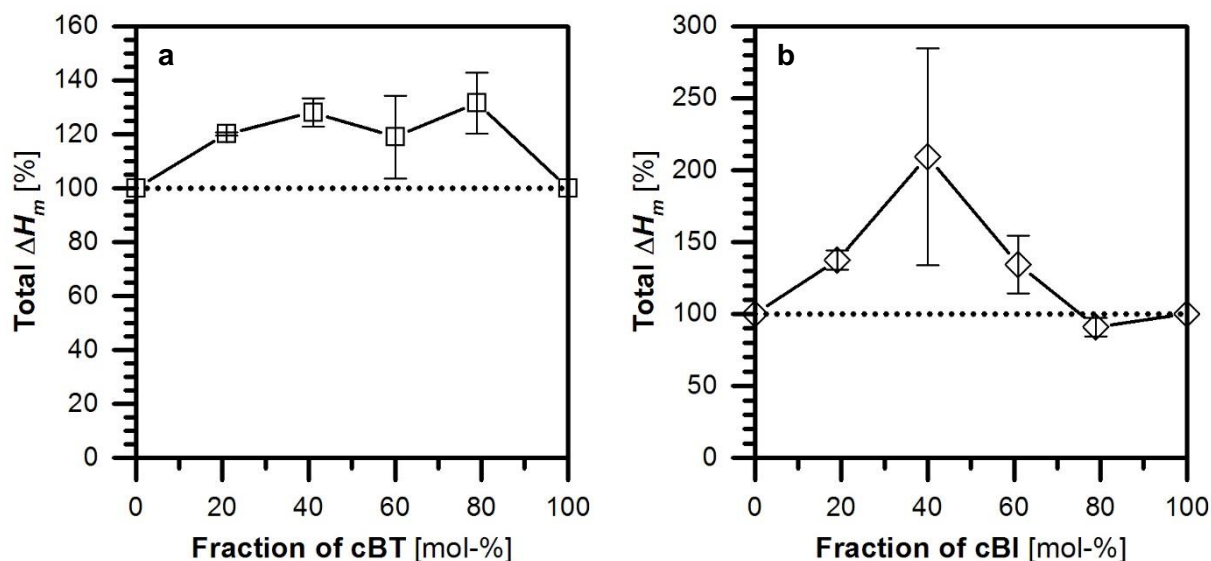


Figure 59: Average of the ΔH_m of all melting endotherms during the 1st heating of the 2nd and 3rd run of mixtures a) of cBT and cPT and b) of cBI and cPT.

The similarity of the phase diagrams of the combinations of cBT or cBI with cPT is obvious. The amount of the low-melting phase is, however, smaller for cBI/cPT blends than for cBT with cPT (concluding from the ΔH_m of the respective DSC peaks; Figure 60). The melting peaks of the pure components cBT and cPT are at significantly higher temperatures (lowest melting peak of cBT >126 °C and of cPT >212 °C). It is not clear whether the low-melting phase in the combination of cBI with cPT is of similar character to that of cBT with cPT, as cBI itself has a fraction melting at a similar temperature. A distinction between newly formed phase and previously existing crystal structure is challenging. However, it seems likely that the low-melting fraction is formed by the combination of monomers, as well, because the ΔH_m of the peak at low temperature (Figure 60) shows no dependency on the fraction of cBI.

In the time between two DSC measurements, an enhanced crystallization can be derived for both mixtures of cPT with cBT or cBI, respectively, from their ΔH_m of the first melting in the third cycle (Figure 59).

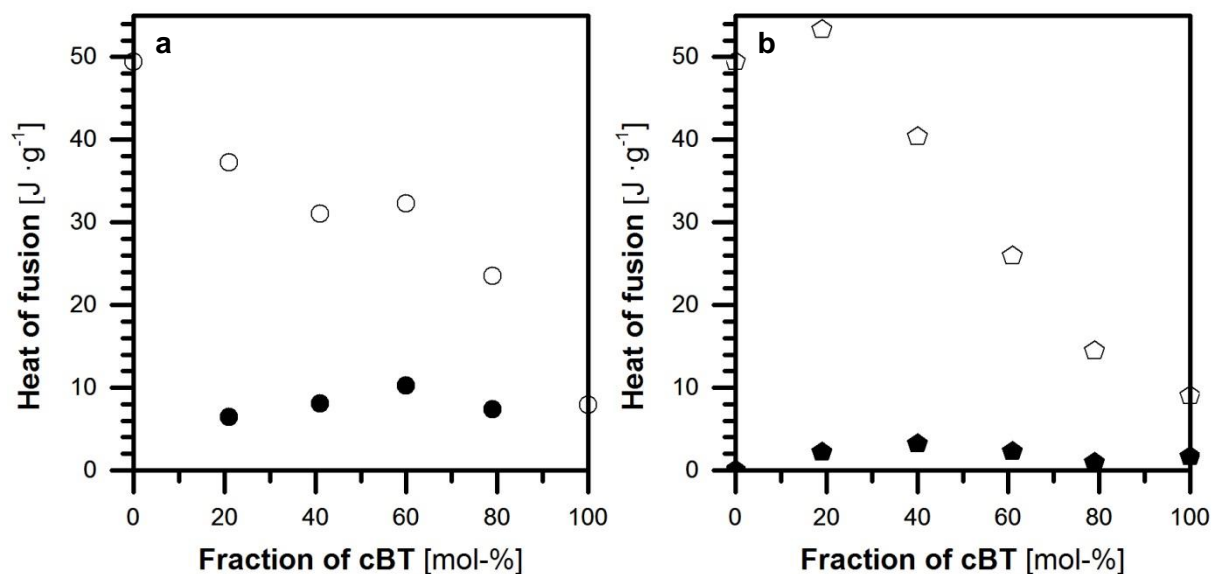


Figure 60: Values of ΔH_m of the lowest (filled markings) and highest melting endotherm (hollow markings) for mixtures of a) cBT and cPT and b) cBI and cPT during the 1st heating of the 3rd run.

A change of crystalline phase takes place in the mixtures of cBI and cPT between runs in DSC. The fraction-dependent melting temperature and to a lesser extent the crystallization temperature shift with runs to smaller values, while ΔH_m remains within the same dimension (Figure 61; data of the first to third run in light grey to black). The difference is up to 23 °C between the runs. The peak form is identical for every sample, at least for the second and third run (initial melting and mixing takes place in the first run). This excludes a degradation or transformation of the sample as cause.

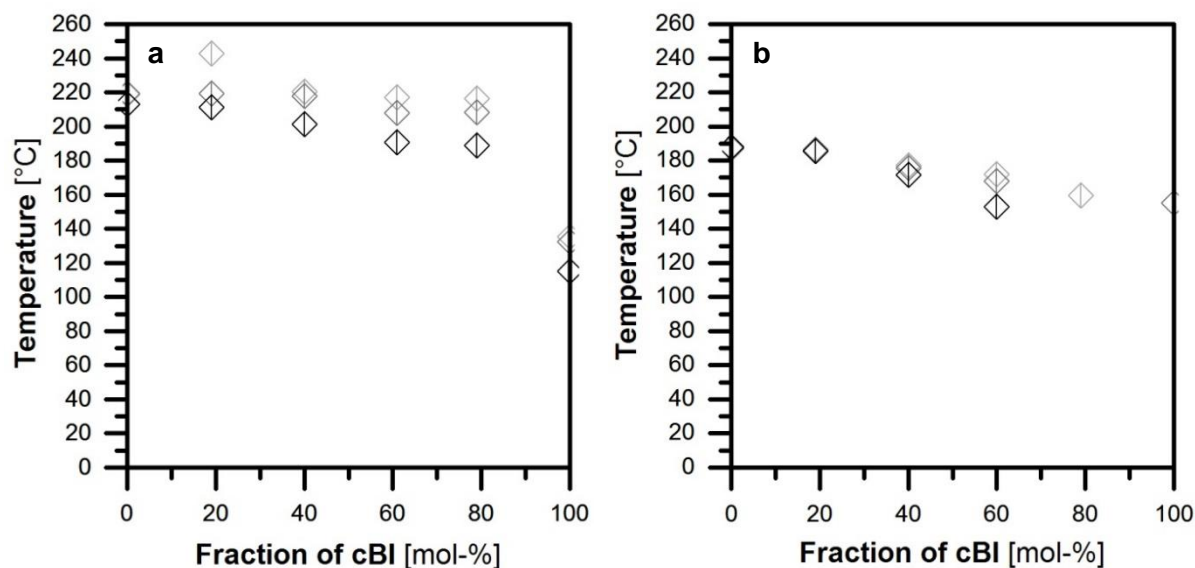


Figure 61: a) Endset temperature of the melting and b) high limit of crystallization of blends of cBI/cPT (1st DSC run in light grey, 2nd in dark grey and 3rd in black).

Comparing mixtures containing only BDO as diol (cBT/cBI) with those containing only PDO instead (cPT/cPI), it has been noted that a stronger interaction seemed to occur in mixtures of cBT and cBI than in those of cPT and cPI. The reduction of the melting temperature for mixtures of cPT and cPI is smaller than that in the comparative combinations of cBT with cBI, although the respective difference between the pure monomers' melting temperatures is higher for cPT and cPI than for cBT and cBI (102 vs. 52 °C). The longer aliphatic chain seems crucial for a stronger interaction. The latter is also indicated by the higher maximum of the relative ΔH_m of mixtures of cBT and cBI in the first melting, implying a larger amount of crystalline phase.

5.2.2.3.4 Mixture of the isophthaloyl-containing MCOs cBI and cPI among each other

Mixtures of cBI and cPI exhibit a hindered crystallization, which resulted in only very small endotherms during the heating segments of DSC measurements and in no crystallization exotherms. The thermograms had a noisy baseline with an inaccurate determination of the melting peaks, preventing meaningful evaluation of the values. At the same time, a glass transition was clearly observed, especially for high amounts of cPI. This implies a high fraction of amorphous material, which is further discussed below on basis of Figure 64a in context of the glass transition of the aromatic mixtures.

5.2.2.3.5 Supercooling of the aromatic MCO combinations

ΔT_{sc} of the samples was similar for all tested mixtures (about 48 – 65 °C, when considering the melting temperatures in the second cycle of the third DSC run). Values could only be obtained when both crystallization and melting peaks were detected.

Differences were observed with respect to the melting data from the first heating cycle (Figure 62). Larger ΔT_{sc} were observed for the mixtures of cBT/cPI, cBI/cPI and cPT/cPI, i.e. all mixtures with an isophthalate and a PDO moiety. A maximum at about equimolar composition is apparent. The presence of isophthalate or PDO alone is not sufficient for enhanced supercooling in contrast to the observation on polyesters.^{232,233}

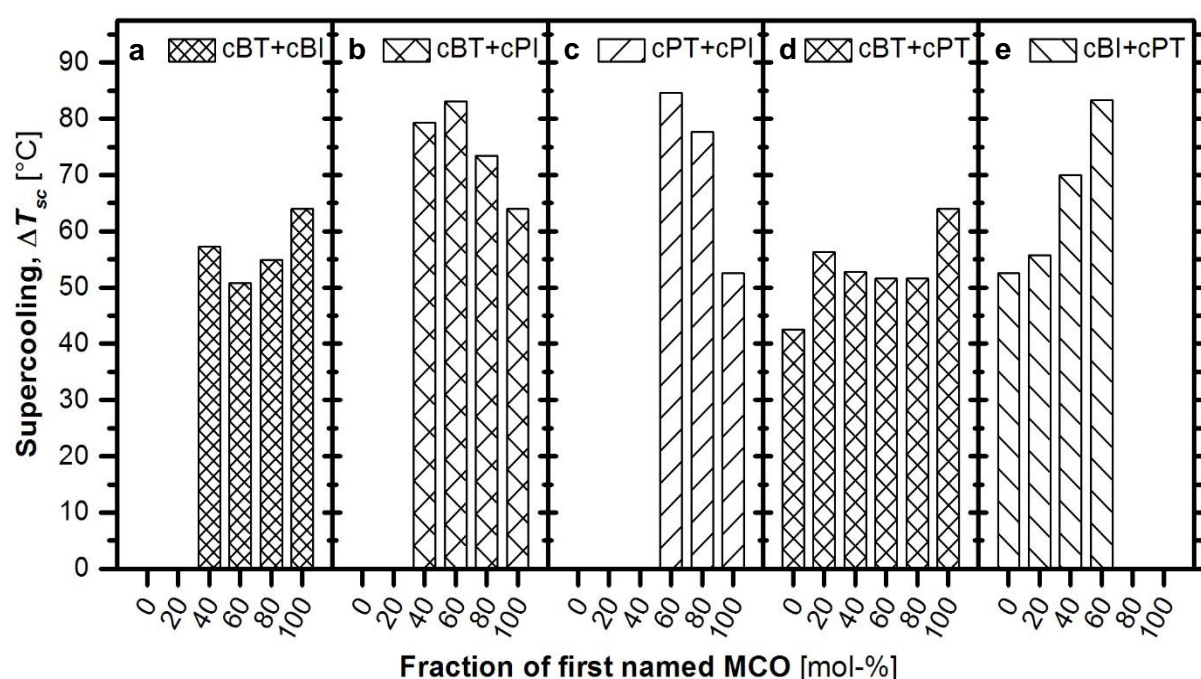


Figure 62: Supercooling (difference between highest melting and crystallization temperature) of the first heating and cooling segment of the 3rd DSC run for the mixtures of the aromatic MCOs. No melting or crystallizing was observed for the mixture of cBI/cPI.

5.2.2.3.6 Glass transition of the aromatic MCO combinations and their cold crystallization

Only one glass transition was observed for all tested combinations of aromatic MCOs, which is a reliable indication of successful mixing of the monomers in the melt. The dependency of the T_g 's on the fraction of the respective monomers obeys the FOX equation except for the blend of cBT with cPT (Figure 63, Figure 64 and Figure 67). The size of the markings in the figures indicates the intensity of the glass transition by means of ΔC_p . The difference between the glass transitions of the pure MCOs in the respective mixtures is

rather small in all cases (below 18 °C) compared to those in the mixtures with the aliphatic monomers cBA and cBS. Hence, systematic deviations from the expectations by the Fox equation (broken lines) would be rather small and hard to detect.²⁴³

A comparatively large amorphous fraction was found in combinations of cBT, cBI or cPT with cPI. High values of ΔC_p were measured for these three mixes (Figure 63b, Figure 64a and b), which is consistent with the poor crystallizing of cPI itself and of its mixtures. The amount of this amorphous phase seems to be rather constant over the whole range of sample composition of the cBT/cPI and the cBI/cPI mixtures (Figure 63a and Figure 64), but decreases with the cPT content in blends of cPT and cPI (Figure 64b). The thermograms of the three combinations of cBT, cBI or cPT with cPI show a good reproducibility between the runs.

The ΔH_{cc} after the glass transition is generally smaller ($< 25 \text{ J}\cdot\text{g}^{-1}$) than in mixtures with the aliphatic monomers (Figure 65 and Figure 52). The ΔH_{cc} increases for cBT/cPI mixtures with the ratio. It has a maximum around equimolar composition with cPT and is zero with cBI. The ΔH_m during both heatings of the third run decreases with the cPI content for cBT/cPI and cPT/cPI blends. No melting endotherm is detectable for cBI/cPI mixes (Figure 66a). The different behavior of the three cPI mixtures can be summarized as follows:

- No crystallization nor cold crystallization occur in mixtures of cBI with cPI (at least within three weeks); the amount of amorphous fraction is constantly high over time and composition of the blend.
- The amount of amorphous fraction in cBT/cPI blends is constant over sample composition. An increasing crystallite formation is observable for an increasing cBT content according to ΔH_{cc} and the consecutive ΔH_m . The difference between ΔH_m and ΔH_{cc} increases at the same time. However, the final crystallinity is below the expectations for all compositions.
- The forming of crystalline instead of amorphous phase grows with increasing cPT content in cPT/cPI mixes. The preferences for the two phases overlap at about equimolar composition, resulting in a maximum of cold crystallization in this range.

A minor influence of the diol chain length on the mentioned properties is found. A comparable behavior to that of cPT/cPI mixtures is observed, i.e. when cPI is exchanged for the longer-chained cBI (Figure 64 to Figure 66). The same is true for the comparison between cBT/cPI mixtures and of cBT/cBI (Figure 63 to Figure 66). The influence of a terephthalate moiety in cPT and cBT seems to be dominant for the behavior of the glass transition and crystallinity and not so much the length of the diol in the second MCO. The

minor influence of the diol length is sufficient to alter the behavior of cPI mixtures with cBT in comparison to cPT to some extent.

In samples with cBT and cPT, a smaller amount of energy is necessary for softening the comparatively small glass phase compared to the FOX assumptions, which involves a higher free volume. The T_g is smaller than expected by the FOX equation for all ratios of the two MCOs (Figure 67a). The ratio of amorphous to crystalline fraction seems to be rather constant. ΔC_p of all mixtures are of the same dimension as of the pure monomers and the ΔH_m after the glass transition decreases only marginally with the content of cBT (Figure 66b). Cold crystallization after the glass transition is only observed for high cBT contents (Figure 65b) indicating a fast crystallization of the other mixtures during cooling.

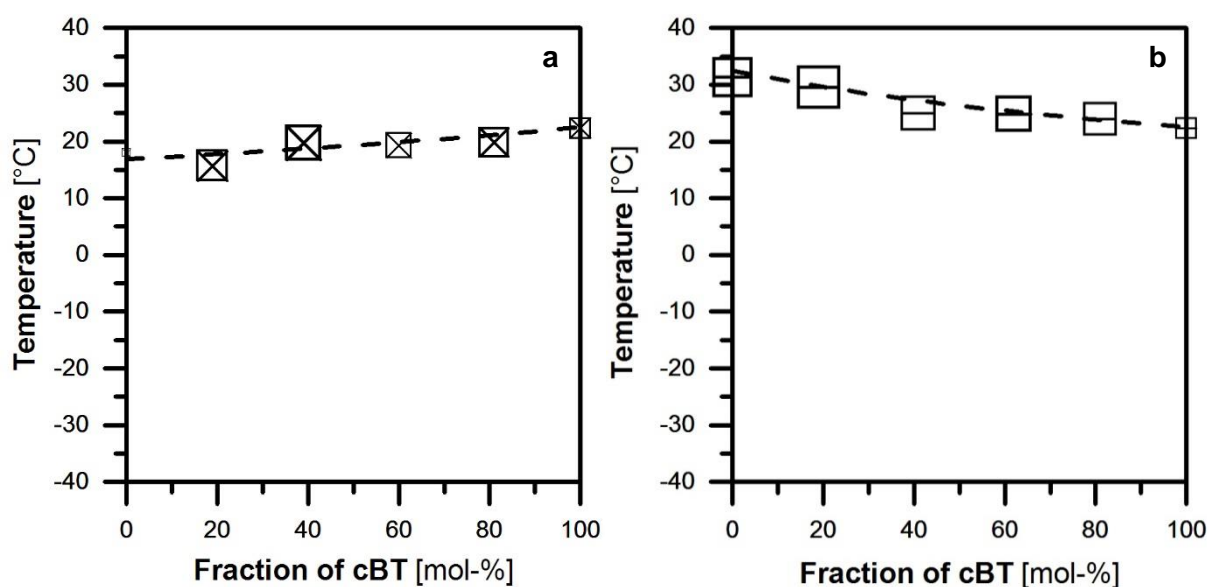


Figure 63: Dependency of the T_g of the 2nd heating of the 3rd run on the composition and the fitting according to FOX for blends of a) cBT and cBI and b) cBT and cPI.

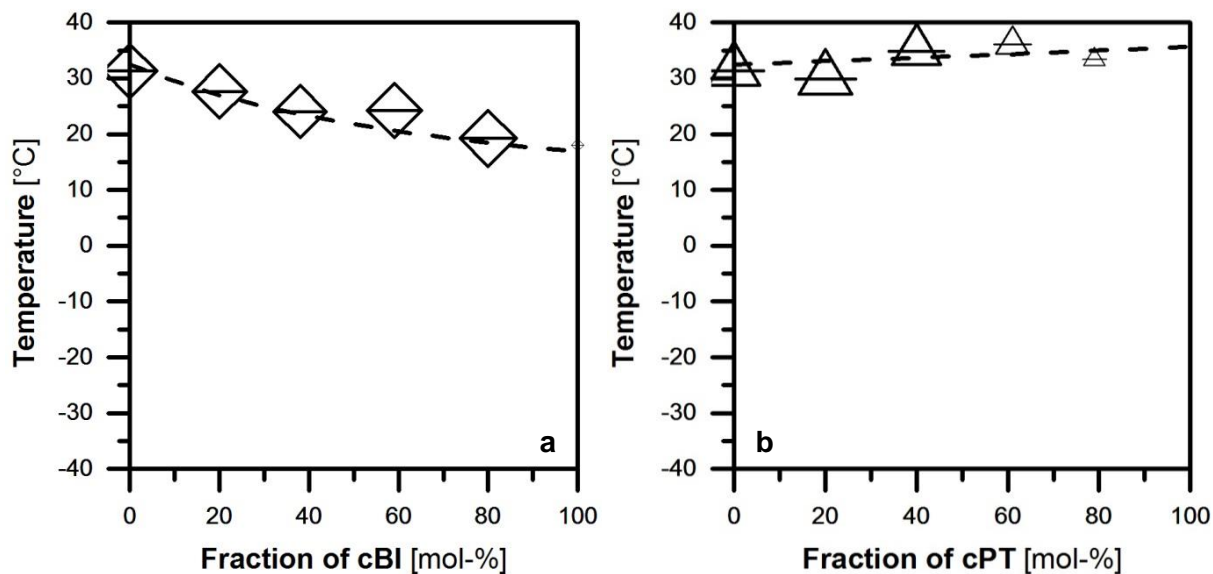


Figure 64: Dependency of the T_g of the 2nd heating of the 3rd run on the composition and the fitting according to FOX for combinations of a) cBI and cPI and b) cPT and cPI.

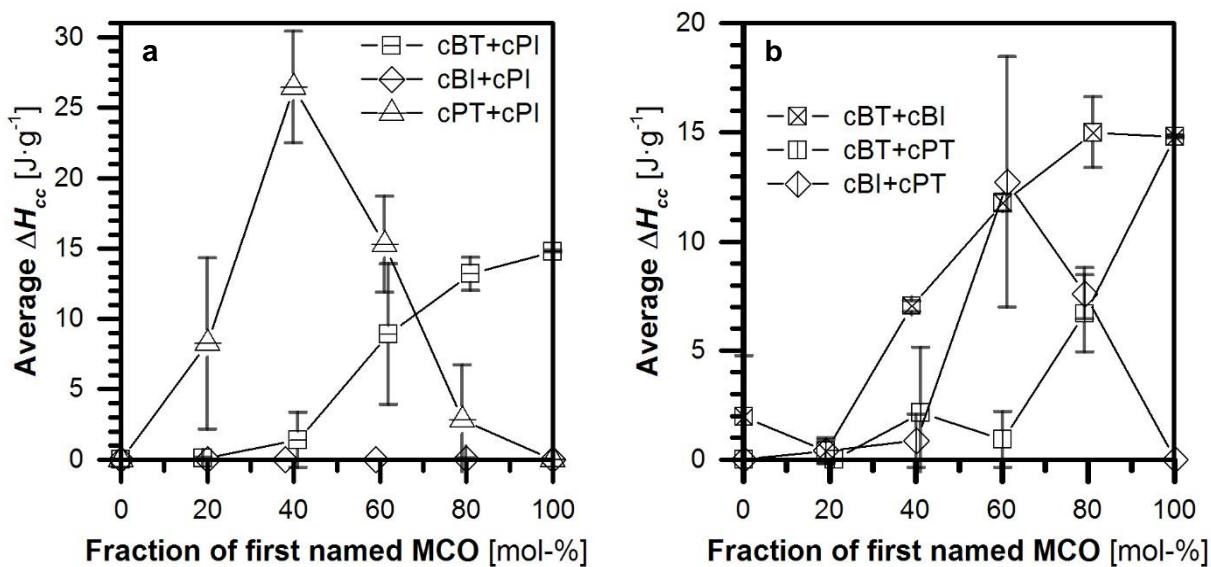


Figure 65: Heat of cold crystallization ΔH_{cc} in the 3rd DSC run of the mixtures of a) cBT, cBI or cPT with cPI and b) cBT with cBI and cBT or cBI with cPT.

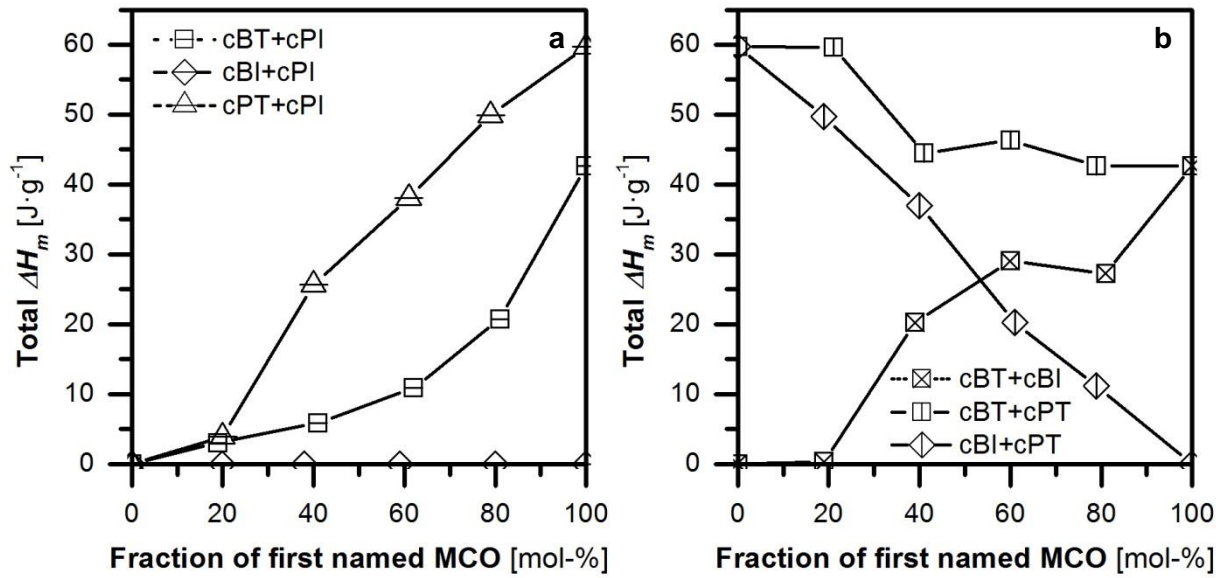


Figure 66: ΔH_m during 2nd heating of the 3rd DSC run of the mixtures a) of cBT, cBI or cPT with and cPI and b) of cBT/cBI, cBT/cPT and cBI/cPT.

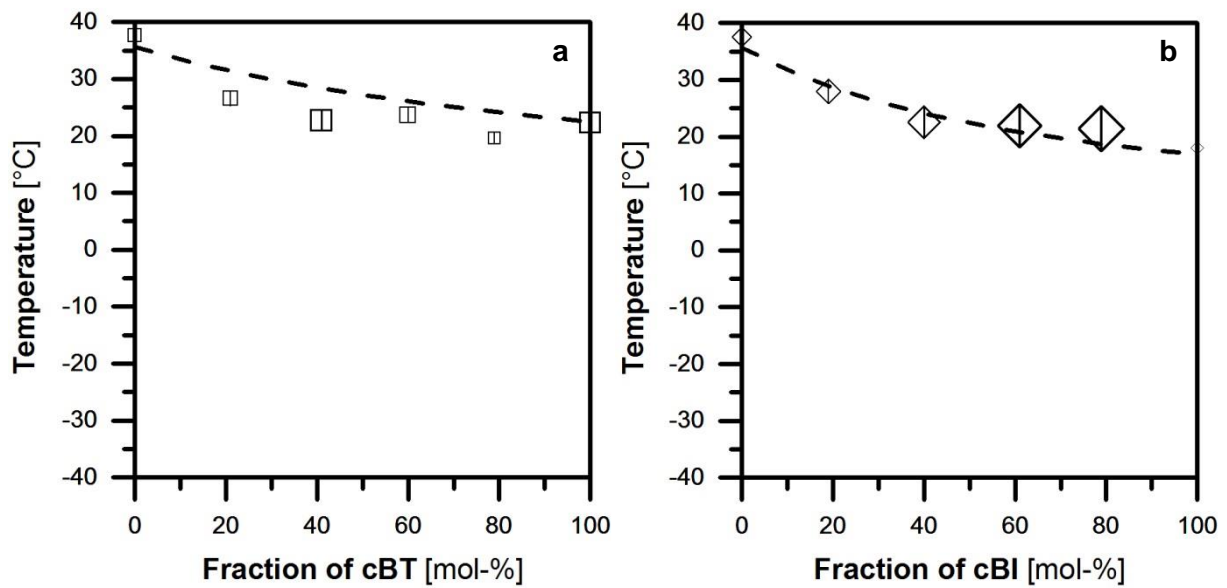


Figure 67: Relation between the T_g of the 2nd heating of the 3rd run and the composition as well as the fitting to the FOX equation for blends of a) cBT with cPT and b) cBI with cPT.

5.2.3 Interpretation of the results of the monomeric mixtures

All monomers studied are miscible in each other as a dependency of T_m , T_c and T_g on the sample composition was observed in blends and as only one T_g was found. Mixing was complete after the initial melting. A further shift of the initially found T_m and T_c with the number of DSC runs was only observed for blends of cBI with cPT. The phase diagrams, i.e. the temperature of the lowest and the highest melting endotherm of a particular binary mixture, appeared as to be expected of miscible substances. The influence of the monomer ratio on the highest melting peak, taken as the end of melting, was generally small. A high influence in terms of reduction of the highest melting temperature was only observed for high contents of significantly lower melting monomers as in the combinations of cBT or cPT with cBS, cBA, cBI or cPI.

Structural similarities of the aromatic monomers generally led to a comparable behavior in mixtures with an aliphatic monomer. Both monomers based on terephthalic acid, cBT and cPT, and those with isophthalic acid, cBI and cPI, had similar phase diagrams and glass transition dependencies in combinations with cBA or cBS. This is in agreement with equations of mixing theory for the chemical potential. A similar melting behavior was observed for the two mixtures of one particular aromatic monomer with cBS and with cBA, despite of the different melting temperatures of the aliphatic components (cBS 69 °C, cBA 95 °C) showing colligative properties of the compounds. The total ΔH_m of mixtures, as an indicator of crystallinity, was usually higher if cBA instead of cBS was utilized, which is consistent with reports in literature.^{232,233,236} Exceptions are the combinations of cBS or cBA with cPT – a monomer with rather high ΔH_m – where equally high values were found for both mixtures. The exact crystallinity could not be calculated on basis of the DSC measurements because the respective molar heat of fusion for pure crystals and the extent of possible co-crystallization in the mixtures are unknown.

5.2.3.1 The melting temperature

The melting temperature was general higher for the mixtures containing terephthalate than for those with an isophthalate. This is caused by the more bulky isophthalate leading to a distorted zigzag structure in the crystals and hence to a more complicated packing. Similar has been observed for derived polyesters.^{232,233}

The melting temperature of the odd-numbered cPT was found to be more effectively reduced by the aliphatic cBA or cBS than that of cBT with its longer and even-numbered diol. The ΔH_m of mixtures with cPT is larger than with cBT indicating a comparable crystallinity

dependence. This observation is also seen in the linear slope of the crystallization temperature in dependence of the sample composition, which was found for the respective cPT but not the cBT mixtures. It is probably caused by combination of monomers with an odd and an even number of methylene groups present between these polar groups, combined with the small distance between the polar ester groups. It hampers alignment of chains during crystal growth. This is not the case in corresponding mixtures with cPI and cBI with their bulky isophthaloyl moiety, which showed comparable values to each other. The hindering influence of isophthalate on crystallization is obviously dominating over all other effects in these cases.

The distance between the polar groups were found to be of importance for the melting temperature of aromatic mixtures, as well. A smaller reduction of the melting temperature is obtained combining the two aromatic MCOs with only the odd-numbered diol, cPT and cPI. It is possibly due to the smaller distance between the polar groups in their mixture, which is majorly responsible for packing of the crystals. The entropy related to the chain length has proven in this study to have a higher influence than the difference of even- vs. odd-numbered chains discussed in literature for polyesters, at least for the short repetition units explored in this work.

5.2.3.2 Formation of a low-melting fraction

Most mixtures possessed a low-melting fraction, which might stem from the monomers themselves in cases where at least to some part readily crystallizing monomers are involved. Further effort is necessary to evaluate the correlation of the formation of this low-melting phase to the structure of the mixed monomers. The mixture of cBT and cPT is remarkable because the lowest melting temperature of the mixture is far below any other observed in either of the pure monomers. Evidence for the formation of a small fraction with eutectic behavior was observed for blends of cBI or cPI with cBA. The highest amount of these fractions is generally observed close to equimolar ratios of the monomers.

5.2.3.3 Supercooling and short-term hindrance of crystallization

A short-term hindrance of crystallization is observed for all mixtures of aliphatic and aromatic monomers and for most mutual combinations of the aromatics. This can be concluded from ΔT_{sc} until crystallization and from the ΔH_m during the second heating of a DSC run by comparison to the first as well as to the theoretically expected value from the data of the pure monomers.

An isophthaloyl moiety intensifies the effect, as already noticed for polyesters.^{232,233} The reason is probably the necessary orientation of the chain in a zigzag structure for crystallization. The consequence thereof is the absent crystallization in mixtures of cBI or cPI with cBA or cBS above 20 mol-% isophthalate, in those of cBT with cBI or cPI at a high isophthalate concentration and in those of cBI with cPI, where no melting nor crystallization was observed even after a prolonged time (>4 d).

The odd-numbered PDO usually had to be additionally present in the aromatic cycles for a pronounced supercooling, most preferably in one monomer with isophthalate (i.e. as cPI). The enhancing effect of the odd-numbered PDO was expected just like that of the isophthalate.^{232,233,237,240} However, even the presence of both PDO and isophthalate in a mixture are no guarantee for a high ΔT_{sc} .

An influence of the chain length on the hindrance in crystallization was found from a comparison of aliphatic mixtures with cBT or cPT (not in case of cBI and cPI). This is consistent with the observations for T_m discussed above. No difference is found between ΔT_{sc} of cBS and of cBA mixtures. A general influence of the chain length has however been reported for aliphatic²³² as well as for aromatic polyesters^{233,237,238} before. The difference in chain length in case of cPI vs. cBI may be too small to make a difference. The terephthalate part does not have such a leveling influence as isophthalates. A higher ΔT_{sc} is hence observed for cPT blends compared to cBT, especially for mixtures containing an aliphatic monomer, which is caused by the complicated alignment due to its odd-numbered diol.^{232,233} A second effect must be present as deduced from the amount of crystalline phase formed, which is still uncovered. It causes a non-proportional dependency of ΔT_{sc} on the cPT content with a maximum between 20 and 40 mol-% cPT.

5.2.3.4 Long-term crystallization (> 4 d)

Enhanced crystallization between two consecutive DSC measurements was observed in cBS or cPT containing mixtures relative to the total ΔH_m of the first cycle of DSC measurements. High density of polar groups and their comparatively easier chain orientation results in more extensive crystallization.^{232,233,236} No impairing long-term effect of the odd number of carbon atoms, which the aliphatic chain of cPT contains, was found in this study. This was reported differently, but in this study, it may arise from the small distance between the polar groups discussed above. A linear dependency of the respective ΔH_m on the content of cPT was not found. The increased long-term crystallization of mixtures of cBI and cBA at a concomitant short-term hindrance of crystallization can also not be explained on basis of the named properties.

5.2.3.5 Glass transition and the subsequent melting process

A glass transition was found in most studied mixtures in melting segments of the DSC measurements. It was followed by cold crystallization in most cases. A more than proportional increase of the free volume (according to the T_g relative to that from the FOX equation) was recognized if a monomer was present which readily crystallized in pure state. This is a similar condition than for formation of a low-melting fraction. The increase was observed for various combinations, e.g. for cPT with cBT, the first especially being an extensively crystallizing MCO. CBA in only small fractions below 40 or 60 mol-% reduced the T_g below expectations of the FOX equation. Higher fractions of cBA and the combination of cBA with cPT resulted in a general absence of any glass transition and in crystallization only. The reason for the different behavior of the two readily crystallizing monomers cPT and cBA probably arises from the entropy of their different chain length. The rigid ring in cPT does not easily allow a rearrangement in the non-molten state in contrast to the more flexible methylene groups in cBA. Even small amounts of cBA enhance the mobility remarkably and thus lower the T_g . This may also be the explanation for the different effect of cBA compared to cBS.

The amorphous phase is smaller in mixtures of cBA than of those with cBS mixtures (according to the ΔC_p). Additionally, it is smaller in the cBA mixtures containing terephthalate than in those with isophthalate. A maximum of glass was observed in the curves of ΔH_{cc} for the cBA mixtures with about equal weight fractions of the monomers (except for those with cPT). These mixtures with cBA generally have a higher crystallinity if the molar heat capacities of the MCOs are similar as predicted by the rule of WUNDERLICH^{245–247}. The influence of the diol chain length respectively entropy on the amorphous fraction has not been explicitly reported before to best knowledge, but the described dependency is consistent with previous observations made for polyester.^{232,233} The higher mobility by cBA as “solvent” enables the partner in the mixtures to reorganize at temperatures between T_g and T_m . The effect on the readily crystallizing cPT is not as high as on the others.

The glass transition of cBS mixtures containing isophthalate behave differently on changing of the fractions than the glass transition of those containing the terephthalate. The T_g of the two isophthalate-containing blends of cBS follows the FOX equation despite their different diol length. A negligible small effect of steric hindrance on the T_g and a major effect of chain length has been reported before.^{232–234} The amorphous phase is comparatively large for these two blends (as expected from the hindered crystallization discussed above).

The free volume of cBS mixtures with the terephthalate-containing monomers, cBT and cPT, is higher than predicted by the FOX equation. This is consistent with the enhancing

influence of readily crystallizing monomers on the free volume mentioned above. The fraction of amorphous phase decreases with increasing aromatic fraction. The softened amorphous phase is only in the combinations with cBT prone to cold crystallization, which is consistent with the behavior of cPT described and discussed above.

A minor effect on glass transition and cold crystallization was observed with the length of the diol bonded to cyclic isophthalates. The diol length in the second MCO is dominant, if it contains a terephthaloyl rest. It determines not only the behavior in respect of (cold) crystallization as already implied above, but also influences the amount of vitreous and crystalline in solid state. The mixtures of cBT with cPI or cBI behave similar in these respects but different compared to those of cPT with cPI or cBI. In the first group, an almost constant amorphous phase and an increase of crystalline phase is observed with increasing cBT content. In the latter mixtures, a transformation from amorphous to crystalline phase takes place if the cPT content is raised, leading to maximum cold crystallization around equimolar ratios of the MCOs. This is probably caused by the higher tendency for crystallizing of cPT over that of cBT. This larger driving force for crystallizing makes a rearrangement after the first softening redundant. The mixture of cBI and cPI shows no crystallization nor any remarkable change of the fraction of amorphous phase judged by the ΔC_p .

5.3 Enzyme- and metal-catalyzed polycondensation of a new bio-based polyester

The diacid Pripol and the diol PDO have been used in polycondensation in bulk. Both monomers are commercially prepared from renewable resources. The focus of this cooperation with the Technical University Hamburg¹ was on the differences between enzyme catalysis at milder temperatures compared to conventional metal-complex catalysis in respect to reaction progression and constitution of the obtained product.

5.3.1 Characterization of the diacid Pripol by ¹³C NMR

Pripol is the dimerization of two unsaturated C18 fatty acids from vegetable origin. It is claimed to be partly unsaturated (0-1 double bonds per molecule) but its exact structure is not supplied by the manufacturer. NMR analysis indicates a mixture of various compounds.

However, the composition is not easily elucidated from these spectra and Pripol has been used as received as “natural product”.

The ^{13}C NMR experiment with DEPTQ sequence (Figure 68a) indicates a mixture of different structures according to the number of integrals, which is supported by the ^{13}C NMR experiment with IGATED sequence (Figure 68b). Identified peaks and normalized intensities are given in the inscription of the respective figure. Probable linking carbon atoms between the two fatty acids can be recognized in form of -CH- groups in the DEPT spectrum, but only to a small amount according to their integrals. The absence of signals in the range of 160 to 80 ppm (except for the solvent CDCl_3) in both spectra indicates the absence of major olefinic majorities. Further efforts exceeding this study are necessary to reveal the structures and composition of Pripol.

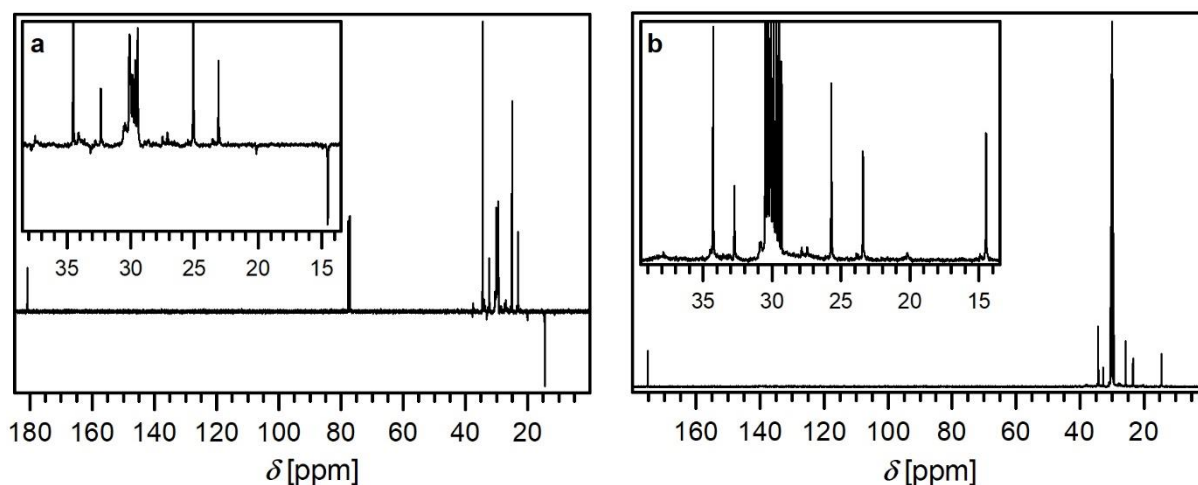


Figure 68: a) ^{13}C NMR spectrum of Pripol in acetone- d_6 from DEPTQ sequence (2000 scans), identified peaks with indication of number of protons: δ [ppm] = 180.9 (-COOH), 37.8 (-CH-), 37.5, 34.5, 34.1 (3x -CH₂-), 33.2 (-CH-), 32.8, 32.3 (2x -CH₂-), 30.8-29.2 (various -CH₂-), 28.6, 27.5, 27.1, 25.1, 23.1 (5x -CH₂-), 20.1 (-CH-), 14.5 (-CH₃). b) Corresponding spectrum with IGATED sequence (2000 scans). Identified peaks and normalized integrals: δ [ppm] = 175.1 (2.0 C), 37.8 (0.3 C), 34.4 (0.4 C), 34.3 (2.7 C), 32.7 (1.0 C), 30.9 (0.5 C), 30.8 (0.6 C), 30.3 (1.5 C), 30.2 (2.6 C), 27.8 (0.4), 27.5 (0.6 C), 25.7 (2.4 C), 23.4 (1.6 C), 20.2 (0.3 C), 14.5 (2.0 C).

5.3.2 Polycondensation of Pripol and 1,3-propanediol

The polycondensation was carried out following two different protocols in order to obtain data to compare enzyme- and metal-catalysis performances (compare to Table 5):

- i) a two stage process consisting of precondensation at 180 °C and 600 mbar with only autocatalysis for a time of 125 min, followed by the transesterification phase with addition of catalyst (A: no catalyst, M: $\text{Ti}(\text{OnBu})_4$, E1: *CalB immo*) and with altering of the settings to 220 °C and below 1 mbar,
- ii) a two-stage process with an enzyme-catalyzed precondensation (E2) at 80 °C and 100 mbar for 150 min, followed by condensation at 80 °C and below 1 mbar.

The precondensation phase was terminated in all cases at acid conversions in the range of 75 – 80 % to start the determinative second phase with similar conditions.

Table 5: Polycondensation procedures for the different routes of metal- (M), enzyme- (E) and autocatalysis (non-catalyzed) (A). (Index a indicates polycondensation in air.)

Protocol	Reaction	Atmosphere	Conditions first stage (Precondensation)		Conditions second stage (Transesterification)	
i)	M	Ar	180 °C, 600 mbar 125 min	No catalyst	220 °C, ≤ 1 mbar 365 min to 24 h	$\text{Ti}(\text{OnBu})_4$
	M _a	Air				No catalyst
	A	Ar				
	E1	Ar			80 °C, ≤ 1 mbar 48 to 55 h	<i>CalB immo</i>
	E1 _a	Air				
ii)	E2	Ar	80 °C, 100 mbar 150 min	<i>CalB immo</i>		
	E2 _a	Air				

All reactions were carried out either in Ar (no index) or in air (index a) to investigate the role of oxygen. No obvious difference was noticeable, neither in reaction progression nor in product constitution. Hence, the following discussion is concentrated on polycondensation in Ar atmosphere but is valid for the reactions in air, too. No effect was observed either for the addition of a small amount of 1,4-dihydroxybenzene to the reaction mixture of either route E1 or A before reaction termination in order to prevent possible oxygen-mediated crosslinking reactions. Hence, the addition of 1,4-dihydroxybenzene was stopped. Both findings can be explained by the fact that polycondensation has been carried out in vacuum, so the influence of oxygen is minimized.

5.3.2.1 Precondensation

The reaction progression was monitored by regular titration of samples from the reaction vessel with potassium hydroxide (Figure 69 for reactions under Ar, Figure 70 for those under

air). The resulting curves showed the expected appearance for a step-growth polymerization with continuous removal of the formed side product water and excess diol.¹⁶⁹ They are similar for the first step of precondensation (up to 75 – 80 %) for the routes M, A and E1. This proves a good reproducibility of the autocatalyzed reaction in the equipment.

A comparable conversion of about 75 % was chosen at the end of the first phase of the second protocol (E2), i.e. precondensation at a lower temperature and lower pressure in the presence of *CalB immo* (Table 5): The high catalytic activity of the enzyme is observable in the only somewhat smaller rate of acid conversion in route E2 despite of the drastically reduced temperature (80 °C instead of 180 °C). The decreased rate is most probably caused by the limited removal of diol and water at these reaction conditions. An increase of the temperature was not possible because of an inactivation of the enzyme at higher temperatures.²⁴⁸

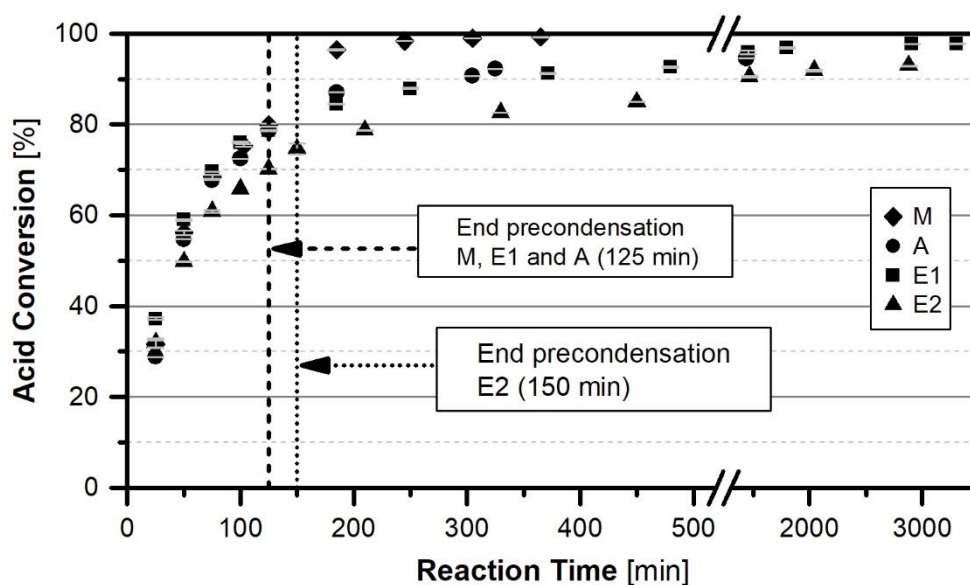


Figure 69: Time-dependent conversion of acid in the metal- (M), enzyme- (E) and non-catalyzed (autocatalyzed) (A) polycondensation in Ar atmosphere.

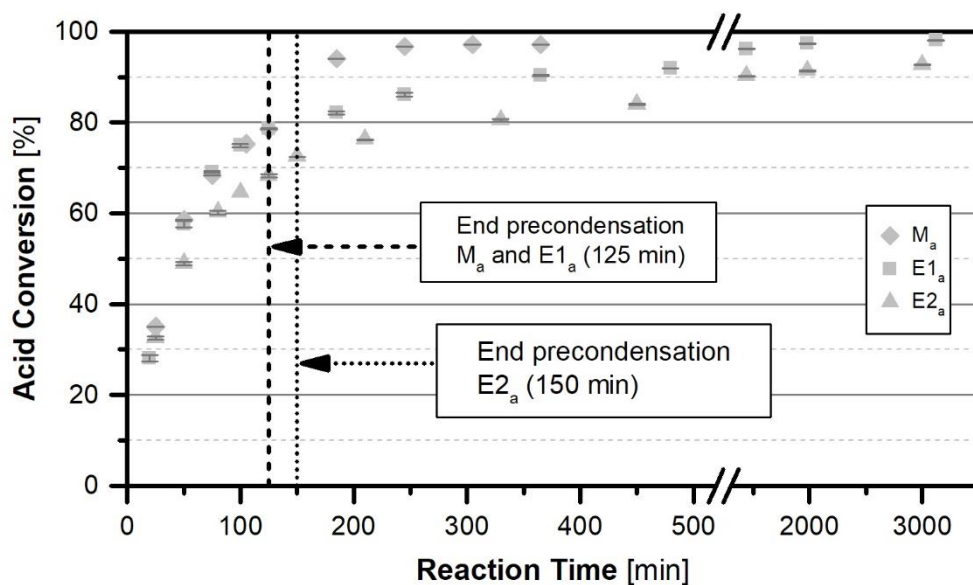


Figure 70: Time-dependent conversion of acid in the metal- (M), enzyme- (E) and non-catalyzed (autocatalyzed) (A) polycondensation in air.

The molecular weight distribution was determined by GPC in the same intervals as the acid conversion. The resulting elugrams for the precondensation show four oligomers with retention times between 23 and 28 min (selected samples in Figure 71). This corresponds to the weight average molecular weight $M_w \approx 4200 \text{ g} \cdot \text{mol}^{-1}$ at maximum (relative to PS standards), which is a potentially useful polymer as polyol in polyurethane synthesis, provided only hydroxy end groups are present.

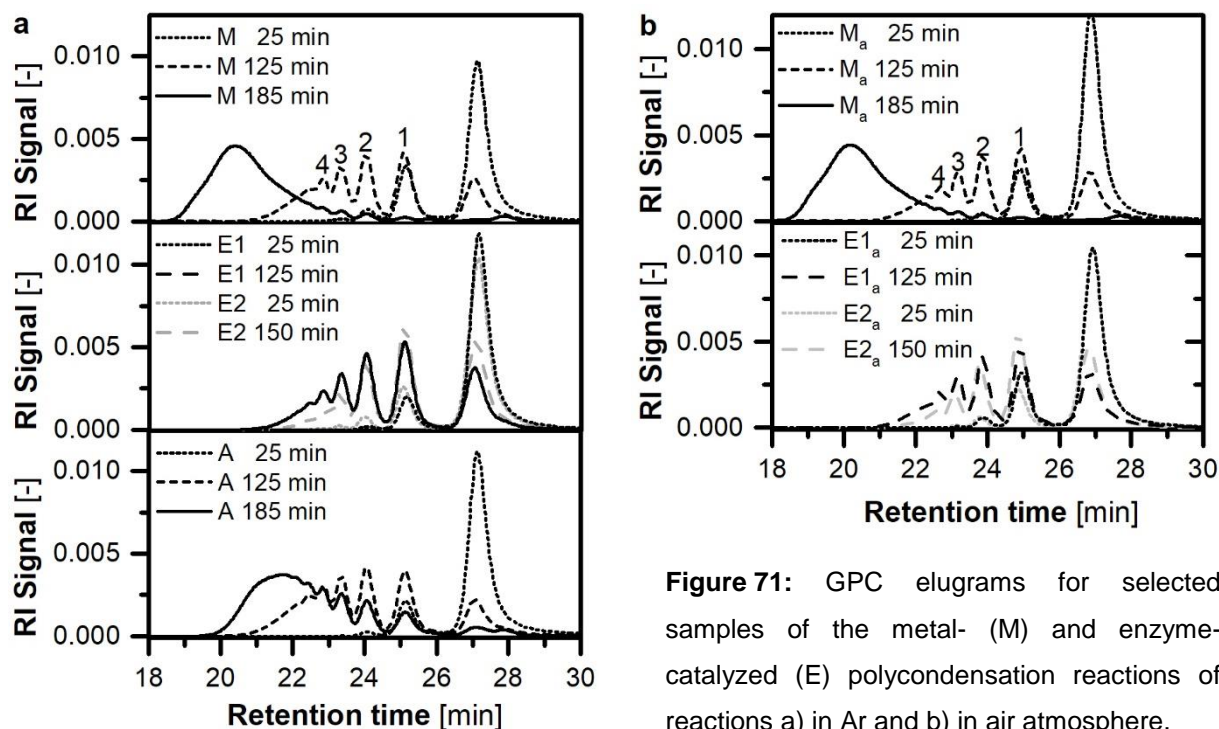


Figure 71: GPC elugrams for selected samples of the metal- (M) and enzyme-catalyzed (E) polycondensation reactions of reactions a) in Ar and b) in air atmosphere.

5.3.2.2 Transesterification and the final polyesters

The products obtained by the different routes were isolated as yellow, highly viscous oils. The autocatalyzed polycondensation (A) gives a final acid conversion of 95 % and polymer with $M_w = 28.4 \text{ kg} \cdot \text{mol}^{-1}$ according to GPC analysis after 24 h (Table 6). The presence of $\text{Ti}(\text{OnBu})_4$ after the precondensation step (M and M_a) leads to the formation of high-molecular weight polyester (up to $M_w = 84.6 \text{ kg} \cdot \text{mol}^{-1}$, dependent on the conversion) in only 365 min. The initially formed oligomers are rapidly linked to polymer chains in the period between 125 to 185 min of the reaction (Figure 71) in accordance with expectations regarding step-growth polymerizations.

The variation in conversion of this route in air or in Ar atmosphere of 97 or 99 %, respectively, are most probably caused by small variations in pressure. The vacuum pump created vacuum in the reactor between 0.3 and 0.6 mbar at the end of the polycondensation. The removal of the byproduct water (and PDO) shifts the equilibrium decisively towards the product and is hence directly linked to conversion and molecular weight.

Table 6: Conversion X , M_w , PDI (including low molecular weight fractions) and zero shear viscosity $|\eta^*|_0$ of the end products. (Index a indicates polycondensation in air.)

Route	Time	T	Conversion X	M_w	PDI	$ \eta^* _0$
-------	------	-----	----------------	-------	-------	--------------

	[h]	[°C]	[%]	[kg · mol ⁻¹]		[Pa · s]
M	6	220	97	49.3	3.0	320
M _a	6	220	99	84.6	4.4	4370
A	24	220	95	28.4	2.6	45
E1	52	80	98	26.7	2.3	38
E1 _a	55	80	98	25.5	2.3	56
E2	50	80	93	15.6	2.0	7
E2 _a	48	80	93	15.1	2.0	12

A comparatively high *PDI* (Table 6) was determined for the metal-catalyzed reactions from GPC elugrams. The broadening of the molecular weight distribution is most likely caused by the higher viscosity in the reaction M (and M_a) and cannot simply be assigned to a different catalytic behavior of the metal complex compared to the enzyme. Mixing of the reaction mixture could not be adequately realized both for the waterlike viscosity at the beginning of the reaction and the high viscous mixture at the end. Therefore, a not ideal stirring of the viscous polymer melt at the end probably led to an inhomogeneous reaction in the reactor.

It should be noted that the *PDI* was calculated over the whole range of molecular weight excluding only the monomers because by this procedure the value has the highest significance for application of the product. Additionally, oligomeric cycles may have formed to a small extent in metal and enzyme-catalyzed reactions as to be expected of a polycondensation in bulk. Small signals for cyclic structures are observed in MALDI-TOF spectra for both means of catalysis (exemplary spectra see Figure 72 and Figure 73). An unequivocally identification, however, could not be accomplished because of the complexity of the spectra combined with the fact that Pripol is already a mixture of compounds. Improvement of the spectra was not possible despite recordings in repulsion as well as in linear mode and with different matrices as 2,5-dihydroxybenzoic acid or dithranol. A determination of the ring-chain equilibrium and of the distribution of cycles exceeds the scope of this study as it is a field of extensive studies itself.^{249–252} The dominant formation of rings containing Pripol is not expected, as large membered rings (>20 atoms) are thermodynamically and kinetically not favored.

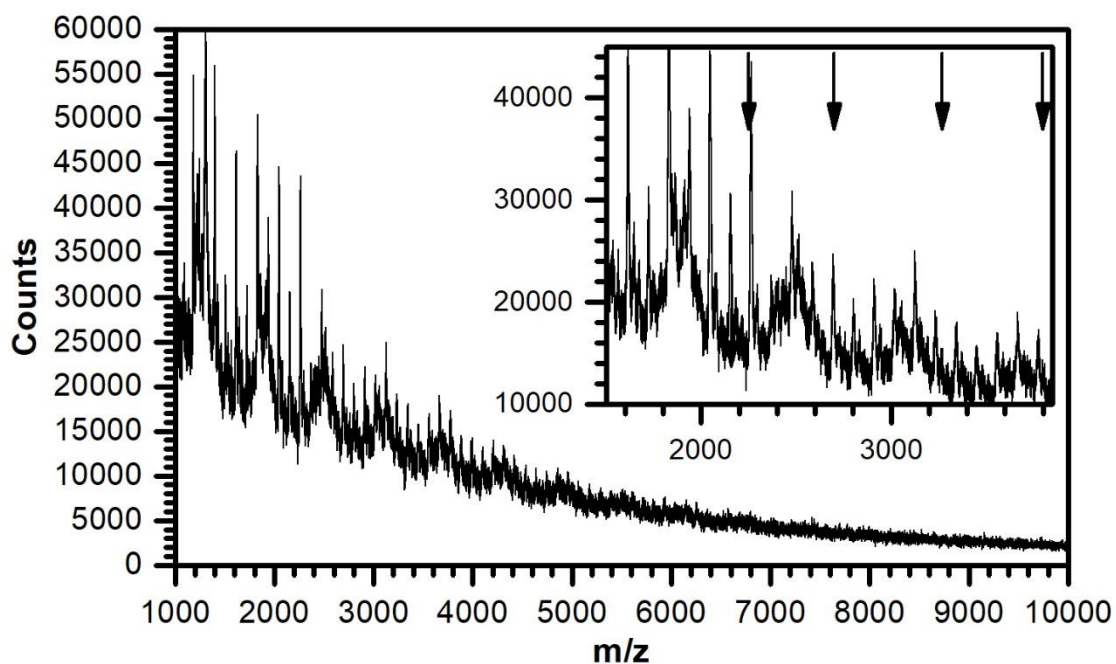


Figure 72: Exemplary MALDI-TOF spectrum of reaction E1_a (linear mode with dithranol as matrix and AgTFA as ionization agent) including an extension with indication of possible cyclic compounds.

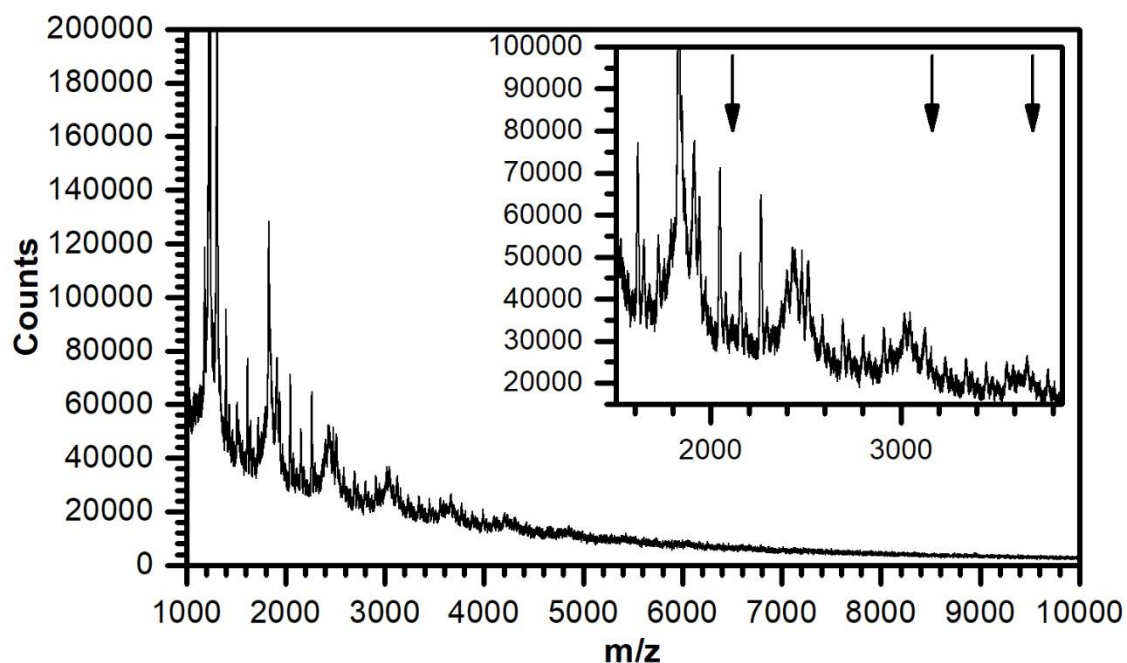


Figure 73: Exemplary MALDI-TOF spectrum of reaction M_a (linear mode with dithranol as matrix and AgTFA as ionization agent) including an extension with indication of possible cyclic compounds.

Enzyme-catalysis at 80 °C for 50 h (E1) yielded a polymer with a M_w in the same order of magnitude as the autocatalyzed route at 220 °C after 25 h (A) (compare $26.7 \text{ kg} \cdot \text{mol}^{-1}$ to $28.4 \text{ kg} \cdot \text{mol}^{-1}$). This illustrates well the capabilities of enzymatic catalysis even at low temperatures but also its limitations. The reaction rate becomes more dependent on the removal of the side products (H_2O and PDO) from the reaction vessel with increasing conversion. The higher temperature selectable in case of the metal complex improves the distillation. The reaction mixture has additionally a lower dynamic viscosity at a higher temperature, which enhances the distillation even further. The concentration of active sites was in the same order of magnitude for route M (0.005 mol-%) and routes E1 and E2 (0.003 mol-% with an estimated enzyme loading 5.6 wt-% *CalB immo*).

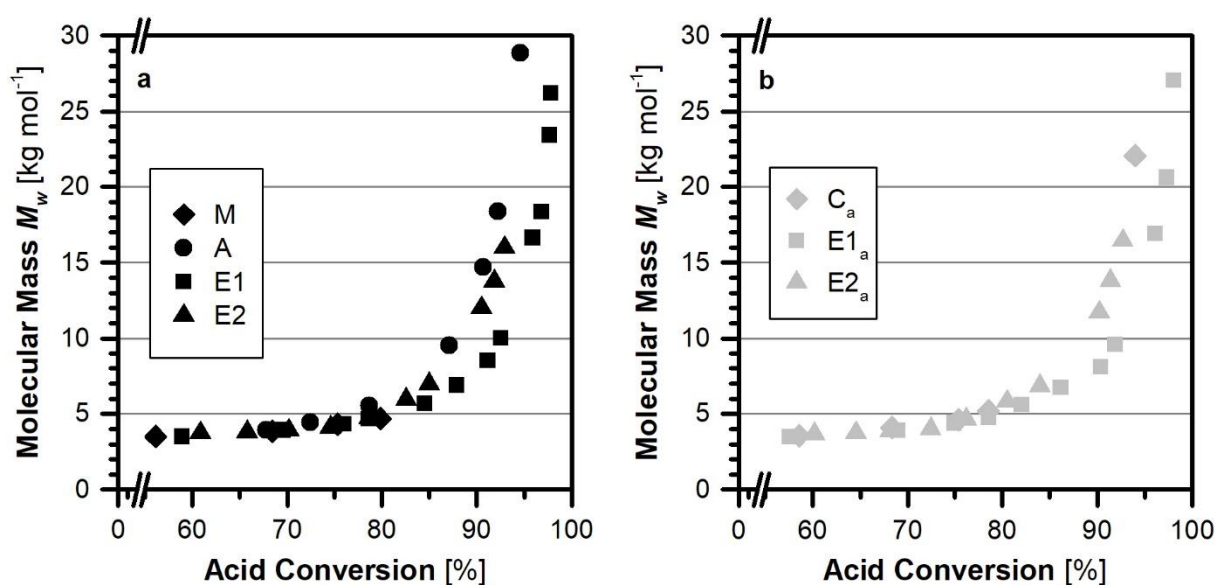


Figure 74: M_w as function of acid conversion for reaction a) in Ar or b) in air atmosphere.

Comparing the two enzyme-catalyzed reactions E1 and E2, a discrepancy in the achievable acid conversion (98 % compared to 93 %) and molecular weight ($26.7 \text{ kg} \cdot \text{mol}^{-1}$ compared to $15.6 \text{ kg} \cdot \text{mol}^{-1}$) is obvious (Figure 69, Figure 74 and Table 6). This seems mainly caused by the different stoichiometric ratios of diacid and diol given after the precondensation step (Figure 69). The higher temperature at a higher pressure during precondensation in E1 was more effective for ester formation than the lower pressure at a lower temperature in E2. These latter reaction conditions lead to a less than stoichiometric ratio of diol to diacid in route E2. Consequently, the molecular weight and the acid conversion are limited here. The final achievable molecular weight is consequently higher in E1 despite the lower molecular weight at comparable levels of acid conversions in the second phase (Figure 74). The latter is caused by the higher content of PDO via route E1 and hence more hydroxy end groups,

which are distilled off with further reaction progression giving the final polymer chains as described in chapter 3.4 (p. 29 ff.). The molecular weight or resulting viscosity in E2 does not seem to limit the conversion by the enzyme in general as higher molecular weights at higher viscosities were obtained with *CalB immo* under the same conditions in the second transesterification phase of E1.

Molecular, thermal and rheological characterization of the crude products show no obvious differences in dependency of the different applied protocols and routes. No evidence for a significant side reaction, e.g. cross-linking, can be found neither by ^1H NMR spectroscopy nor by rheology. The proton spectra are comparable (Figure 75). Signals around 4.16 ppm (4.3 – 3.6 ppm) belong to the terminal methylene groups of the PDO moiety, those at 1.97 ppm to its internal methylene group and signals at 2.30, 1.62, 1.27, 0.89 ppm to the methylene and methyl groups of Pripol. The methylene groups adjacent to an oxygen atom (of polymer chain, hydroxyl terminus of polymer chain and PDO) create the signals in the area of 4.5 to 3.6 ppm in the ^1H NMR spectra, which are observed with different intensities in the different products.

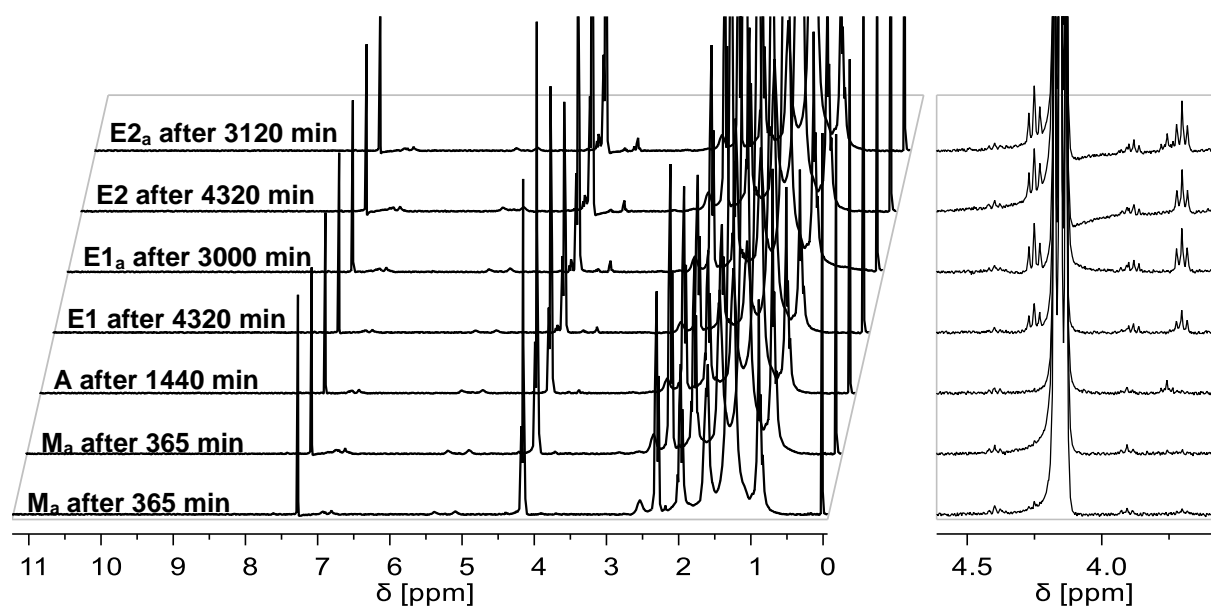


Figure 75: ^1H NMR(CDCl_3) spectra of the final products, synthesized on the different routes M, A, E1 and E2 (index a indicates reactions in air atmosphere).

The thermal behavior in DSC and TGA measurements was similar for all products, independently of the route of preparation (Figure 76 for experiments under Ar, Figure 77 for those in air). Glass transition temperatures of about $-55\text{ }^\circ\text{C}$ within the standard uncertainty of DSC measurements were observed for all products. No noteworthy melting occurred during heating of the second cycle in DSC measurement as expected for polyesters from dimerized

fatty acids.^{253,254} Two merging decomposition processes were observed by TGA, with inflection points at about 427 and 464 °C for all prepared polymers, the second step being less intense. The values are similar to comparable polyesters and have previously been ascribed to ester cleavage, dehydrogenation and alkyl group decomposition.^{192,201,254}

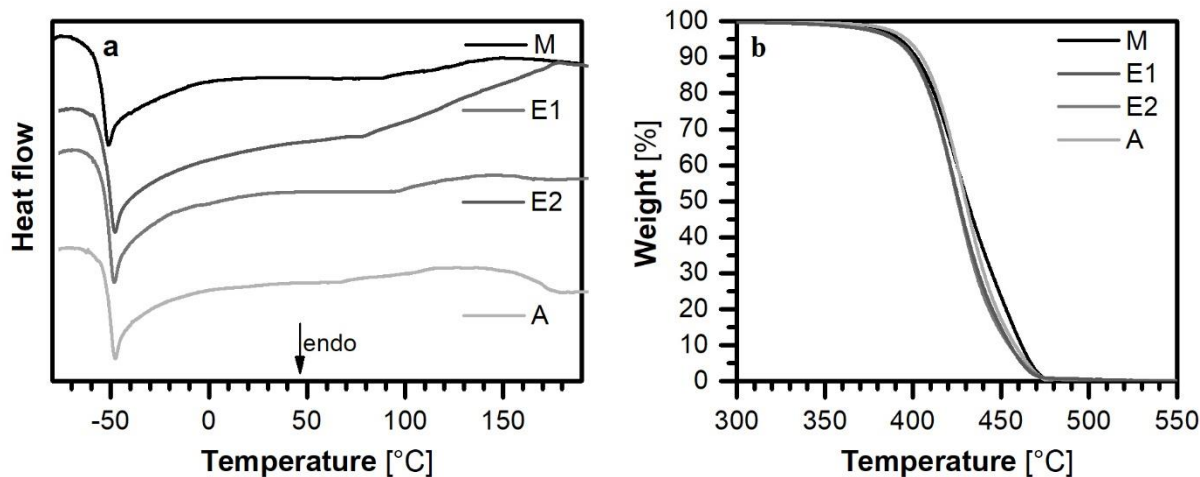


Figure 76: Analysis by a) DSC and b) TGA of the final products obtained on the different routes under Ar atmosphere.

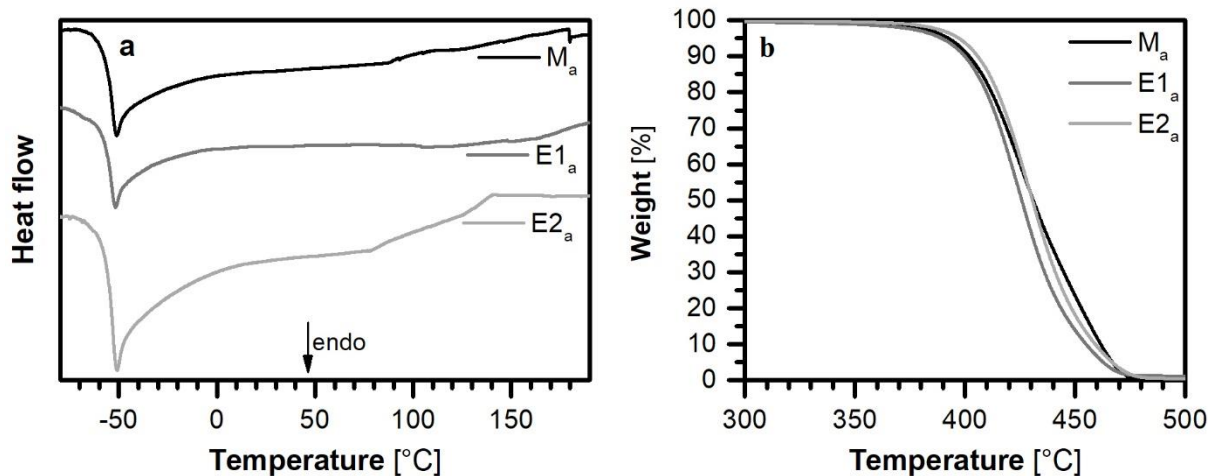


Figure 77: Analysis by a) DSC and b) TGA of the final products obtained on the different routes in air atmosphere.

The polyester products are rheologically simple fluids according to the dynamic viscosity determined by rheology (Figure 78).²⁵⁵ The shear rate in shear experiments was limited by the usual sample discharge of low viscous samples (Figure 78a). The corresponding data obtained in oscillatory mode extend over the accessible frequency domain.

The flow curves in shear and oscillation experiments at 80 °C in the linear viscoelastic regime show that the samples follow the COX-MERZ rule, indicating that non-branched polymers have formed. The zero-shear viscosity increases with the molecular weight along the usual power law with an exponent of 3.7 ± 0.0 (3.7 ± 0.2 including polycondensation under Ar as well as in air). This value is typical for most non-branched polymer systems above the critical entanglement molecular weight (including linear as well as of cyclic polyester chains).²⁵⁶ No systematic difference from this power law was noticed for either the enzymatic or the chemically catalyzed obtained products. The samples showed a regular terminal flowing in oscillatory measurements with the slopes of the storage moduli G' curves being approximately two and of the loss modulus G'' curves one (Figure 79). Both observations indicate comparable polymer structures of the differently prepared polymers. The absolute values of G' and G'' depend on the molecular weight.

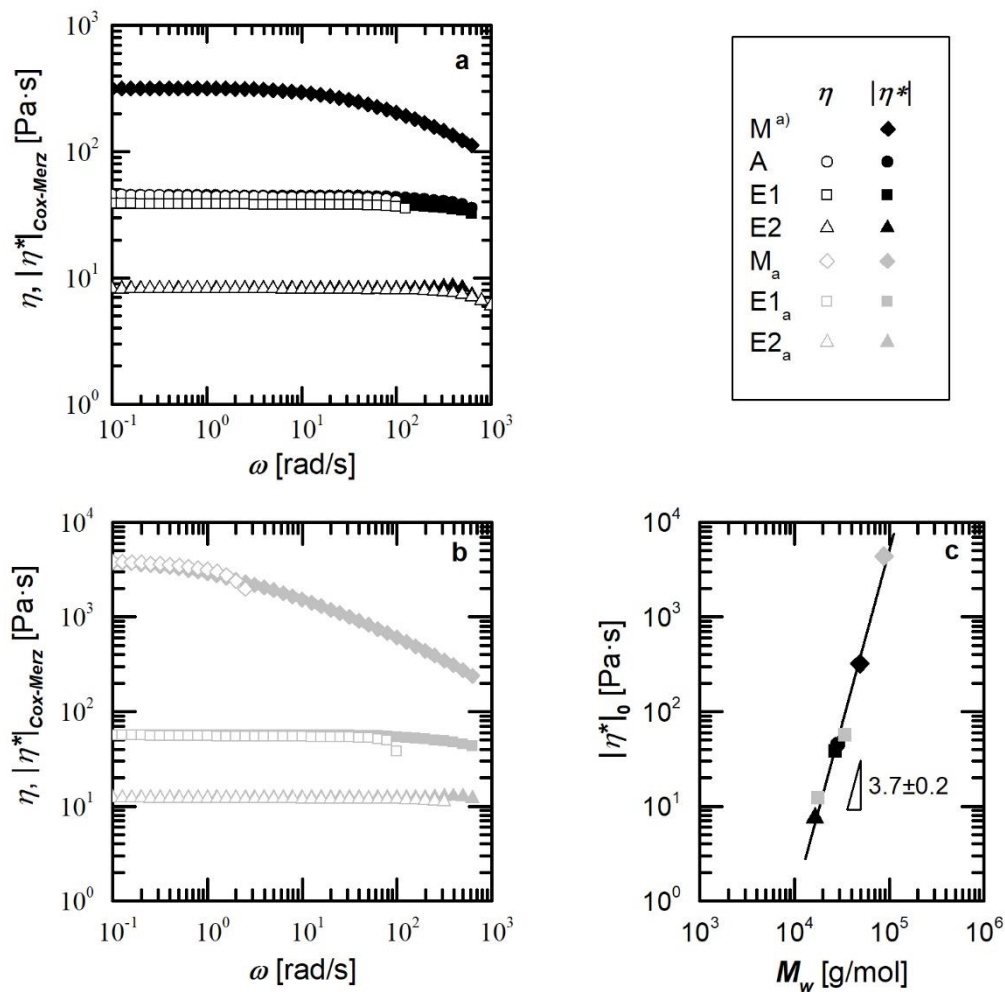


Figure 78: Determination of the viscosity by steady state shear (η) and oscillatory ($|\eta^*|$) experiments at 80 °C of a) experiments in Ar and b) in air atmosphere as well as c) the dependency of zero shear viscosity on the molecular weight. ^{a)} Steady state viscosity was not possible to determine because of early sample discharge.

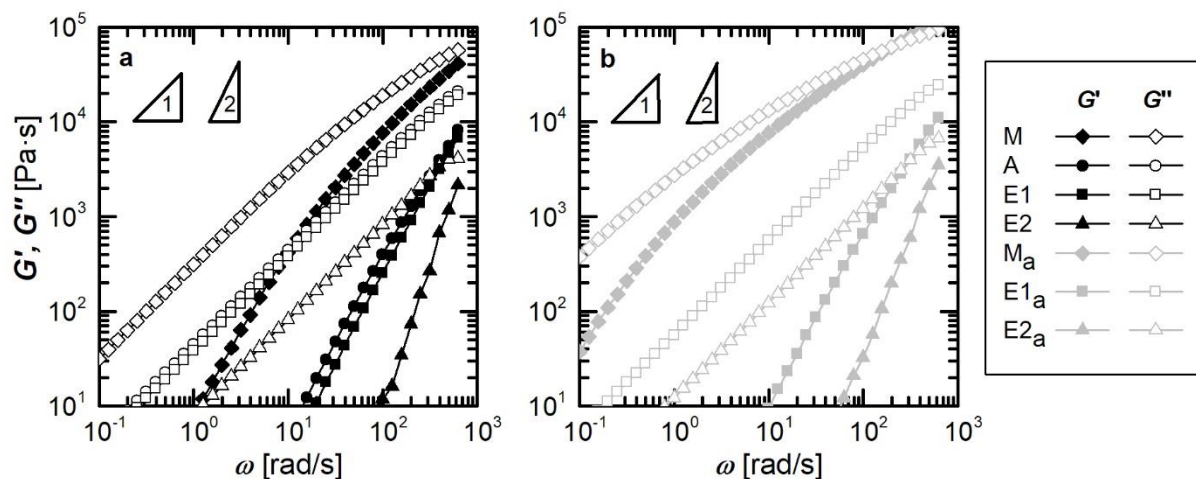


Figure 79: Elastic and viscous moduli vs. angular frequency of oscillatory measurements at 80 °C of experiments a) in Ar and b) in air atmosphere.

5.3.2.3 Exemplary polyurethane preparation from prepared polyesterol

An exemplary polyurethane elastomer has been prepared from a polyesterdiol prepolymer of $M_n = 6.0 \text{ kg} \cdot \text{mol}^{-1}$ as soft segment component to give a proof of concept for one possible application of the polyester. The often used 1,4-butanediol and 4,4'-methylene diphenyl diisocyanate (MDI) were chosen as chain extender and isocyanate, respectively, with an isocyanate index of 100. Synthesis of the polyesterdiol has been accomplished along route M with two intermediate additions of PDO during the transesterification step to obtain hydroxy end groups by splitting the chains with diol.

The obtained opaque polyurethane had a light yellow color similar to previous reports on similar products.²⁰¹ Its thermal and mechanical characterization demonstrated the comparability of the derived polyurethane to previously reported polyurethanes from bio-derived precursors despite its potential for optimization. A glass transition temperature of -53 °C was observed in DSC stemming from the Pripol-based soft phase.²⁵⁷ This value is comparable to those of polyurethanes from natural or dimerized rapeseed oil with MDI and 1,4-butanediol in literature (-47 to -51 °C).^{202,203} A degradation behavior in TGA was observed comparable to that of similar polyurethanes, too. Three degradation processes were determined in the first derivation of the TGA curve with inflection point temperatures of 311, 430 and 465 °C. The first inflection point is assigned in literature to the breaking of the urethane bonds and the latter two to the degradation of the polyester.^{192,201,254}

Mechanical testing of the obtained elastomer showed a Young modulus of 2.5 MPa, an elongation at break of 554 %, an ultimate tensile strength of 3.5 MPa and a hardness of Shore 38A. The Young modulus and the elongation at break are in the reported range for

comparable polyurethanes with polyesters basing on fatty acids.^{201,202} A maximal elongation of 100 to 600 % has been reported for polyurethanes with diacids from renewable resources, with often-used polyols or polyesterols and with various hard-segment contents. The found tensile strength of the prepared polyurethane elastomer is at the lower edge of the range (1.3 to up to 32 MPa) reported for various polyurethanes from different dimeric fatty acids with MDI and with different chain extenders like 1,2-ethandiol or 1,4-butanediol.

6 Experimental Part

6.1 Materials

CBT was obtained from IQ Tec (Schwarzheide, Germany) as CBT100 free from catalyst residues. The following chemicals were used as received, if not stated otherwise: 1,4-butanediol (BDO, Merck 801532), 1,3-propanediol (PDO, Merck 807481 for MCO synthesis; Sigma-Aldrich for polycondensation), 2-propanol (BASF), isophthaloyl chloride (IphCl₂, Alfa Aesar A15904), terephthaloyl chloride (TerCl₂, Sigma-Aldrich 120871), dimethyl isophthalate (DMIph, Sigma-Aldrich 194239), poly(1,4-butylene terephthalate) (PBT, BASF Ultradur B2550), adipic acid (Merck 818650), succinic acid (Sigma-Aldrich W502707), triethylamine (Merck 808352), 1,4-diazabicyclo[2.2.2]octane (DABCO, Sigma-Aldrich D27802), hydrochloric acid (Geyer Chemsolute 00000836), 4-dimethylaminopyridine (DMAP, Fluka 39405), sodium hydroxide (NaOH, Grüssing 12156), potassium hydroxide ethanol solution (0.1 N, Sigma-Aldrich 1.09115), tetrahydrofuran (THF, donated by BASF) dichloromethane (DCM, BASF), chloroform (CHCl₃, BASF), chloroform-d (CDCl₃, Euriso-Top D007H, 99.8% deuterated), cyclohexane (CY, Merck), 1,2-dichlorobenzene (oDCB, Burdick und Jackson 65952), cyclohexanone (Grüssing 10263), tetramethylsilane (TMS, Sigma-Aldrich) and 1,1,1,3,3,3-hexafluoroisopropanol (HFIP, Fluorochem 003409), sodium(I) trifluoroacetate (NaTFA) and silver(I) trifluoroacetate (AgTFA), dithranol. Chloroform and THF were distilled for all analytic purposes. Titanium(IV) tetra-*n*-butanolat (Ti(*On*Bu)₄, Merck 821084) and tin(II) 2-ethylhexanoate (Sn(Oct)₂, Sigma-Aldrich S3252) were vacuum distilled prior to use. In polycondensation experiments additionally *Pripol*TM 1012 (Pripol, donated by Croda chemicals), immobilized *CalB immo* (c-LEcta), an anti-foaming agent on silicon basis (donated by BASF), catalyst for polyurethane synthesis (a mixture of phenylmercury(II) 2-(dodec-1-en-1-yl)succinate and 2-ethylhexanoic acid, donated by BASF), the isocyanates Lupranat MM103 and IsoMMDI (both donated by BASF) and 2-butanone (Sigma-Aldrich 02469) have been used as received.

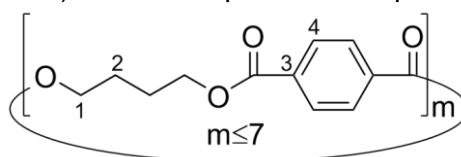
6.2 Analytical Measurements

DSC measurements were carried out on a *DSC 821* or a *DSC 1* (both Mettler Toledo), each equipped with an auto sampler and a liquid nitrogen tank. Calibration in temperature and energy was obtained with high-purity standards (indium and zinc). Evaluation was carried out with the *STARe Evaluation Software* (Mettler Toledo), Version 9.00 or 11.00, respectively. Samples of 7 to 15 mg were measured under a nitrogen atmosphere in one of three methods. The first two methods consist of cooling from 25 to 0 °C, heating to 250 °C, cooling to -25 and heating to 250 °C with a rate of 10 K · min⁻¹ in all steps (Method A) or in all except for the second heating where 5 K · min⁻¹ was applied (Method B). The third method has been applied for products from the polycondensation experiments and consisted of heating from 100 to 150 °C followed by cooling to -100 °C and a second heating to 230 °C, all steps with a rate of 10 K · min⁻¹ (Method C).

TGA curves of 10 to 20 mg sample were recorded by heating from 25 to 550 °C with 10 K · min⁻¹ in a nitrogen atmosphere.

NMR spectra were recorded on Bruker *AVANCE 400 MHz*, a *Fourier 300 MHz* or a *DRX500 MHz* spectrometer (all Bruker) in chloroform-*d* (CDCl₃) or in acetone-*d*₆ (only for characterization of Pripol) with tetramethylsilane as internal standard. Depending on the sample solubility, samples were spiked with several drops of HFIP.

The following peaks were observed for cBT fractions in the experiments described below: ¹H NMR (400 & 300 MHz, CDCl₃-*d*) δ[ppm] = 8.20-8.04 (m, H^{Ar, Polymer}) & 7.87 (s, H^{Ar, Oligomer}), 4.43 (m, 4 H, -CH₂-O-), 2.13-1.80 (m, 4 H, -CH₂-). Additional peaks from opened cycles: 3.76-3.69 (t, J = 6.4 Hz, 2 H, -CH₂-OH), 2.05-1.98 (m, J = 8.3 Hz, 2 H, -CH₂-CH₂-OH). Further degradation: 8.24-8.15 (m, 2H, H^{Ar}), 1.83-1.75 (m, 5H, -CH₂-), 1.72-1.62 (m, 9H, -CH₂-).



MALDI-TOF spectra were recorded on an *UltrafleXtreme with Smartbeam II Laser* (Bruker) with Dithranol (1,8,9-anthracenetriol) as matrix and AgTFA or NaTFA as ionization agent. Solutions of both (in CHCl₃ or Methanol, respectively) were mixed with a solution of the sample before applying on the target plate. Measurements were carried out in reflection mode of the analyzer and the corresponding peaks of the cycles attached to sodium, potassium and silver were analyzed.

SEM was conducted on a *LEO 1525 (Gemini)* with a field emission cathode and a SE as well as an In-Lens detector. Samples of the respective fraction were coated by carbon prior to imaging and investigated in top view and cross section.

Optical microscopy in form of inverse microscopy imaging was carried out with a *DMi8 A* (Leica) in reflection and transmission mode with magnification of 2.5 to 5 and digital processing.

The average molecular weight and dispersity of cBT fractions isolated from CBT100 were determined in some cases as well as polyesters from polycondensation by GPC with distilled THF as eluent. Separation of oligomers was achieved by a precolumn *MZ Gel SDplus* (100 Å, 5 µm, MZ-Analysentechnik) and a column *MZ-Gel SDplus* (100 Å, 3 µm) (MZ-Analysentechnik). Polyesters from polycondensation were analyzed by the named precolumn followed by a series of three columns (a *Polypore linear*, 1000 Å, 5 µm by Polymer Laboratories (now Agilent), a *MZ-Gel SDplus linear*, 1000 Å, 5 µm and a *MZ-Gel SDplus 100 Å*, 3 µm both by MZ-Analysentechnik). A solution of 5 mg · mL⁻¹ of sample in THF were filtered with a 0.45 µm PTFE filter and, after adding 3 µl of toluene as internal standard, injected into the SEC. The flow rate was in all cases 1 mL · min⁻¹. The instrumentation consisted of an *Intelligent Pump AI12* (Flom), a *PLDG 802 degaser* (Polymer Laboratories, now Agilent) and a detector *RI 101* (Shodex) with a *hs 2600 interface* (hs GmbH). Evaluation was carried out by the software *NTeQGPC V 6.4* in Version 1.0.25 (hs GmbH). The system was conventionally calibrated with seven narrow distributed polystyrene standards (980, 2000 11870, 22480, 46790, 119900, 222100, 630000 and 1000000 g · mol⁻¹).

The determination of unit cell parameters of crystals was carried out on *SuperNova* (Oxford Diffraction, former Agilent Technologies) with an automatic four-circle diffractometer with monochromated CuK α radiation up to an angle of $2\theta = 65^\circ$ at 100 K.

Rheological measurements of the polycondensation products were performed on an *AR 2000ex controlled stress rheometer* (TA Instruments, New Castle, USA) with a plate-plate geometry (25 mm diameter). Small amplitude oscillatory shear (SAOS) experiments were carried out at a frequency range of 628 to 0.1 rad · s⁻¹ at a temperature of 80 °C. The strain (8 to 40 %) was kept within the limits of the linear viscoelastic regime. A steady state shear experiment has been carried out after each SAOS experiment in a frequency range of 0.1 to 1000 Hz. Time sweeps of all samples were carried out at a constant oscillatory frequency at 80 °C. No significant changes of G' , G'' , δ and $|\eta^*|$ of the samples were detected. The model of CROSS resulted the best fits for obtaining the zero shear viscosity, except for the measurements of the polymer of route M under air which was fitted according to MIN.

Acid value (AV) titration was performed to determine the acid conversion in polycondensation reactions. The withdrawn samples were dissolved in 40 ml THF and titrated with 0.1 M potassium hydroxide in ethanol using a *Brand Titrette* on a 1 L *Schott* bottle and with phenolphthalein as indicator. AV was calculated from the volume V_{KOH} of

potassium hydroxide solution, its concentration $c_{\text{KOH}} = 0.1 \text{ mol} \cdot \text{L}^{-1}$, its molar mass $M_{\text{KOH}} = 56.1 \text{ g} \cdot \text{mol}^{-1}$ the sample mass m accordingly to:

$$AV = \frac{V_{\text{KOH}} \cdot c_{\text{KOH}} \cdot M_{\text{KOH}}}{m} \quad (6)$$

The conversion was calculated therefrom together with AV_0 at the beginning (derived from the masses of the reactants).

$$X = \frac{AV_0 - AV}{AV_0} \quad (7)$$

The dilution by addition of immobilized catalyst during the reactions has been considered by adjusting the measured AV upwards by the factor 1.05. The loss of mass by removing water as well as dilution by adding metal catalyst in the chemical route has not been taken into account.

6.3 Reduction of melting temperature of cBT by separation

The experiments in order to explore a possible reduction of the melting temperature of cBT basing on CBT100 are collected in this subchapter. The conditions are summarized in tables were reasonable.

6.3.1 Manipulation of the melting temperature of cBT by precipitation with variation of solvent polarity

6.3.1.1 Time and temperature dependency of precipitation of cBT oligomers

650.80 g oDCB were placed under an Ar atmosphere in a 3-neck flask, equipped with a DIMROTH condenser, an internal thermometer and a septum for sampling. The solvent was heated to 180 °C by a heating jacket under stirring with a magnetic stirring bar. Afterwards, 50.04 g CBT100 and 0.1 mL $\text{Ti}(\text{OnBu})_4$ (0.3 mmol) were added giving a yellow solution. Stirring at 180 °C was continued for 2 h with sampling every 15 min. After this period, the temperature was reduced to 120 °C in steps of 10 degrees within 5 hours with 40 min before sampling for equilibration after a temperature change. The samples were filtrated at room temperature and the precipitate analyzed by DSC following Method A. The details of sampling are summarized in Table 7. Peaks in ^1H NMR spectra were accordingly to the list

given above with noticeable fractions of opened and of degraded cycles (p. 138). MALDI-TOF spectra of selected samples were recorded with Dithranol and NaTFA.

Table 7: Conditions of the time and temperature dependent precipitations of cBT from oDCB.

Exp. no.	Time of sampling [min]	Solvent temperature [°C]	Yield of isolated cBT [wt-%]	Highest T_m [°C]
8.01	15	180	19.8	224.7
88.02	30	181	22.4	224.0
8.03	45	182	22.0	224.9
8.04	60	181	22.5	225.4
8.05	75	181	24.9	222.8
8.06	90	182	24.1	223.5
8.07	105	182	23.1	225.1
8.08	120	182	25.8	221.2
8.09	180	171	23.8	222.2
8.10	243	160	23.7	228.2
8.11	286	151	26.7	223.4
8.12	327	138	23.9	224.8
8.13	370	130	28.4	228.7
8.14	421	121	25.7	224.2
8.15	431	121	24.1	230.7
8.16	431	121	13.6	200.9
8/I	--	22		231.3
8/II		22		148.8

6.3.1.2 Variation of solvent polarity

50 g CBT100 (dried over night at 60 °C in a vacuum oven), 530 mL oDCB (distilled and dried over molecular sieves (4 Å) over night), and 0.12 g Sn(Oct)₂ (0.30 mmol, 0.13 mol-%) were weighed into a 3-necked 1L flask. The flask was equipped with a DIMROTH condenser, a heating jacket with temperature control, and a magnetic stirring bar. The manipulations

were carried out under an Ar atmosphere in glassware dried previously at 150 °C over night. The mixture was heated under stirring by the magnetic stirring bar to reflux for 2.5 h before cooling to the respective temperature of 108 (± 5) °C for reactions with toluene or to 60 °C for those with CHCl₃. Toluene or CHCl₃, respectively, was added stepwise to increase the ratio in relation to oDCB up to about 1:1. Samples were taken through the septum after 25 min after variation of the solvent ratio to equilibrate the system and immediately filtrated through a small BÜCHNER funnel (Table 8 and Table 9). The precipitates were dried *in vacuo* at 40 °C. The filtration of the reaction mixture after complete addition of the respective solvent was carried out in hot state through a hot BÜCHNER funnel (precipitate P1). A second filtration after further precipitation was necessary in case of toluene addition 3 d later (precipitate P2). Only very small further precipitate was found in experiment with CHCl₃ even one week later. It was very similar to the final precipitate P3 and hence united with it. The filtrate of the second filtrate was evaporated to dryness for reason of completeness (precipitate P3). DSC thermograms of the samples were measured according to Method A. Peaks of cyclic, opened and degraded MCOs were observed in ¹H NMR spectroscopy following the list given above (p. 138). MALDI-TOF was carried out utilizing Dithranol and AgTFA as matrix and ionization agent.

Table 8: Conditions of precipitations of cBT from oDCB with toluene.

Exp. no.	Time of sampling [min]	Fraction of added toluene [vol-%]	Solvent temperature [°C]	Yield of isolated cBT [wt-%]	Highest T_m [°C]	Oligomeric ratio by ¹ H NMR [mol-%]	Ratio of hydroxy termini [mol-%]
9.1	282	0.0	108	8.7	211.8	9.4	5.8
9.2	310	9.5	113	9.3	210.2	10.2	5.6
9.3	345	17.1	108	8.0	210.3	9.9	7.1
9.4	370	23.6	108	8.4	212.8	8.4	6.0
9.5	400	29.3	103	9.0	211.6	7.8	6.0
9.6	435	38.7	103	8.6	212.8	7.7	6.2
9.7	468	48.6	103	8.7	213.2	7.1	6.4
9/P1	480	48.6	103	8.7	218.4	1.2	7.4
9/P2	3 d	48.6	22	14.6	241.7	1.2	1.2
9/P3	---	48.6	22	36.2	179.4	N/A	N/A

Table 9: Conditions of precipitations of cBT from oDCB with CHCl₃.

Exp. no.	Time of sampling [min]	Fraction of added CHCl ₃ [vol-%]	Solvent temperature [°C]	Yield of isolated cBT [wt-%]	Highest T _m [°C]	Oligomeric ratio by ¹ H NMR [mol-%]	Ratio of hydroxy termini [mol-%]
10.1	255	0	62	11.7	210.8	8.4	6.5
10.2	320	7.9	62	11.5	210.7	7.9	6.7
10.3	336	17.5	61	11.2	210.7	8.4	6.6
10.4	358	23.9	61	10.2	211.5	8.2	6.6
10.5	388	32.6	59	10.6	213.2	7.5	7.2
10.6	411	41.1	60	10.6	212.7	7.5	6.8
10.7	440	47.8	61	10.2	213.5	6.6	7.1
10/P1	450	47.8	61	9.1	219.1	0.8	8.2
10/P3	---	47.8	22	48.7	158.0	42.7	0.3

6.3.2 Isolation of low-melting cBT (LM-cBT) by utilization of low-boiling solvents

6.3.2.1 Separation of cBT in presence of transesterification catalyst in CHCl₃

25 g CBT100 were dried at 60 °C in vacuum for 60 h and placed into a 3-neck flask with a stirring bar, equipped with a heating jacket and a DIMROTH condenser and closed by a septum. 380 g CHCl₃ (HPLC grade and dried over 4 Å molecular sieves (4 Å)) (6.57 wt-%, 9.7 % (w/v) of CBT100) and 0.14 g SnOct₂ (0.35 mmol, 0.30 mol-%) were added. The mixture was heated to reflux. All steps so far were carried out under an Ar flow in dried glassware (150 °C, over night). Filtration through a BÜCHNER funnel was carried out in hot condition after 50 h giving a white powder in 11.7 wt-% yield. A second filtration of newly formed precipitate was conducted 12 d later yielding a white powder (3.2 wt-%). DSC thermograms were recorded following Method A and MALDI spectra with Dithranol as matrix and NaTFA as ionization agent. Peaks in ¹H NMR were in accordance with the list above (chapter 6.2).

6.3.2.2 Isolating of low-melting cBT (LM-cBT) from single solvent system

20 g CBT100 and about 275 g CHCl_3 (distilled and over molecular sieves 4 Å for 4 weeks) or 107 g CY (distilled and over molecular sieves 4 Å for 3 days) (11 and 15 % (w/v), respectively) were refluxed under Ar while stirred for 1 to 3 hours. The non-soluble cBT fraction was filtrated off through a preheated BÜCHNER funnel. The yield of the white to beige precipitate was not determinable. Newly formed precipitate was separated the next day before the filtrate was evaporated to dryness. A white powder was isolated in a yield of up to 76.7 wt-% for experiments with CHCl_3 and of 1 wt-% for CY. Method A was applied for DSC measurements. The ^1H NMR peaks of cyclic, opened and degraded MCOs were observed following the list given above (p. 138). MALDI-TOF was carried out utilizing Dithranol and NaTFA as matrix and ionization agent.

6.3.2.3 Isolating of low-melting cBT (LM-cBT) by precipitating from a solution in CHCl_3 with cyclohexane

20 g CBT100 (not dried) were placed together with CHCl_3 (distilled and dried over molecular sieves 4 Å for several days) (8 to 18 % (w/v)) in a flask and refluxed for two hours under Ar atmosphere. Depending on the experiment, insoluble cBT was filtered off in hot condition at this stage. CY (quality *purissimum*, dried over molecular sieves of 4 Å for at least one day) was added to the filtrate in a ratio of CHCl_3 :CY \approx 1:1 (v/v). The precipitate formed after refluxing was filtrated off. The filtrate was evaporated to dryness and the residue was dried *in vacuo* at 40 °C at least over night. The cBT fraction insoluble in CHCl_3 was quickly separated by filtration in hot condition prior to addition of the precipitating solvent in one variation of the experiment. In this case, a further addition of CHCl_3 was necessary to refill the volume after filtration. The influence of water content was evaluated by usage of CBT100 unprocessed or after drying *in vacuo* at 40 or 80 °C for several days. Scale-up experiments with 40 g CBT100 were carried out accordingly with a ratio CHCl_3 :CY \approx 1:1 or 2:1 (v/v). Yields of 78 or 67 wt-%, respectively, were obtained. DSC measurements were carried out according to Method A or B, ^1H NMR spectroscopy showed signals according to the list (p. 138) and MALDI experiments were carried out utilizing Dithranol as matrix and AgTFA or NaTFA as ionization agent.

Table 10: Conditions for separation of cBT fractions by utilization of low-boiling solvents with the key figures of the LM-cBT isolated from the respective filtrate.

Exp. no.	Mass of used cBT [g]	Solvent	Volume solvent [mL]	Precipitation solvent	Volume for Precipitation [mL]	Time for precipitation [h]	Yield [wt-%]	Highest T_m [°C]	Oligomeric ratio by ^1H NMR [mol-%]	Ratio of hydroxy termini [mol-%]
11	25.00	CHCl_3	255 ^{a)}	---	---	1	3	155	N/A	N/A
12	20.00	CHCl_3	179	---	---	1+0.5 ^{b)}	45	163	22	0.1
13	19.94	CHCl_3	190	---	---	3+38 ^{b)}	77	161	22	0.1
14	19.98	CY	137	---	---	4	1	172	61	ca. 0.0
15	19.90	CHCl_3	104	CY	118	1+0.5 ^{b)}	55	164	N/A	N/A
16	20.00	CHCl_3	101	CY	175	2+0.5 ^{c)}	79	160	25	0.1
17	40.00	CHCl_3	280	CY	275	1.3+1.3 ^{c)}	78	158, 187 ^{d)}	23	0.1
18	42.55	CHCl_3	349	CY	351	4.7	67	157, 245 ^{d)}	40	0.8

^{a)} Addition of 0.14 g SnOct_2 as transesterification catalyst.

^{b)} A 2nd filtration was necessary after the 1st giving the filtrate with the final fraction of cBT.

^{c)} Insoluble cBT was filtrated off previously to addition of precipitation solvent.

^{d)} Further of cBT precipitates from LM-cBT with time inhibiting a higher T_m .

6.3.3 Isolation of LM-cBT by extraction

6.3.3.1 Small-scale iterative extractions

15 g of CBT100 were placed in an extraction thimble (cellulose MN 501) after drying in a vacuum oven at 40 °C for at least 2.5 days. The thimble was put in the respective extractor (according to KNÖFLER-BÖHM or to SOXHLET) equipped with a DIMROTH condenser and connected to an Ar supply. All glassware was dried in an oven prior to use and assembled under an Ar flow. A flask with a stirring bar and with the respective solvent (CHCl_3 , CY or THF) was placed under the extractor in a temperature regulated oil bath. The flask was exchanged for a new flask with fresh solvent for time dependent analysis. After extraction, the solvent was evaporated to give a white powder, which was dried at 40 °C in a vacuum

drying oven. The results and conditions of the relevant extractions are summarized in Table 11. The samples were analyzed by DSC according to Method A (BNU122, 260) or B (BNU170) for deconvolution of melting and crystallization processes in the second cycle of DSC measurements. Signals in ^1H NMR (300 and 400 MHz) were observed in accordance with the list given above with negligible integrals for degradation products present (p. 138). MALDI-TOF analysis was conducted with Dithranol and AgTFA and partly NaTFA.

Table 11: Conditions of the small-scale extractions. Exp. no. 19: extraction of 15.11 g CBT100 with CY in a Knöfler-Böhm setup at 120-125 °C; exp. no. 20: extraction of 15.17 g by CY in a Soxhlet apparatus at 125 °C; exp. no. 21: extraction of 15.00 g by THF in a Knöfler-Böhm apparatus at 128 °C; exp. no. 22: extraction of 15.00 g by CHCl_3 in a Knöfler-Böhm setup at 106 °C.

Exp. no.	Time of sampling [min]	Yield of extracted cBT [%]	Highest T_m [°C]	Endset T [°C]	High Limit [°C]	Oligomeric Ratio by ^1H NMR [mol-%]	Ratio of hydroxy termini [mol-%]
19.1	105	10.4	167.0	190.6	187.7	50.9	0.6
19.2	231	16.5	166.5	179.5	187.5	52.0	0.9
19.3	365	22.8	164.4	175.8	188.6	53.1	0.6
19.4	470	27.9	163.6	176.7	182.8	53.3	0.3
19.5	1235	47.6	167.6	179.7	189.4	50.9	0.4
19.Rest	---	---	208.4		228.39		
20.1	125	3.6	168.7		183.2	55.0	0.1
20.2	251	5.1	173.2		189.71	56.3	0.3
20.3	380	9.5	166.1		181.44	51.4	0.3
20.4	490	12.1	172.1		189.61	56.5	0.3
20.5	1286	23.9	186.5		197.19	44.9	0.4
20-Rest	---	---	207.9		225.08		

Exp. no.	Time of sampling [min]	Yield of extracted cBT [%]	Highest T_m [°C]	Endset T [°C]	High Limit [°C]	Oligomeric Ratio by ^1H NMR [mol-%]	Ratio of hydroxy termini [mol-%]
21.1	123	47.5	153.8	171.7	180.9	38.3	4.4
21.2	251	57.7	158.6	171.8	176.5	42.3	4.4
21.3	367	63.7	156.9	188.2	179.3	41.1	3.2
21.4	488	68.3	158.5	166.4	182.6	40.3	2.1
21.5	607	72.3	148.6	173.9	193.0	38.6	5.7
21-Rest	---	---	197.8	221.5	237.0		
22.1	130	62.8	161.3	167.1	183.4	35.4	0.2
22.2	248	77.5	188.1	194.7	198.1	34.7	0.2
22.3	363	85.9	191.8	201.5	206.7	35.4	0.2
22.4	481	92.1	191.0	197.5	201.9	33.6	0.9
22.5	594	94.5	192.4	199.4	204.7	28.3	0.5
22.6	1381	95.4	195.1	205.3	209.4	13.2	2.3
22-Rest	---	---	225.8	228.3	233.3	0.0	69.1

a) Exp. no. 19: extraction of 15.11 g CBT100 with CY in a KNÖFLER-BÖHM setup at 120-125 °C.

b) Exp. no. 20: extraction of 15.17 g by CY in a SOXHLET apparatus at 125 °C.

c) Exp. no. 21: extraction of 15.00 g by THF in a KNÖFLER-BÖHM apparatus at 128 °C.

d) Exp. no. 22: extraction of 15.00 g by CHCl_3 in a KNÖFLER-BÖHM setup at 106 °C.

6.3.3.2 Larger-scale extractions (>100 g cBT) with frits continuously passed by a solvent

Scale-ups of the extraction were carried out of 130 or 335 g CBT100 in various grain sizes and distributions. Therefore, CBT100 was grinded in a mortar (fine or rough), crumbled between steel plates and milled in a cutting mill or rotor speed mill (FRITSCH PULVERISETTE type 15.303 with 2810 rpm or type 17.702, respectively, with various sieves or inserts). The processed cBT or mixtures thereof or with PBT was given in glass frits of 6 cm diameter and a length of 12 or 26 cm (for about 130 or 335 g, respectively) and with a fused silica bottom of a porosity of G0, G1 or G2 (with maximal nominal pore sizes of 160 – 250 (P250), 100 – 160 (P160) or 40 – 100 μm (P100), respectfully, according to ISO 4793) (Table 12). The glass frit was placed in a vacuum isolated glass tube connected by a glass joint on the lower end to the solvent flask and on the upper end to a DIMROTH condenser. Heating of the

solvent was carried out by a heating jacket with thermal control. Evaporated solvent CY heated the glass frit by passing it, cooled at the condenser and dropped into the frit. The solvent was distilled and dried for several days over molecular sieves of size 4 Å prior to use. All glassware was dried before use at 150 °C at least over night and assembled in an Ar stream. The solvent flask was exchanged against a new flask with fresh solvent in case of temporal screening. In an additional experiment, an Ar stream was led into the frit by a cannula to enhance the passing of the solvent (exp. no. 7).

The respective solvent was evaporated after extraction giving a white to yellow powder, depending on the extraction conditions. The product was dried *in vacuo* at 40 °C. Samples as well as samples taken from the residue in the extraction frit were analyzed by DSC by Method A (exp. no. 1, 2, 4 – 7) or B for a better resolution of melting and cold crystallization processes (exp. no. 3). ¹H NMR spectra were recorded on instrumentation with 300 and 400 MHz resulting in peaks according to the list mentioned above (p. 138). MALDI-TOF spectra were recorded with Dithranol and AgTFA. Samples of the residues were investigated by SEM. The results are summarized in Table 13.

Table 12: Conditions of extractions in larger scale.

Exp. no.	Porosity of silica frit G...	Mass of used cBT [g]	Mass of cyclo-hexane [g]	Condition of CBT and further reaction conditions	Time of extraction [h]
23	0	130	550	CBT100	11
24	1	131	502	CBT100	17
25	2	130	501	CBT100	17
26 (I&II)	2	340	799	CBT100	20+24
27	0	130	660	grinded	40
28	2	330	525	grinded	29
29	0	65+65	551	1/2 grinded + 1/2 CBT100	24
30	0	114	531	grinded + 63 g PBT pellets	24
31	0	131	550	roughly grinded	24
32	0	130	470	crumbled	20+24
33	0	130	368	milled, Ar flow	9

Table 13: Results of extractions in larger scale.

Exp. no.	Yield of extracted cBT [%]	Highest T_m [°C]	Oligomeric Ratio by ^1H NMR [mol-%]	Ratio of hydroxy termini [%]
23	20.2	166.3	54.0	0.1
24	38.1	156.2	48.4	0.0
25	44.4	170.3	51.5	0.0
26/I	36.8	150.3	44.1	0.0
26/II	20.0	177.0	N/A	N/A
2	0.3	118.2	46.8	2.9
1	1.5	196.4	49.2	8.7
3	21.4	161.1	51.7	0.3
4	7.7	163.5	52.4	0.3
5	55.6	161.5	48.0	0.3
6/I	39.0	162.5	34.8	0.3
6/II	4.5	165.5	50.2	0.0
7	0.8	163.2	52.6	0.0

6.3.3.3 Extraction of CBT100 with supercritical carbon dioxide

Extraction with scCO_2 as extracting agent was conducted at the Technical University of Hamburg, Institute of Thermal Separation Processes by Dr. C. Zetzl. It was carried out of 31.18 g unprocessed CBT100 pellets, which were previously dried *in vacuo* at 40 °C for 16 h. It was placed in an autoclave continuously flushed by scCO_2 with a flow of $40 \text{ g}\cdot\text{min}^{-1}$ at a temperature of 45 °C and a pressure of 300 bar. The pressure was dropped by a needle valve leaving the extracted cBT in vials. ^1H NMR spectra were recorded on the 400 MHz instrument giving peaks as listed above (p. 138). DSC thermograms were recorded according to Method A and MALDI-TOF spectra using Dithranol and AgTFA.

6.3.3.4 Ring-opening of cBT with 1-butanol as reference for analytics

About 4.4 g CBT100 (20 mmol) were placed in a SCHLENK tube and melted in an oil bath at 225 °C under Ar under stirring. 60 μL transesterification catalyst $\text{Ti}(\text{O}n\text{Bu})_4$ (0.1 mol-%) and

0.4 mL 1-butanol (4.4 mmol) were added before the tube was sealed again and mixed by shaking. After 1.5 h in the oil bath, the cBT was poured on a glass plate to solidify. MALDI analysis was carried out with Dithranol as matrix and with NaTFA or AgTFA as ionization agent. The MALDI and NMR spectra showed signals of cycles and those plus the mass of 1-butanol and the respective ion Na⁺ or Ag⁺.

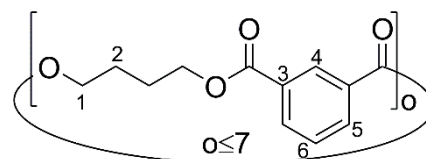
6.4 Mixtures of MCO and their influence on the thermal behavior

6.4.1 Preparation of aliphatic and aromatic lactones

6.4.1.1 Pseudo-high dilution synthesis

6.4.1.1.1 Preparation of cyclic 1,4-butylene isophthalate (cBI)

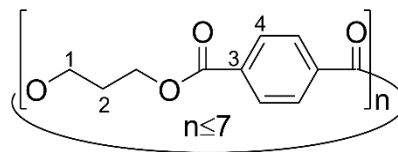
8.00 g lphCl₂ (39.4 mmol) were dissolved in 130 g DCM (distilled and dried over magnesium sulfate) and placed in a nitrogen flask together with an excess of trimethylamine (12.8 g, 217 mmol, 2.7 equivalents) and a catalytic amount of DABCO under stirring by a magnetic stirring bar. 3.55 g BDO (39.4 mmol) were diluted in 21 mL THF and added slowly by a syringe pump at 0 – 1 °C to the solution in 2 h. After 20 min of additional stirring and cooling, the light yellow suspension was allowed to warm up to room temperature. An excess of several hundred milliliters of water was added and the suspension was carefully neutralized with aqueous HCl. The aqueous phase was removed and the resulting DCM phase washed with water three times before the DCM phase was dried to give finally the light beige brittle product in a yield of 81 mol-%. A comparable preparation with simultaneous addition of the two reactants to a solution containing DMAP (1.1 mmol) as catalyst and pyridine as base (142 mmol) led to 94 mol-% yield but with a comparably high ratio of hydroxyl termini (ca. 14 mol-%). ¹H NMR (400 MHz, CDCl₃) δ [ppm] = 8.64 – 8.58 (m, 1H, H⁴), 8.24 – 8.19 (dd, *J* = 7.9, 1.7 Hz, 2H, H⁵), 7.59 – 7.52 (m, 1H, H⁶), 4.41 – 4.35 (m, 4H, H¹), 2.05 – 1.90 (m, 4H, H²). ¹³C NMR



(101 MHz, CDCl_3) δ [ppm] = 167.4 (-COO-) 134.4 (C^5), 130.9 (C^4) 130.4 (C^3), 129.2 (C^6), 65.69 (C^1), 25.3 (C^2). $T_m(\text{DSC}) = 131$ °C.

6.4.1.1.2 Preparation of cyclic 1,3-propylene terephthalate (cPT)

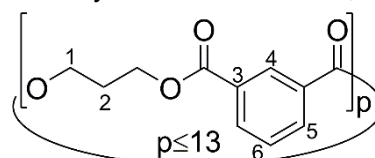
12.69 g TerCl_2 (62.51 mmol) and 4.39 g (57.7 mmol) PDO, dried at 80 °C at a rotary evaporator at 10 mbar for 6 h and stored over molecular sieves (4 Å) overnight, were each placed in a nitrogen flask and degassed by changes between vacuum and Ar for three times. The dichloride was dissolved in a mixture of DCM (dried by passing through a column of molecular sieves of 4 Å) and THF (distilled from sodium) (ratio of 4:5) to give 50 mL in total. The diol was diluted to 50 mL by THF, (distilled from sodium). Both solutions were simultaneously dosed by a syringe pump through a septum



into a third flask containing 200 mL DCM, an excess of trimethylamine (14.44 g, 244.3 mmol) and a catalytic amount of DMAP (0.38 g, 3.1 mmol), while it was cooled in an ice bath and stirred at 350 – 400 rpm with a magnetic stirring bar. After complete addition in 2.5 h, stirring was continued for another hour before the ice bath was removed and the temperature was increased until moderate reflux. The heating was stopped and 100 mL of ice water was added before the pH was adjusted to about 6 with aqueous hydrogen chloride. The precipitate was isolated, suspended in 200 mL water and again treated with HCl to give pH 6. The precipitate was washed with water and small amounts of THF. Drying in a vacuum oven at 40 °C at about 10 mbar overnight gave the colorless powdery product in a yield of 71 mol-%. ^1H NMR (400 MHz, CDCl_3) δ [ppm] = 8.01 – 7.91 (m, 4H, $\text{H}^{\text{aromatic}}$), 4.50 – 4.39 (tt, $J = 6.2$ Hz, 4H, H^1), 2.27 – 2.17 (m, 2H, H^2). ^{13}C NMR (101 MHz, CDCl_3) δ [ppm] = 166.7 (-COO-), 129.8 ($\text{C}^{\text{aromatic}}$), 62.60 (C^1), 28.06 (C^2). $T_m(\text{DSC}) = 222$ °C.

6.4.1.1.3 Preparation of cyclic 1,3-propylene isophthalate (cPI)

12.69 g (62.51 mmol) lphCl_2 were solved in THF under Ar, previously dried with sodium, to give 24 mL. 4.39 g PDO (57.7 mmol) were diluted to 24 mL by the dried THF, as well. 14.4 g trimethylamine (142 mmol, 2.27 equivalents) and 0.38 g DABCO (3.4 mmol) were dissolved in about 200 mL THF in a third nitrogen flask, which was sealed by a silicone septum, stirred at 350 rpm and cooled in an ice bath. The reactant solutions were simultaneously added by a syringe pump in 2.5 h. 4 h after start of dosing, ice water was added, the mixture poured into a beaker and neutralized by diluted HCl solution. The precipitate was isolated and treated once more on the same way giving a colorless



power. The washings were extracted by DCM twice and the organic solvent evaporated to give a second part of product. After drying *in vacuo* at 40 °C for four days, a yield was determined of 32 and 45 mol-% yield, respectively. ^1H NMR (400 MHz, CDCl_3) δ [ppm] = 8.58 – 8.47 (m, 1H, H⁴), 8.16 – 8.04 (dd, J = 8.0, 1.7 Hz, 2H, H⁵), 7.48 – 7.34 (m, 1H, H⁶), 4.51 – 4.40 (m, 4H, H¹), 2.29 – 2.16 (m, 2H, H²). ^{13}C NMR (101 MHz, CDCl_3) δ [ppm] = 166.4 (-COO-), 134.1 (C⁵), 130.7 (C⁴), 130.2 (C³), 128.9 (C⁶), 62.4 (C¹), 27.9 (C²). $T_m(\text{DSC})$ = 120 °C.

6.4.1.1.4 Attempted preparation of cBI from transesterification of DMIph with BDO in dilution

A solution of 11.32 g DMIph (58.3 mmol, dried in a vacuum cabinet at 40 °C) in 182.74 g oDCB (dried over molecular sieves (4 Å)) was refluxed in presence of 0.10 g $\text{Ti}(\text{O}^n\text{Bu})_4$ under an Ar atmosphere in a 2-neck-flask and a cooler. 5.33 g BDO (59.1 mmol, dried over molecular sieves) were dosed by syringe pump for 4 h. The solution was cooled down and evaporated to dryness to give after further drying the final precipitate as mixture of cBI, DMIph and end groups with BDO (ratio by ^1H NMR 1.0 : 10.4 : 3.5). ^1H NMR of DMIph (400 MHz, CDCl_3) δ [ppm] = 8.66 (s, 1H), 8.21 (dd, J = 7.7, 1.7 Hz, 2H), 7.52 (t, J = 7.8 Hz, 1H), 3.95 (s, 4H). Signals BDO end groups: 4.40 (t, J = 6.6 Hz, 2H), 3.74 (t, J = 6.4 Hz, 2H), 1.97 – 1.85 (m, 2H), 1.81 – 1.70 (m, 2H) and 3.68 (t, J = 5.8 Hz, 2H), 1.72 – 1.63 (m, 2H).

6.4.1.1.5 Attempted preparation of cBT from TerCl_2 and BDO by removing HCl

Equimolar solutions of TerCl_2 in toluene and of BDO in Tol:THF=1:1 (v/v) (0.9 M) or of both in cyclohexanone (1.7 M) were prepared with each volume being about 50 mL. All solvents used in the reactions were dried prior to use by a solvent drying system. 200 mL of toluene or cyclohexanone, respectively, were placed under Ar in a 3-neck-flask equipped with a magnetic stirrer, a heating jacket and a DIMROTH condenser. The solutions were simultaneously dosed into the flask with a speed of $10 \text{ mL}\cdot\text{h}^{-1}$, while the mixture refluxed. At the same time, Ar was led through the liquid to facilitate the driving out of formed HCl. 30 min after complete addition (ca. 5.8 h in total), the reaction was quenched by addition of 200 mL water and the organic phase was extracted three further times with water. The resulting organic phase was evaporated to dryness. ^1H NMR (300 MHz, CDCl_3) δ [ppm] = 8.09 (d, J = 10.8 Hz, 4H), 4.51 – 4.30 (m, 4H), 1.99 (s, 4H). BDO end groups: 4.51 – 4.30 (m, 2H) 3.83 – 3.73 (m, 2H), 1.88 (p, J = 6.9 Hz, 2H), 1.76 (q, J = 7.2 Hz, 2H). (Ratio repeating units : end groups = 1 : 0.7 to 0.8.)

6.4.1.1.6 Attempted Preparation of cBT from TerCl_2 and BDO with NaOH at elevated temperature

10.15 g TerCl_2 (50.0 mmol) were dissolved in 45 g toluene and 4.51 g BDO (50.0 mmol) in 24 g toluene and 25 g THF (solvents from a drying system). Both solutions were slowly dosed by a syringe pump into a 3-neck-flask containing 175 mL toluene, 2.86 g NaOH (71.5 mmol) and 38 g 2-propanol to increase the polarity without providing a reactive nucleophile. The flask was heated to reflux magnetically stirred and equipped with a condenser. After 5.8 h, the addition was finished and the reaction was quenched by adding 200 mL of water after cooling of the yellow suspension to about 50 °C. The organic phase was separated from the aqueous and two more times extracted by water. The united aqueous phases were extracted three times by DCM. The two organic phases were separately dried at a rotational evaporator giving the same product according to ^1H NMR in total yields between 66 – 86 mol-%. ^1H NMR (300 MHz, CDCl_3) δ [ppm] = 8.20 – 8.01 (m, 3H), 4.52 – 4.33 (m, 3H), 2.06 – 1.95 (m, 1H). BDO end group: 3.78 (t, J = 6.4 Hz, 2H), 1.95 – 1.82 (m, 21H), 1.84 – 1.68 (m, 12H). (Ratio repeating units : end groups = 1 : 2.8 to 3.6).

6.4.1.2 Depolymerization of PBI in dilution

PBI was prepared by polycondensation from 150 g DMlph and an excess of 80 – 90 g BDO in a 250 mL glass reactor analogue to the procedure described elsewhere.¹ ^1H NMR (400 MHz, CDCl_3) δ [ppm] = 8.67 (s, 1H), 8.36 – 8.14 (d, J = 7.8 Hz, 2H), 7.52 (t, J = 7.8 Hz, 1H), 4.43(s, 4H), 1.97 (s, 3H); end groups (in ratio 1:11) 3.73 (t, J = 6.4 Hz, 2H), 1.92 – 1.85 (m, 2H), 1.85 – 1.78 (m, 2H), 1.78 – 1.69 (m, 2H). $T_m(\text{DSC})$ = 142 °C (literature 143 °C¹²⁷).

A solution of the prepared PBI (after drying *in vacuo* at 40 °C over night) in oDCB (dried over molecular sieves) (10 % w/v) was refluxed together with 2.92 g $\text{Ti}(\text{O}^n\text{Bu})_4$ in a three-neck flask under an Ar atmosphere for up to 72 h. Samples were taken at different times, dried and analyzed by DSC. The solvent was reduced and the product filtered off and dried in vacuum at 40 °C. ^1H NMR and DSC were as expected for a mixture of PBI and cBI (ratio of repeating units by ^1H NMR of cBI : PBI \leq 3.8 : 1.0).

6.4.1.3 Depolymerization in bulk

6.4.1.3.1 Attempts for depolymerization of aromatic polyesters in bulk

PBI was prepared as described above from DMlph and BDO.¹ 100 to 150 g PBI or commercial PBT (dried in vacuum at least over night) were placed in a 250 mL glass reactor equipped with an overhead mechanical stirrer, a heating jacket and connected over a micro

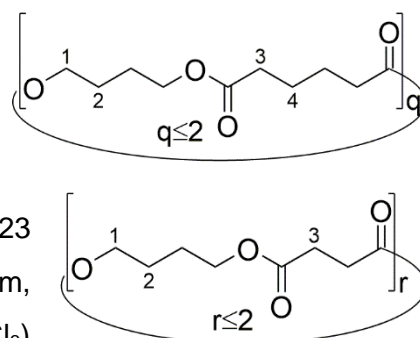
distillation bridge to a vacuum pump with pressure control. The polymer was carefully melted under reduced pressure. The temperature was set to 200 to 250 °C in case of PBT or 250 to 350 °C for PBI and the pressure reduced to the desired value of the rotary vane pump or the diffusion pump. The content of the reactor and the formed distillate was regularly probed and analyzed by ^1H NMR and especially GC-MS in respect to formed cycles without finding hints. Stripping with nitrogen was evaluated by a continuous stream of nitrogen through a cannula leading into the melt of about 79 g PBI at up to 250 °C. No signs for formed MCOs were found, either.

6.4.1.3.2 Preparation of cyclic 1,4-butylene adipate (cBA) and cyclic 1,4-butylene succinate (cBS)

CBA and cBS were prepared in a polymerization-depolymerization process from BDO and adipic or succinic acid in a 5 L steel reactor at 220 to 240 °C and pressures as low as $2 \cdot 10^{-2}$ mbar. The formed cycles were purified by repeated recrystallization and distillation. A description of the general method is given

elsewhere.²³¹ CBA: ^1H NMR (400 MHz, CDCl_3) δ [ppm] = 4.23 – 4.17 (m, 4H, H^b), 2.38 – 2.30 (m, 4H, H^c), 1.87 – 1.81 (m, 4H, H^a), 1.79 – 1.72 (m, 4H, H^d). ^{13}C NMR (101 MHz, CDCl_3)

δ [ppm] = 173.33 (C^e), 64.05 (C^b), 33.97 (C^c), 25.57 (C^a), 23.92 (C^d). T_m (DSC) = 96 °C. CBS: ^1H NMR (500 MHz, CDCl_3) δ [ppm] = 4.21 – 4.14 (m, 1H, H^b), 2.62 – 2.56 (m, 1H, H^c), 1.85 – 1.77 (dt, $J = 5.3, 2.8$ Hz, 1H, H^a). ^{13}C NMR (126 MHz, CDCl_3) δ [ppm] = 172.24 (C^d), 65.21 (C^b), 32.65 (C^c), 26.54 (C^a). T_m (DSC) = 69 °C.



6.5 Enzyme- and metal-catalyzed polycondensation of a new bio-based polyester

6.5.1 Polycondensation of polyesters

Polycondensation reactions were carried out in bulk polymerization of 27.77 g PDO (365.1 mmol) and 149.96 g Pripol (258.0 mmol) in a 250 ml glass reactor. The respective reaction mixture was stirred with an anchor stirrer connected to an overhead agitator. Heating was

achieved by a heating jacket controlled by a PT100 resistance thermometer. Water and the excess of PDO were removed by vacuum through a distillation bridge connected to the reactor and collected in a cooling trap, both cooled with liquid nitrogen. At defined time points, samples were withdrawn from the reactor and analyzed by acid titration and SEC. The final products were additionally characterized by ^1H NMR spectroscopy and rheology.

6.5.1.1 Metal- and auto-catalyzed polycondensation

The reaction mixture was heated to 180 °C at a reduced pressure of 600 mbar and kept at these conditions for 100 min in order to obtain oligomers. Subsequently, the pressure was reduced to 20 mbar within 18 min and the temperature was raised to 220 °C within 7 min. The pressure was reduced to less than 1 mbar by a rotary vane pump after adding 0.005 mol-% of $\text{Ti}(\text{OnBu})_4$ solution in toluene (10 wt-%). The reaction was stopped after 365 min by pouring out of the reaction mixture. The autocatalyzed reaction without any catalyst (route A) was conducted identically for 1440 min. In case of route A, a spatula tip of 1,4-dihydroxybenzene was added to the melt directly before terminating of the reaction to inhibit oxygene-mediated crosslinking.

6.5.1.2 Enzyme-catalyzed polycondensation

Two different types of precondensation were carried out for enzyme-catalyzed polycondensation: Either an uncatalyzed precondensation (route E1), identical to that in the metal-catalyzed route (180 °C, 600 mbar) was performed for 100 min or one at 80 °C and 100 mbar for 125 min with enzyme initially added (route E2). In both cases, the temperature of the reaction mixture was adjusted to 80 °C within the next 18 min after the precondensation step. Subsequently, the pressure was lowered to the final condition of 1 mbar within 7 min and 5 wt-% of the enzyme *CalB immo* (approximately 3 mmol-% active sites) were added in case of route E1. The reactions were terminated after 48 or 55 h (E2 or E1, respectively). In case of route E1, a small amount of 1,4-dihydroxybenzene was added to avoid oxygene-mediated crosslinking.

6.5.2 Exemplary synthesis of a polyurethane elastomer

The polyesterdiol for the exemplary synthesis of a polyurethane elastomer was prepared accordingly to the metal-catalyzed route (chapter 6.5.1.1) with 0.08 mL $\text{Ti}(\text{OnBu})_4$. Two times the formed polymer chains were scissored by dosing of additional PDO (16 and 14 mL)

to ensure hydroxy end groups before the final polyesterol was obtained. Its hydroxide number was determined by a titrator *TA 20* and the software *TitriSift 2.6* (both by Schott Geräte) according to DIN 53240-2 (half scale, double determination) with 30 mL 2-butanone as solvation help.








For polyurethane synthesis, the polyesterdiol, isocyanates and chain extender 1,4-butanediol were heated to 100 °C before use. Every component or mixture was extensively mixed by a *SpeedMixer DAC400 FV* at 2500 rpm for 30 s prior to further use. The polyol component (component A) consisted of 91.6 wt-% polyesterdiol, 8.0 wt-% 1,4-butanediol, 0.3 wt-% anti-foaming agent and 0.1 wt-% catalyst. In the isocyanate component (component B), equal amounts by weight were present of Lupranat MM103 and IsoMMDI. After regaining a temperature of 100 °C in 30 min of both components, the A component was mixed again before the B component was added with an isocyanate index of 100. After mixing for 30 s, the reaction mixture was spread with a layer thickness of 2 mm on a preheated aluminum plate (70 °C), kept there for another 30 min and was annealed for 4 h at 80 °C afterwards. The PU sheet was conditioned at about 20 °C and 60 % relative air humidity for 14 d before tensile testing by a *ZwickRoell machine* with *videoXtens* (in accordance with DIN 53504) and determining of the Shore A hardness (according to DIN 53505) were carried out.











7 H- and P-Clauses and Disposal









Annotations for safety, disposal and health in respect of carcinogenicity, reproductive toxicity and mutagenicity (CMR) are given for the chemicals used within this work in the following subchapters.

7.1 Safety^{258–260}

Table 14: The used chemicals with their safety relevant data.

Substance	Pictogram	H clause	P clause
Acetone-d6		225, 319, 336	210, 261, 305+351+338
Adipic acid		319	305+351+338
1,4-Butanediol (BDO)		302, 336	301+P312, 330
2-Butanone		225, 319, 336	210, 305+351+338, 403+233
CBT100			
Chloroform (CHCl ₃)		302, 315, 319, 331, 336, 351, 361d, 372	261, 281, 305+351+338, 311
Chloroform-d (CDCl ₃)		302, 315, 319, 331, 351, 361d, 372	260, 280, 301+312+330, 304+340+312, 305+351+338, 403+233
Cyclic 1,4-butylene isophthalate (cBI)	N/A		
Cyclic 1,4-butylene terephthalate (cBT)	---	---	---
Cyclic 1,3-propylene isophthalate (cBT)	N/A		
Cyclic 1,3-propylene terephthalate (cPT)	N/A		
Cyclohexane (CY)		225, 304, 315, 336, 410	210, 240, 273, 301+330+331, 302+352, 403+233

Substance	Pictogram	H clause	P clause
Cyclohexanone		226, 302+312+332, 315, 318	280, 305+351+338
1,4-Diaza-bicyclo[2.2.2]octane (DABCO)		228, 302, 315, 318	210, 240, 241, 264, 270, 280
1,2-Dichlorobenzene (oDCB)		302+332, 315, 319, 317, 335, 410	261, 280, 301+312+330, 305+351+338
Dichloromethane		315, 319, 335, 336, 351, 373	261, 281, 305+351+338
1,4-Dihydroxybenzene		351, 341, 302, 318, 317, 400	273, 280, 305+351+338, 302+352, 313
Dimethyl isophthalate (DMlph)	---	---	---
4-Dimethylaminopyridine (DMAP)		301, 310, 315, 319, 335	280, 301+310+330, 302+352+310, 304+340+312, 305+351+338, 337+313
Dithranol		315, 319, 335	261, 305+351+338
1,1,1,3,3,3-hexafluoroisopropanol (HFIP)		302, 314, 361d	260, 280, 301+312+330, 303+361+353, 304+340+310, 305+351+338
Hydrochloric acid		290, 314, 335	260, 280, 303+361+353, 304+340+310, 305+351+338
IsoMMDI		320, 315, 332, 334, 317, 335, 373	280, 271, 260, 261, 284, 272, 264, 312, 305+351+338, 304+340, 314, 303+352, 333+311, 332+313, 362+364, 337+311, 403+233, 405, 501

Substance	Pictogram	H clause	P clause
Isophthaloyl chloride (IphCl ₂)		331, 312, 314	261, 280, 305+351+338, 310
Mixture of phenylmercury(II) 2-(dodec-1-en-1-yl)succinate and 2-ethylhexanoic acid (catalyst for polyurethane synthesis)	N/A		280, 271, 260, 261, 284, 272, 264, 312, 305+351+338,
Lupranat MM103		320, 315, 332, 334, 317, 335, 373	304+340, 314, 303+352, 333+311, 332+313, 362+364, 337+311, 403+233, 405, 501
Phenolphthalein		341, 350, 361f	201, 280, 308+313
Poly(1,4-butylene isophthalate) (PBI)	---	---	---
Poly(1,4-butylene terephthalate) (PBT)	---	---	---
Potassium hydroxide in ethanol, 0.1 mol · L ⁻¹		225, 315, 319	210, 240, 302+352, 305+351+338, 403+233
PripolTM 1012 (Pripol)	N/A		210, 233, 240, 305+351+338, 403+235
2-Propanol		225, 319, 336	210, 233, 240, 305+351+338, 403+235
1,3-Propanediol (PDO)	---	---	---
Silver(I) trifluoroacetate (AgTFA)		315, 319	305, 351, 338
Sodium hydroxide		290, 314	280, 301+330+331, 305+351+338, 308+310
Sodium(I) trifluoroacetate (NaTFA)	---	---	---
Succinic acid		318	280, 305+351+338, 313

Substance	Pictogram	H clause	P clause
Terephthaloyl chloride (TerCl ₂)		331, 314	261, 280, 303+361+353, 304+340, 305+351+338, 310
Tetrahydrofuran (THF)		225, 302, 319, 335, 351, EUH019	210, 280, 301+312+330, 305+351+338, 370+378, 403+235
Tetramethylsilane (TMS)		224	210
Tin(II) 2-ethylhexanoate (SnOct ₂)		317, 318, 361, 412	273, 280, 305+351+338
Titanium(IV) tetra-n- butanolate (Ti(OnBu) ₄)		226, 315, 318, 335, 336	210, 280, 304+340+312, 305+351+338+310, 403+235
Toluene		225, 361d, 304, 373, 315, 336	210, 240, 301+310+330, 302+352, 308+313, 314, 403+233
Triethylamine		225, 302, 311+331, 314, 335	210, 280, 303+361+353, 304+340, 310, 305+351+338, 403+233

7.2 Disposal

The substances were disposed according to the Chemicals Act, the Ordinance on Hazardous Substances and the applicable technical rules comprised in the disposal guide of the University of Hamburg²⁶¹. Liquids were separately collected in containers for halogenated and non-halogenated solvents. Acids and bases were separately collected and disposed. Solids and contaminated working materials were disposed after drying in adequate bags.

7.3 Usage of CMR substances^{258,259}

No chemicals with CMR of category 1A or 1B were used according to EC regulation No.1272/2008. The used CMR substances with category 2 are summarized in the following table.

Table 15: Used CMR substances (C: carcinogenic, M: mutagenic and R: reproductive toxic).

Substance	CAS No.	Used method, number of experiments and quantity	Category
Chloroform	67-66-3	Precipitation: 1x0.1 L, 3x0.2 L, 2x0.3 L, 1x0.4 L, 1x0.5 L, 1x2.1 L	2 (C, H351)
		Extraction: 1x0.5 L	2 (R, H361d)
		Ultrasonic degradation: 2.1 L	
Chloroform-d	865-49-6	NMR: 334x0.7 mL	2 (C, H351)
			2 (R, H361d)
Dichloromethane	75-09-2	Reactions: 1x15 mL, 3x20 mL, 1x40mL, 1x45 mL, 1x200mL	2 (C, H351)
1,4-Dihydroxybenzene	123-31-9	3x ca. 20 mg	2 (C, H351)
			2 (M, H341)
1,1,1,3,3,3-hexafluoroisopropanol	920-66-1	NMR & MALDI: 189x0.05 mL	2 (R,H361d)
		Ultrasonic degradation: 1x260 mL	
		GPC: 1x2 L	
Petrolether	8032-32-4	Purification: 1x50 mL, 1x150 mL, 1x250 mL, 1x680 mL, 1x1 L	2 (R, H361f)
Phenolphthalein	77-09-8	2x50 mg	1B (C, H350)
			2 (M, H341)
Tetrahydrofuran	109-99-9	Extraction: 1x450 mL	2 (C, H351)
		Reaction: 3x20 mL, 1x25 mL, 1x30 mL, 3x50 mL, 1x80 mL	
		Purification: 2x0.1 mL	
Tin(II) 2-ethylhexanoate	301-10-0	Catalyst for depolymerization: 4x0.1 g	2 (R, H361)
		Catalyst for ROP: 1x0.7 mL, 5x2.5 mL	
Toluene	108-88-3	Precipitation/purification: 1x10 mL, 1x50 mL, 1x80 mL, 1x130 mL, 2x250 mL, 1x280 mL, 1x400 mL	2 (R, H361d)
		Reaction: 2x70 mL	
		Extraction: 1x500 mL	
		Catalyst solution for ROP: 1x3 mL, 2x2 mL, 3x3 mL, 4x5 mL, 5x10 mL, 2x15 mL, 1x20 mL	

8 References

1. Gebhard, J., Neuer, B., Luinstra, G. A. & Liese, A. Enzyme- and Metal-Catalyzed Synthesis of a New Biobased Polyester. *Org. Process Res. Dev.* **21**, 1245–1252 (2017).
2. Mülhaupt, R. Green Polymer Chemistry and Bio-based Plastics: Dreams and Reality. *Macromol. Chem. Phys.* **214**, 159–174 (2013).
3. PlasticsEurope. *Plastics - The Facts 2015: An analysis of European plastics production, demand and waste data.* (2015).
4. PlasticsEurope. *Plastics - The Facts 2016: An analysis of European latest plastics production, demand and waste data.* (2016).
5. PlasticsEurope Deutschland e. V. *Geschäftsbericht 2017.* (2017).
6. Michael Herrmann. *Geschäftsbericht 2015 - PlasticsEurope Deutschland e. V.* (2016).
7. PlasticsEurope. *Plastics – the Facts 2017: An analysis of European plastics production, demand and waste data.* (2018).
8. E.V., E. B. *Bioplastics market data 2018.* (2018).
9. Lundquist, L., Leterrier, Y., Sunderland, P. & Månson, J.-A. E. *Life Cycle Engineering of Plastics.* (Elsevier, 2000).
10. Tobita, H. & Hamielec, A. E. Polymerization Processes, 2. Modeling of Processes and Reactors. in *Ullmann's Encyclopedia of Industrial Chemistry* 1–50 (Wiley-VCH Verlag GmbH & Co. KGaA, 2015). doi:10.1002/14356007.o21_o01.pub2
11. Elias, H.-G. *Makromoleküle - Band 1: Chemische Struktur und Synthesen.* (Wiley-VCH, 2003).
12. Hodge, P. Entropically Driven Ring-Opening Polymerization of Strainless Organic Macrocycles. *Chem. Rev.* **114**, 2278–2312 (2014).
13. Kricheldorf, H. R. H. R., Berl, M. & Scharnagl, N. Poly(lactones). 9. Polymerization Mechanism of Metal Alkoxide Initiated Polymerizations of Lactide and Various Lactones. *Macromolecules* **21**, 286–293 (1988).
14. Duda, A. & Penczek, S. Polymerization of ϵ -Caprolactone Initiated by Aluminum Isopropoxide Trimer and/or Tetramer. *Macromolecules* **28**, 5981–5992 (1995).
15. O'Keefe, B. J., Breyfogle, L. E., Hillmyer, M. A. & Tolman, W. B. Mechanistic Comparison of Cyclic Ester Polymerizations by Novel Iron(III)–Alkoxide Complexes: Single vs Multiple Site Catalysis. *J. Am. Chem. Soc.* **124**, 4384–4393 (2002).
16. Youk, J. H., Kambour, R. P. & MacKnight, W. J. Polymerization of Ethylene Terephthalate Cyclic Oligomers with Antimony Trioxide. *Macromolecules* **33**, 3594–3599 (2000).
17. Youk, J. H., Kambour, R. P. & MacKnight, W. J. Preparation and Polymerization of Ethylene 2,6-Naphthalenedicarboxylate Cyclic Oligomers †. *Macromolecules* **33**, 3606–3610 (2000).
18. Youk, J. H., Boulares, A., Kambour, R. P. & MacKnight, W. J. Polymerization of Ethylene Terephthalate Cyclic Oligomers with a Cyclic Dibutyltin Initiator. *Macromolecules* **33**, 3600–3605 (2000).

-
19. Brunelle, D. J. *et al.* Semicrystalline Polymers via Ring-Opening Polymerization: Preparation and Polymerization of Alkylene Phthalate Cyclic Oligomers. *Macromolecules* **31**, 4782–4790 (1998).
 20. Brunelle, D. J. Cyclic oligomer chemistry. *J. Polym. Sci. Part A: Polym. Chem.* **46**, 1151–1164 (2008).
 21. Mohd Ishak, Z. A., Shang, P. P. & Karger-Kocsis, J. A modulated DSC Study on the in situ Polymerization of Cyclic Butylene Terephthalate Oligomers. *J. Therm. Anal. Calorim.* **84**, 637–641 (2006).
 22. Samsudin, S. A. Cyclic Polyesters Evolution. 1–30 (2014).
 23. Tripathy, A. R., Chen, W., Kukureka, S. N. & MacKnight, W. J. Novel poly(butylene terephthalate)/poly(vinyl butyral) blends prepared by in situ polymerization of cyclic poly(butylene terephthalate) oligomers. *Polymer* **44**, 1835–1842 (2003).
 24. Brunelle, D. J. Synthesis and Polymerization of Cyclic Polyester Oligomers. in *Modern Polyesters: Chemistry and Technology of Polyesters and Copolyesters* (eds. Scheirs, J. & Long, T. E.) 117–142 (John Wiley & Sons, Ltd, 2003). doi:10.1002/0470090685.ch3
 25. Parton, H. & Verpoest, I. In situ polymerization of thermoplastic composites based on cyclic oligomers. *Polym. Compos.* **26**, 60–65 (2005).
 26. Mohd Ishak, Z. A., Leong, Y. W., Steeg, M. & Karger-Kocsis, J. Woven glass fabric composites via in-situ polymerized cyclic butylene terephthalate oligomers. in *ANTEC* 186–189 (2006).
 27. McLauchlin, A., Bao, X. & Zhao, F. Organoclay polybutylene terephthalate nanocomposites using dual surfactant modified montmorillonite prepared by the masterbatch method. *Appl. Clay Sci.* **53**, 749–753 (2011).
 28. Jiang, Z. *et al.* Poly(butylene terephthalate)/silica nanocomposites prepared from cyclic butylene terephthalate. *Composites Part A* **40**, 273–278 (2009).
 29. Fabbri, P., Bassoli, E., Bon, S. B. & Valentini, L. Preparation and characterization of poly(butylene terephthalate)/graphene composites by in-situ polymerization of cyclic butylene terephthalate. *Polymer* **53**, 897–902 (2012).
 30. Wu, F. & Yang, G. Synthesis and Properties of Poly(butylene terephthalate)/Multiwalled Carbon Nanotube Nanocomposites Prepared by In Situ Polymerization and In Situ Compatibilization. *J. Appl. Polym. Sci.* **118**, 2929–2938 (2010).
 31. Bernnat, A., Eibeck, P. & Dirlenbach, J. Polybutylene Terephthalate (PBT). *Kunststoffe* **10**, 106–110 (2013).
 32. Global Industry Analysis Inc. Press Release - February 3rd, 2016. Available at: <http://www.strategyr.com/pressMCP-6509.asp>. (Accessed: 29th August 2016)
 33. Baur, E., Osswald, T. A., Rudolph, N. & Saechtling, H. Polybutylenterephthalat (PBT). in *Saechtling Kunststoff Taschenbuch* 583–584 (Carl-Hanser, 2013).
 34. McIntyre, J. E. *et al.* *Modern Polyesters: Chemistry and Technology of Polyesters and Copolyesters*. (2003).
 35. Hill, J. W. & Carothers, W. H. Studies of Polymerization and Ring Formation. XX. Many-membered Cyclic Esters. *J. Am. Chem. Soc.* **55**, 5031–5039 (1933).
 36. Hubbard, P., Brittain, W. J., Simonsick, W. J. & Ross, C. W. Synthesis and Ring-Opening Polymerization of Poly(alkylene 2,6-naphthalenedicarboxylate) Cyclic
-

-
- Oligomers. *Macromolecules* **29**, 8304–8307 (1996).
37. Lahcini, M., Castro, P. M., Kalmi, M., Leskelä, M. & Repo, T. The Use of Tetra(phenylethynyl)tin as an Initiator for the Ring-Opening Polymerization of Lactide. *Organometallics* **23**, 4547–4549 (2004).
 38. Tripathy, A. R., Elmoumni, A., Winter, H. H. & MacKnight, W. J. Effects of Catalyst and Polymerization Temperature on the In-Situ Polymerization of Cyclic Poly(Butylene Terephthalate) Oligomers for Composite Applications. *Macromolecules* **38**, 709–715 (2005).
 39. Kamau, S. D., Hodge, P., Williams, R. T., Stagnaro, P. & Conzatti, L. High Throughput Synthesis of Polyesters Using Entropically Driven Ring-Opening Polymerizations. *J. Comb. Chem.* **10**, 644–654 (2008).
 40. Vuorinen, S. *et al.* Bismuth(III) Alkoxide Catalysts for Ring-Opening Polymerization of Lactides and ϵ -Caprolactone. *Macromol. Chem. Phys.* **214**, 707–715 (2013).
 41. Ouhadi, T., Stevens, C. & Teyssié, P. Mechanism of ϵ -Caprolactone Polymerization by Aluminum Alkoxides. *Die Makromolekulare Chemie, Suppl.* **1**, 191–201 (1975).
 42. Storey, R. F. & Sherman, J. W. Kinetics and Mechanism of the Stannous Octoate-Catalyzed Bulk Polymerization of ϵ -Caprolactone. *Macromolecules* **35**, 1504–1512 (2002).
 43. Kricheldorf, H. R., Kreiser-Saunders, I. & Boettcher, C. Polylactones: 31. Sn(II)octoate-initiated polymerization of L-lactide: a mechanistic study. *Polymer* **36**, 1253–1259 (1995).
 44. Kricheldorf, H. R., Kreiser-Saunders, I. & Stricker, A. Polylactones 48. SnOct₂-Initiated Polymerizations of Lactide: A Mechanistic Study. *Macromolecules* **33**, 702–709 (2000).
 45. Kricheldorf, H. R. Tin-initiated polymerizations of lactones: mechanistic and preparative aspects. *Macromol. Symp.* **153**, 55–65 (2000).
 46. Zhang, X., MacDonald, D. A., Goosen, M. F. A. & McAuley, K. B. Mechanism of Lactide Polymerization in the Presence of Stannous Octoate: The Effect of Hydroxy and Carboxylic Acid Substances. *J. Polym. Sci. Part A: Polym. Chem.* **32**, 2965–2970 (1994).
 47. Kowalski, A., Duda, A., Stanis & Penczek, S. Kinetics and mechanism of cyclic esters polymerization initiated with tin(II) octoate, 1, Polymerization of ϵ -caprolactone. *Macromolecules* **19**, 567–572 (1998).
 48. Libiszowski, J., Kowalski, A., Duda, A. & Penczek, S. Kinetics and mechanism of cyclic esters polymerization initiated with covalent metal carboxylates, 5, End-Group Studies in the Model ϵ -Caprolactone and L,L-Dilactide/Tin(II) and Zinc Octoate/Butyl Alcohol Systems. *Macromol. Chem. Phys.* **203**, 1694–1701 (2002).
 49. Kohn, F. E., Van Ommen, J. G. & Feijen, J. The mechanism of the ring-opening polymerization of lactide and glycolide. *Eur. Polym. J.* **19**, 1081–1088 (1983).
 50. Davies, A. G., Kleinschmidt, D. C., Palan, P. R. & Vasishtha, S. C. Organotin Chemistry. Part XI. The Preparation of Organotin Alkoxides. *J. Chem. Soc. C Org.* **0**, 3972–3976 (1971).
 51. Goodman, I. & Nesbitt, B. The structures and reversible polymerization of cyclic oligomers from poly(ethylene terephthalate). *J. Polym. Sci.* **48**, 423–433 (1960).
 52. Schmidt, S. Untersuchung der Aktivität verschiedener Initiatoren zur ring-öffnenden Copolymerisation von cyclischem 1,4-Butylenterephthalat und ϵ -Caprolacton bei
-

- Temperaturen unterhalb 200 °C. (University of Hamburg, 2015).
53. Hodge, P. & Colquhoun, H. M. Recent work on entropically-driven ring-opening polymerizations: some potential applications. *Polym. Adv. Technol.* **16**, 84–94 (2005).
 54. Zhang, J. *et al.* Living lamellar crystal initiating polymerization and brittleness mechanism investigations based on crystallization during the ring-opening of cyclic butylene terephthalate oligomers. *Polym. Chem.* **4**, 1648–1656 (2013).
 55. Mohd Ishak, Z. A., Gatos, K. G. & Karger-Kocsis, J. On the In-Situ Polymerization of Cyclic Butylene Terephthalate Oligomers: DSC and Rheological Studies. *Polym. Eng. Sci.* **46**, 743–750 (2006).
 56. Parton, H. *et al.* Properties of poly(butylene terephthalate) polymerized from cyclic oligomers and its composites. *Polymer* **46**, 9871–9880 (2005).
 57. Chen, H., Yu, W. & Zhou, C. Entropically-driven ring-opening polymerization of cyclic butylene terephthalate: Rheology and kinetics. *Polym. Eng. Sci.* **52**, 91–101 (2012).
 58. Hakmé, C. *et al.* In situ monitoring of cyclic butylene terephthalate polymerization by dielectric sensing. *J. Non. Cryst. Solids* **353**, 4362–4365 (2007).
 59. Archer, E. *et al.* Monitoring the Degree of Conversion of Cyclic Butylene Terephthalate using Dielectric Analysis. *Polym. Polym. Compos.* **16**, 365–374 (2008).
 60. Derdouri, A., Tatibouet, J. & Sammut, P. Rheological and ultrasonic monitoring of the in-situ polymerization of cyclic butylene terephthalate. *AIP Conf. Proc.* **1027**, 467–469 (2008).
 61. Nakayama, Y., Sakaguchi, K., Tanaka, R., Cai, Z. & Shiono, T. Synthesis of Aliphatic Polyesters via Ring-Opening Polymerization of Macrocyclic Oligoesters. *Macromol. Symp.* **350**, 7–13 (2015).
 62. Labruyère, C., Talon, O., Berezina, N., Khousakoun, E. & Jérôme, C. Synthesis of poly(butylene succinate) through oligomerization-cyclization-ROP route. *RSC Adv.* **4**, 38643 (2014).
 63. Brunelle, D. J. & Shannon, T. G. Preparation of functionalized polycarbonates via ring-opening polymerization of diverse mixed oligomeric cyclic carbonates. *Makromol. Chem.-M. Symp.* **42–43**, 155–166 (1991).
 64. Szopinski, D., Neuer, B., Scheliga, F., Auhl, D. & Luinstra, G. A. Ultra-High Molecular Weight Biodegradable Polyesters Synthesized by Non-Enzymatic Ring-Opening Polymerization (ROP). in *Macromolecular Colloquium* (2016).
 65. Carothers, W. H. & Hill, J. W. Studies of polymerization and ring formation. XII. Linear superpolyesters. *J. Am. Chem. Soc.* **54**, 1559–1566 (1932).
 66. Ishii, M., Okazaki, M., Shibasaki, Y., Ueda, M. & Teranishi, T. Convenient Synthesis of Aliphatic Polyesters by Distannoxane-Catalyzed Polycondensation. *Biomacromolecules* **2**, 1267–1270 (2001).
 67. Mochizuki, M. *et al.* Structural Effects upon Enzymatic Hydrolysis of Poly(butylene succinate-co-ethylene succinate)s. *Macromolecules* **30**, 7403–7407 (1997).
 68. Yoda, K. & Kimoto, K. Ring-opening Polymerization of the Macrocyclic Ester. *Bull. Chem. Soc. Jpn.* **41**, 1687–1689 (1968).
 69. Monvisade, P. & Loungvanidprapa, P. Synthesis of poly(ethylene terephthalate-co-isophthalate) via ring-opening polymerization of their cyclic oligomers. *J. Polym. Res.* **15**, 381–387 (2008).
 70. Burch, R. R. R., Lustig, S. R. S. & Spinu, M. Synthesis of cyclic oligoesters and their

- rapid polymerization to high molecular weight. *Macromolecules* **33**, 5053–5064 (2000).
71. Harsch, M., Karger-Kocsis, J. & Apostolov, A. A. Crystallization-induced shrinkage, crystalline, and thermomechanical properties of in situ polymerized cyclic butylene terephthalate. *J. Appl. Polym. Sci.* **108**, 1455–1461 (2008).
 72. Baets, J., Dutoit, M., Devaux, J. & Verpoest, I. Toughening of glass fiber reinforced composites with a cyclic butylene terephthalate matrix by addition of polycaprolactone. *Composites Part A* **39**, 13–18 (2008).
 73. Baets, J., Godara, A., Devaux, J. & Verpoest, I. Toughening of polymerized cyclic butylene terephthalate with carbon nanotubes for use in composites. *Composites Part A* **39**, 1756–1761 (2008).
 74. Baets, J., Godara, A., Devaux, J. & Verpoest, I. Toughening of isothermally polymerized cyclic butylene terephthalate for use in composites. *Polym. Degrad. Stab.* **95**, 346–352 (2010).
 75. Mäder, E., Gao, S.-L., Plonka, R. & Wang, J. Investigation on adhesion, interphases, and failure behaviour of cyclic butylene terephthalate (CBT)/glass fiber composites. *Compos. Sci. Technol.* **67**, 3140–3150 (2007).
 76. Wu, C.-M. & Jiang, C.-W. Crystallization and morphology of polymerized cyclic butylene terephthalate. *J. Polym. Sci. Part B Polym. Phys.* **48**, 1127–1134 (2010).
 77. Wu, C.-M. & Huang, C.-W. Melting and crystallization behavior of copolymer from cyclic butylene terephthalate and polycaprolactone. *Polym. Eng. Sci.* **51**, 1004–1013 (2011).
 78. Verrey, J., Wakeman, M. D., Michaud, V. & Månson, J.-A. E. Manufacturing cost comparison of thermoplastic and thermoset RTM for an automotive floor pan. *Composites Part A* **37**, 9–22 (2006).
 79. Cyclics Corporation. Material Safety Data Sheet - CBT160 resin. 1–5 (2007).
 80. Zhang, J. *et al.* Correlation between polymerization of cyclic butylene terephthalate (CBT) and crystallization of polymerized CBT. *Chinese J. Polym. Sci.* **33**, 1104–1113 (2015).
 81. Noh, Y. J. *et al.* Ultra-high dispersion of graphene in polymer composite via solvent free fabrication and functionalization. *Sci. Rep.* **5**, 9141 (2015).
 82. Samsudin, S. A. The Thermal Behaviour and Isothermal Crystallisation of Cyclic Poly(Butylene Terephthalate) and Its Blends. (University of Birmingham, 2010).
 83. Balogh, G., Hajba, S., Karger-Kocsis, J. & Czigány, T. Preparation and characterization of in situ polymerized cyclic butylene terephthalate/graphene nanocomposites. *J. Mater. Sci.* **48**, 2530–2535 (2012).
 84. Ben-Haida, A., Conzatti, L., Hodge, P., Manzini, B. & Stagnaro, P. An Introduction to Entropically-driven Ring-opening Polymerizations. *Macromol. Symp.* **297**, 6–17 (2010).
 85. Repin, H. & Papanikolaou, E. Synthesis and Properties of Cyclic Di(ethylene Terephthalate). *J. Polym. Sci. Part A-1 Polym. Chem.* **7**, 3426–3427 (1969).
 86. Shiono, S. Separation and identification of poly(ethylene terephthalate) oligomers by gel permeation chromatography. *J. Polym. Sci. Polym. Chem. Ed.* **17**, 4123–4127 (1979).
 87. Wick, G. & Zeitler, H. Cyclische Oligomere in Polyestern aus Diolen und aromatischen Dicarbonsäuren. *Die Angew. Makromol. Chemie* **112**, 59–94 (1983).
 88. Burzin, K., Holtrup, W. & Feinauer, R. Cyclische Ester in Poly(alkylterephthalaten).

-
- Die Angew. Makromol. Chemie* **74**, 93–103 (1978).
89. Jacobson, H. & Stockmayer, W. H. Intramolecular Reaction in Polycondensations. I. The Theory of Linear Systems. *J. Chem. Phys.* **18**, 1600 (1950).
 90. Jacobson, H., Beckmann, C. O. & Stockmayer, W. H. Intramolecular Reaction in Polycondensations. II. Ring-Chain Equilibrium in Polydecamethylene Adipate. *J. Chem. Phys.* **18**, 1607 (1950).
 91. Hubbard, P. & Brittain, W. Ring-size distribution in the depolymerization of poly (butylene terephthalate). *Macromolecules* **9297**, 1518–1522 (1998).
 92. Kricheldorf, H. R. Cyclic polymers: Synthetic strategies and physical properties. *J. Polym. Sci. Part A: Polym. Chem.* **48**, 251–284 (2010).
 93. Ruggli, P. Über einen Ring mit dreifacher Bindung. *Justus Liebig's Ann. der Chemie* **392**, 92–100 (1912).
 94. Ziegler, K. & Aurnhammer, R. Über vielgliedrige Ringsysteme: V. Die Bildungstendenz cyclischer Verbindungen. *Justus Liebig's Ann. der Chemie* **513**, 43–64 (1934).
 95. Ziegler, K. Über Ringschluß-Reaktionen. *Berichte der Dtsch. Chem. Gesellschaft (A B Ser.)* **67**, A139–A149 (1934).
 96. Stepto, R. F. T. & Waywell, D. R. A Study of Intramolecular Reaction during Linear Polyurethane Formation. *Die Makromol. Chemie* **152**, 263–275 (1972).
 97. Stanford, J. L., Stepto, R. F. T. & Waywell, D. R. Rate Theory of Irreversible Linear Random Polymerisation. Part 2. Application to Intramolecular Reaction in A-A + B-B Type Polymerisations. *J. Chem. Soc. Faraday Trans. 1 Phys. Chem. Condens. Phases* **71**, 1308 (1975).
 98. Gordon, M. & Temple, W. B. Ring-Chain Competition Kinetics in Linear Polymers. *Die Makromol. Chemie* **152**, 277–289 (1972).
 99. Gordon, M. & Temple, W. B. The Graph-Like State of Molecules. III. Ring-Chain Competition Kinetics in Linear Polymerisation Reactions. *Die Makromol. Chemie* **160**, 263–276 (1972).
 100. Kim, Y. H., Calabrese, J. & McEwen, C. CaCl₃- or Ca₂Cl₄ Complexing Cyclic Aromatic Amide. Template Effect on Cyclization. *J. Am. Chem. Soc.* **118**, 1545–1546 (1996).
 101. Memeger, W., Campbell, G. C. & Davidson, F. Poly(aminophosphazene)s and Protophosphatranes Mimic Classical Strong Anionic Base Catalysts in the Anionic Ring-Opening Polymerization of Lactams. *Macromolecules* **29**, 6475–6480 (1996).
 102. Peng, P. & Hodge, P. Cyclic oligo(undecanamide)s (nylon 11 s) and cyclic alternating oligo(undecanamide-undecanoate)s: their synthesis using high dilution conditions and their analysis. *Polymer* **39**, 981–990 (1998).
 103. Ben-Haida, A., Hodge, P. & Colquhoun, H. M. Ring-Chain Interconversion in High-Performance Polymer Systems. 3. Cyclodepolymerization of Poly(m-phenylene isophthalamide) (Nomex) and Entropically Driven Ring-Opening Polymerization of the Macrocylic Oligomers so Produced. *Macromolecules* **38**, 722–729 (2005).
 104. Winnacker, M., Neumeier, M., Zhang, X., Papadakis, C. M. & Rieger, B. Sustainable Chiral Polyamides with High Melting Temperature via Enhanced Anionic Polymerization of a Menthone-Derived Lactam. *Makromol. Rapid Commun.* **37**, 851–857 (2016).
 105. Fürstner, A. Olefin Metathesis and Beyond. *Angew. Chemie* **39**, 3012–3043 (2000).
-

-
106. Gautrot, J. E. & Zhu, X. X. Main-Chain Bile Acid Based Degradable Elastomers Synthesized by Entropy-Driven Ring-Opening Metathesis Polymerization. *Angew. Chemie Int. Ed.* **45**, 6872–6874 (2006).
 107. Tastard, C. Y., Hodge, P., Ben-Haida, A. & Dobinson, M. Entropically driven ring-opening metathesis polymerization (ED-ROMP) of macrocyclic olefin-containing oligoamides. *React. Funct. Polym.* **66**, 93–107 (2006).
 108. Kamau, S. D., Hodge, P., Hall, A. J., Dad, S. & Ben-Haida, A. Cyclo-depolymerization of olefin-containing polymers to give macrocyclic oligomers by metathesis and the entropically-driven ROMP of the olefin-containing macrocyclic esters. *Polymer* **48**, 6808–6822 (2007).
 109. Kang, S. *et al.* Polypseudorotaxanes via Ring-Opening Metathesis Polymerizations of [2]Catenanes. *J. Am. Chem. Soc.* **130**, 15246–15247 (2008).
 110. Goldring, W. P. D., Hodder, A. & Weiler, L. Synthesis of macrocyclic lactams and lactones via ring-closing olefin metathesis. *Tetrahedron Lett.* **39**, 4955–4958 (1998).
 111. Choon Woo Lee & Grubbs, R. H. Formation of macrocycles via ring-closing olefin metathesis. *J. Org. Chem.* **66**, 7155–7158 (2001).
 112. Litinas, K. E. & Salteris, B. E. Unsaturated macrocyclic lactone synthesis via catalytic ring-closing metathesis. *J. Chem. Soc. Perkin Trans. 1* **6**, 2869–2872 (1997).
 113. Grubbs, R. H. *Handbook of Metathesis*. (Wiley-VCH Verlag GmbH, 2003). doi:10.1002/9783527619481
 114. Chen, M. & Gibson, H. W. Communications to the Editor. Large-Sized Macrocyclic Monomeric Precursors of Poly(ether ether ketone): Synthesis and Polymerization. *Macromolecules* **29**, 5502–5504 (1996).
 115. Teasley, M. F. & Hsiao, B. S. Synthesis and Characterization of Poly(oxy-1,3-phenylenecarbonyl-1,4-phenylene) and Related Polymers. *Macromolecules* **29**, 6432–6441 (1996).
 116. Bryant, J. J. L. & Semlyen, J. A. Cyclic polyesters: 6. Preparation and characterization of two series of cyclic oligomers from solution ring-chain reactions of poly(ethylene terephthalate). *Polymer* **38**, 2475–2482 (1997).
 117. Wang, Y.-F., Paventi, M. & Hay, A. S. Novel macrocyclic aryl ether oligomers containing a diphenylacetylene moiety: synthesis, characterization and ring-opening polymerization. *Polymer* **38**, 469–482 (1997).
 118. Teasley, M. F., Wu, D. Q. & Harlow, R. L. Synthesis, Characterization, and Ring-Opening Polymerization of the Cyclic Oligomers of Poly(Oxy-1,3-phenylenecarbonyl-1,4-phenylene). *Macromolecules* **31**, 2064–2074 (1998).
 119. Baxter, I. *et al.* Sulfone-Linked Paracyclophanes via Macrocyclic Aromatic Thioethers: Synthetic and Structural Investigations. *Chem. Eur. J.* **6**, 4285–96 (2000).
 120. Kobayashi, U. Enzymatic Ring-Opening Polymerisation of Lactones by Lipase Catalyst: *Bull. Chem. Soc. Japan* **68**, 56–61 (1995).
 121. Commercial Information of IQ Tec Germany. Available at: www.iq-holding.com/. (Accessed: 31st July 2016)
 122. Ross, S. D., Coburn, E. R., Leach, W. A. & Robinson, W. B. Isolation of a Cycle Trimer from Polyethylene Terephthalate Film. *J. Polym. Sci.* **13**, 406–407 (1945).
 123. Evans, T. L., Brunelle, D. J., Bradt, J. E., Pearce, E. J. & Wilson, P. R. Polymerization of Macrocyclic Poly(alkylene dicarboxylate) Oligomers. 1–7 (1995).
-

-
124. Papadopoulou, C. P. Blends of an amorphous copolyester with poly(butylene terephthalat). **33**, 191–197 (1997).
 125. Lee, S.-W., Huh, W., Hong, Y.-S. & Lee, K.-M. Synthesis and Thermal Properties of Poly(cyclohexylene dimethylene terephthalate-co-butylene terephthalate). *Korea Polym. J.* **8**, 261–267 (2000).
 126. Wan, X.-H. *et al.* Synthesis, characterization, and ring opening polymerization of poly(1,4-cyclohexylenedimethylene terephthalate) cyclic oligomers. *J. Polym. Sci. Part A: Polym. Chem.* **38**, 1828–1833 (2000).
 127. Finelli, L., Siracusa, V., Lotti, N., Gazzano, M. & Munari, A. Synthesis and thermal properties of randomly branched poly(butylene isophthalate) containing sodium sulfonate groups. *J. Appl. Polym. Sci.* **99**, 1374–1379 (2006).
 128. Conzatti, L., Alessi, M., Stagnaro, P. & Hodge, P. Syntheses of random PET-co-PTTs and some related copolyesters by entropically-driven ring-opening polymerizations and by melt blending: Thermal properties and crystallinity. *J. Polym. Sci. Part A: Polym. Chem.* **49**, 995–1005 (2011).
 129. Lurgi Zimmer GmbH. PBT Polybutylene Terephthalate Process. *Brochure* Available at: <http://lurgi.info/website/Broschueren.25.0.html>. (Accessed: 25th April 2015)
 130. Spanagel, E. W. & Carothers, W. H. Macrocyclic Esters. *J. Am. Chem. Soc.* **57**, 929–934 (1935).
 131. Carothers, W. H. & Spanagel, E. W. Preparation of Macrocyclic Lactones by Depolymerization. *J. Am. Chem. Soc.* **58**, 654–656 (1936).
 132. Carothers, W. H. & Van Natta, F. J. Studies of Polymerization and Ring Formation. XVIII. Polyesters from ω -Hydroxydecanoic Acid. *J. Am. Chem. Soc.* **55**, 4714–4719 (1933).
 133. Van Natta, F. J., Hill, J. W. & Carothers, W. H. Studies of Polymerization and Ring Formation. XXIII. ϵ -Caprolactone and its Polymers. *J. Am. Chem. Soc.* **1772**, 5–7 (1934).
 134. Berr, C. E. Isolation of a Cyclic Dimer during Synthesis of Polyethylene Isophthalate. *J. Polym. Sci.* **15**, 591–592 (1955).
 135. Ehrhart, W. A. Synthesis of macrocyclic o-phthalate esters from the corresponding polyesters. *J. Org. Chem.* **33**, 2930–2933 (1968).
 136. Burzin, K. & Frenzel, P.-J. Massenspektrometrischer Nachweis cyclischer Oligomerer in Poly(butylenterephthalat) und Isolierung des cyclischen Di(butylenterephthalats). *Die Angew. Makromol. Chemie* **71**, 61–66 (1978).
 137. Nagahata, R. *et al.* Solid-Phase Thermal Polymerization of Macrocyclic Ethylene Terephthalate Dimer Using Various Transesterification Catalysts. *J. Polym. Sci. Part A Polym. Chem.* **38**, 3360–3368 (2000).
 138. Brunelle, D. J. & Takekoshi, T. Process for preparing macrocyclic polyester oligomers (US 5407984). 1–6 (1995).
 139. Brunelle, D. J., Kailasam, G., Serth-Guzzo, J. A. & Wilson, P. R. Process for Depolymerizing Polyesters. 1–5 (1997).
 140. Cooper, D. R. & Semlyen, J. a. Equilibrium ring concentrations and the statistical conformations of polymer chains: Part 11. Cyclics in poly(ethylene terephthalate). *Polymer* **14**, 185–192 (1973).
 141. González-Vidal, N., Martínez de Ilarduya, A. & Muñoz-Guerra, S. Poly(hexamethylene
-

- terephthalate-co-caprolactone) copolymers: Influence of cycle size on ring-opening polymerization. *Eur. Polym. J.* **46**, 792–803 (2010).
142. Brunelle, D. J., Serth-Guzzo, J. A., Kailasom, G. & Wilson, P. R. Verfahren zur Depolymerisation von Polyestern (DE 697 20 579 T2). 1–15 (1997).
143. Bryant, J. J. L. & Semlyen, J. A. Cyclic polyesters: 7. Preparation and characterization of cyclic oligomers from solution ring-chain reactions of poly (butylene terephthalate). *Polymer* **38**, 4531–4537 (1997).
144. Hall, A., Hodge, P., McGrail, C. S. & Rickerby, J. Synthesis of a series of cyclic oligo(alkylidene isophthalate)s by cyclo-depolymerisation. *Polymer* **41**, 1239–1249 (2000).
145. Hodge, P., Yang, Z., Ben-Haida, A. & McGrail, C. S. Cyclo-depolymerisation of poly(ethylene naphthalene-2,6-dicarboxylate) and ring-opening polymerisations of the cyclic oligomers obtained. *J. Mater. Chem.* **10**, 1533–1537 (2000).
146. Montero, G., Hinks, D. & Hooker, J. Reducing problems of cyclic trimer deposits in supercritical carbon dioxide polyester dyeing machinery. *J. Supercrit. Fluids* **26**, 47–54 (2003).
147. Kawahara, Y. *et al.* Oligomer deposition on the surface of PET fiber in supercritical carbon dioxide fluid. *Macromol. Mater. Eng.* **291**, 11–15 (2006).
148. Weijers, C., de Rooij, R. D., Agarwal, U. S., de Wit, G. & Lemstra, P. J. Supercritical fluid extraction of cyclic oligomers from depolymerizing PBT. *J. Appl. Polym. Sci.* **101**, 4487–4492 (2006).
149. Meraskentis, E. & Zahn, H. Synthesis of cyclic tris(ethylene terephthalate). *J. Polym. Sci. Part A-1 Polym. Chem.* **4**, 1890–1891 (1966).
150. Meraskentis, E. & Zahn, H. Darstellung cyclischer Ester aus Terephthalsäure und Diolen. *Chem. Ber.* **103**, 3034–3040 (1970).
151. Zahn, H. & Repin, J. F. Synthese einer homologen Reihe von cyclischen Äthylenterephthalaten. *Chem. Ber.* **103**, 3041–3049 (1970).
152. Nagahata, R., Sugiyama, J., Nakao, Y., Asai, M. & Takeuchi, K. Selective synthesis of macrocyclic ethylene isophthalate dimer. *Macromolecules* **36**, 2582–2583 (2003).
153. Brunelle, D. J. Cyclic Oligomers of Polycarbonates and Polyesters. in *Cyclic Polymers* (ed. Semlyen, J. A.) 185–228 (Springer, 2000).
154. Guggenheim, T. L., McCormick, S. J. & Colley, A. M. Method for preparing cyclic polyarylate oligomers (EP 0 402 670). (1990).
155. Brunelle, D. J. & Shannon, T. G. Preparation and polymerization of bisphenol A cyclic oligomeric carbonates. *Macromolecules* **24**, 3035–3044 (1991).
156. Brunelle, D. J. & Bradt, J. E. Method for preparation of macrocyclic Poly(alkylene dicarboxylate) oligomers (US 5,214,158). 1–5 (1993).
157. Brunelle, D. J. & McDermott, J. B. Method for preparation of macrocyclic Poly(alkylene dicarboxylate) oligomers from Bis(hydroxyalkyl) dicarboxylates (US 5,231,161). 1–5 (1993).
158. Hodge, P. & Peng, P. Polymer-supported syntheses of some cyclic oligoamides and some cyclic alternating oligo(amide-ester)s. *Polymer* **40**, 1871–1879 (1999).
159. Karger-Kocsis, J., Shang, P. P., Mohd Ishak, Z. A. & Rösch, M. Melting and crystallization of in-situ polymerized cyclic butylene terephthalates with and without organoclay: a modulated DSC study. *Express Polym. Lett.* **1**, 60–68 (2007).

-
160. Wu, F. & Yang, G. Poly(butylene terephthalate)-functionalized MWNTs by in situ ring-opening polymerization of cyclic butylene terephthalate oligomers. *Polym. Adv. Technol.* **22**, 1466–1470 (2011).
 161. Balogh, G. Development of Cyclic Butylene Terephthalate Matrix Composites. *Omikk.Bme.Hu* (Budapest University of Technology and Economics, 2012).
 162. Steinke, J. & Wald, H. Isolation of cyclic oligomers of poly(butylene glycolterephthalate). *Melliand Textil. Int.* **58**, 494–5 (1977).
 163. Müller, F.-J. Über cyclische Oligomere des Polybutylenterephthalats und Untersuchungen an der technischen Faser. (TH Aachen, 1978).
 164. Phelps, P. D. Specific Modification in Macrocyclic Polyester Oligomers and Compositions prepared thereby (US 6,713,601 B2). 1–15 (2004). doi:10.1021/n10602701.
 165. Tripathy, A. R., MacKnight, W. J. & Kukureka, S. N. In-Situ Copolymerization of Cyclic Poly(butylene terephthalate) Oligomers and ϵ -Caprolactone. *Macromolecules* **37**, 6793–6800 (2004).
 166. González-Vidal, N., Martínez de Ilarduya, A., Herrera, V. & Muñoz-Guerra, S. Poly(hexamethylene terephthalate-co-caprolactone) Copolyesters Obtained by Ring-Opening Polymerization. *Macromolecules* **41**, 4136–4146 (2008).
 167. González-Vidal, N., Martínez de Ilarduya, A. & Muñoz-Guerra, S. Poly(ethylene-co-1,4-cyclohexylenedimethylene terephthalate) copolyesters obtained by ring opening polymerization. *J. Polym. Sci. Part A Polym. Chem.* **47**, 5954–5966 (2009).
 168. Pepels, M. P. F., van der Sanden, F., Gubbels, E. & Duchateau, R. Catalytic Ring-Opening (Co)polymerization of Semiaromatic and Aliphatic (Macro)lactones. *Macromolecules* **49**, 4441–4451 (2016).
 169. Carothers, W. H. Polymers and polyfunctionality. *Trans. Faraday Soc.* **32**, 39–49 (1936).
 170. Banach, T. E. & Colonna, M. New catalysts for poly(butylene terephthalate) synthesis. 2. Kinetic comparison using model compounds. *Polymer* **42**, 7517–7522 (2001).
 171. Kricheldorf, H., Mang, T. & Jonté, J. M. Polylactones. 1. Copolymerizations of glycolide and ϵ -caprolactone. *Macromolecules* **17**, 2173–2181 (1984).
 172. Yu, Y. *et al.* Lipase/esterase-catalyzed synthesis of aliphatic polyesters via polycondensation: A review. *Process Biochem.* **47**, 1027–1036 (2012).
 173. Yang, Y. *et al.* Two-Step Biocatalytic Route to Biobased Functional Polyesters from ω -Carboxy Fatty Acids and Diols. *Biomacromolecules* **11**, 259–268 (2010).
 174. Vilela, C. *et al.* The quest for sustainable polyesters – insights into the future. *Polym. Chem.* **5**, 3119–3141 (2014).
 175. Gross, R. A., Ganesh, M. & Lu, W. Enzyme-catalysis breathes new life into polyester condensation polymerizations. *Trends Biotechnol.* **28**, 435–443 (2010).
 176. Jiang, Y., Woortman, A. J. J., Alberda van Ekenstein, G. O. R. & Loos, K. Environmentally benign synthesis of saturated and unsaturated aliphatic polyesters via enzymatic polymerization of biobased monomers derived from renewable resources. *Polym. Chem.* **6**, 5451–5463 (2015).
 177. Scherkus, C. *et al.* A Fed-Batch Synthetic Strategy for a Three-Step Enzymatic Synthesis of Poly- ϵ -caprolactone. *ChemCatChem* **8**, 3446–3452 (2016).
 178. Wedde, S. *et al.* An alternative approach towards poly- ϵ -caprolactone through a
-

- chemoenzymatic synthesis: Combined hydrogenation, bio-oxidations and polymerization without the isolation of intermediates. *Green Chem.* **19**, 1286–1290 (2017).
179. Varma, I. K., Albertsson, A. C., Rajkhowa, R. & Srivastava, R. K. Enzyme catalyzed synthesis of polyesters. *Prog. Polym. Sci.* **30**, 949–981 (2005).
180. Kobayashi, S. Enzymatic ring-opening polymerization and polycondensation for the green synthesis of polyesters. *Polym. Adv. Technol.* **26**, 677–686 (2015).
181. Gustini, L. *et al.* Green and selective polycondensation methods toward linear sorbitol-based polyesters: enzymatic versus organic and metal-based catalysis. *ChemSusChem* **9**, 2250–2260 (2016).
182. Pedersen, S. Industrial aspects of immobilized glucose isomerase. in *Industrial applications of immobilized biocatalysts* (eds. Tanaka, A., Tosa, T. & Kobayashi, T.) (Dekker, 1993).
183. Bommarius, A. S. *et al.* Synthesis and use of enantiomerically pure tert-leucine. *Tetrahedron: Asymmetry* **6**, 2851–2888 (1995).
184. Hilterhaus, L., Thum, O. & Liese, A. Reactor concept for lipase-catalyzed solvent-free conversion of highly viscous reactants forming two-phase systems. *Org. Process Res. Dev.* **12**, 618–625 (2008).
185. Thum, O. Enzymatic Production of Care Specialties Based on Fatty Acid Esters. *Tenside Surfactants Deterg.* **41**, 287–290 (2004).
186. Liese, A. & Hilterhaus, L. Evaluation of immobilized enzymes for industrial applications. *Chem. Soc. Rev.* **42**, 6236 (2013).
187. Poojari, Y., Beemat, J. S. & Clarson, S. J. Enzymatic synthesis of poly(ϵ -caprolactone): thermal properties, recovery, and reuse of lipase B from *Candida antarctica* immobilized on macroporous acrylic resin particles. *Polym. Bull.* **70**, 1543–1552 (2013).
188. Szmercsányi, I. V., Maros, L. K. & Zahran, A. A. Investigations of the kinetics of maleate–fumarate isomerization during the polyesterification of maleic anhydride with different glycols. *J. Appl. Polym. Sci.* **10**, 513–522 (1966).
189. Ordelt, Z., Novák, V. & Krátký, B. Über die Umkehrbarkeit der Diolenaddition an die olefinische Doppelbindung der Äthylen-1,2-dicarbonensäuren bei der Polykondensation in der Schmelze. *Collect. Czechoslov. Chem. Commun.* **33**, 405–415 (1968).
190. Hollmann, F., Gumulya, Y., Tölle, C., Liese, A. & Thum, O. Evaluation of the laccase from *Myceliophthora thermophila* as industrial biocatalyst for polymerization reactions. *Macromolecules* **41**, 8520–8524 (2008).
191. Gross, R. A., Kalra, B. & Kumar, A. Polyester and polycarbonate synthesis by in vitro enzyme catalysis. *Appl. Microbiol. Biotechnol.* **55**, 655–660 (2001).
192. Yu, F., Saha, P., Suh, P. W. & Kim, J. K. Green polyurethane from dimer acid based polyether polyols: Synthesis and characterization. *J. Appl. Polym. Sci.* **132**, 41410 (1–9) (2015).
193. Ferrario, V., Pellis, A., Cespuogli, M., Guebitz, G. & Gardossi, L. Nature Inspired Solutions for Polymers: Will Cutinase Enzymes Make Polyesters and Polyamides Greener? *Catalysts* **6**, 205 (2016).
194. Kobayashi, S. & Makino, A. Enzymatic polymer synthesis: an opportunity for green polymer chemistry. *Chem. Rev.* **109**, 5288–5353 (2009).

-
195. Nguyen, H. D., Löf, D., Hvilsted, S. & Daugaard, A. E. Highly branched bio-based unsaturated polyesters by enzymatic polymerization. *Polymers (Basel)*. **8**, 1–12 (2016).
 196. Kim, D. *et al.* The studies of physical properties of dimeric fatty acid-modified thiodiphenyl epoxy resins. *Polym. Bull.* **74**, 4595–4605 (2017).
 197. Liu, H., Xu, Y., Zheng, Z. & Liu, D. 1,3-Propanediol and its copolymers: Research, development and industrialization. *Biotechnol. J.* **5**, 1137–1148 (2010).
 198. Biebl, H., Menzel, K., Zeng, A. P. & Deckwer, W. D. Microbial production of 1,3-propanediol. *Appl. Microbiol. Biotechnol.* **52**, 289–97 (1999).
 199. Katarzyna Leja, Czaczyk, K. & Myszka, K. The use of microorganisms in 1,3-Propanediol production. *African J. Microbiol. Res.* **5**, 4652–4658 (2011).
 200. Hablot, E., Zheng, D., Bouquey, M. & Avérous, L. Polyurethanes based on castor oil: Kinetics, chemical, mechanical and thermal properties. *Macromol. Mater. Eng.* **293**, 922–929 (2008).
 201. Bueno-Ferrer, C. *et al.* Relationship between morphology, properties and degradation parameters of novative biobased thermoplastic polyurethanes obtained from dimer fatty acids. *Polym. Degrad. Stab.* **97**, 1964–1969 (2012).
 202. Bueno-Ferrer, C. *et al.* Structure and Morphology of New Bio-Based Thermoplastic Polyurethanes Obtained From Dimeric Fatty Acids. *Macromol. Mater. Eng.* **297**, 777–784 (2012).
 203. Reulier, M. & Avérous, L. Elaboration, morphology and properties of renewable thermoplastics blends, based on polyamide and polyurethane synthesized from dimer fatty acids. *Eur. Polym. J.* **67**, 418–427 (2015).
 204. Reulier, M. & Avérous, L. Corrigendum to ‘Elaboration, morphology and properties of renewable thermoplastics blends, based on polyamide and polyurethane synthesized from dimer fatty acids’. *Eur. Polym. J.* **67**, 418–427 (2015).
 205. Poussard, L., Lazko, J., Mariage, J., Raquez, J.-M. & Dubois, P. Biobased waterborne polyurethanes for coating applications: How fully biobased polyols may improve the coating properties. *Prog. Org. Coatings* **97**, 175–183 (2016).
 206. Petrović, Z. S., Milić, J., Zhang, F. & Ilavsky, J. Fast-responding bio-based shape memory thermoplastic polyurethanes. *Polymer* **121**, 26–37 (2017).
 207. *ASTM D3418-15, Standard Test Method for Transition Temperatures and Enthalpies of Fusion and Crystallization of Polymers by Differential Scanning Calorimetry.* ASTM International (2015). doi:10.1520/D3418-15
 208. Widmann, G., Riesen, R., Schawe, J., Schubnell, M. & Wagner, M. *Thermal Analysis in Practice - Collected Applications.* (Mettler-Toledo, 2009).
 209. Chiou, J. S., Barlow, J. W. & Paul, D. R. Polymer crystallization induced by sorption of CO₂ gas. *J. Appl. Polym. Sci.* **30**, 3911–3924 (1985).
 210. Beckman, E. & Porter, R. S. Crystallization of bisphenol a polycarbonate induced by supercritical carbon dioxide. *J. Polym. Sci. Part B Polym. Phys.* **25**, 1511–1517 (1987).
 211. Lambert, S. M. & Paulaitis, M. E. Crystallization of poly(ethylene terephthalate) induced by carbon dioxide sorption at elevated pressures. *J. Supercrit. Fluids* **4**, 15–23 (1991).
 212. Shieh, Y. *et al.* Interaction of supercritical carbon dioxide with polymers. I. Crystalline polymers. *J. Appl. Polym. Sci.* **59**, 695–705 (1996).
-

-
213. Zhong, Z., Zheng, S. & Mi, Y. High-pressure DSC study of thermal transitions of a poly(ethylene terephthalate)/carbon dioxide system. *Polymer* **40**, 3829–3834 (1999).
214. Brantley, N. H., Kazarian, S. G. & Eckert, C. A. In situ FTIR measurement of carbon dioxide sorption into poly(ethylene terephthalate) at elevated pressures. *J. Appl. Polym. Sci.* **77**, 764–775 (2000).
215. Shieh, Y.-T. & Lin, Y.-S. Glass transition and cold crystallization in carbon dioxide treated poly(ethylene terephthalate). *J. Appl. Polym. Sci.* **113**, 3345–3353 (2009).
216. de Gooijer, J. M., Scheltus, M., Jansen, M. A. G. & Koning, C. E. Carboxylic acid end group modification of poly(butylene terephthalate) in supercritical fluids. *Polymer* **44**, 2201–2211 (2003).
217. Sabirzyanov, A. N., Il'in, A. P., Akhunov, A. R. & Gumerov, F. M. Solubility of water in supercritical carbon dioxide. *High Temp.* **40**, 203–206 (2002).
218. Kitano, Y., Ishitani, A. & Ashida, T. Crystal Structure of Cyclic Dimer of Poly(butylene terephthalate). *Polym. J.* **23**, 949–954 (1991).
219. Suehiro, K., Shigaki, T. & Kuramori, M. Crystal Structure of Cyclic Di(ethylene terephthalate). *Polym. J.* **27**, 840–845 (1995).
220. Nagahata, R. *et al.* Thermal polymerization of uniform macrocyclic ethylene terephthalate dimer. *Polym. Commun.* **42**, 1275–1279 (2001).
221. Chatani, Y., Suehiro, K., Ôkita, Y., Tadokoro, H. & Chujo, K. Structural properties of polyesters. I. Crystal Structure of Polyglycolide. *Die Makromol. Chemie* **113**, 215–229 (1968).
222. Chatani, Y., Okita, Y., Tadokoro, H. & Yamashita, Y. Structural Studies of Polyesters. III. Crystal Structure of Poly- ϵ -caprolactone. *Polym. J.* **1**, 555–562 (1970).
223. Ueda, A. S., Chatani, Y. & Tadokoro, H. Structural Studies of Polyesters. IV. Molecular and Crystal Structures of Poly(ethylene succinate) and Poly(ethylene oxalate). *Polym. J.* **2**, 387–397 (1971).
224. Yokouchi, M., Chatani, Y., Tadokoro, H., Teranishi, K. & Tani, H. Structural studies of polyesters: 5. Molecular and crystal structures of optically active and racemic poly (β -hydroxybutyrate). *Polymer* **14**, 267–272 (1973).
225. Yokouchi, M. *et al.* Structures of Two Crystalline Forms of Poly(butylene terephthalate) and Reversible Transition between Them by Mechanical Deformation. *Macromolecules* **9**, 266–273 (1976).
226. Minke, R. & Blackwell, J. Polymorphic Structures of Poly(tetramethylene Adipate). *J. Macromol. Sci. Part B* **16**, 407–417 (1979).
227. Minke, R. & Blackwell, J. Single crystals of poly(tetramethylene adipate). *J. Macromol. Sci. Part B* **18**, 233–255 (1980).
228. Aylwin, P. A. & Boyd, R. H. Aliphatic polyesters as models for relaxation processes in crystalline polymers: 1. Characterization. *Polymer* **25**, 323–329 (1984).
229. Aleman, C. & Puiggali, J. Effect of the Folding of Methylene Units in the Conformational Preferences of Small Diesters. *J. Org. Chem.* **62**, 3076–3080 (1997).
230. Díaz, A., Katsarava, R. & Puiggali, J. Synthesis, Properties and Applications of Biodegradable Polymers Derived from Diols and Dicarboxylic Acids: From Polyesters to Poly(ester amide)s. *Int. J. Mol. Sci.* **15**, 7064–7123 (2014).
231. Neuer, B. Einfluss verschiedener Alkohole auf die ringöffnende Polymerisation von zyklischem 1,4-Butylenadipat. (Universität Hamburg, 2012).
-

-
232. Gilbert, M. & Hybart, F. J. Effect of chemical structure on crystallization rates and melting of polymers: Part 1. Aromatic polyesters. *Polymer* **13**, 327–332 (1972).
233. Gilbert, M. & Hybart, F. J. Effect of chemical structure on crystallization rates and melting of polymers: 2. Aliphatic polyesters. *Polymer* **15**, 407–412 (1974).
234. Albanese, M., Boyenval, J., Marchese, P., Sullalti, S. & Celli, A. The aliphatic counterpart of PET, PPT and PBT aromatic polyesters: effect of the molecular structure on thermo-mechanical properties. *AIMS Mol. Sci.* **3**, 32–51 (2016).
235. Dangseeyun, N., Srimoan, P., Supaphol, P. & Nithitanakul, M. Isothermal melt-crystallization and melting behavior for three linear aromatic polyesters. *Thermochim. Acta* **409**, 63–77 (2004).
236. Berti, C. *et al.* The effect of aliphatic chain length on thermal properties of poly(alkylene dicarboxylate)s. *e-Polymers* **7**, 1–18 (2007).
237. Youk, J. H., Ha, W. S., Jo, W. H. & Park, C. R. Effect of chemical structure on crystallization behavior of poly(phenylene alkylene dicarboxylate) (PPAD). *J. Appl. Polym. Sci.* **66**, 1575–1582 (1997).
238. Chisholm, B. J. & Zimmer, J. G. Isothermal crystallization kinetics of commercially important polyalkylene terephthalates. *J. Appl. Polym. Sci.* **76**, 1296–1307 (2000).
239. Prigogine, I. & Defay, R. *Chemical Thermodynamics*. (Longmans Green, 1954).
240. Zorba, T., Chrissafis, K., Paraskevopoulos, K. M. & Bikiaris, D. N. Synthesis, characterization and thermal degradation mechanism of three poly(alkylene adipate)s: Comparative study. *Polym. Degrad. Stab.* **92**, 222–230 (2007).
241. Lee, S. W. *et al.* Synthesis and non-isothermal crystallization behaviors of poly(ethylene isophthalate-co-terephthalate)s. *Polymer* **40**, 7137–7146 (1999).
242. Wu, T.-M., Chang, C.-C. & Yu, T. L. Crystallization of poly(ethylene terephthalate-co-isophthalate). *J. Polym. Sci. Part B Polym. Phys.* **38**, 2515–2524 (2000).
243. Menczel, J. D. & Prime, R. B. Differential Scanning Calorimetry (DSC). in *Thermal Analysis of Polymers* **1**, 7–239 (Wiley, 2009).
244. Finelli, L., Lotti, N. & Munari, A. Crystallization kinetics and melting behavior of poly(butylene isophthalate/terephthalate) random copolyesters. *Eur. Polym. J.* **37**, 2039–2046 (2001).
245. Wunderlich, B. Study of the change in specific heat of monomeric and polymeric glasses during the glass transition. *J. Phys. Chem.* **64**, 1052–1056 (1960).
246. Jin, Y. & Wunderlich, B. Single run heat capacity measurements. *J. Therm. Anal.* **36**, 765–789 (1990).
247. Jin, Y. & Wunderlich, B. Single run heat capacity measurements - II. Experiments at subambient temperature. *J. Therm. Anal.* **36**, 1519–1543 (1990).
248. Hunsen, M., Abul, A., Xie, W. & Gross, R. Humicola insolens Cutinase-Catalyzed Lactone Ring-Opening Polymerizations: Kinetic and Mechanistic Studies. *Biomacromolecules* **9**, 518–522 (2008).
249. Berkane, C., Mezoul, G., Lalot, T., Brigodiot, M. & Maréchal, E. Lipase-Catalyzed Polyester Synthesis in Organic Medium. Study of Ring-Chain Equilibrium. *Macromolecules* **30**, 7729–7734 (1997).
250. Wallace, J. S. & Morrow, C. J. Biocatalytic synthesis of polymers. II. Preparation of [AA–BB]_x polyesters by porcine pancreatic lipase catalyzed transesterification in anhydrous, low polarity organic solvents. *J. Polym. Sci. Part A: Polym. Chem.* **27**,
-

-
- 3271–3284 (1989).
251. Linko, Y.-Y., Wang, Z. & Seppälä, J. Lipase-catalyzed linear aliphatic polyester synthesis in organic solvent. *Enzyme Microb. Technol.* **17**, 506–511 (1995).
252. Kricheldorf, H. R. The role of ring-ring equilibria in thermodynamically controlled polycondensations. *Macromol. Symp.* **199**, 15–22 (2003).
253. Kozłowska, A. & Ukielski, R. New type of thermoplastic multiblock elastomers - Poly(ester-block-amide)s - Based on oligoamide 12 and oligoester prepared from dimerized fatty acid. *Eur. Polym. J.* **40**, 2767–2772 (2004).
254. Liu, X. *et al.* Preparation and properties of waterborne polyurethanes with natural dimer fatty acids based polyester polyol as soft segment. *Prog. Org. Coatings* **72**, 612–620 (2011).
255. Cox, W. P. & Merz, E. H. Correlation of dynamic and steady flow viscosities. *J. Polym. Sci.* **28**, 619–622 (1958).
256. Bueche, F. Melt viscosity of polymers: Effect of polydispersity. *J. Polym. Sci.* **43**, 527–530 (1960).
257. Zhang, S.-L. *et al.* Impact properties, Phase Structure, Compatibility, and Fracture Morphology of Polyamide-1010/Thermoplastic Poly(ester urethane) Elastomer Blends. *J. Polym. Sci. Part B Polym. Phys.* **43**, 1177–1185 (2005).
258. Institut für Arbeitsschutz der Deutschen Gesetzlichen Unfallversicherung. GESTIS-Stoffdatenbank. (2017). Available at: www.dguv.de/ifa/gestis/gestis-stoffdatenbank/index.jsp. (Accessed: 27th March 2017)
259. Sigma-Aldrich. Online catalog. (2017). Available at: www.sigmaaldrich.com/germany.html. (Accessed: 27th March 2017)
260. BASF. Online Database MSDS. (2018). Available at: <https://worldaccount.basf.com/wa/msds/eu/search>. (Accessed: 3rd January 2019)
261. Devison for Waste and Disposal. Abfallhandbuch Universität Hamburg (ohne UKE). (2008). Available at: www.chemie.uni-hamburg.de/sicherheit/entsorgung.html. (Accessed: 1st April 2017)

9 Acknowledgements and Credits

An erster Stelle möchte ich Herrn Professor Dr. Luinstra für die Aufgabenstellung und die konstruktive Betreuung dieser Doktorarbeit sowohl bei den praktischen Teilen als auch bei der schriftlichen Ausarbeitung danken. In meiner Promotionszeit konnte ich zahlreiche Einblicke gewinnen, die ich auf keinen Fall missen möchte. Ich möchte in diesem Zusammenhang ebenfalls Herrn Priv. Doz. Dr. Wutz für die Beurteilung dieser schriftlichen Arbeit sowie Herrn Prof. Dr. Maison und Herrn Dr. Hackl für Ihre Bereitschaft danken, mich in dieser anspruchsvollen Zeit bei meiner Disputation mündlich zu prüfen.

Ein großer Dank gilt außerdem meinem gesamten Arbeitskreis, einschließlich der ehemaligen Mitglieder, der mir eine unvergessliche Zeit mit wunderbaren Erinnerungen beschert hat und der meiner Promotionszeit die nötige Würze verliehen hat. Ganz besonders möchte ich dabei allen danken, die es mit mir als ihrem Laborpartner ausgehalten haben, und denen, die mich anderweitig (fachlich oder persönlich) unterstützt haben. Eine besondere Stellung nimmt hierbei Dr. Felix Scheliga ein, dem ich sehr viel verdanke. Auch meinen Bachelor- und Masterstudenten danke ich für ihre indirekte Unterstützung.

Mein weiterer Dank gilt Stefan Bleck und Kathrin Rehmke, die meine zahllosen Anfragen und Messungen per DSC, TGA und GPC u.a. allesamt erfüllt haben. Der Dank gilt nicht minder den weiteren Abteilungen der Universität Hamburg: So hat der massenspektrometrische Service, namentlich v. a. Christine Christ, eine ungeheure Anzahl an Messungen für mich durchgeführt. Die NMR-Abteilung hat – meistens prompt – meine zahlreichen Spektren aufgenommen, obwohl ich diese manchmal als ganzen Strauß von NMR-Röhrchen abgegeben habe. Unermüdlich und geduldig hat auch Renate Walter meine SEM-Proben vermessen. Nicht unerwähnt lassen möchte ich auch Kathleen Pruntsch für ihre so erfrischende Hamburger Art und zahlreiche kleine und große Gefallen über die Jahre. Auch Peter Harry möchte ich für seine Unterstützung bei Glasbruch und Sonderwünschen danken. Der Verwaltung des Fachbereichs sowie dem Einkauf, der mir so manchen ungewöhnlichen Einkaufswunsch erfüllt hat, gilt ebenfalls mein Dank.

Außerdem möchte ich mich bei meinen Vorgesetzten und Kollegen bei meinem Arbeitgeber nach der Laborzeit für die Unterstützung bei der Fertigstellung dieser Arbeit bedanken.

Ein ganz besonderer Dank gilt noch meinen Eltern, die mich all die Jahre meines Studiums stets auf so viele Weisen unterstützt haben und immer für mich da waren. Auch meinen Großeltern möchte ich an dieser Stelle posthum meinen tiefen Dank für ihre stete

Unterstützung und ihre Anteilnahme aussprechen. Mein größter Dank gilt allerdings meiner Frau Sabine, die mein steter Halt und sicherer Hafen war, ist und bleibt. Ihre Unterstützung und ihre Nachsicht mit mir und mit dieser Arbeit sind in meinen Augen beispiellos. Ich bin dankbar für das Geschenk unserer beiden Kinder Nele und Mats und froh, dass ich mein Leben mit euch verbringen darf.

Statutory Declaration

I hereby affirm that the present thesis was written by me and that I used no source material or aids other than those stipulated. I assure that this thesis was not submitted for a previous doctorate examination procedure.

signed Björn Neuer

Hamburg, April 2020